A sensitivity study on the natural frequency of high-rise structures in the Netherlands

K.M.S. Tempelman

TUDelft   Aronsohn   **TNO** innovation for life

A sensitivity study on the natural frequency of high-rise structures in the Netherlands

by

K.M.S. Tempelman

to obtain the degree of Master of Science

in Civil Engineering, in the field of Structural Mechanics,

at the Delft University of Technology,

to be defended publicly on Friday, February 25, 2022 at 15:00.

An electronic version of this thesis is available at `http://repository.tudelft.nl/`.

TUDelft   **Aronsohn**   **TNO** innovatior for life

Preface

The completion of this thesis is the last requirement to obtain the degree of Master of Science in Civil Engineering, in the field of Structural Mechanics, at the Delft University of Technology. The thesis was written in collaboration with Aronsohn Consulting Engineers and TNO, without whose help it would not have been possible.

First, I would like to express my gratitude to Paul Lagendijk, from Aronsohn Consulting Engineers, he has helped me on this journey from day one. Thank you for all the help over the period of my thesis, for always being available when I had questions, and taking the time to explain countless topics.

Second, I would like to thank Okke Bronkhorst from TNO, who joined as my second daily supervisor shortly after Paul. Thank you for coming up with new topics and furthering my interest in this topic. I have learnt a lot from both of you and will use what I have learnt going forward.

Then I would like to thank Apoatolos Tsouvalas and Sergio Gomez, who were my supervisors from the Technical University of Delft. Thank you both for the sound advice and steering me in the right direction.

Lastly, I would like to thank my parents, without whose help none of this would have been possible. Thank you for supporting me from the first day I told you I wanted to study engineering. Thank you for always being there through the ups and down, and keeping me motivated when things got tough. It would have been a tougher journey without you.

<div align="right">

K.M.S. Tempelman
Delft, February 2022

</div>

Abstract

As the world's population keeps increasing and the rate of urbanizations increases, The rate at which high-rise structures are being built is skyrocketing. In the Netherlands, this is no different. It is expected that the amount of high-rise structures taller than 70 meters will more than double in the coming 20 years. As these structures become taller and more slender, they also become more susceptible to wind-induced excitations. Where once the design of a structure was predominantly governed by the Ultimate Limit State (ULS) design criteria, for tall structures, the Serviceability Limit State (SLS) design criteria becomes as, if not more, important. Therefore, the accurate prediction of the dynamic characteristics are becoming increasingly important. One of these dynamic characteristics is the natural frequency, also called the eigen frequency, of the structure.

The natural frequency is a parameter which is largely influenced by the mass and the stiffness of the structure. One would think that after the completion of structure, that the magnitudes of parameters can be determined with a high level of certainty, and that the natural frequency can be calculated accurately, but this is not the case. When comparing the measured natural frequencies of several high-rise structures in the Netherlands, to their natural frequencies determined in the design phases, an underestimation of between 20% to 50% was seen. Although the likelihood that these underestimations will lead to structural failure are small, it does lead to larger design forces and higher peak accelerations, which are used in determining occupant comfort in the structures. The aim of this research is to find the reasons for the discrepancies between the measured and the calculated natural frequencies.

A literature study was performed to determine what the most common methods of determining the natural frequency are during the design phase. There are three main methods which are used throughout different stages of the design phase to approximate the natural frequencies. At the start of the design phase, when structural parameters have not yet been determined, the natural frequency is approximated using empirical formulae. These formulae mostly only depend on 1 or 2 spatial parameters. As the design progresses and the structural parameters are specified, dynamic beam theory can be used to determine the natural frequency. These calculations take the stiffness of the super- and sub-structure, and the mass of the structure, into account. As the design nears completion, the structure is modelled in a FE software package. The natural frequency can then be calculated by the software to give a final impression of the natural frequency.

The main parameters influencing the natural frequency of a system are the stiffness and the mass. This is no different for high-rise structures, but how do these parameters affect the natural frequency, and which of these parameters has the greatest effect on the natural frequency? A sensitivity study, looking at 5 existing high-rise structures in the Netherlands, was performed. Each structure was represented by 5 different beam models. One structural parameter was added to each subsequent beam model as to be able to quantify the influence of the added parameter. Lower and upper bounds were determined for each structural parameter. By varying these parameters and calculating the natural frequencies, the effect this variation has on the natural frequency can be determined. It was found that there are 3 parameters which have significant influence on the natural frequencies, namely, the superstructure stiffness, the superstructure density and the rotational stiffness of the foundation. For all cases with a flexible foundation, the measured natural frequencies could not be reached, even after determining the natural frequencies using the extreme parameter combination, the natural frequencies were still underestimated. The analyses were done for both uniform beam models and multibeam models. The general trend was that the multibeam model produced higher frequencies. This is due to more of the overall stiffness and mass of the structure being situated in the bottom sections of the structure. Using a multibeam can lead to an increase in natural frequency of up to 15%. Although the natural frequencies were increased, they were still nowhere near the measured natural frequencies.

The underestimation of the natural frequencies using the beams models, led to the question if there are other factors which are not yet taken into account when determining the natural frequencies. In

the calculation of the stiffness of the new Erasmus Medical Centre (NEMC), it was assumed that the beams, columns, non-structural elements and the low-rise structure have a negligible influence on the stiffness of the structure. The underestimation in the natural frequencies, led to the conclusion that the stiffness of the structure is underestimated. A complete model of the NEMC was modelled using the SCIA Engineer software. All the structural systems were added to the model. Modal analyses, including different combinations of structural systems and parameter magnitudes, were performed. It was found that for the NEMC the assumption that the beams and columns have a negligible contribution to the natural frequency, was correct. The main contributors to the stiffness of the superstructure were the outer tube and the central cores. The partition walls were added to the model using low stiffness wall elements, by added the walls, the natural frequency was increased by 8.5%. Assumptions were made to include the influence of the low-rise structure. The determined natural frequency was increased past the measured natural frequency, however, this result might not be realistic.

The final conclusion of the thesis is that the stiffness of the superstructure is underestimated. This leads to the conclusion that there are certain elements which provide the structure with extra stiffness, which is not yet taken into account. At the end of the thesis several recommendations are made as to determine where this extra stiffness comes form.

Contents

List of Figures

List of Tables

1

Introduction

1.1. Introduction

For almost 4000 years, the Great Pyramid of Giza held the title of the tallest structure in the world, until it was overtaken by Old St. Paul's Cathedral at the start of the 13th century. Since then, this title has been passed down from churches, to towers, to radio masts and now to the famous Burj Khalifa. Builders and engineer throughout the ages have kept themselves busy with trying to exceed new heights and claim this prestigious title. In the Netherlands, this was no different, as just before the end of the 14th century the Domtoren in Utrecht was finished, with a height of 112 meters. In 1898 the first high-rise building in Europe, was built in Rotterdam. This being only 13 years after the world's first high-rise building in Chicago. Since the completion of the Witte Huis, more than 220 buildings higher than 70 meters have been built in the Netherlands, with the highest building being the Zalmhaventoren at 215 meters tall. It is predicted that the number of high-rise buildings above 70 meters will rise to 450 by 2040 [36].
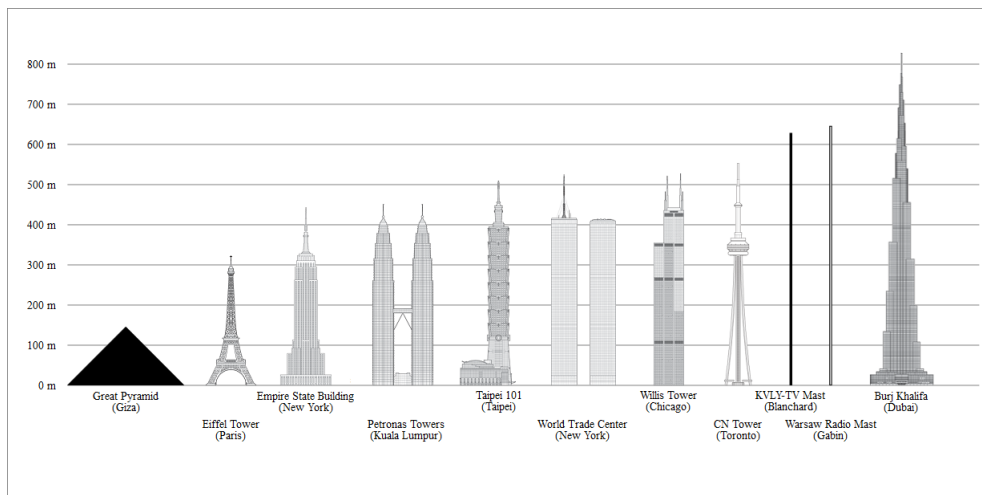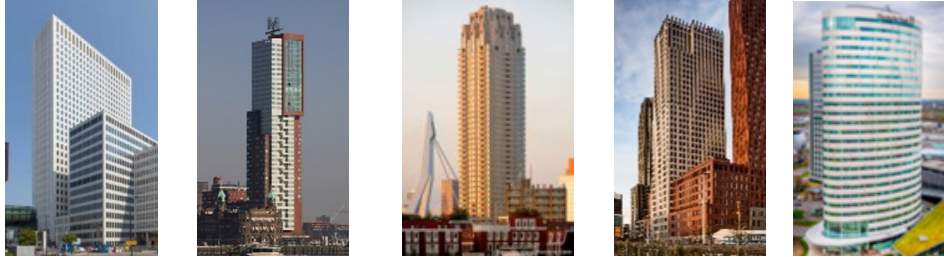
Figure 1.1: Some of the tallest structures in the world throughout history [Google images]

As the race to the sky continues and the height and slenderness of structures keeps increasing, the dynamic properties become increasingly important. As these structures become higher, and their designs more complex, it becomes increasingly difficult to predict these dynamic properties. As these tall buildings are more susceptible to wind excitations, the design criteria shifts from a predominant Ultimate Limit State (ULS) governed design, to a combined ULS and SLS (Serviceability Limit State) governed design. Instead of solely focusing on the structural integrity of the structure, maximum allowable deflection and occupant comfort must now also be taken into account. One of the important parameters

Table 1.1: Weak-axis frequencies of five tall buildings in the Netherlands.

Bronkhorst, O. (2020). 'Long-term vibration and wind load monitoring on a high-rise building' [Conference presentation].ISMA-USD 2020.

Method	NEMC (121m)	Montevideo (140)	New Orleans (155)	JuBi (153)	Oval (98)
Measured	$0.53\,Hz$	$0.41\,Hz$	$0.28\,Hz$	$0.46\,Hz$	$0.40\,Hz$
NEN 6702 (Design)	$0.27\,Hz$	$0.19\,Hz$	$0.19\,Hz$	$0.27\,Hz$	$0.33\,Hz$
NEN-EN 1991-1-4	$0.38\,Hz$	$0.33\,Hz$	$0.30\,Hz$	$0.30\,Hz$	$0.46\,Hz$

used in the dynamic designs of these tall buildings, is the natural frequency. The natural frequency provides insight into the dynamic behaviour of the structure and is often used in the determination of base forces and peak acceleration during the design. Engineers and academics have dedicated large efforts to finding accurate methods of predicting the natural frequency. Due to the complex designs of tall buildings today, simplifying assumptions of structural properties are often made when during the design phase, which often leads to discrepancies between the predicted and measured natural frequencies.

1.2. Problem Statement

In the next 20 years, it is estimated that more than 200 high-rise buildings of over 70 meters will be built in the Netherlands. As these structures become taller and more slender, the importance of the dynamic properties keep increasing. During the design phase of a high-rise structure, the natural frequency is used to give a first indication of the moments and shear forces at the base of the structure, used to approximate the damping in the structure and used to determine the occupant comfort level. These are just a few properties which are influenced by the natural frequency. It is thus easy to see why being able to accurately predict the natural frequency is important. In table 1.1 the first natural frequency of five high-rise structures in the Netherlands can be seen. The table shows the measured frequencies, the frequencies used during the design phase using NEN 6702 and the frequencies determined by the current European standards. When comparing the measured frequencies with the design frequencies, it can be seen that an underestimation of up to 50% is not uncommon. The table also shows that even though the frequencies determined using the current European standards, are closer to the measured frequencies, there is still a significant amount of error.

(a) Base Moment vs Frequency

(b) Base Shear vs Frequency
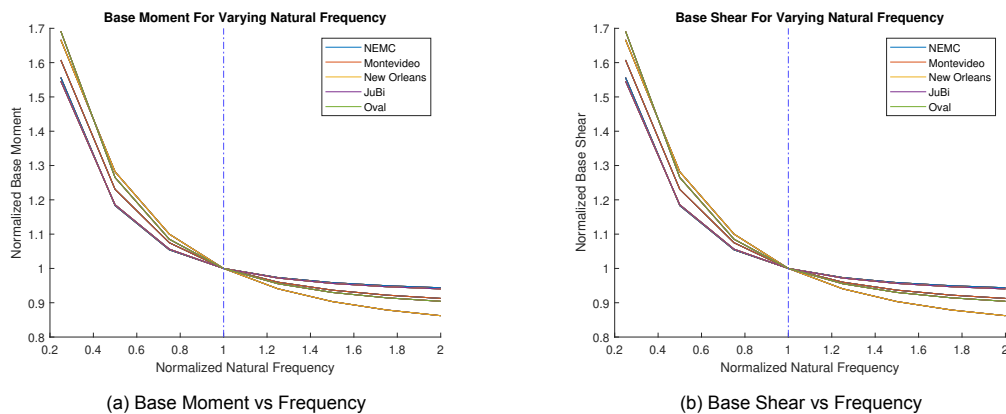
Figure 1.2: Normalized base moment and base shear for varying frequencies

Although wind-induced vibrations in tall buildings seldom result in structural failure, the inaccurate approximation of the natural frequencies can have other consequences. In figure 1.2 the base moment and base shear, calculated using the methods described in NEN-EN 1991-1-4, for the five high-rise buildings can be seen for a varying natural frequency. It can be seen that the underestimation of the natural frequencies can lead to an increased base moment and base shear, which can lead to over designing the structure, which in turn leads to an uneconomical structure. Inaccurate prediction of the natural frequency, can also have a negative effect on the comfort experienced by the occupants of the structure.

1.3. Research Objective and Approach

The literature provides many different methods for the determination of the natural frequency of tall buildings. These methods range from elaborate finite element models, to using beam theory, to using empirical formulae. Each method having their own advantages and disadvantages. Often, simplifying assumptions are made during the determination of the frequencies, which often lead to discrepancies between the calculated and measured frequencies. As shown in table 1.1 these discrepancies also occur during the designing of high-rise buildings in the Netherlands. It is, however, not always clear what the exact cause of these differences in frequencies is caused by. This leads to the objective of this thesis:

> *To determine the reasons for the underestimation of the natural frequency of high-rise structures in the Netherlands.*

To be able to complete the research objective, four main research questions are investigated. These questions will provide insight and narrow done the search to the cause of the underestimation of the natural frequency in high-rise structures in the Netherlands. Certain chapters in the thesis will be dedicated to answering specific questions.

1. *What are the most common methods of determining the natural frequency during the design phase of a high-rise structure?*

To be able to answer this question, a look will be taken at the literature. Firstly, the literature study will provide basic insight into what the natural frequency is. The study will shed light on some of the main parameters that influence the natural frequency by describing the motion of a single degree of freedom system. Hereafter, common methods of determining the natural frequency during the design phase of a tall building will be researched.

2. *What are the main factors influencing the natural frequency of a high-rise structure during the design phase?*

3. *What is the influence of these factors on the natural frequency?*

Question 2 and 3 will be answered by means of a sensitivity study regarding five analytic beam models. A series of calculations will be done to determine which of the parameters included in the different beam models have the most influence on the natural frequencies of the beam. Different beam theories will be used, as to determine if different theories result in different natural frequencies. A lower and upper bound of each of the beam model's parameters will be determined. By calculating the frequency using different parameters values, the effect of the parameter uncertainty has of the natural frequency can be observed.

To be able to determine if the factors influencing the frequency behave the same for all structures, five existing high-rise structures in the Netherlands will be looked at. Each structure will have different parameter ranges, as no structural design is the same. This way, it can be determined if different parameter combinations react differently when parameters varying from their lower bound to their upper bounds.

4. *Are there other factors that influence the natural frequency which are not taken into account*?

Question 4 will be answered by means of a second sensitivity study. In this study, a full model of the new Erasmus Medical Centre will be created in SCIA Engineer. The model will be as complete as possible in regard to the structural specifications given in the design documentation. The focus will mainly be on structural systems which are usually neglected or simplified in the beam models, like beams, floors,

columns and large pile foundations. Certain parameter values and structural system in the model will either be included of excluded from subsequent modal analyses. In this way, the effect in the change in parameter values or the exclusion of certain structural systems have on the frequencies of the structure can be quantified. internal and external non-structural systems will also be looked at, to see how these systems might affect the frequency.

1.4. Thesis Layout

The body of this thesis is divided into 6 main chapters. Chapter 2 presents a literature study regarding the background of the natural frequency and how it is determined during the design phase. The focus of this study is to provide insight on what the natural frequency of a system is. Hereafter, the different methods on how the natural frequency is determined is looked at. The background of the well known empirical formula adopted by the current European Standards is explained. The calculation of the natural frequency using beam models of FEM software is also discussed. Different beam models and theories throughout literature are given. Parameters which influence the frequencies in the different beam models and FEM software is also looked at.

Chapter 3 presents the first sensitivity study. This sensitivity study focuses on the use of beam theory to determine the natural frequency of high-rise buildings. First, a description of the five high-rise buildings used as case studies are describes. In this section, different properties and structural systems are introduced. The measurement setup done by TNO and the measured frequencies of the structure is given. Hereafter, the five different analytic models used in the sensitivity study are described. For each subsequent model, a structural parameter is added to the system. In this way, the influence of this parameter can be quantified. Then the lower and upper bounds for each parameter of the different buildings are determined. Lastly, the results of the different sensitivity calculations are given and discussed.

Chapter 4 discusses the second sensitivity study. In this chapter, structural systems which are usually neglected in the beam models are focused on. This is done by creating a complete model of the new Erasmus Medical centre, according to the specifications given in the design documentation. The first section in this chapter discusses the FEM model which was made during the design of the structure, and the editions added to the model for the purpose of this study. Hereafter, the sensitivity of the frequency due to different structural and non-structural systems is examined.

Chapters 5 and 6 conclude the work covered in this thesis and provides recommendations for further research, to gain more understanding into the complex topic that is the natural frequency of high-rise structures.

2

Literature Study

2.1. Introduction

As buildings become taller and more flexible, the need for lightweight and innovative solutions to complex designs to be able to reach the new heights increases. As the materials and the structural system of these tall buildings change, so does the structure's response to dynamic wind loads. For this reason, to be able to accurately determine the structural response, it is important to first be able to accurately determine the structural parameters playing a role in this response. In older practice it was thought that the parametric uncertainty was due to the variability in the wind environment, meteorological data and wind-structure interaction and that structural properties were deterministic, but according to Kareem [39] the uncertainty in the structural properties of tall buildings also play a large role in their dynamic response. Structural properties which are obtained using the dimensions of the structure, like the height or area of the structure, are usually quite easy to determine accurately. However, for properties such as the building mass, stiffness of the superstructure and influence of the soil-foundation interaction a lot of uncertainty can arise. These uncertainties are mainly caused by variation in the properties of the used materials due to inconsistencies during fabrications, or variations in the mathematical idealization of these properties [39].

One of the dynamic properties heavily influenced by the structural properties is the natural frequency. During the design phase of a building, the natural frequency is an important parameter as it is used to determine the peak acceleration and peak displacement at SLS, and the dynamic factor in ULS. In table 2.1 the natural frequency calculated during the design phase, and the measured natural frequencies of 5 high-rise buildings in the Netherlands are shown. It can be seen that in all cases there is an underestimation of the natural frequencies. Two of the main causes of the inaccurate estimation of these frequencies is due to an inaccurate estimation of the structural parameters and not having a full understanding of how the interconnected structural mechanisms influence the natural frequency [39].

Table 2.1: Calculated natural frequencies in the design phase and the measured natural frequency [9]

Building	Calculated Frequency [Hz]	Measured Frequency [Hz]
New Erasmus MC	0.27	0.53
Montevideo	0.19	0.41
New Orleans	0.19	0.29
JuBi	0.27	0.46
Oval	0.28	0.40

There are several methods how to predict the natural frequency of a structure. These methods range from empirical estimators to detailed FEM simulations. Often early in the design phase of a structure, empirical formulae are used to get a first impression of the value of the natural frequency. As the design progresses and values of the structural parameters are defined, beam theory can be used to

calculate the natural frequencies. This is discussed further in chapter 3 and Appendices A and B. As the final design of the structure nears completion, the structure is modelled using FEM software. The FEM software can then also be used to determine the natural frequency of the system. The following sections provide insight of the different methods used when predicting the natural frequency of a structure. In section 2.2.1 past and current methods of determining the natural frequency according to Dutch standards are discussed. Section 2.2.2 gives background on the empirical formula used in NEN-EN 1991-1-4, and also provides insight into other empirical frequency predictors. Section 2.2.4 discusses the use of FEM software to obtain the natural frequency and how different aspects of the model influence the natural frequency.

2.2. Determining the natural frequency of high-rise structures

The natural frequency, also referred to as the eigen frequency, is the frequency at which an object (or system) oscillates in the absence of a repeated external force. Knowing the natural frequency of a system is important, because when a system is excited at the same frequency as the natural frequency, resonance can occur if sufficient damping is not present. The natural frequency is also one of the parameters needed to predict the dynamic response of a system, and errors in its determination can lead to errors in the prediction and assessment of the dynamic behaviour of a system.

Each natural frequency has a certain mode of vibration. According to Ellis [19] for most buildings the fundamental modes which mainly determine the dynamic behaviour are the two lowest translational modes and the first one torsional mode. These modes contribute more than 90% of the overall motion caused by wind. The higher modes are disregarded [19].

There are several methods how to predict the natural frequency of a structure. For simple systems, the natural frequency can be determined exactly. For instance, in the case of a lumped mass attached to a spring, forming a single degree of freedom system, the natural frequency can be determined with equation 2.1. Where ω_n is the natural frequency, k is the spring stiffness and m is the lumped mass. As the systems under consideration get more complex, the difficulty of accurately predicting the natural frequency increases.

$$\omega_n = \sqrt{\frac{k}{m}} \tag{2.1}$$

Two of the most renowned theories to model a structure are the Euler-Bernoulli beam theory and the Timoshenko beam theory, founded in 1744 and 1921 respectively [16]. The former model is an accurate predictor of the bending behaviour of a beam, but does not account for transverse deformations, whereas the latter model introduces a uniform shear distribution along the beam's cross-section. A drawback of both theories is that they do not take effects such as localised boundary conditions, in- and out of plane deformations, warping and torsional-bending coupling into account [16].

2.2.1. Design codes
2.2.1.1   NEN 6702

Even though high-rise building are complex systems existing of many parts, it is reasonable to represent a high-rise building with a beam element. Often an Euler-Bernoulli beam is used, as high-rise buildings are relatively flexible for their height. During the design phase of a structure, it is necessary to predict the natural frequency of the structure. The NEN 6702 also adopts a vertical beam model [51], which is supported at one end and free at the other end as shown in figure 2.1, to determine the natural frequency. The formula for the natural frequency used in NEN 6702 is given in equation 2.2.

$$f_e = \sqrt{\frac{a}{\delta}} \rightarrow f_e = \sqrt{\frac{0.384}{\delta}} \tag{2.2}$$

With f_e being the first eigen frequency of the beam,
δ being the maximum displacement at the top of the beam due to the vertical load of the structure

applied as a horizontal load against the structure, and
a being the acceleration of the beam. For a cantilever beam as shown in figure 2.1, the acceleration is taken ass 0.384 $\frac{m}{s^2}$.

This formula can be derived using the three well known equation shown below. From the theory of the dynamics of an Euler-Bernoulli beam, discussed in appendix B, the following equation is obtained by rearranging equation B.26. For a cantilever beam with a fixed support, it is known that for the first eigen frequency $(\beta L)^2 = 1.8751$.

$$\omega_e^2 = \frac{(1.8751)^2 EI}{mL^2} \tag{2.3}$$

with ω_e being the first eigen angular frequency of the beam,
EI being the stiffness of the beam, and
m being the mass of the beam.
L being the length of the beam.

The second formula is the well known equation for the maximum deflection of a cantilever beam loaded by a uniform distributed load. Considering a horizontal beam, where the only acting load is the own weight of the beam, then $q = mg$. With g being the gravitational acceleration of 9.81 $\frac{m}{s^2}$.

$$\delta = \frac{qL^4}{8EI} = \frac{m(9.81)L^4}{8EI} \tag{2.4}$$

q being the distributed load.

By rearranging equation 2.4, combining it with equation 2.3 and converting the angular frequency to frequency in Hertz, the formula in equation 2.2 is obtained.

$$f_e = \sqrt{\frac{9.81(1.8751)^4}{4\pi^2 \times 8\delta}} = \sqrt{\frac{0.384}{\delta}} \tag{2.5}$$
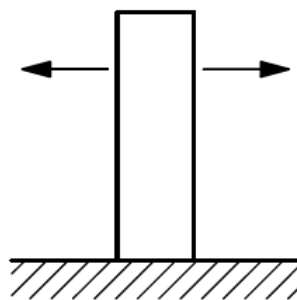
Figure 2.1: Beam adopted by NEN 6702 to determine the natural frequency [51]

2.2.1.2 NEN-EN 1991-1-4

Upon the publication of the NEN-EN 1991-1-4, the method of determining the natural frequency for a high-rise building was replaced. The current empirical formula used to determine the natural frequency was found by Ellis [19]. The formula was determined by plotting the lowest natural frequency measured for the buildings, against the height of the respective buildings of 163 rectangular shaped buildings. The plot is shown in figure 2.2.
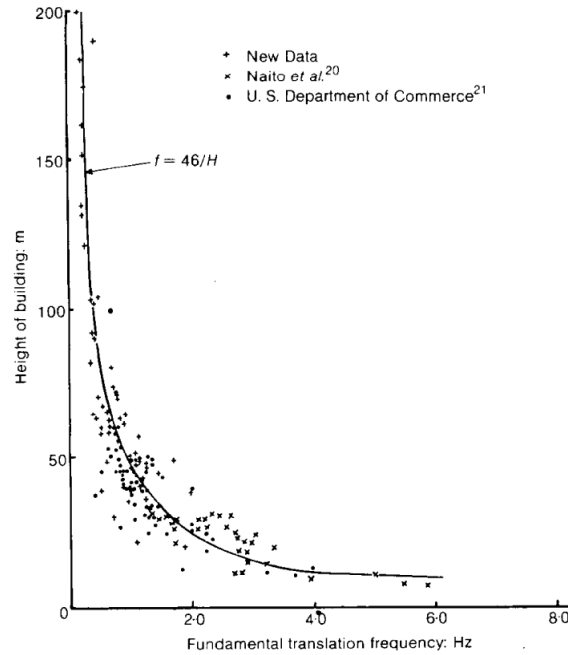
Figure 2.2: Translational natural frequency plotted against building height for 163 rectangular buildings [19]

The best fit line has a correlation of 0.8828 to the data and is easy to use, as it only depends on the height of the building. Equation 2.6 shows the best fit empirical formula, it can also be seen in figure 2.2. This is the equation NEN-EN 1991-1-4 has adopted for determining the first translational natural frequency for structure with a height larger than 50m. In the same study, empirical formulae for the natural frequency in the second translational and torsional direction, as shown in equation 2.7

$$f_{n,1} = \frac{46}{H} \tag{2.6}$$

$$f_{n,2} = \frac{58}{H}$$
$$f_{n,3} = \frac{72}{H} \tag{2.7}$$

With,
$f_{n,1}$ the first translational natural frequency,
$f_{n,2}$ the second translational natural frequency,
$f_{n,3}$ the torsional natural frequency respectively, and
H being the height of the building.

2.2.2. Emperical formlae
Ellis [19] set out to find the best simple predictor for the natural frequency. Using data gathered by the U.S. Department of Commerce, Naito et al. and his own, Ellis plotted the lowest translational frequency measured for the buildings, against the height of the respective buildings of 163 rectangular shaped buildings. This is shown in figure 2.2. In equations 2.6 and 2.7 Ellis opted for the empirical formulae which had a high correlation to the measured data, but which were also simple to use. The fact is that in the same study, Ellis found curves with a higher correlation to the data than the formulae adopted by NEN-EN 1991-1-4, with the highest correlation being 0.8918. The other empirical formulae obtained by Ellis and their correlation to the measured data is shown in table 2.2. In the table, it can be seen that the empirical formula with the highest correlation is

$$f_{n,1} = 42.22D^{0.2}H^{-1.2}. \tag{2.8}$$

In figure 2.3 the equations 2.6 and 2.8 are plotted for buildings with a height between 50m and 200m. Equation 2.8, represented in the dashed lines, is plotted for 4 different building lengths (D). In the figure can be seen that the frequencies determined by equation 2.8 predict a lower frequency than equation 2.6.
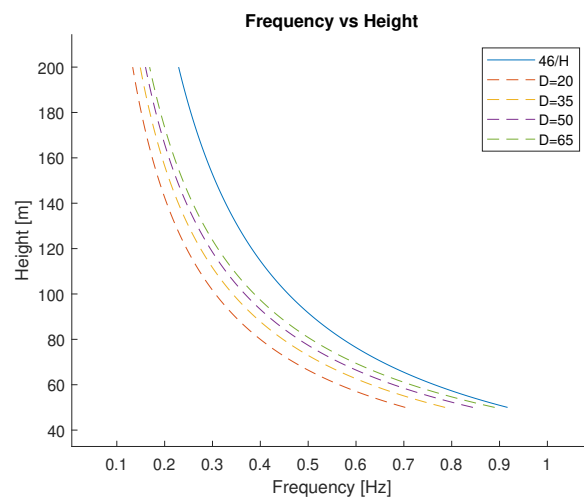
Figure 2.3: Best fit line for the empirical formula used by NEN-EN 1991-1-4 and the formula with the highest correlation for different building lengths, plotted for buildings with a height between 50m and 200m.

Table 2.2: Correlation of measured and predicted lowest fundamental translation frequency for 163 rectangular buildings [19]

Predictor frequency proportional to	Correlation coefficient r	Best fit formula
$H^{-1.5}$	0.8835	$220.60H^{-1.5}$
$H^{-1.4}$	0.8851	$162.60H^{-1.4}$
$H^{-1.3}$	0.8859	$119.27H^{-1.3}$
$H^{-1.2}$	0.8860	$87.10H^{-1.2}$
$H^{-1.1}$	0.8850	$63.32H^{-1.1}$
H^{-1}	0.8828	$45.84H^{-1}$
$H^{-0.9}$	0.8793	$33.05H^{-0.9}$
$H^{-0.8}$	0.8743	$23.72H^{-0.8}$
$H^{-0.7}$	0.8676	$16.95H^{-0.7}$
$H^{-0.6}$	0.8591	$12.05H^{-0.6}$
BH^{-1}	0.5530	$2.17BH^{-1}$
$B^{0.5}H^{-1}$	0.7565	$10.33B^{0.5}H^{-1}$
$B^{0.3}H^{-1}$	0.8217	$18.90B^{0.3}H^{-1}$
$B^{0.1}H^{-1}$	0.8680	$34.21B^{0.1}H^{-1}$
$D^{0.3}H^{-1}$	0.8846	$15.35D^{0.3}H^{-1}$
$D^{0.2}H^{-1}$	0.8874	$22.17D^{0.2}H^{-1}$
$D^{0.1}H^{-1}$	0.8869	$31.92D^{0.1}H^{-1}$
$D^{0.2}H^{-1.2}$	0.8918	$42.22D^{0.2}H^{-1.2}$
H = height; D = length; B = width; All dimensions in meters.		

Throughout the years, there have been numerous studies with regard to finding an accurate natural frequency predictor. Equation 2.1 shows that for a basic mass-spring system, the natural frequency depends on the mass of the system and the stiffness of the spring. This raises the question whether predicting the frequency using only the height of the structure might be too simple. literature provides several factors which influence the natural frequency of a building, a few are the configuration of the stability system of the structure, the mass density and distribution over the building height, the distribution of stiffness of the building, material properties and foundation parameters [61]. There are also studies showing that non-structural elements, such as partition walls and masonry in the structure, influence

the natural frequency of a building [44, 42, 57]. One can see why it is difficult determining an empirical formula which takes into account all the different influencing factors. For this reason, the buildings used to determine an empirical formula are often clustered into groups with some of the same attributes. In table 2.3 empirical formulae to determine the natural frequency of high-rise buildings with a height of at least 50m, can be found. In the table the study of origin, formula and the range in which the formula can be applied is seen. Figure 2.4 shows the different empirical formula plotted against height. The buildings heights range from 50m to 200m. For formulae dependent of the number of storeys (N) and the width (D) of the building, a range of 12 to 50 storeys and 30m is used respectively.

Table 2.3: Empirical formulae used to estimate the fundamental frequencies of high-rise buildings

Study	Formula	Application
NRCC [15]	$20H^{-0.75}$	"Bases on measured periods of buildings"
Gilles [22]	$52.6H^{-1}$	"Regression analysis to test goodness of fit of different equations of the mean-value curve"
Hong [28]	$34H^{-0.804}$	"Predicts median fundamental vibration period of RC moment resisting frame (MRF) building with given height"
ICBO [30]	$20D^{0.5}H^{-1}$	"According to 1970 edition of Uniform Building Code"
ICBO [31]	$13.7H^{-0.75}$	"Evaluates fundamental vibration period of RC MRF building"
Goel [23]	$19.7H^{-0.92}$	"Obtains measured periods of RC MRF buildings n California using unconstrained regression analysis"
Goel [23]	$18.9H^{-0.9}$	"For RC structures"
Goel [23]	$21.5H^{-0.9}$	"Based on lower bound of data; proposed for RC frames"
CEN [20]	$13.3H^{-0.75}$	"According to the European seismic design regulations; only for RC structures"
Hatzigeorgiou [25]	$13.7H^{-0.745}$	"Considers influence of infill and concrete shear walls, soil flexibility, and building height "
ASCE [2]	$13.8H^{-0.8}$	"General buildings"
Crowley [17]	$11.1D^{0.5}H^{-1}$	"Vibration of RC moment resisting frames with rigid infills"
BIS [13]	$10N^{-1}$	"Earthquake-resistant design of structures"
Michel [49]	$76.9H-1$	"RC and masonry buildings"
Pan [52]	$10.8N^{-0.8183}$	"RC and masonry buildings"
Velani [59]	$111.1H^{-1.1}$	"RC buildings above 20 floors (>60m)"
H = height; D = length; N = Number of storeys.		
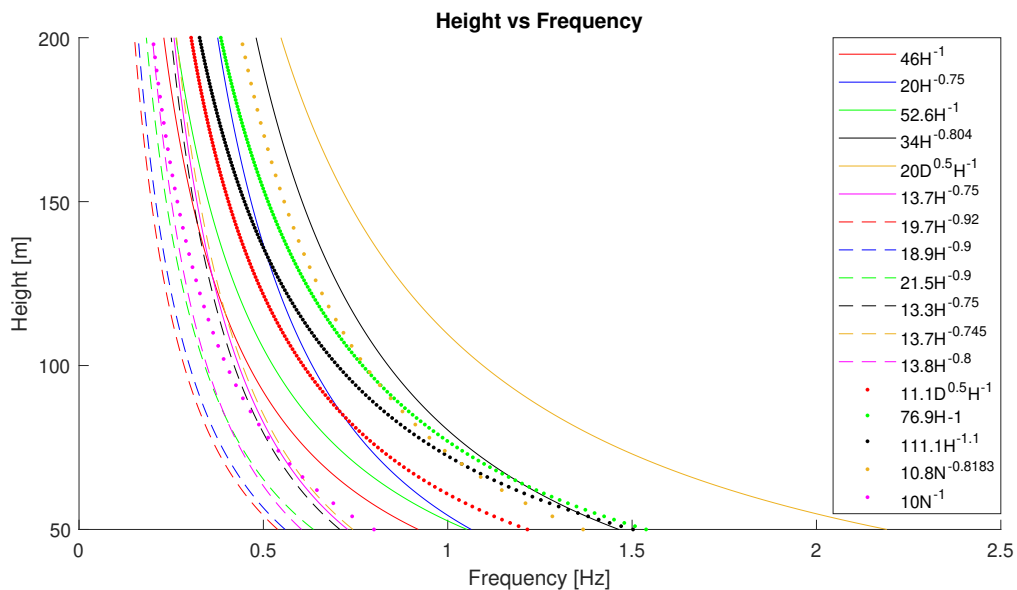
Figure 2.4: Empirical formulae given in table 2.3 plotted vs height ranging from 50m to 200m. Formulae dependent on N or D, a range of 12 to 50 storeys and a width of 30m is used.

2.2.3. Beam Theory

As high-rise structures become higher and more slender, they are often relatively flexible owing to their height. For this reason, it is generally accepted to use Euler-Bernoulli and Timoshenko beam theory to represent these tall structures. High-rise structures are represented by cantilever beams, where the top is free and the base of the beam has a set of boundary conditions. The boundary conditions are commonly either fixed, to represent a structure build on bedrock. Or, the boundary conditions can be represented by a series of springs to represent the soil-structure interaction.

In the 1750s mathematicians Euler and Lagrange described dynamic beam theory for a bending beam with a uniform stiffness and density [16]. Using this beam theory, the dynamic behaviour of beams could be predicted. This theory is still used today to predict the dynamic behaviour of beams. Applying this theory to a cantilever beam which represents a tall building, the dynamic behaviour of this building can be approximated. Properties like the eigen frequencies, mode shapes and free and forced vibration behaviour can be predicted. The first three translational mode shapes of a cantilever Euler-Bernoulli beam can be seen in figure 2.5. These are the shapes the beam will assume when excited by the first three translational eigen frequencies.
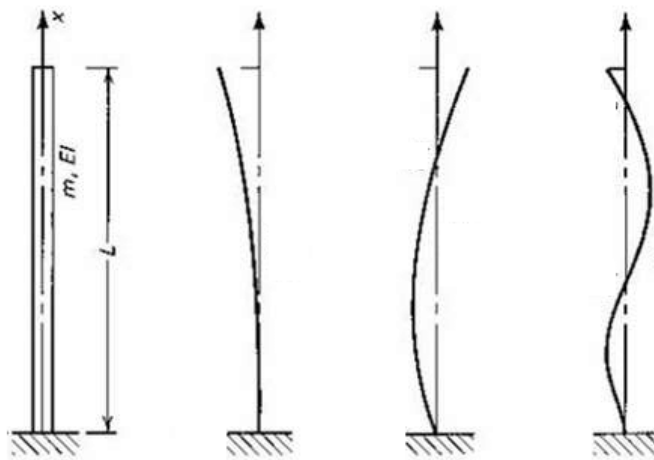
Figure 2.5: First three translational modes of a cantilever Euler-Bernoulli beam.

When using dynamic beam theory to predict the dynamic behaviour, one of the main assumptions is that the beam is seen as a continuous system. This means that there are an infinite number of degrees of freedom. This also means that the system has an infinite number of eigen frequencies. The equation of motion of an Euler-Bernoulli beam is shown in equation 2.9. When the differential equation os solved for a cantilever beam with a fixed base, the natural frequency can be determined with equation 2.10. Where n is the number of the wanted eigen frequency and β_n is a value which corresponds to each individual eigen frequency. In equation 2.10 is can be seen, just like for the SDoF system, that the eigen frequencies of a beam increase as the stiffness of the beam increases, and decreases when the mass of the beam increases. The change in frequency due to an increased stiffness or mass is graphically represented in figure 2.6.

$$\rho A \frac{d^2 v}{dt^2} + \frac{d^2}{dx^2}\left(EI\frac{d^2 v}{dx^2}\right) = q \tag{2.9}$$

$$\omega_n = \beta_n \sqrt{\frac{EI}{\rho A}} \tag{2.10}$$
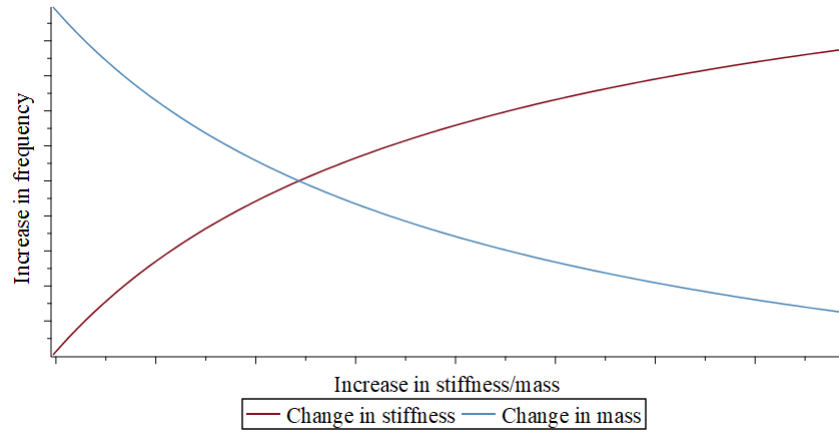
Figure 2.6: General change in frequency due to an increase in stiffness of mass parameters

Since the dynamic beam theory was proposed, many researches have been inspired to build on this theory, or to introduce theories of their own. One of the assumptions often made when simplifying a high-rise structure with a cantilever beam, is that the parameters do not vary in the height of the structure. In some cases, this can have a significant influence on the frequencies. Many studies have researched the effect of changes in the stiffness and density in the longitudinal direction have on the frequency. Jang and Bert [33, 32] proposed a method for the free vibration of a stepped Euler-Bernoulli beam. The beam had a single step, and the neutral axis of the two stepped sections were collinear. Ju et al. [38] presented a differential equation which exceeded the restriction of Jang and Bert, and solved the free vibration for beams with multiple steps with non-collinear neutral axes. Jategaonkar and Chehil [37] investigated the problem of calculating the natural frequency of a beam with a varying inertia, area and mass. Studies have also been done on bending-shear and bending-torsional coupled beams [18] [7]. These are only a few studies that touch on the topic of the free vibration of beams.

As high-rise structures are often not constant in stiffness and mass over their height, it is easy to question if a beam with uniform parameters is an accurate simplification? Or what if the beam acts more like a shear beam, rather than a bending beam? With the wide variety of structural types and complex designs of tall buildings today, modern buildings are often difficult to simplify accurately. In the work of Bartolini [5], he describes a Differential Degree of Cantilever Action (dDCA) shown in equation 2.11. The dDCA calculates how the actual mode shape of an existing building, differs from an idealized bending beam. If the dDCA calculates a value of 1, the structure is an ideal bending beam. Whereas, if the dDCA calculates a value of 0, the beam is an ideal shear beam. Values between 0 and 1 will thus show if the structure is dominated by cantilever action, or by shear action. This method is currently being used to reclassify high-rise structures in America [5].

$$d = 1 - \frac{1}{N} \Sigma_{i=1}^{N} \frac{\Delta C_i(h_i)}{T_i(h_i)} \tag{2.11}$$

Where N is the amount of steps where measurements were taken,
h_i is the height where the ith measurement was taken,
$\Delta C_i(h_i)$ is the difference between the measured data and the ideal bending beam, and
$T_i(h_i)$ is the difference between the measured data and the ideal shear beam.

2.2.4. Finite Element Method Software
As the design phase progresses and the structural systems are more defined, models of the structure are often created in FEM software. One of the many advantages of using FEM software is that structural systems, such as beams, floors, outriggers, etc., as well as non-structural systems, can easily be taken into account when performing dynamic analyses. Although these FEM software packages can determine the natural frequency quite accurately, simplifications in the creation of the models are still
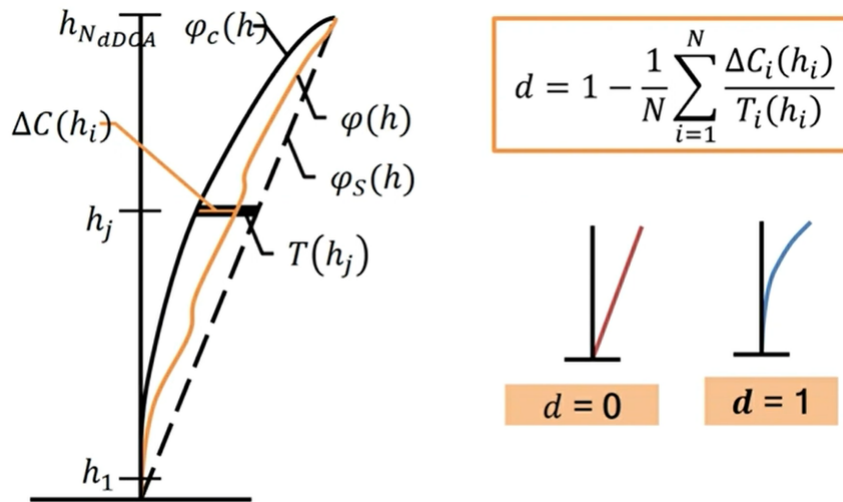
Figure 2.7: Differential Degree of Cantilever Action.
[5]

made to save time and computation power. These simplifications often lead to discrepancies when comparing the FEM determined results to the measured data [42]. Table 2.4 shows a few studies where measured frequencies were compared to the frequencies determined by FEM software. The table shows the type of structure, what was included in the FEM model and the comparison in frequencies. It can be seen that in most studies, there is a significant difference between the measured frequencies and the frequencies determined by the FEM software.

Certain structural and non-structural systems are commonly assumed to be negligible when calculating the frequencies, but this is often found not to be accurate. This has been the topic of many studies. Kim et al. [44] studied three towers in Korea. All three towers had a similar structural system, which consisted of a perimeter beam-column frame and concrete cores is the centre of the structure. The initial FEM models only included these structural systems. The underestimation of the first natural frequency for the initial FE models was between 70% and 85%. Hereafter, several changes were made to the models which influence the frequencies. Beam-end-offset [1] was introduced to the models and increased the natural frequencies by 1%-6%. Floor slabs were modelled, instead of rigid diaphragms [2], this further increased the translational frequencies by 3%-11%, and the torsional frequencies by 16%-23%. After plain concrete and concrete brick walls were added to the model, the first translational frequency was increased by 5%-12%. According to Kim [44], the Korean Building Code states that to assure the quality of concrete, the compressive strength of concrete used during construction must, on average, be 21% higher than stated in the design. By introducing this increase to the FE model, the frequencies were raised further by 7%-12%. After introducing all these changes, the highest error in FEM determined frequency was only 4%.

Su et al. [57] did a similar study of three high-rise structures in China. In the study, only the major structural elements of the structural were added to the FE model. Floors were again modelled by rigid diaphragms, as in the previous study. For the three models, the initial frequencies calculated by the FEM software, were underestimated by more than 100%. The first structure was a 15-storey reinforced concrete (RC) building. The lateral stability system consisted of RC moment resisting (MR) frames attached to a concrete core in the centre of the structure, and 4 shear walls at the edges of the structure. According to Su [57], the Hong Kong construction regulations state that the concrete strength used during construction must be $5 MPa$ higher than specified in the design. The increase in the concrete strength lead to an increase in frequency of between 15%-16%. The addition of concrete

---

[1] "In conventional analysis of frame, beams and columns are modelled in such a way that they are connected at dimensionless nodal points. However, in reality a joint has finite dimensions and generally acts as a rigid body, so it is believed that that FE models considering beam-end-offset at the joints can more accurately represent the actual behaviour." [44]

[2] Rigid diaphragms are kinematic constraints imposed on the lateral displacements of the floor nodes, so these nodes can only displace as a rigid body. [44]

Table 2.4: Measured frequency compared to FEM determined frequency

Researcher	Material & type of structure	Height [m]	Mode of vibration	Natural frequency [Hz]		Difference %	Components included in FEM model
				Measured	FEM		
J.M.W. Browinjohn, et al. [12]	RC core and concrete filled tube columns	280	1st	0.191	0.194	1.6	Bare frame,
			2nd	0.199	0.215	8.0	wall opening and core
			3rd	0.566	0.605	6.9	thin wall in the core
M. Miwa, et al. [50]	Steel frame	63	1st	0.76	0.76	0.0	Bare frame and
			2nd	0.87	0.86	-1.1	composite beams
			3rd	1.15	1.11	-3.5	
Y. Tamura, et al. [58]	Steel frame	108	1st	0.57	0.57	0.0	Bare frame
			2nd	2.18	2.15	-1.4	
			3rd	4.58	4.48	-2.2	
Q.S. Li, et al. [45]	RC frame and core walls	200	1st	0.368	0.3	-18.5	Not specified
			2nd	1.395	1.109	-20.5	
			3rd	2.979	2.451	-17.7	
E. Ho, et al. [27]	RC shear wall	218	1st	0.31	0.18	-41.9	Bare frame
			2nd	0.31	0.18	-41.9	
			3rd	0.53	0.16	-69.8	
s. Campbell, et al. [14]	RC shear wall	206	1st	0.36	0.18	-50.0	Bare frame
			2nd	0.37	0.19	-48.6	
			3rd	0.58	0.15	-74.1	
	RC frame and core walls	51	1st	1.67	0.82	-50.9	Bare frame
			2nd	1.75	0.63	-64.0	
			3rd	2.38	1.03	-56.7	
R.K.L. Su, et al. [57]	RC frame and core walls	53	1st	1.79	0.53	-70.4	Bare frame
			2nd	1.72	0.66	-61.6	
			3rd	2.63	0.62	-76.4	
	RC shear wall	113	1st	0.78	0.38	-51.3	Bare frame
			2nd	0.72	0.36	-50.0	
			3rd	0.65	0.38	-41.5	
J.Y. Kim, et al. [43]	RC frame and core walls	148	1st	0.35	0.23	-34.3	Bare frame
			2nd	0.38	0.28	-26.3	
			3rd	0.74	0.46	-37.8	
Q.S li, et al. [46]	Steel and RC	420	1st	0.147	0.162	10.2	Not specified
			2nd	0.381	0.446	17.1	
			3rd	0.576	0.664	15.3	

brick walls to the model, added 74%-140% to the frequencies. All secondary beams, which were not taken into account in the bare frame model, had less than 2% effect on the frequencies. Lastly, floor slabs were added to the model, instead of the rigid diaphragm assumption. This lead to an increase of around 12%. After the model was updated, the difference between the FE software determined frequencies and the measured frequencies were minimized to between -6% to 3%.

For the other two structures, similar results were obtained. With final differences between determined and measured frequencies of -1.7% to 5.5%.

Several similar studies can be found in literature. This shows that even though FE software is able to predict frequencies quite accurately, the engineer should be wary in the assumptions which are made. the wrong assumptions could often lead to an over simplification of the model, which could provide inaccurate results.

3

Sensitivity Study I: Analytic Models of 5 Existing High-Rise Structures in the Netherlands

3.1. Introduction

As the literature discussed in the previous chapter shows, there are several factors which influence the accurate determination of the natural frequencies. The aim of chapter 3 is to gain a better understanding of how certain properties of a structure affect its natural frequency. As stated by Kareem [39] the uncertainty in the determination of structural properties of tall buildings play a large role in their dynamic response. For this reason, a closer look will be taken at the building parameters with high uncertainty and what this uncertainty does to the natural frequency. The 5 high-rise buildings discussed in chapter 2 (the New Erasmus Medical Center, The Montevideo tower, the New Orleans tower, the JuBi tower and the Oval tower), will be used as case studies to show the sensitivity of the natural frequency.

As it is quite difficult to quantify an exact amount of uncertainty for the different structural parameters, this will be done in the form of determining a lower and upper bound for each parameter influencing the natural frequencies of the structures. These are the parameters related to the mass and stiffness of the superstructure and the foundation, and bounds will be determined for the superstructure's bending stiffness and density and the foundation's rotational and translational stiffness and the mass of the foundation. Spatial parameters such as the surface area and height of the structure are assumed to be deterministic and will be calculated exactly. As the structures are not uniform over their height, the mass and stiffness parameters of the superstructure are calculated for each section where there is a significant change in these parameters. FEM results determined during the design phase of the respective structures, and the calculated sectional parameters are used to determine a bending stiffness for the structure which is uniform throughout the height of the structure.

Once the parameter ranges are determined, the influence of these ranges on the natural frequencies can be determined. This is done by calculating the natural frequency using 5 different analytical beam models as stated below. Each of these models will provide insight on how the addition or exclusion of certain structural parameters influence the natural frequency. Two different beam theories are used, Euler-Bernoulli and Timoshenko, so that the most suitable theory for the given buildings can be found. Two different analytic approaches are used. First, a one beam model is used with uniform parameters throughout the height of the beam, second, a multibeam model is used with the calculated sectional properties.

1. Case 1: Cantilever Euler-Bernoulli beam with fixed support

2. Case 2: Cantilever Euler-Bernoulli beam with rotational spring support

3. Case 3: Cantilever Euler-Bernoulli beam with rotational and translational spring support

4. Case 4: Cantilever Euler-Bernoulli beam with rotational and translational spring support including foundation mass

5. Case 5: Cantilever Timoshenko beam with rotational and translational spring support including foundation mass

In this chapter, section 3.2 provides background of the 5 high-rise buildings used in this sensitivity study. Important aspects of the design of each structure are discussed, and the measured natural frequency of each structure is given. Section 3.4 describes the 5 different analytical models used in the study, and the relevance of the different models. Section 3.5 describes how the lower and upper bounds of the sectional and uniform structural parameters are determined, and gives reference to the appendices where the calculations can be found. Section 3.6 describes the methodology used to obtain the results, and section 3.8 will conclude the findings of the study.

3.2. Building Descriptions and Measurements

To determine the influence the different structural parameters have on the natural frequency, five different existing buildings are looked at. These buildings are the New Erasmus Medical Center, the Montevideo tower, the New Orleans tower, the JuBi tower and the Oval tower. TNO has gathered data regarding the natural frequencies of each of these buildings. The following section describes the key structural aspects of the five structures, the setup of the measurement apparatus and the natural frequencies measured by TNO.

3.2.1. The New Erasmus Medical Center

The new Erasmus Medical Center (NEMC) is a hospital building in the center of Rotterdam. The building is 121m tall, consists of 31 floors and has a constant rectangular shape throughout the entire height of the building as shown in figure 3.1. The load carrying system of the structure exists of a concrete tube and three central concrete cores, which are marked in red in figure 3.1a. The lower part of the concrete tube, up to level 4 marked by '1' in figure 3.1b, is made in situ, whereas the rest of the structure (marked by '2') exists out of layered prefabricated concrete elements. The lateral stability of the structure is provided by the concrete tube and core of the structure. The structure rests on a 2m thick concrete foundation slab supported by 352 piles. Between the ground floor and the foundation slab, there is a crawl space of about 1.5m. Connected to the lower part of the tower is a low-rise building of 14 storeys high. Between the two structures, movement joints are placed, and it is thus assumed that the low-rise structure does not provide stiffness to the high-rise structure.

On the top floor of the tower, 6 accelerometers were placed as shown in figure 3.1a [54]. In figure 3.1a can be seen that accelerometers 1, 3 and 5 are placed facing the direction of the strong-axis as to measure the accelerations in the y-direction, in the same figure can be seen that accelerometers 2, 4 and 6 are placed facing the weak-axis as to measure the accelerations in the x-direction. With the data gathered by TNO, the first three eigenfrequencies were determined and are shown in table 3.1. These are the measured frequencies in the weak (x), strong (y) and the torsional (ϕ) direction.

Direction	Frequency [Hz]
x	0.53
y	0.68
ϕ	1.28

Table 3.1: Eigenfrequency in the x, y and torsion direction of the new Erasmus Medical Center

(a) Plan view of NEMC top floor
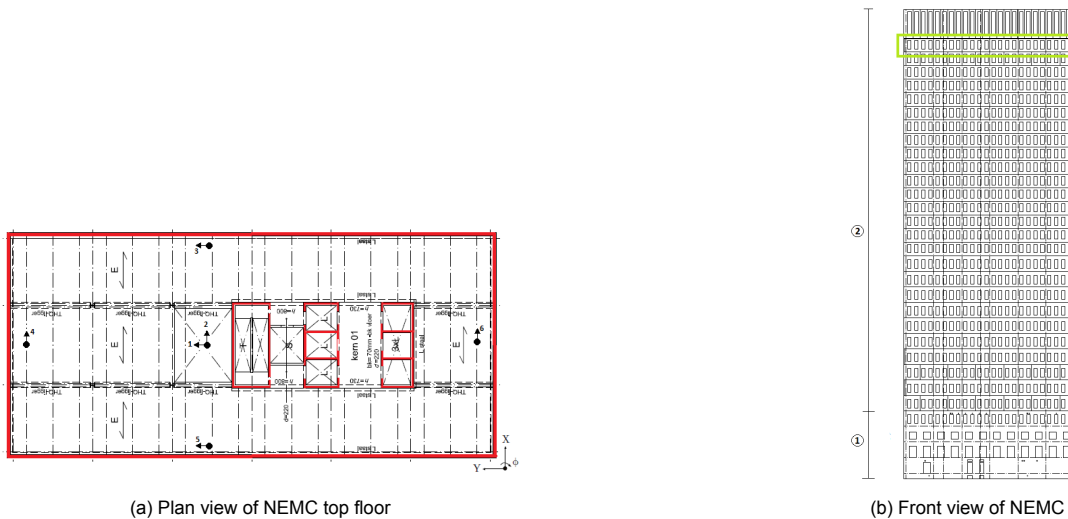
(b) Front view of NEMC

Figure 3.1: Plan and front view of the NEMC showing the lateral stability system, concrete core and the placement of the measuring apparatus

3.2.2. The Montevideo Tower

The Montevideo tower is a residential building situated in the centre of Rotterdam. The tower has 43 floors above ground and is 140m tall (close to 150m when including the 8m high letter 'M' on the roof). The structure has a rectangular shape throughout the height of the building. The lateral stability system of the tower is split into 3 parts: the top part, stretching from the 28th floor to the 42nd floor, exists of a steel frame system shown in green in figure 3.2. On the outer side of the steel frame, the beams and columns are connected by diagonally placed steel beams stretching from floors 28 to 35 and from floor 35 to floor 42. The middle of the structure, from the 2nd floor to the 28th floor, exists of a concrete structure of load bearing walls given by the red lines in figure 3.2. Lastly, the bottom part of the structure, from the ground floor to the 2nd floor, exists of a concrete core and steel braces. Beneath the ground floor there is a parking garage stretching 2 levels down. The floor of level -2 is a concrete foundation slab of 2m thick which rests on 238 prefabricated concrete piles. Connected to the lower part of the tower is a building of 8 storeys high. Between the two structures, movement joints are placed, and it is thus assumed that the low-rise structure does not provide stiffness to the high-rise structure.
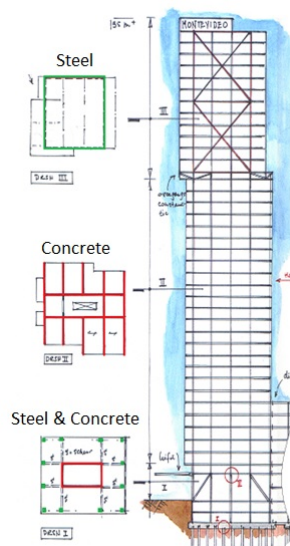
Figure 3.2: The lateral stability system of the three parts of the Montevideo tower

In the Montevideo tower, 6 accelerometers were placed on the 27th floor and 5 accelerometers were

placed on the 42nd. Accelerometers 1, 3 and 5 (27th floor) and 7, 8 and 10 (42nd floor) are placed facing the direction of the strong-axis as to measure the accelerations in the y-direction [54]. Accelerometers 2, 4 and 6 (27th floor) and 9 and 11 (42nd floor) are placed facing the weak-axis as to measure the accelerations in the x-direction [54]. The setup of the accelerometers can be seen in figure 3.3. With the data gathered by TNO, the first three measured eigenfrequencies were determined and are shown in table 3.2.

Direction	Frequency [Hz]
x	0.41
y	0.49
ϕ	1.06

Table 3.2: Eigenfrequency in the x, y and torsion direction of the Montevideo tower
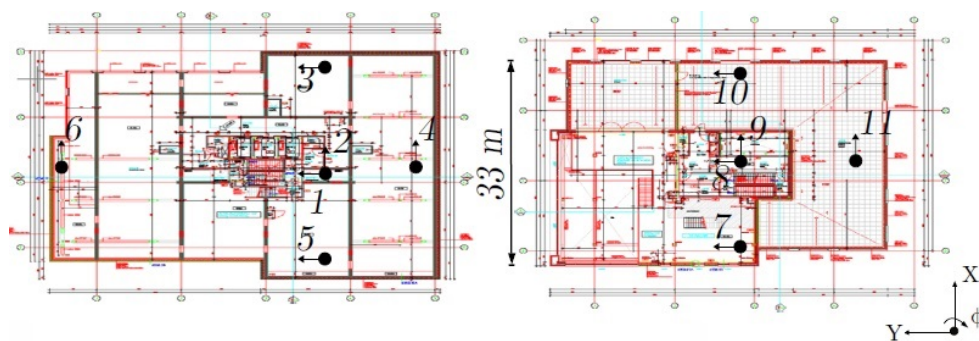
Figure 3.3: Accelerometer setup of the Montevideo tower. [54]

3.2.3. The New Orleans Tower
The New Orleans tower is a residential tower located next to the Montevideo tower. The building has 44 storeys above ground, a 2-storey parking area below ground and is 155m tall. From level 2 and upwards, the stability of the structure is given by the concrete core shown in red in figure 3.4a, the concrete walls acting as outriggers spreading from the central core shown in blue, and the outer walls shown in green. The walls marked in blue act like outriggers as they transfer the loads in the structure to the columns of the lower levels, also marked in blue in figure 3.4b, which in turn transfers the load to the foundation. Beneath the parking area, the structure rests on a 2.5m thick concrete foundation slab, which transfers the loads to the 323 concrete piles found below the foundation slab.

On the 34th floor of the New Orleans tower, 4 accelerometers were placed. Accelerometers 1 and 3 are placed facing the direction of the strong-axis as to measure the accelerations in the y-direction and accelerometers 2 and 4 are placed facing the weak-axis as to measure the accelerations in the x-direction [56]. The setup of the accelerometers is shown in figure 3.4a. With the data gathered by TNO, the first three measured eigenfrequencies were determined and are shown in table 3.3.

Direction	Frequency [Hz]
x	0.28
y	0.29
ϕ	0.67

Table 3.3: Eigenfrequency in the x, y and torsion direction of the New Orleans tower.

(a) stability system above level 1

(b) Stability system levels 0 and 1
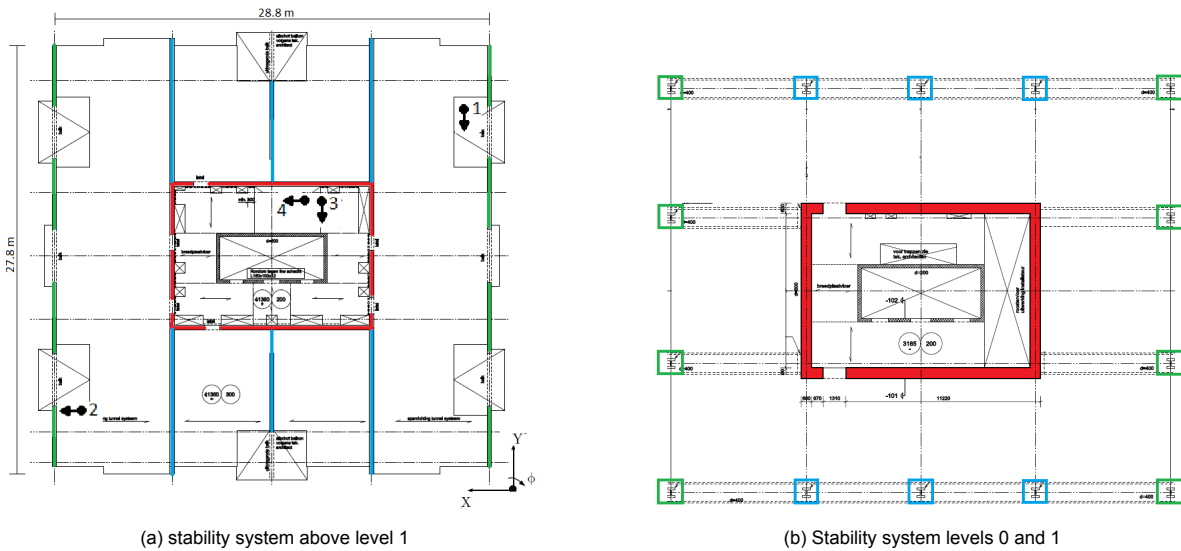
Figure 3.4: Lateral stability system of the New Orleans tower and the placement of the measuring apparatus

3.2.4. The JuBi Tower

The JuBi towers are office buildings situated in the centre of the Hague. Both towers have 38 storeys and are 146m high. Connecting the two towers there is a low-rise building of 10 storeys high. Movement joints are present between the low-rise building and the towers and for this reason the low-rise building is neglected in the analysis. The highlighted tower in figure 3.5a will be considered further in this report. The stability of the structure is provided by a tube-in-tube system. The outer tube exists out of prefabricated concrete elements and the inner tube are a set of concrete cores, as respectively shown in red and blue in figure 3.5b. Beneath the ground level of the building is a 2-storey parking area which rests on a concrete foundation slab varying in thickness between 1.2m and 800mm. The foundation slab is supported by 529 concrete piles.

(a) Considered JuBI tower

(b) Stability system of the JuBi tower
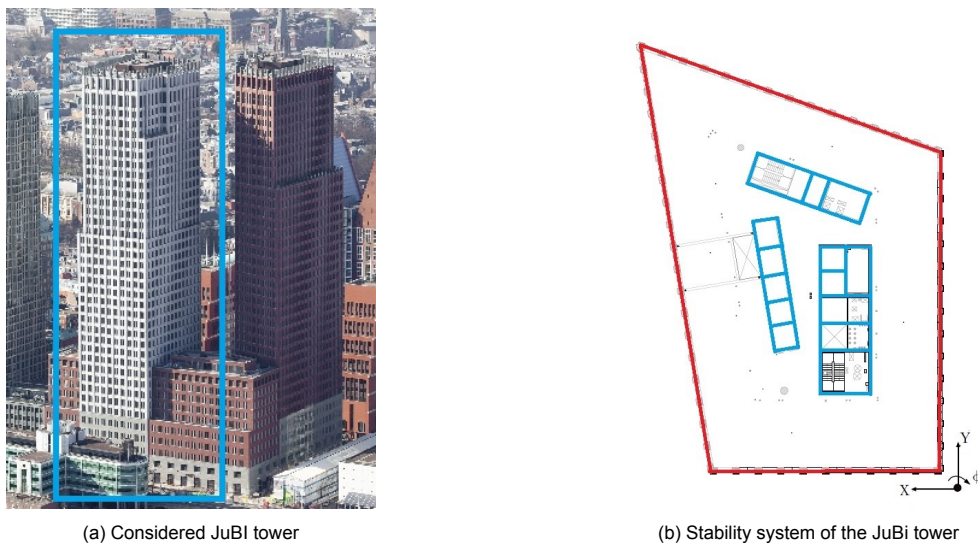
Figure 3.5: The considered JuBi tower and it's stability system.

In the JuBi tower, accelerometers were placed on the 9th, 22nd and 37th floor and can be seen in figure 3.6. Accelerometers 2, 4 and 6 were placed in the direction of the strong-axis as to measure the acceleration of the y-axis and accelerometers 1, 3, 5, 7 and 8 were placed facing the direction of the weak-axis as to measure the acceleration in the x-axis.With the data gathered by TNO, the first three measured eigenfrequencies were determined and are shown in table 3.4.

Direction	Frequency [Hz]
x	0.46
y	0.55
ϕ	1.00

Table 3.4: Eigenfrequency in the x, y and torsion direction of the JuBi tower.
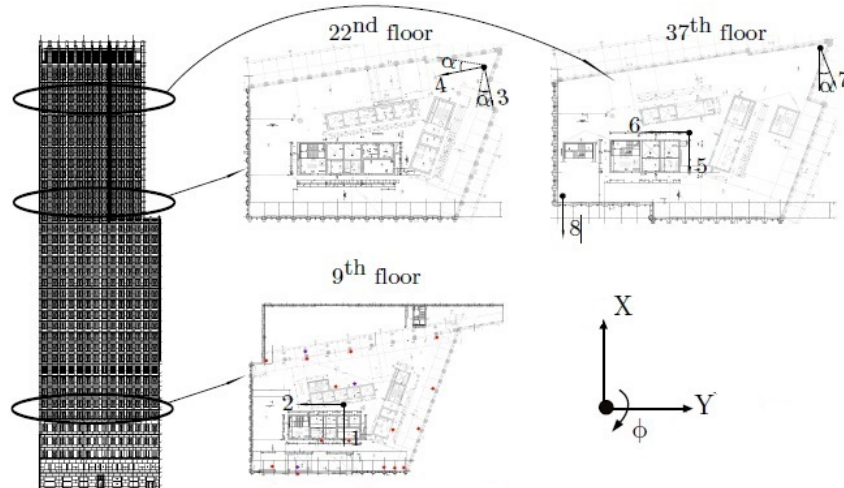
Figure 3.6: Accelerometer setup of the JuBi tower [54]

3.2.5. The Oval Tower
The Oval tower is an office building in Amsterdam and gets its name due to its uniform oval shape throughout the entire height of the building. The building has 24 floors above ground, one level below ground and is 98m high. The inner concrete core of the building is the main load bearing structure, and the outer perimeter is closed off by aluminium walls. The stability of the structure is provided by the concrete core, as well as 8 concrete columns on the outer perimeter of the structure, which are connected to the central core by outriggers. The stability system is shown in red in figure 3.7a. Below the core of the structure the foundation plate is 1.5m thick and under the rest of the structure it has a thickness of 400mm. The foundation plate rest on 185 concrete piles.

The top floor of the Oval tower was provided with 6 accelerometers. Accelerometers 2, 4 and 6 are placed facing the direction of the strong-axis as to measure the accelerations in the y-direction and accelerometers 1, 3 and 5 are placed facing the weak-axis as to measure the accelerations in the x-direction [54]. The setup of the accelerometers is shown in figure 3.7b. With the data gathered by TNO, the first three measured eigenfrequencies were determined and are shown in table 3.5.

Direction	Frequency [Hz]
x	0.40
y	0.57
ϕ	0.82

Table 3.5: Eigen frequency in the x, y and torsion direction of the Oval tower.

(a) Horizontal stability system

(b) Accelerometer setup [54]
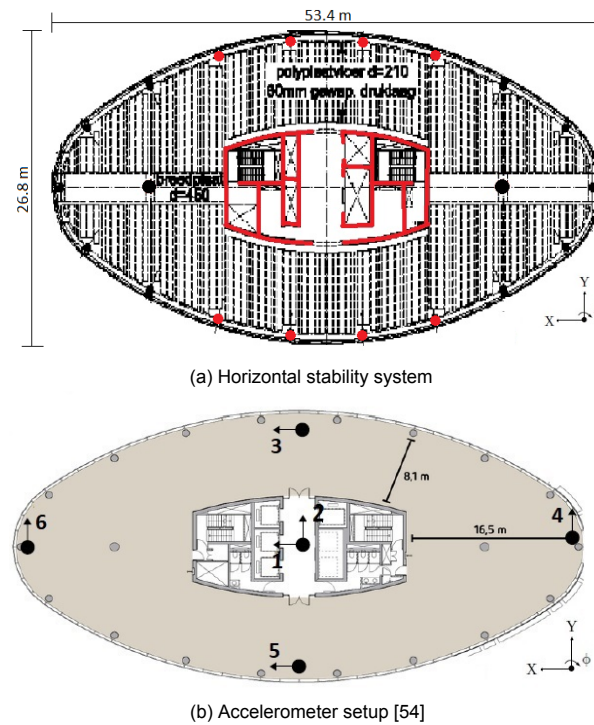
Figure 3.7: The horizontal stability system and the accelerometer setup of the Oval tower.

3.3. Determining the natural frequency using measured data

The setup of the measurement apparatus used to gather acceleration data for the 5 high-rise structures was discussed in the previous section. Each accelerometer is placed facing one of the principal directions, as to record the accelerations only in that direction if that vibration mode is activated. Figure 3.8a shows the setup of the accelerometers in the NEMC. Accelerometer 2, 3 and 4 are set up to record the accelerations in the strong direction, and accelerometers 1, 5 and 6 are set up to record the accelerations in the weak direction. Figures 3.8b shows the accelerations for a short time period for accelerometers 1 and 2.

(a) Accelerometer Setup

(b) Measured acceleration for accelerometer 1 and 2
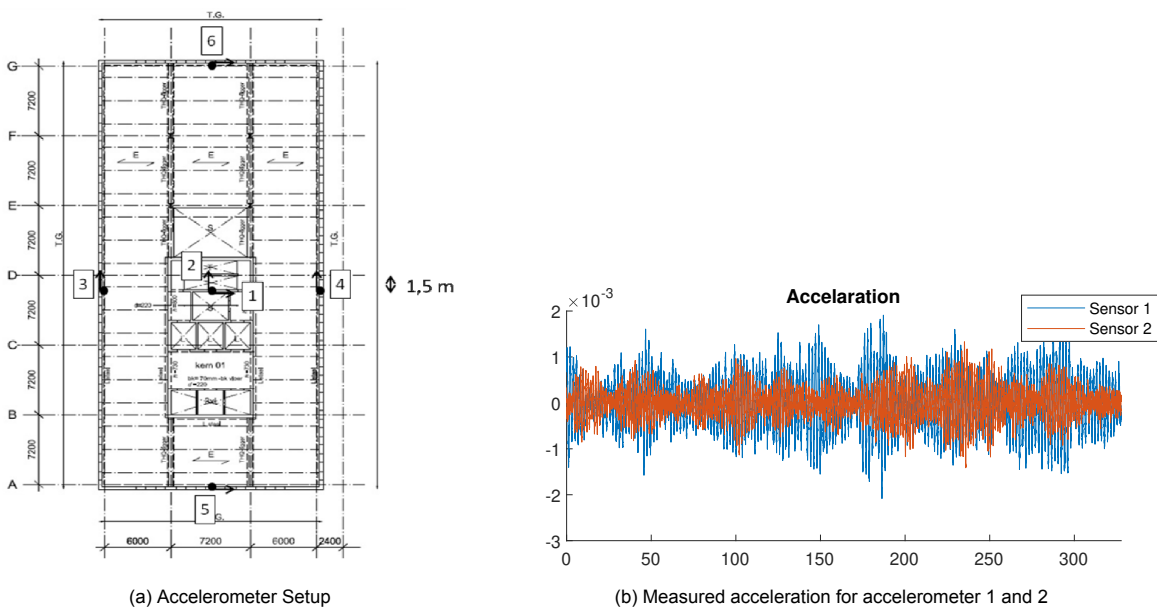
Figure 3.8: Accelerometer direction setup and the measured accelerations of sensor 1 and 2 in the NEMC

3.3.1. Natural frequency in the time domain

A first approximation of the natural frequencies can be made by considering the acceleration-time signal. First a segment of the recorded accelerations, where a visible vibration is present. These segments are shown between the black lines in the top two graphs of figure 3.9. When zooming in on these segments, as shown in the bottom figures of figure 3.9, the oscillations in the accelerations can be seen. The natural frequency can be calculated by dividing the number of oscillations with the time in which these oscillations take place.
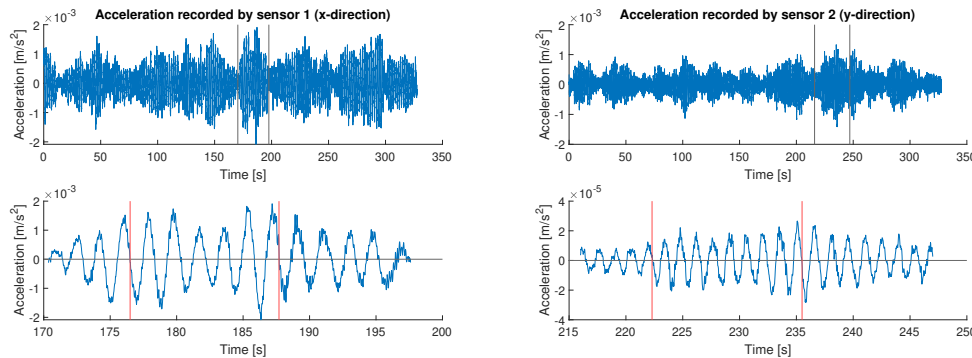
Figure 3.9: Acceleration signal of sensor 1 and 2 (top). Segment of each signal (bottom).

Considering the oscillations for the time period between the red lines, for sensor 1, it can be seen that 6 full oscillations are made in between seconds 176.5 and 187.7. The natural frequency is thus

$$f_1 = \frac{6}{187.7 - 176.5} = 0.536 Hz \tag{3.1}$$

this corresponds to the first translational frequency given in section 3.2.1. The same can be done for the accelerations of sensor 2, where there are 9 oscillations between seconds 222.3 and 235.5, which equates to a frequency of

$$f_1 = \frac{9}{235.5 - 222.3} = 0.682 Hz \tag{3.2}$$

and corresponds to the second translational frequency.

3.3.2. Natural frequency in the frequency domain

There are several methods how to extract the natural frequencies from acceleration data. One of the most used methods is the method proposed by Peter Welch [60]. In this method, the measured acceleration data is divided into several segments. Each segment partly overlaps with the previous and following segment, as shown in figure 3.10. The frequency spectrum is then calculated for each section using the Fast Fourier Transform (FFT) method. The sectional spectra are then averaged to create a full spectrum for the accelerations signal. The averaging of the spectra results in a smoother spectrum when compared to taking the FFT of the whole spectrum [6]. The method is explained in detail in [60] and will not be discussed further.
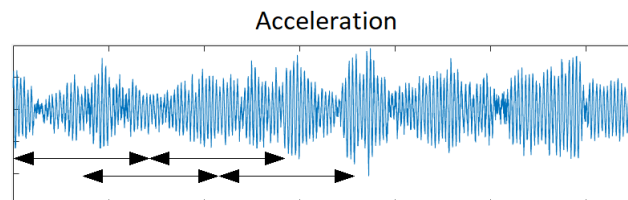
Figure 3.10: Sectioning of measured accelerations.

This method was performed on the data measured by the all 6 of the accelerometers in the NEMC, using the **pwelch** function in MATLAB R2020a. The acceleration data in inputted into the **pwelch** function.

For the NEMC, 20 accelerations data sets of around 10 minutes long, for each sensor were used. The signal is then split into a user define amount of segments. In the case of the NEMC, 1 segment was chosen to be the length of 1 data set. So the total acceleration data was split into 20 segments. Each segment is then windowed by a Hamming window with a length that corresponds to the length of the segments. The power spectral density (PSD) for each sensor was then calculated. The computed PSD for accelerometers 1, 5 and 6, and accelerometers 2, 3 and 4, are shown in figure 3.11. From the top graph, two clear frequency peaks can be seen in the first 1.5 Hz. The frequency peaks are situated at 0.53 and 1.28 Hz, where the former of these two frequencies corresponds to the first translational eigen frequency of the NEMC. In the bottom graph, again two frequency peaks can be seen in the first 1.5 Hz. The first being at 0.68 Hz, which corresponds to the second translational frequency. The second peak is also situated at 1.28 Hz. When considering figure 3.12, the power spectral densities of all the sensors are shown. It can be seen that for all sensors, there is a peak at 1.28 Hz. This means that both principal directions were excited at this frequency, leading to the conclusion that this is the first torsional eigen frequency of the NEMC.
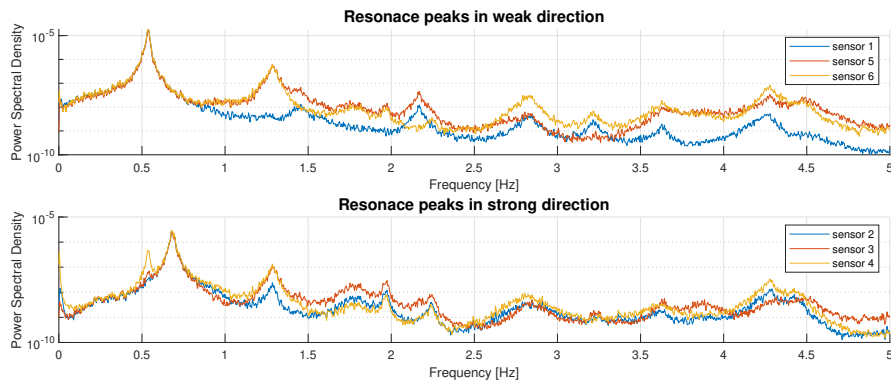
Figure 3.11: Power spectral density for frequencies excited in the x-direction (top), and in the y-direction (bottom)
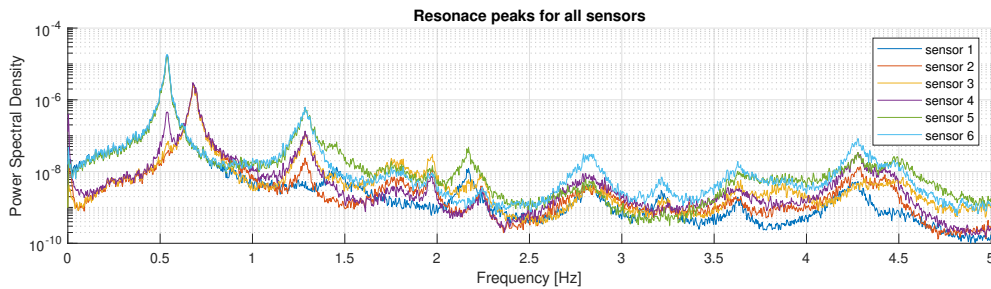
Figure 3.12: Power spectral density for all sensors

In figure 3.12 is can also be seen that sensor 4, which is placed facing the strong direction, recorded a vibration when the structure was excited at 0.53 Hz. This leads to the belief that the sensor was not installed perfectly along the principal strong direction. According to Gomez [54], this can be overcome by manipulating the acceleration signals by means of rigid body kinematics. This can be performed due to the assumption that the floors in the structure act as rigid bodies, resulting that the velocity at any point ($\vec{v}_B$), can be computed with the product of the velocity at a certain point ($\vec{v}_A$) and the angular velocity times the distance from A to B ($\vec{\Omega} \times \vec{r}_B^A$). This can be seen in equation 3.3. Gomez has applied this transformation to the acceleration signals of the NEMC, whereafter he used the Half Power Band Width method (HPBW) to compute the power spectral densities in the principal directions, this can be seen in figure 3.13.

$$\vec{v}_B = \vec{v}_A + \vec{\Omega} \times \vec{r}_B^A \tag{3.3}$$
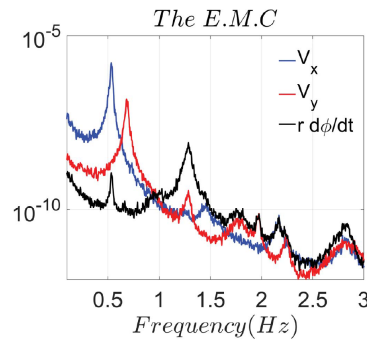
Figure 3.13: Single mode power spectral densities for the NEMC [54]
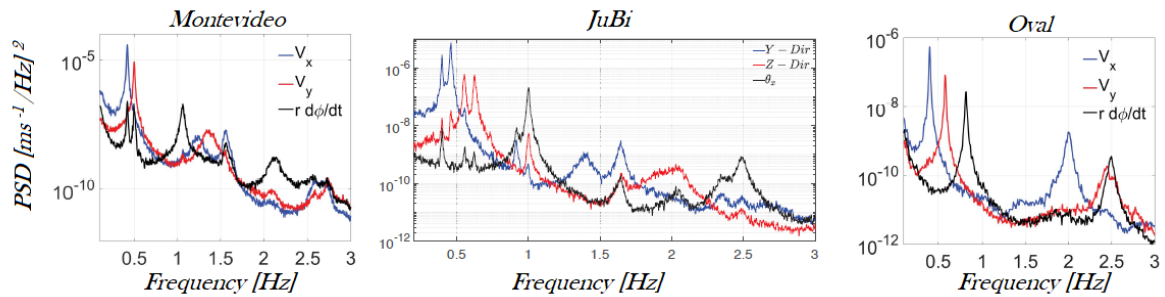
Figure 3.14: Single mode power spectral densities for the Montevideo, JuBi and Oval towers. [54]

In the figure, three clear frequency peaks can be seen at 0.53 Hz, 0.68 Hz and 1.28 Hz. These frequencies coincide with the frequencies determined above, validating the frequencies determined using the Welch method. In figure 3.13, it can be seen that the spectral density for the first translational mode has no peak at the second translational frequency, and vice versa. This shows that the signals have successfully been transformed to the principal directions. In a study by Bronkhorst et al. [9], the same procedure used by Gomez was performed on the acceleration measurements of the New Orleans tower. The natural frequencies shown in figure 3.15 were obtained.
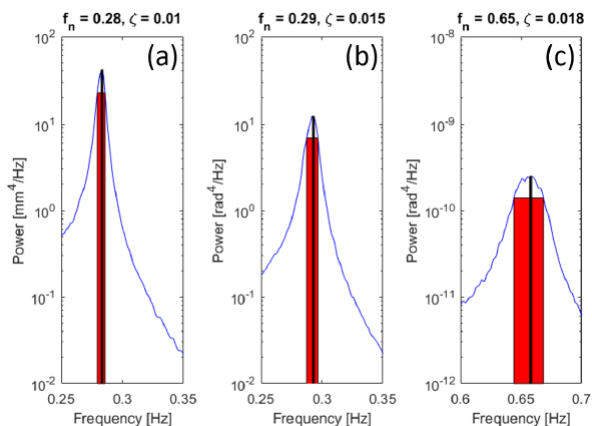
Figure 3.15: Natural frequencies of the New Orleans tower determined by the HPBW method [9]

3.3.3. Measured Mode Shapes

It was previously mentioned that the natural frequencies, calculated during the design phase, are often underestimated when compared to the measured frequencies. It was also mentioned in the previous section, that the frequencies measured by the accelerometers, are sensitive to the placement of the

accelerometers. Considering this, the question arises if there might not be a frequency smaller than the first measured natural frequency which might not have been recorded by the accelerometers? One method to validate that the first and second natural frequencies, are indeed the smallest, is by looking at the mode of vibration of the structure at these frequencies.

In a study done by Bronkhorst [10], acceleration measurements were recorded of the New Orleans tower in Rotterdam. To be able to determine the modes shapes of a structure using measurements, the measurements must be made at several heights in the structure. For the New Orleans tower, measurements were made on 3 different levels. The positions and heights of the accelerometers are shown in figure 3.16. To determine the natural frequencies and mode shapes of the structure, the Frequency Domain Decompostion was used. This technique was proposed by Brincker et al. [8] and is well-established, and will thus not be discussed further. The validity of the mode shapes were then check using the Modal Assurance Criterion (MAC) [26]. The MAC checks whether the mode shapes are orthogonal, by determining a correlation between two mode shapes.

Figure 3.17 shows several natural frequencies of the New Orleans tower. It can be seen that these are the same frequencies as shown in figure 3.15. The mode shapes for these frequencies were also determined for several frequencies. The mode shapes corresponding to the first two natural frequencies can be seen in figure 3.18a and 3.18b. It can be seen that these mode shapes are the same as the expected first and second translational mode shapes. For this reason, it can be concluded that the possibility that a natural frequency smaller than the first measured natural frequency, was not recorded by the measuring apparatus is quite small.
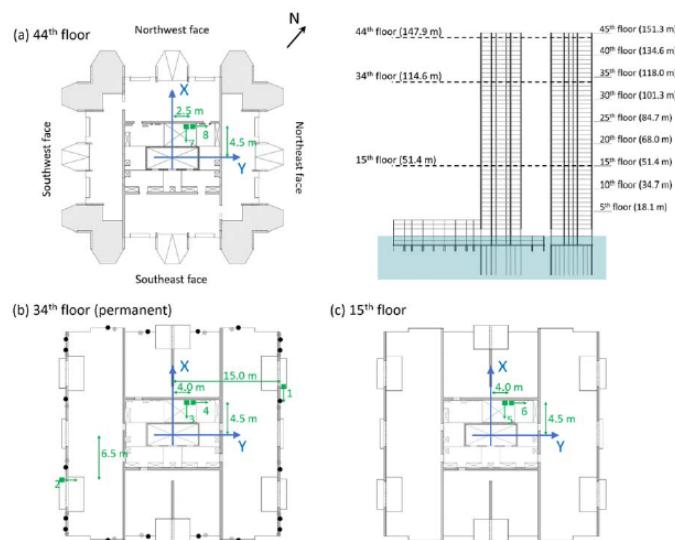
Figure 3.16: Positions and heights of the accelerometers in the New Orleans tower [10].
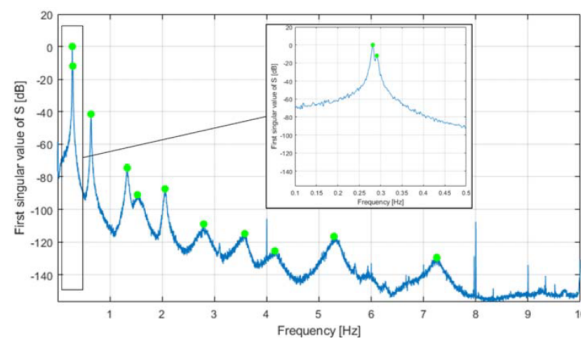
Figure 3.17: Natural frequencies of the New Orleans tower determined by the FDD [10].
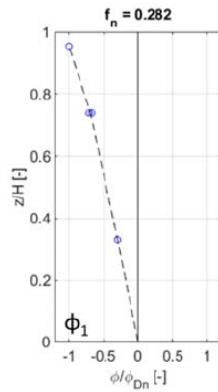
(a) Mode shape of first natural frequency
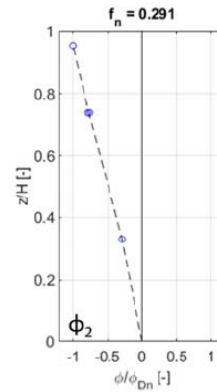
(b) Mode shape of second natural frequency

3.4. Analytic Model Description

In the following section, the analytic models used for the sensitivity study will be discussed. In figure 3.19a a sketch is shown of a high rise-building supported by a pile foundation. Often in practice, a beam element, as shown in figure 3.19b, is used to represent a high-rise structure. This is a reasonable assumption due to the fact that high-rise structures are rather flexible in regard to their height. Due to the soft soil conditions in the Netherlands, most high-rise structures are situated on a large foundation slab, which sits atop of a pile group. One might think that the foundation fixes the base of the superstructure to the ground, but in reality it merely restrains the base from translating and rotating. On account of this, the foundation is often represented by translational and rotational springs, as shown in figure 3.19b. It must be noted that the stiffness of the spring does not only represent the stiffness of the foundation, but takes into account the interaction between the foundation slab, the piles and the soil. The mass of the foundation block (M_f) is introduced to the beam model by adding a lumped mass to the base of the beam. The height of the beam (L), represents the height of the superstructure above ground. The bending stiffness and building density of the superstructure are given by EI and ρ, respectively.
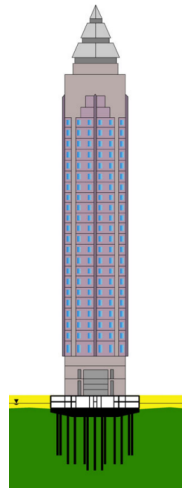
(a) High-rise building on pile foundation
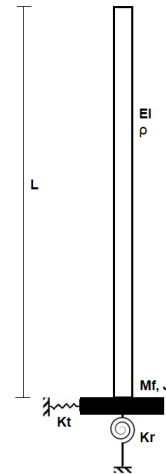
(b) Beam model representing a high-rise structure

Figure 3.19: High-rise structure supported by pile foundation and its beam model representation.

It must be noted that the focus of this chapter is on the natural frequency of the structure. For this reason, all damping mechanisms are neglected in the beam model shown above. The following five beam models will be discussed in more detail. The beams given in blue represent Euler-Bernoulli beams, and the beam in orange represents a Timoshenko beam. The beam theory regarding the two different beams can be found in A. For the Timoshenko beam, G represents the shear modulus of the superstructure.
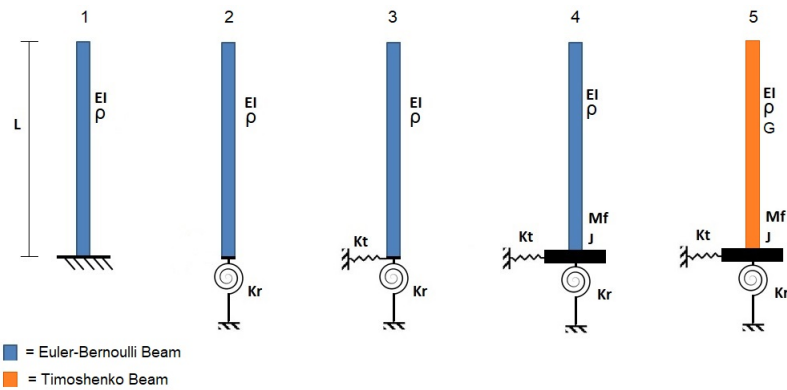
Figure 3.20: Five beam models representing a high-rise building for the inclusion of different structural parameters

3.4.1. Case 1: Cantilever Euler-Bernoulli Beam with Fixed Support

The first case which will be looked at is a cantilever Euler-Bernoulli beam with a fixed support, as shown in figure 3.21. This case will act as a reference case to be able to quantify the influence of different structural elements added to the proceeding cases. The support of the beam is fixed in all translational and rotational directions. This is a simplified representation of a foundation supported by a bedrock. The foundation, and thus the bottom of the structure, has no possibility of rotation or translation. If the fixed support were to be represented by springs, the stiffness of the springs would be infinitely large.
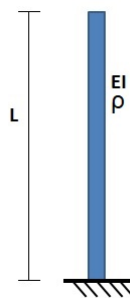
Figure 3.21: Case 1: Cantilever Beam with Fixed Support

3.4.2. Case 2: Cantilever Euler-Bernoulli Beam with Rotational Spring Support

For structures built on soil where the foundation can not reach the bed rock, movement in the foundation and the base of the superstructure is possible. For this reason, it is appropriate to add this interaction to the analytic models when calculating the natural frequency of a building. As previously stated, a widely accepted method to include the movement of the base of the superstructure is to add rotational and translational springs to the support of the beam model. This allows the base of the beam to rotate and translate in the specified directions, with the spring's stiffness representing the resistance of the soil-pile-structure interaction.

The second analytic case which is looked at is an Euler-Bernoulli beam with a rotational spring at it's support. This means the base of the beam is fixed in all translational directions (i.e. that the translational spring stiffness is infinitely large), but free to rotate around the axes the rotational spring is applied to. By comparing the results of case 2 to the reference case (case 1), the influence of the rotational spring on the natural frequency can be quantified. Case 2 is shown in figure 3.22. This case is often used in the preliminary design phase to get an initial indication of the behaviour of the structure.
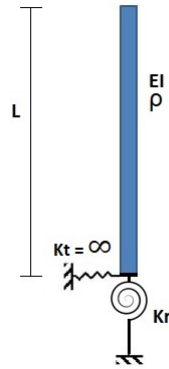
Figure 3.22: Case 2: Cantilever Beam with Rotational Spring Support

3.4.3. Case 3: Cantilever Euler-Bernoulli Beam with Rotational and Translational Spring Support

For the third case, the base of the superstructure is allowed to translate. In this case, the translational spring stiffness is not infinitely large, but set to a specific value. This value represents the horizontal resistance of the soil and foundation.
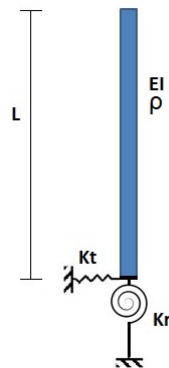
Figure 3.23: Case 3: Cantilever Beam with Rotational and Translational Spring Support

3.4.4. Case 4: Cantilever Euler-Bernoulli Beam with Rotational and Translational Spring Support including Foundation Mass

For each of the above-mentioned cases, the density used in the computations originates from the superstructure above ground level. This means that the mass of sub-zero levels and the foundation is not taken into account. To be able to quantify the influence the foundation mass has on the natural frequency of the buildings, a lumped mass is added to the base of the beam model. Included in the lumped mass is the mass of the foundation slab and, where applicable, the mass and accompanying loads of the sub-zero levels of the building. It must be noted that the length of the beam still equates to the height of the building above ground. The beam model for case 4 is shown in figure 3.24.
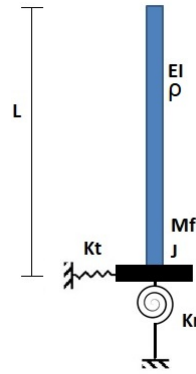
Figure 3.24: Case 4: Cantilever Beam with Rotational and Translational Spring Support including Foundation Mass

3.4.5. Case 5: Cantilever Timoshenko Beam with Rotational and Translational Spring Support including Foundation Mass

The final case that is looked at, is the same as case 4, with the only difference that the beam element is now a Timoshenko beam. This means that the assumption that the shear deformation is zero, as explained in Appendix A, does not hold any more. This model will provide insight of how the shear modulus influences the natural frequency of the beam model. The theory regarding the Timoshenko beam can be found in Appendix A.2. A graphical representation of the model is shown in figure 3.25.
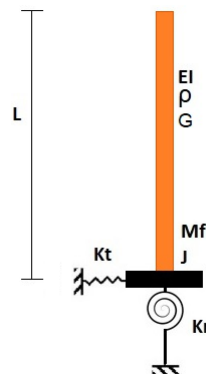
Figure 3.25: Case 4: Cantilever Timoshenko Beam with Rotational and Translational Spring Support including Foundation Mass

3.5. Structural Parameters

As previously stated, there is a significant amount of uncertainty when it comes to the exact value of different structural parameters. In this section, an upper and lower bound for all the structural parameters where there is uncertainty is determined. These are the building stiffness (EI), building density (ρ), rotational and translational spring stiffnesses (K_r and K_t) representing the resistance caused by the soil and foundation, the foundation mass (M_f) and for the Timoshenko case the shear modulus (G). Parameters based on the geometry of the structure, such as the height of the building (L), the area (A) and the moment of inertia (J) of the foundation are assumed to be deterministic. The main focus of this chapter lays on the first and second natural frequency of the different buildings. For this reason, the directional parameters will be determined in correspondence with the two lowest natural frequencies, as given in tables 3.1 to 3.5. For simplicity, all the axes have been chosen in such a manner that the first natural frequency for each building is in the x-direction, and the second natural frequency is in the y-direction.

3.5.1. Bending Stiffness

For complex buildings, as most buildings today are, it is quite difficult to accurately determine the flexural stiffness of the building. In this section, a range for the bending stiffness will be found. As a cantilever beam is used to represent the buildings in the proceeding analysis, the stiffness of the beam model exists out of two part: the Young's modulus (E-modulus) and the moment of inertia of the structural configuration of the structure.

During the design phase, it is especially difficult to accurately estimate the stiffness of a structure. Due to the horizontal loading caused by wind and the vertical loading cause by the self-weight of the structure, the stability elements of the structure experience bending and axial loads. As a consequence of these loads, the formation of cracks can occur in the concrete stability elements. Once cracks form in the concrete, the stiffness of the structure decreases. As the loading continues, the stiffness of the concrete decreases further, this is illustrated in the moment-axial force-curvature diagram in figure 3.26. In practise, it is customary to keep calculating with the moment of inertia of the uncracked sections through out the calculations. For this reason, the reduction in stiffness is introduced by reducing the E-modulus of the stability elements. The magnitude of the reduction of the E-modulus is affected by the geometry of the structure, the amount of reinforcement in the concrete and the magnitude of the axial force and bending moment in the structure. In the design phase these factors can not always be quantified and thus reducing the E-modulus accurately is not easy. This is why an arbitrary E-modulus is often chosen in the design phase. In an article in Cement, it is said that a good estimation for the E-modulus of cracked concrete is 10 GPa [29].
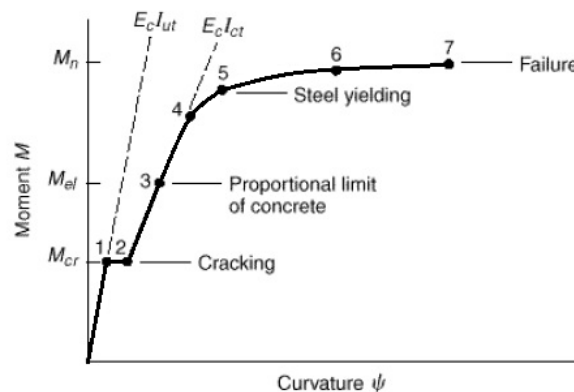
Figure 3.26: M-N-κ diagram of reinforced concrete

In the figure can be seen that before the cracking moment (M_{cr}) has been reached, the bending stiffness of the concrete ($E_c I_{ut}$) is at it's maximun and remains constant. When the M_{cr} is reached, there is an instant decrease in the bending stiffness ($E_c I_{ct}$) whereafter the bending stiffness again remains constant. After the elastic moment (M_{el}) has been reached, the bending stiffness decreases with every increase in moment.

To be conservative, an E-modulus of 7.5 GPa will be used in determining the lower bound of the bending stiffnesses. This will represent a scenario where cracks have formed in the concrete of the stability system. In the design documentation of the buildings described in section 3.2 the E-modulus used ranges from 20 to 38 GPa. Higher E-moduli are often a result of the assumption that the structural elements of the building are mostly in compression, which makes crack formation less likely. For the upper bound of the bending stiffnesses, the E-modulus of concrete will be chosen as 38 GPa. During the determination of the bending stiffnesses, it is assumed that the only reduction in E-modulus occurs in concrete elements. For all steel members, a constant E-modulus of 210 GPa is used, as it is assumed that the steel does not crack and remains in the elastic deformation zone.

The second part of the bending stiffness of the structures is the moment of inertia. The moment of inertia is a geometric property describing the distribution of points with regard to an axis. The structural configuration of the building's stability system is represented by the moment of inertia. The determina-

tion of the moment of inertia of the different buildings can be found in Appendix C.1. As the direction of the lowest natural frequency is chosen in the x-direction, the corresponding moment of inertia will be around the y-axis, and vice versa. Throughout the height of the structure, the moment of inertia of the building often changes. The moment of inertia is calculated for each section of the building height where a significant change in the moment of inertia is present. Only the load bearing system will be used to calculate the moment of inertia in each case, as it is assumed that the non-structural elements have a negligible influence on the stiffness.

3.5.1.1   New Erasmus Medical Center

As described in section 3.2 the load bearing system of the NEMC is a concrete tube and three concrete cores, marked in blue and red respectively in the figure shown below. The calculation of the stiffness of the NEMC can be found in Appendix C.1.1. Throughout the height of the building, the moment of inertia of the stability systems is mostly constant. The changes in moment of inertia are small and are thus considered negligible.
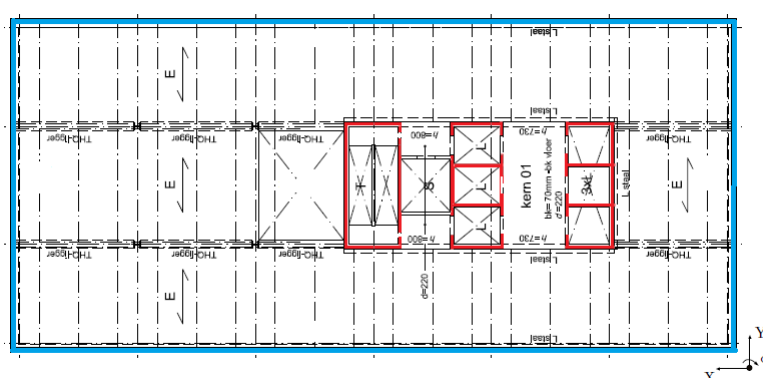
Figure 3.27: Concrete tube (blue) and core (red) of the NEMC

Design Value
In the design phase, it was assumed that shear deformation will be dominant in the structure. The reason for this is due to the many openings in the concrete tube creating a frame like system. This is why a rather low E-modulus of 10 GPa was chosen for concrete in the design. For the moment of inertia only the concrete tube was taken into account as the core only contributes 6% and 7.5% to the total stiffness in the x and y-direction, respectively. In the design, the cores are seen as a connected system. The design moment of inertia and bending stiffness in both directions are shown in tables 3.6 and 3.7. It must be noted that the method of calculating the moment of inertia reduction due to the openings in the tube structure, in the design documentation slightly differs from the method used in the calculations in Appendix C.1, this is the reason for the difference in the moment of inertia seen in table 3.6,

Lower and upper bound
The total moment of inertia of the structure is taken as the product of all the systems which provide stiffness to the structure. In the case of the NEMC, this is the outer tube and the three cores. The moment of inertia for the different systems are shown in table 3.6. As all the stability systems are made of concrete, the lower and upper bound of the bending stiffness is obtained by the multiplication of the total moment of inertia with 7.5 GPa and 38 GPa respectively. The lower bound, design value and the upper bound of the bending stiffness can be found in table 3.7.

Equivalent bending stiffness
For the one beam model, an equivalent uniform bending stiffness is also needed. As previously stated, the NEMC is taken as uniform throughout the height of the structure. For this reason, the lower and

upper bound for the equivalent uniform bending stiffness is the same as the lower and upper bound for the three beam model given in table 3.7.

Table 3.6: Moment of inertia of the stability systems of the NEMC

	Outer Tube	Left Core	Middle Core	Right Core	Total	Design
I_{yy}	1863.67	37.59	34.37	41.67	1977.30	1868
I_{xx}	6614.82	5.64	5.73	9.52	6635.70	6875

Table 3.7: Lower and upper bound of bending stiffness

	Lower Bound	Design	Upper Bound
EI_x	1.48×10^{13}	1.87×10^{13}	7.51×10^{13}
EI_y	4.98×10^{13}	6.88×10^{13}	2.52×10^{14}

3.5.1.2 Montevideo

The different stability systems and their corresponding positions are given in figure 3.28. The bottom part, which exists of a concrete core and steel columns, is 8m tall. The middle section is a concrete core with concrete walls in a roster orientation. This section is 78m tall. Lastly, the top part of the building exists of a steel structure which is 50m tall. In figure 3.28, the red section represent concrete elements and the blue sections represent the steel elements. The moment of inertia and bending stiffness calculations can be found in Appendix C.1.2.
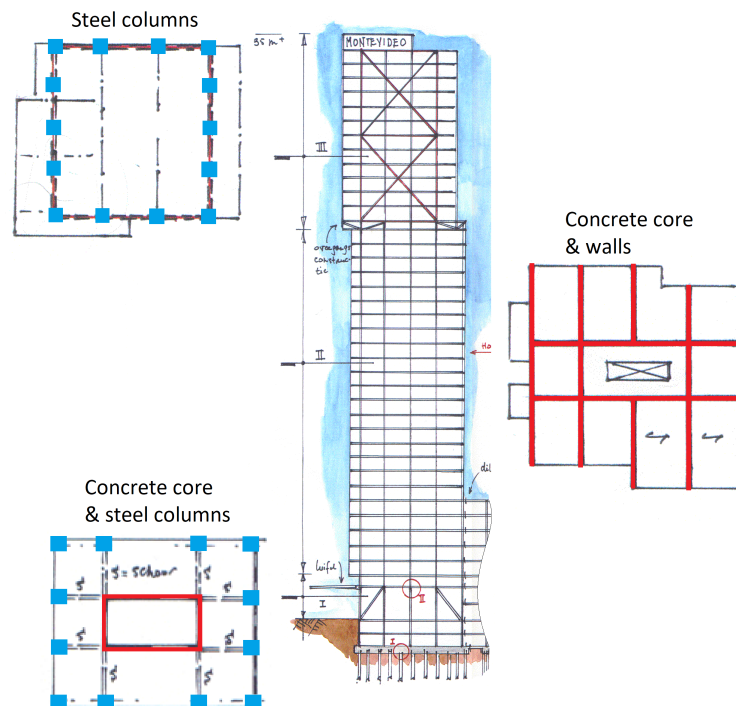
Figure 3.28: Different structural systems of the Montevideo tower

Design Value

During the design phase a model of the Montevideo tower was made in the finite element software DIANA. The model existed of the three stability systems and the pile foundation. In a static analysis a load was applied to the structure and a top displacement of 161mm was found. A second calculation was done in EPW software to calculate the uniform equivalent stiffness of the structure. A beam, representing the superstructure, and a rotational spring, which represented the pile foundation, were

modelled in EPW. The rotational spring was given a spring stiffness of $1.42 \times 10^{12} \frac{Nm}{rad}$. The same load as in the DIANA model was applied in EPW and the stiffness of the beam was calibrated until the top displacement of the beam equated to 161mm. A uniform equivalent stiffness of $2.79 \times 10^{13} Nm^2$ was found. In the design phase an equivalent stiffness around the x-axis (strong-axis) was not determined.

Lower and Upper Bound

As done in the previous case, the E-modulus of concrete used to calculate the lower and upper bound stiffness is 7.5 and 38 GPa, respectively. The stability system of the Montevideo does, however, not only exist out of concrete, but also steel. It is assumed that no cracks form in the steel, and thus a reduction of the E-modulus of the steel is not needed. The E-modulus for steel is 210 GPa for the lower and upper bounds of the stiffness. The moment of inertia for the different stability sections is shown in table 3.8. The lower and upper bounds for the different sections can be determined by multiplying the concrete and steel parts with their respective Young's moduli. The bending stiffness of levels 0 - 1 is taken as the product of the bending stiffness of the concrete and steel part. The results of the lower and upper bounds are given in table 3.9.

Equivalent uniform bending stiffness

To find the lower and upper bound for the equivalent uniform bending stiffness, a 1D model was made using MatrixFrame. The model consists of three beams, each representing one of the three sections of table 3.9. The lower and upper bounds of the stiffnesses for each section are inputted into the MatrixFrame model. After applying a load to the model, a static analysis is done and a top displacement is calculated. The load and displacement is then used to determine an equivalent uniform stiffness, using the well-know displacement formula for a cantilever beam with a fixed base. The equivalent uniform stiffnesses can be seen in table 3.10. The calculations can be found in appendix C.1.2.

The same analysis was done using the Young's modulus of $16GPa$ and $210GPa$ for concrete and steel, respectively. These are the same Young's moduli which were used to determine the design stiffness. After applying the same load as used in the design to the MatrixFrame model, a top displacement and uniform stiffness of 110mm and $3.35 \times 10^{13} Nm^2$, in the x-direction, was calculated. This is a stiffness of 1.2 times greater than the design stiffness and a displacement of 1.46 times smaller than that calculated by the EPW model. The same was done in the y-direction, and a displacement of 64.8mm was calculated by MatrixFrame, whereas the EPW model calculated a displacement of 67mm.

Table 3.8: Moment of inertia of the stability systems of the Montevideo tower

		Concrete section	Steel section
Level 0 - 1	I_{yy}	315.00	134.82
	I_{xx}	549.70	153.64
Level 2 - 27	I_{yy}	2786.86	-
	I_{xx}	4421.06	-
Level 28 - 42	I_{yy}	-	13.95
	I_{xx}	-	16.67

Table 3.9: Lower and upper bound of bending stiffness

		Lower Bound	Upper Bound
Level 0 - 1	EI_x	3.07×10^{13}	4.03×10^{13}
	EI_y	3.64×10^{13}	5.32×10^{13}
Level 2 - 27	EI_x	2.09×10^{13}	1.06×10^{14}
	EI_y	3.32×10^{13}	1.68×10^{14}
Level 28 - 42	EI_x	2.93×10^{12}	2.93×10^{12}
	EI_y	3.50×10^{12}	3.50×10^{12}

Table 3.10: Lower and upper bound of the equivalent uniform bending stiffness

	Lower Bound	Design	Upper Bound
EI_x	2.00×10^{13}	2.80×10^{13}	5.06×10^{13}
EI_y	2.92×10^{13}	$-$	7.28×10^{13}

3.5.1.3 New Orleans

The stability system of the New Orleans tower is split into three parts. The first system ranges from the ground floor to level 2 and exists concrete core and steel columns, which can be seen respectively in red and green in figure 3.29a. The second and third stability system both exist of a concrete core with connected walls and disconnected walls, which are represented by the red and blue lines shown in figures 3.29b and 3.29c. A distinction is made between the connected and disconnected walls, due to the disconnected walls only contributing to the stiffness of the structure in one direction.

(a) Bottom stability system   (b) Middle stability system   (c) Top stability system
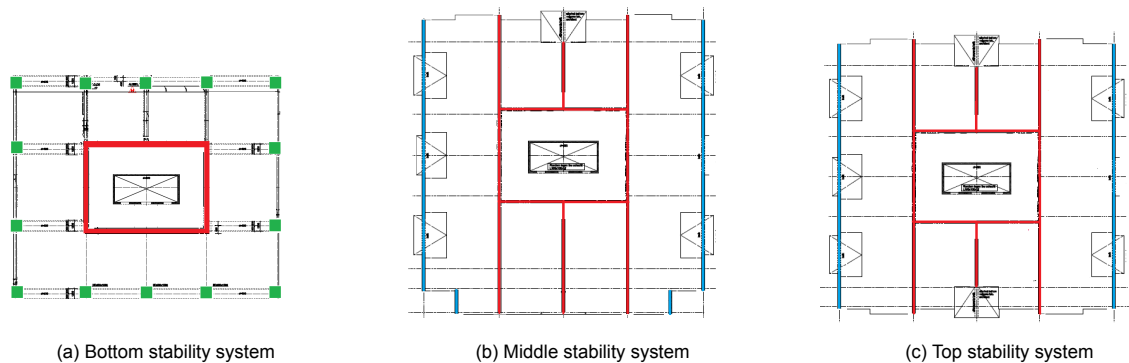
Figure 3.29: Stability systems contributing to the bend stiffness of the New Orleans Tower

Design Value
To determine the bending stiffness used in the design phase, the concrete core and connecting walls (without openings) were modelled in ESA Prima Win FEM-software package using a single beam model. A 100 kN point load was applied to the top of the beam and a displacement of 5mm was calculated by the FEM-software. Using a simple deflection formula for a fixed-free cantilever beam, a uniform bending stiffness of $2.8 \times 10^{13} Nm^2$ over the whole height of the structure was determined. The stiffness was then reduced by 15%, as this was assumed to be the reduction due to the openings in the structure, thus a final uniform bending stiffness of $2.43 \times 10^{13} Nm^2$ was found. In this calculation, a total height of 162m was used. This is the height of the sub-zero levels added to the height of the superstructure.

Lower and Upper Bound
The bending stiffness is determined for the three different sections by multiplying each system contributing to the bending stiffness with their corresponding E-moduli. For the lower and upper bound, 7.5 and 38 GPa is used for the concrete section and for steel the E-modulus is 210 GPa. Per section, the different systems are then added to each other. The moment of inertia for the different systems and the bending moment for the different sections are shown in tables 3.11 and 3.12.

Equivalent uniform bending stiffness
To find the lower and upper bound for the equivalent uniform bending stiffness, the same approach is used as explained in the previous section. The lower and upper bounds for the equivalent stiffnesses is both direction is shown in table 3.13. The calculations can be found in appendix C.1.3.

The same analysis was done using the design Young's modulus of $35 GPa$ for concrete and $210 GPa$ for steel. After applying the same load as used in the design to the MatrixFrame model, a top displacement

and uniform stiffness of 131mm and $2.79 \times 10^{13} Nm^2$, in the x-direction, was calculated. This is a stiffness equating to the stiffness calculated in the design phase before the opening reduction was done. The top displacement of the MatrixFrame model is also 10mm smaller than that calculated by the ESA Prime model. The same was done in the y-direction, and a displacement of 56.7mm was calculated by MatrixFrame, resulting in a stiffness of 7.06×10^{13}, whereas the ESA Prime model calculated a displacement of 116mm, resulting in a stiffness 2.05 times smaller than MatrixFrame.

Table 3.11: Moment of inertia of the stability systems of the New Orleans tower

		Steel columns	Concrete core	Disconnected section	Connected section	Lift core
Level 0 - 2	I_{yy}	24.16	653.63	-	-	25.46
	I_{xx}	136.23	416.7	-	-	6.13
Level 3 - 10	I_{yy}	-	-	-	907.82	25.46
	I_{xx}	-	-	1149.32	1621.00	6.13
Level 11 - 45	I_{yy}	-	-	-	844.55	25.46
	I_{xx}	-	-	751.68	1299.87	6.13

Table 3.12: Lower and upper bound of bending stiffness

		Lower Bound	Upper Bound
Level 0 - 2	EI_x	1.02×10^{13}	3.09×10^{13}
	EI_y	3.18×10^{13}	4.47×10^{13}
Level 3 - 10	EI_x	7.00×10^{12}	3.55×10^{13}
	EI_y	2.08×10^{13}	1.06×10^{14}
Level 11 - 45	EI_x	6.53×10^{12}	3.31×10^{13}
	EI_y	1.54×10^{12}	7.82×10^{13}

Table 3.13: Lower and upper bound of the equivalent uniform bending stiffness

	Lower Bound	Design	Upper Bound
EI_x	7.45×10^{12}	2.43×10^{13}	3.34×10^{13}
EI_y	2.04×10^{13}	3.06×10^{13}	7.17×10^{13}

3.5.1.4   JuBi

The stability systems of the JuBi tower all made of concrete. For the first 9 level, stability is provided by walls, columns and three central cores. Between levels 10 to 27 and 28 to 38, stability is provided by a tube structure and three central cores. The three central cores only differ slightly for the three sections. The stability systems for the different sections can be seen in figure 3.30. The calculations for the moment of inertia and the bending stiffness for the different sections can be found in Appendix C.1.4.

Design Value
During the design phase, the JuBi tower was also modelled using the ESA Prima win software. The model consisted of the concrete tube and the three central cores, and the base of the model was clamped, representing a rigid foundation. After applying a moment of $1.5 \times 10^6 kNm$ to the top of the structure, a top displacement of 135.5 mm was calculated by the FEM software. Using the well-known displacement formula for a fixed-free cantilever beam loaded by a moment, the uniform bending stiffness over the whole height of the structure of $1.29 \times 10^{14} Nm^2$ was determined.

Lower and Upper Bound
For the lower and upper bounds, the bending stiffness was divided into three different sections. All stability systems contributing to the stiffness of the structure are made of concrete, thus the moment of inertia of the different systems per section can easily be added to each other. The lower and upper

bounds of the bending stiffnesses are then determined by multiplying the total moment of inertia of each section with their corresponding E-moduli. The moment of inertia and the bending stiffnesses for the different sections can be seen in tables 3.14 and 3.15.

(a) Bottom stability system   (b) Middle stability system   (c) Top stability system
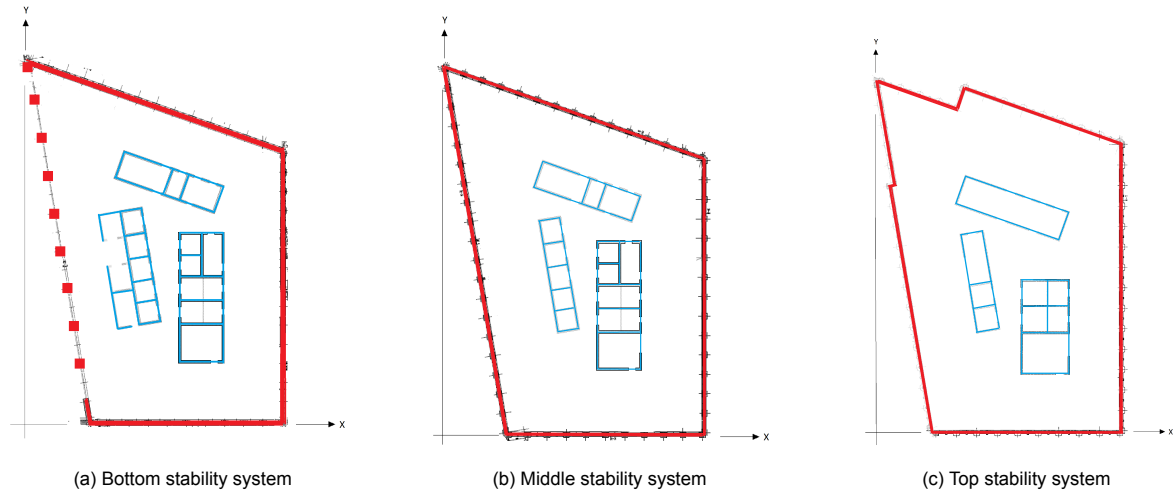
Figure 3.30: Stability systems contributing to the bend stiffness of the JuBi Tower

Equivalent uniform bending stiffness

For the JuBi tower, the same method as previously stated was used to find the lower and upper bound for the equivalent uniform bending stiffness. The lower and upper bounds for the equivalent stiffnesses is both direction is shown in table 3.16. The calculations can be found in appendix C.1.4.

To compare the equivalent stiffnesses and the stiffness of the 3D ESA Prime model, the MatrixFrame analysis was done using the design Young's modulus for concrete of $35 GPa$. The same load used in the ESA Prime model was applied to the MatrixFrame model and a static analysis was done. This lead to a top displacement of 40.8mm and 20.4mm in the x- and y-direction, respectively, which leads to a stiffness of 1.90×10^{14} and 3.40×10^{14}. The ESA Prime model, with the same applied UDL load, found displacements of 94mm and 29mm in the x- and y-direction.

Table 3.14: Moment of inertia of the stability systems of the JuBi tower

		Concrete columns	Concrete tube	Left core	Top core	Right core	Total
Level 0 - 9	I_{yy}	2015.06	4097.47	83.88	250.26	121.17	6567.84
	I_{xx}	1203.04	9276.85	496.88	68.28	596.81	11641.84
Level 10 - 27	I_{yy}	-	3917.20	29.14	250.26	121.17	4317.77
	I_{xx}	-	6767.62	321.51	68.28	596.81	7754.22
Level 28 - 38	I_{yy}	-	2907.33	11.67	149.05	49.12	3117.17
	I_{xx}	-	5658.1	109.00	39.01	150.48	5956.60

Table 3.15: Lower and upper bound of bending stiffness

		Lower Bound	Upper Bound
Level 0 - 9	EI_x	4.93×10^{13}	2.50×10^{14}
	EI_y	8.73×10^{13}	4.42×10^{14}
Level 10 - 27	EI_x	3.24×10^{12}	1.64×10^{14}
	EI_y	5.82×10^{13}	2.95×10^{14}
Level 28 - 38	EI_x	2.34×10^{13}	1.18×10^{14}
	EI_y	4.47×10^{13}	2.26×10^{14}

Table 3.16: Lower and upper bound of the equivalent uniform bending stiffness

	Lower Bound	Design	Upper Bound
EI_x	4.26×10^{13}	1.29×10^{14}	2.16×10^{14}
EI_y	7.61×10^{13}	$-$	3.86×10^{14}

3.5.1.5 Oval Tower

The stability system of the Oval tower is split into two sections. The first section stretching from the ground floor to the 13th floor, and the second section stretching from the 14th floor to the 28th floor. For both sections, the stiffness is provided by two cores and four columns attached to each core by an outrigger on the top floor. Between the two sections, there is only a small difference in the configuration of the cores. The cores and the attached columns can be found in figure 3.31. The calculations of the moment of inertia for the two sections are given in Appendix C.1.5.

(a) Bottom stability system

(b) Top stability system

(c) Concrete columns contributing to stiffness
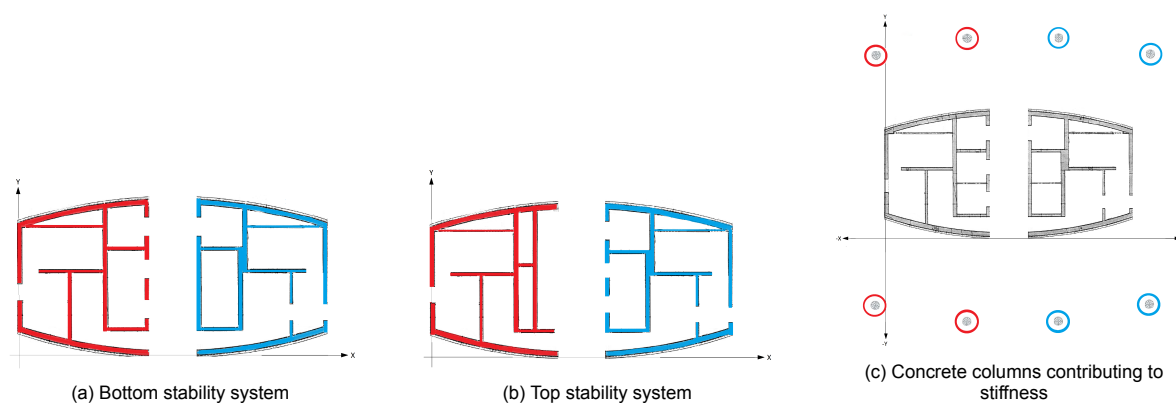
Figure 3.31: Stability systems contributing to the bend stiffness of the Oval Tower

Design Value
During the design, the moment of inertia of the right cores were determined for the two section. Using Technosoft Framework software, only the right core was modelled as two beam elements with a user-defined moment of inertia of $145.9m^4$ and $145.3m^4$ and E-modulus of $33.5 \times 10^9 \frac{N}{m^2}$. Only two columns were modelled, also by user-defined beam elements, and were attached to the core beam at the top. A uniform distributed load of $40.33 \frac{kN}{m}$ was applied to the core beams and a displacement of 106.7mm was calculated. Using this displacement and the well-known formula for the displacement of a fix-free cantilever beam, a uniform bending stiffness of $4.47 \times 10^{12} Nm^2$ was determined. This bending stiffness was then taken as the uniform bending stiffness for the whole tower.

Lower and Upper Bound
As all the stability systems are made of concrete, the total moment of inertia is a simple addition of the different stability systems. For the lower and upper bound of the bending stiffness, the total moment of inertia is multiplied with their corresponding E-moduli. The total moment of inertia and bending moments for the different sections can be seen in tables 3.17 and 3.18.

Equivalent uniform bending stiffness
For the Oval tower, no complete 3D model was made during the design phase. For this reason, the same approach as for the Montevideo, New Orleans and JuBi towers could not be used. It is assumed that as the tower displaces, most of the bending takes place in the bottom half of the structure. For this reason, the bending stiffness of the bottom half of the Oval tower is used as the equivalent uniform bending stiffness. As there is no significant difference in the bending stiffnesses of the bottom half and the top half of the structure, it is assumed that using the bottom stiffness will not have a large impact on

the final results. The lower and upper bounds for the equivalent stiffnesses is both direction is shown in table 3.19. The calculations can be found in appendix C.1.5.

Table 3.17: Moment of inertia of the stability systems of the JuBi tower

		Concrete columns	Left core	Right core	Total
Level 0 - 13	I_{yy}	18.78	97.11	110.22	246.17
	I_{xx}	187.14	142.96	147.60	664.86
Level 14 - 28	I_{yy}	20.05	84.86	99.41	221.86
	I_{xx}	187.15	138.50	145.56	658.39

Table 3.18: Lower and upper bound of bending stiffness

		Lower Bound	Upper Bound
Level 0 - 13	EI_x	1.85×10^{12}	9.35×10^{12}
	EI_y	4.99×10^{12}	2.53×10^{13}
Level 14 - 28	EI_x	1.66×10^{12}	8.43×10^{12}
	EI_y	4.94×10^{12}	2.50×10^{13}

Table 3.19: Lower and upper bound of the equivalent uniform bending stiffness

	Lower Bound	Design	Upper Bound
EI_x	1.85×10^{12}	4.47×10^{13}	9.35×10^{12}
EI_y	4.99×10^{12}	9.50×10^{12}	2.53×10^{13}

3.5.2. Building Mass
3.5.2.1 Superstructure Density

It is well-known that when the mass of a system is increased, the natural frequency decreases. For a simple SDoF system, this can be seen in equation 2.1. For high-rise structures, it is no different. As the density of the structure is increased, the frequency of the structure decreases. In the case of the structure being represented by a cantilever Euler-Bernoulli beam with a fixed base, this can be seen in equation 3.4. When the density of a structure is not distributed evenly over the height, the higher the increased density is found from the bottom of the structure, the greater influence this density increase will have on the natural frequency. This is due to more mass taking part in the vibration when the mass is found at a higher level, than when it is found closer to the bottom.

$$\omega = \sqrt{\frac{\beta^4 EI}{\rho A}} \tag{3.4}$$

To determine the lower and upper bounds for the building density of the 5 structure, the loads contributing to the mass of the structure is divided into three parts, the structural load, the permanent load and the variable load. The structural loads consist of all the dead loads originating from all the systems contributing to the structural integrity of the structure. These are the dead loads of the load bearing walls, cores, floors etc. The permanent loads are all dead loads which do not contribute to the structural integrity of the structure. These are the loads of the floor finishings, piping, ceilings etc. Lastly, the variable loads are all the live loads which originate due to the functionality of the building. The lower bound of the building density is determined by the summation of all the structural loads. The upper bound of the building density is the sum of all the structural loads, permanent loads and variable loads. The equations for the lower and upper bounds are given in equation 3.5. It must be noted that the variable load is multiplied by a combination factor as used in the European Standards. This is due to the assumption that not all variable loads are present at the same time.

$$\rho_{lower} = \frac{\Sigma G_{structural}}{gAL}$$

$$\rho_{upper} = \frac{\Sigma(G_{structural} + G_{permanent} + \Psi Q_{variable})}{gAL} \quad (3.5)$$

For the multibeam models, the building density is again split into different sections. These sections coincide with the sections made for the bending stiffnesses. For the single beam model, the density is determined by dividing the total mass with the volume of the structure. The density in the x- and y-direction is taken as constant. The calculation of the lower and upper bounds can be found in Appendix C.2. To determine the loads for the bounds, a combination of the design documentation and technical drawings of each building was used. In table C.47a lower and upper bounds for the building densities for the different building sections can be seen, whereas table C.47b shows the uniform building densities for the single beam models.

Table 3.20: Sectional building densities

Building	Section	Density [$\frac{kg}{m^3}$]	
		Lower	Upper
NEMC	Level 0-32	358	436
Montevideo	Level 0-1	257	269
	Level 2-27	406	503
	Level 28-42	362	448
New Orleans	Level 0-2	495	656
	Level 3-10	405	502
	Level 11-45	405	493
JuBi	Level 0-9	444	542
	Level 10-27	433	532
	Level 28-38	314	418
Oval	Level 0-13	248	314
	Level 14-28	250	324

Table 3.21: Uniform building densities

Building	Density [$\frac{kg}{m^3}$]		
	Lower	Design	Upper
NEMC	358	400	436
Montevideo	382	460	470
New Orleans	410	500	504
JuBi	393	530	504
Oval	249	340	318

The table C.47b shows that the design density of the JuBi and Oval tower falls outside the defined bounds. In the case of the JuBi tower, this is due to the fact that in the design, the density is calculated using the area of the top section of the tower and does not take into account the larger areas in the bottom of the tower. In the case of the Oval tower, the variable load used in the design is not multiplied by the combination factor, as done for the defined lower and upper bounds.

3.5.2.2 Foundation Mass

For the foundation mass, the same principle was used as for the building density. The only difference being that the total mass is determined, and not the density, as shown in equation C.3. For the foundation mass, all sub-zero levels are taken into account. As the foundation mass is added to the single

beam and multibeam models, by adding a lumped mass to the bottom of the beam, the determined added mass is the same for both models.

$$M_{f\,lower} = \frac{\Sigma G_{structural}}{g}$$

$$M_{f\,upper} = \frac{\Sigma(G_{structural} + G_{permanent} + \Psi Q_{variable})}{g}$$

(3.6)

Table C.58 shows the lower and upper bound for the foundation mass for each building.

Table 3.22: Lower and upper bound of the foundation mass

Foundation Mass [kg]	
Lower Bound	Upper Bound
5.97E+06	6.03E+06
6.06E+06	6.32E+06
4.98E+06	5.21E+06
8.90E+06	9.54E+06
5.95E+06	6.38E+06

3.5.3. Foundation Stiffness

For structures built on soil where the foundation does not reach the bedrock, the rigid base assumption is an overestimation of the stiffness of the foundation. When structures are built on soft soils, as is the case for most structures in the Netherlands, they have the capability to translate and rotate to a certain extent. The resistance the surrounding soil and foundation structure provides, can be represented by springs, as done for case 2 to case 5.

3.5.3.1 Rotational Spring Stiffness

Lower Bound

In a study done by Furgo, the rotational spring stiffnesses of the structures were determined using the D-Pile Group software. During the D-Pile Group analysis, the pile group is modelled with an infinitely stiff foundation slab. Due to the size of the pile group, the software calculates the rotational stiffness using the Poulus model. This is a static model which considers two layers of fully elastic soil. The top layer is along the entire height of the piles, the second layer is located below the tip of the pile. The stiffness of these soil layers is specified by the user. In the analysis done by Furgo, large shear strains in the soil were assumed. This leads to a relatively small E-modulus of the soil, which is approximated by $E = 2G(1 + v)$, with G being the shear modulus and v the Poisson's ratio. Figure 3.32 shows the shear modulus vs shear strain reduction curve for soil. In the figure, it can be seen that the larger the strain gets, the smaller the shear modulus is. Strains typically associated with wind vibrations are small strains, for this reason, the large strain assumption made for the D-Pile Group analysis is seen as conservative.

After the pile group and foundation slab is modelled, and the soil stiffness is specified, a moment is applied to the foundation. D-Pile Group then determined the rotation of the pile heads. Using the determined rotation and the applied force, the rotational spring stiffness can then be determined. Table 3.23 shows the input parameters and the results of the D-Pile Group analysis.
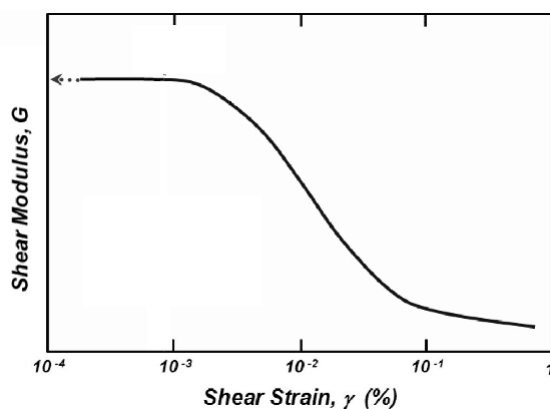
Figure 3.32: Shear modulus vs shear strain reduction curve for soil

Table 3.23: Input parameters and the results of the D-Pile Group analysis for the rotational spring stiffness

Building	E surface	E below pile	Applied Moment	Rotation pile head		Kr	
	$\frac{kN}{m^2}$	$\frac{kN}{m^2}$	kNm	x direction [rad]	y direction [rad]	x direction $[\frac{kNm}{rad}]$	y direction $[\frac{kNm}{rad}]$
NEMC	3000	60000	1.00E+06	7.57E-03	2.96E-03	1.23E+08	3.38E+08
Montevideo	6000	70000	1.00E+06	6.98E-03	5.98E-03	1.42E+08	1.67E+08
New Orleans	5000	70000	1.00E+06	4.78E-03	5.65E-03	2.10E+08	1.77E+08
JuBi	35000	100000	1.00E+06	1.19E-03	8.12E-04	8.40E+08	1.23E+09
Oval	25000	70000	1.00E+06	1.29E-03	2.88E-03	7.75E+08	3.47E+08

Design Value

For each of the structure, except the Oval tower, the rotational spring stiffness was determined in the design documentation. For the NEMC the rotational spring stiffness was calculated by multiplying the moment of inertia of the pile group with the individual vertical spring stiffness of each pile. For the other three structures, this was done using the FE models which were created during the design. A load was applied to the FE models and a static analysis was done for two cases, one with a fixed base and a second with a flexible base. The difference in the displacement of the top of the structure for the two models, and the applied loads was then used to determine the respective rotational stiffnesses. The design rotational spring stiffnesses are shown in 3.24.

Table 3.24: Rotational spring stiffness used in design

	Design Kr
Building	$[\frac{kNm}{rad}]$
NEMC	1.13E+9
Montevideo	1.42E+9
New Orleans	1.88E+9
JuBi	1.04E+10
Oval	-

Upper Bound

For the upper bound of the rotational spring stiffness, each pile under the foundation slab is represented by a vertical spring. For each building, the vertical spring stiffness was determined in the design phase by geotechnical institutions. These spring stiffnesses are shown in table 3.25.

Table 3.25: Vertical spring stiffness of an individual pile

	NEMC	Montevideo	New Orleans	JuBi	Oval
$K_z [\frac{kN}{m}]$	87000	90000	85000	210000	190000

The assumption is then made that the foundation slab is infinitely stiff and that it does not deform when the slab rotates. The slab is then rotated around the pile group's centre of gravity, as shown in figure 3.33. Due to the shortening and elongation of the springs, a force is exerted on to the foundation slab. By combining the well-known equations in 3.7, the single rotational spring stiffness of equation 3.8 can be obtained.

$$F_i = k_z \delta_i$$
$$M_i = F_i a_i$$
$$\delta_i = \theta a_i$$
$$k_{r,i} = \frac{M_i}{\theta}$$

where,

F_i is the force of an individual pile,

k_z is the vertical spring stiffness,

δ, i is the shortening/elongation of the springs,

M, i is the moment due to the spring forces,

a, i is the lever arm of the different springs,

θ is the angle of rotation of the foundation slab, and

$k_{r,i}$ is the rotational stiffness of each spring.

(3.7)

$$K_r = \Sigma k_{z,i} a_i^2$$

(3.8)
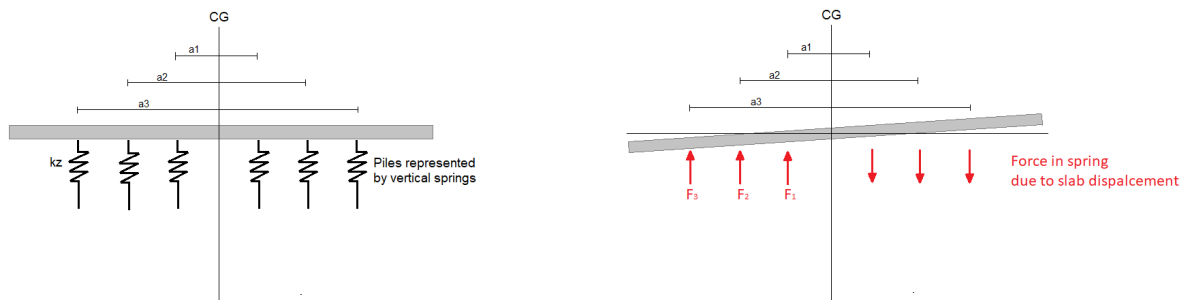
Figure 3.33: Foundation with piles represented by vertical springs (left). Rotated foundation slap with vertical force equilibrium (right)

Following this method, the rotational stiffnesses of the foundations can be determined for each structure in each direction. The calculations of the rotational stiffnesses can be found in Appendix C.4. The rotational stiffnesses in both direction are shown in the table below for each structure.

Table 3.26: Rotational Spring stiffnesses for each structure in both directions

	Rotational Spring Stiffness [kNm/rad]	
Building	K_{rx}	K_{ry}
NEMC	1.75E+9	6.05E+9
Montevideo	1.42E+9	1.75E+9
New Orleans	2.29E+9	2.04E+9
JuBi	1.16E+10	2.16E+10
Oval	4.48E+9	1.49E+9

3.5.3.2 Translational Spring Stiffness

Lower Bound

In the same study done by Fugro, as mentioned for the lower bound of the rotational stiffness, the translational spring stiffness was determined. Again the D-Pile Group software, with the same input parameters, was used. This time, instead of applying a moment to the pile heads, a horizontal force was applied. The software then calculated the displacements of the pile heads. The displacement and the applied force is then used to determine the translational spring stiffness. Table 3.27 shows the input parameters and the results of the D-Pile Group analysis.

Table 3.27: Input parameters and the results of the D-Pile Group analysis for the rotational spring stiffness

Building	E surface $\frac{kN}{m^2}$	E below pile $\frac{kN}{m^2}$	Applied Force kN	Translation pile head x direction [rad]	Translation pile head y direction [rad]	K_t x direction [$\frac{kN}{m}$]	K_t y direction [$\frac{kN}{m}$]
NEMC	3000	60000	1000	7.39E-03	8.13E-03	1.35E+05	1.23E+05
Montevideo	6000	70000	1000	9.00E-03	9.28E-03	1.11E+05	1.08E+05
New Orleans	5000	70000	1000	5.33E-03	5.42E-03	1.89E+05	1.85E+05
JuBi	35000	100000	1000	6.27E-04	5.97E-04	1.59E+06	1.68E+06
Oval	25000	70000	1000	1.06E-03	1.16E-03	9.40E+05	8.62E+05

Upper Bound

The upper bound of the translational stiffness is a combination of two methods proposed by Gazetas [21]. The first part is calculating the translational stiffness provided by a surface foundation on deep inhomogeneous soil. This represents the resistance of the foundation slab. The translational stiffness is determined with equation 3.9. Where G_0 is the shear stiffness of the soil at the surface, and α and n are variables determined by finding the best fit line to the shear stiffness of the soil profile. The method and calculation is described in detail in Foundation Engineering Handbook [21] and in Appendix C.4. The translational stiffness is determined for a foundation strip of 1m and then multiplied by the total width of the foundation.

$$K_t = \frac{2}{2-v} G_0 (1 + \frac{2}{3}\alpha)^n \tag{3.9}$$

The second part of the calculation is determining the translational stiffness of a single pile. The translational stiffness of a pile can be determined with the first part of equation 3.10. where d is the diameter of the pile, $\tilde{E}_s$ is a reference E-modulus of the soil determined using the best fit line of the E-modulus profile of the soil, and E_p is the E-modulus of the pile. The method is also discussed in detail in Foundation Engineering Handbook [21] and in Appendix C.4. After the translational stiffness is determined for a single pile, the stiffness is multiplied by the number of piles in the foundation.

$$K_t = 0.6 d \tilde{E}_s (\frac{E_p}{\tilde{E}_s})^{0.35} \times n_{piles} \tag{3.10}$$

The total translational spring stiffness is then calculated by the product of equations 3.9 and 3.10. The spring stiffness for each structure is given in table 3.28 and 3.29.

Table 3.28: Translational spring stiffness weak direction

	K_{tx} [$\frac{kN}{m}$] Shallow Foundation	n piles	Total
NEMC	3.12E+06	5.23E+06	8.35E+06
MV	1.53E+06	2.40E+06	3.93E+06
NO	1.60E+06	3.28E+06	4.88E+06
JuBi	5.00E+06	9.99E+06	1.50E+07
Oval	4.63E+06	3.94E+06	8.57E+06

Table 3.29: Translational spring stiffness strong direction

	K_{ty} [$\frac{kN}{m}$]		
	Shallow Foundation	n piles	Total
NEMC	2.76E+06	5.23E+06	7.98E+06
MV	1.44E+06	2.40E+06	3.84E+06
NO	1.54E+06	3.28E+06	4.82E+06
JuBi	5.20E+06	9.99E+06	1.52E+07
Oval	4.85E+06	3.94E+06	8.79E+06

3.6. Analytic Models

3.6.1. Single Beam Model

A single beam model is often used to represent high-rise structures. For this model, the parameters are assumed to be constant over the height of the structure. A single beam model is regularly used during the design phase to give an initial idea into the behaviour of a structure, either statically or dynamically. This section discusses the determination of the natural frequency of a single beam model for the 5 buildings. The sensitivity of the model, with regard to a change in stiffness, mass and the addition of foundation parameters, will be looked at. In addition to the parameter sensitivity, the influence of using an Euler-Bernoulli or Timoshenko beam is also looked at.

3.6.1.1   Frequencies Using Design Values

Using the method described in Appendix B, the natural frequencies in the weak and strong direction can be determined for the 5 different beam models. The parameters used in this calculation are the parameters found in the design documentation. For parameters which were not found in the design documentation, the average between the upper and lower bound was used. Figure 3.34 is a graphical representation of the first and second translational frequencies for each building, for the different cases. Table 3.30 shows the values of the frequencies in table form. The results show that for each building, the frequency determined by the single beam model is significantly smaller than the measured frequencies. Even for case 1, representing a structure with a fixed base, the frequencies are severely underestimated. It can be seen that when comparing cases 1 to 3, there is a decrease in frequency. This is an expected result, as the constraints of the base of the beam are relaxed by adding the foundation springs to the model. Looking at the results of case 4, it can be seen that there is no difference in the determined frequencies. The reason for this is that the mass of the foundation is placed at the base of the beam. As previously stated, the lower the mass is placed in the beam, the smaller effect it will have on the frequency, as the participation of the mass is small in the vibration of the beam. When comparing case 4 and 5, using a Timoshenko beam instead of an Euler-Bernoulli beam, there is only a small change in frequency. The general behaviour for the change in cases is the same for all buildings, except for the Oval tower. When looking closed at the frequencies of the Oval tower, it can be seen that there is a significantly smaller change in frequency when comparing cases 2 and 3, compared to the other buildings. In addition to this, the Oval tower is the only building where there is a decrease in frequency when using a Timoshenko beam. This shows that there are parameter combinations which let the beam behave differently for the different cases.
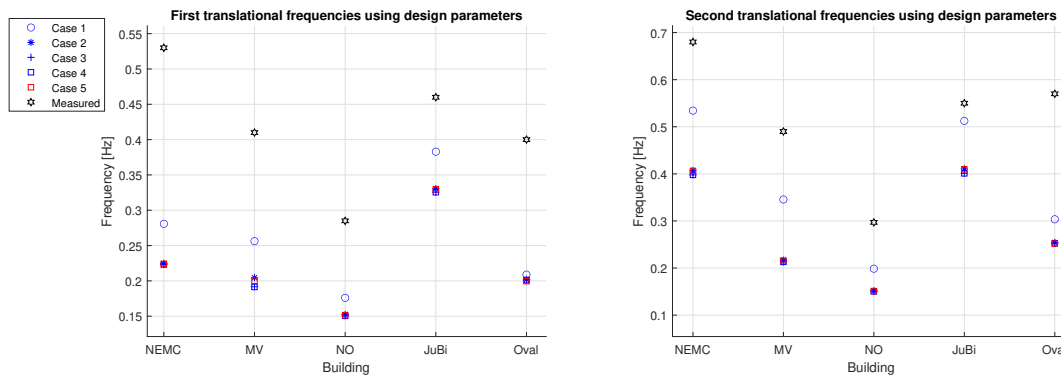
Figure 3.34: The first and second translational frequencies for the different beam models.

Table 3.30: The first and second translational frequencies for the different beam models.

Buildings	Direction	Frequencies [Hz]					
		Case 1	Case 2	Case 3	Case 4	Case 5	Measured
NEMC	f_x	0.281	0.225	0.223	0.223	0.224	0.53
	f_y	0.534	0.407	0.398	0.398	0.406	0.68
Montevideo	f_x	0.256	0.205	0.192	0.192	0.201	0.41
	f_y	0.346	0.217	0.213	0.213	0.216	0.49
New Orleans	f_x	0.176	0.153	0.151	0.151	0.152	0.285
	f_y	0.199	0.152	0.150	0.150	0.151	0.297
JuBi	f_x	0.383	0.330	0.326	0.326	0.330	0.46
	f_y	0.512	0.411	0.401	0.401	0.410	0.55
Oval	f_x	0.209	0.202	0.201	0.201	0.199	0.40
	f_y	0.304	0.254	0.253	0.253	0.252	0.57

3.6.1.2 Influence of Different Structural Parameters on the Frequency

The previous section has shown that the behaviour of the frequency can differ when using different parameter combinations. To see how each parameter influences the frequency, the frequencies for the different cases are calculated using the average between the upper and lower bound. Each parameter is then individually increased from the lower bound to the upper bound, while the rest of the parameters stay constant. This way, the effect the varying parameter has on the frequency can be quantified. This section will only discuss the first translational natural frequency for each building, as the results of the second translational natural frequency behaves in the same way. Table 3.31 shows the ratios between the lower and upper bound for the different varying parameters for each building. Figure 3.35 shows the general trend of the frequency when either a stiffness parameter or mass parameter is increased, while the other parameters stay constant. It can be seen that the rate of change in frequency decreases as the mass or stiffness is increased.

Table 3.31: Ratio between lower and upper bound for different parameters (weak axis)

	Varying Parameter				
	EI	ρ	K_r	K_t	M_f
	Increase Factor				
NEMC	5.07	1.22	13.27	61.82	1.01
Montevideo	2.52	1.23	9.95	35.36	1.04
New Orleans	4.49	1.23	10.91	25.81	1.05
JuBi	5.07	1.25	13.83	9.42	1.07
Oval	5.07	1.28	5.79	9.12	1.07
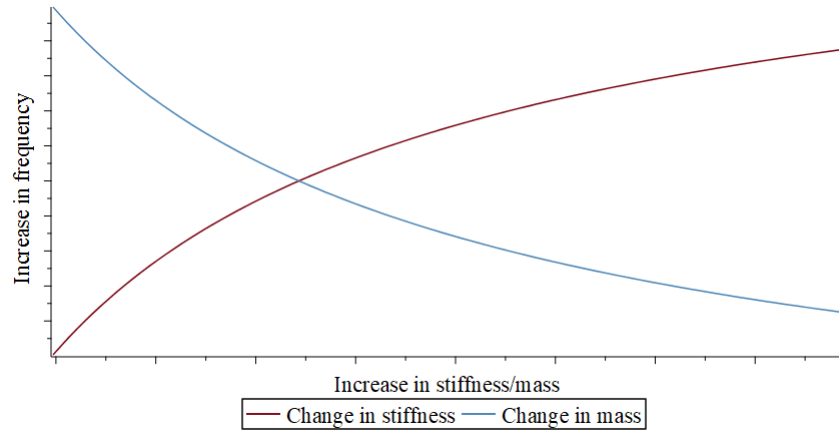
Figure 3.35: General change in frequency due to an increase in stiffness of mass parameters

Figure 3.36 shows the change in frequency as each parameter in the respective cases are varied from the lower to the upper bounds. For case 1, only the bending stiffness and density is varied, respectively. Looking at the red line, which is the frequency when all parameters of the respective case are averaged, it is generally situated around the middle of the frequency band. This means that for this case, when all parameters are averaged, the rate of change in frequency is high. Table 3.33 shows the change in frequency for the varying parameters given in percentage. These percentages are related to the frequency, which is calculated when all parameters are averaged (red line). When comparing the change in frequency, given in table 3.33, for an increase in building stiffness and mass, it can be seen that the change is directly related to the stiffness and mass ratios given in table 3.31, the larger the ratio, the larger the change in frequency.

For case 2, the rotational spring is added to the base of the beam. Figure 3.36 shows the influence of the addition of the rotational spring. In this case, the influence of the rotational spring can no longer be related to the ratio between the lower and upper bound as in the previous case. This can best be seen when comparing the influence of the added rotational spring for the Montevideo and New Orleans tower. The influence of the added spring is much greater for the Montevideo tower, even though the parameter ratio is smaller than that of the New Orleans tower. The influence of the rotational spring is related to the ratio between the building stiffness and the spring stiffness. This ratio can be expressed as a non-dimensional stiffness (η) in the form shown in equation 3.11 [4]. The equation shows the non-dimensional stiffness for the rotational and translational spring. Table 3.32 shows the rotational and translational non-dimensional stiffnesses using the lower and upper bounds for the spring stiffnesses and the averaged bending stiffness. When comparing the percentage change given in table 3.33 to the dimensionless stiffnesses, it can be seen that the lower the dimensionless stiffness, the larger the change in frequency. Figure 3.36 also shows that for most cases, there is a significant reduction in the influence of the building stiffness. It can be seen that the larger the influence of the spring stiffness, the larger the reduction in influence of the bending stiffness. As no mass parameter was added to case 2, the influence of the changing building density equates to that of case 1.

Table 3.32: Lower and Upper non-dimensional stiffnesses (weak axis)

| | η_t | | η_r | |
	Lower	Upper	Lower	Upper
NEMC	5.32	328.70	0.36	4.71
MV	8.66	306.18	0.57	5.65
NO	37.99	980.59	1.76	19.21
JuBi	40.17	378.50	0.99	13.72
Oval	159.92	1458.60	13.62	78.85

$$\eta_r = \frac{K_r L}{EI}$$
$$\eta_t = \frac{K_t L^3}{EI}$$
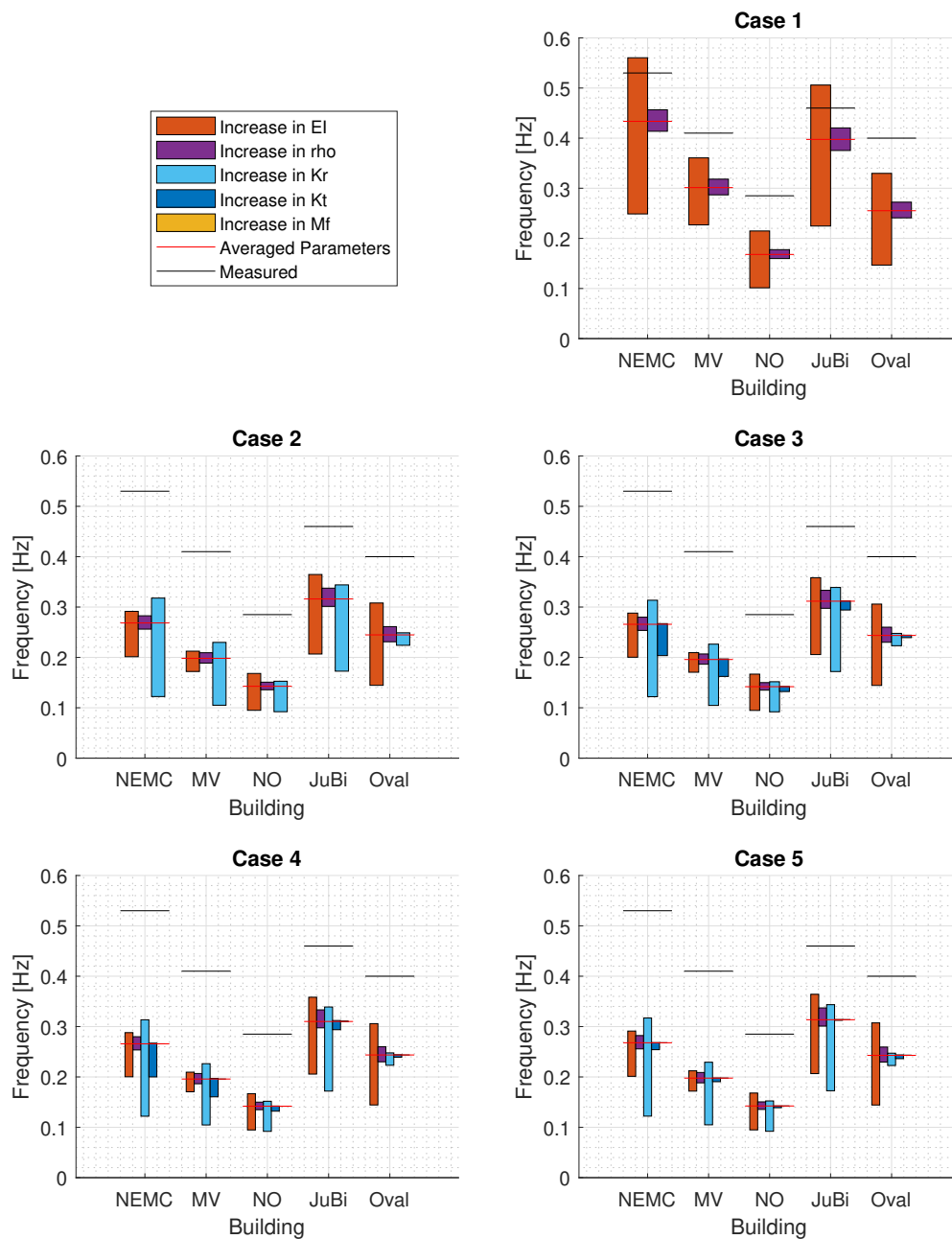
Figure 3.36: Influence of varying parameters on the first translational frequency

Table 3.33: Change in frequency for varying parameters, given in percentage related to the frequency calculated with the averaged parameters

NEMC	Varying in EI Difference [%]		Varying in ρ Difference [%]		Varying in K_r Difference [%]		Varying in K_t Difference [%]		Varying in M_f Difference [%]	
	min	max	min	max	min	max	min	max	min	max
Case 1	-42.6193	29.2573	-4.5772	5.3062	-	-	-	-	-	-
Case 2	-24.9606	8.5831	-4.5772	5.3062	-54.4446	18.3944	-	-	-	-
Case 3	-24.6123	8.3649	-4.5772	5.3062	-54.0900	17.9712	-23.4008	0.4893	-	-
Case 4	-24.6103	8.3631	-4.5769	5.3057	-54.0883	17.9670	-24.7156	0.4922	-1.98E-05	1.96E-05
Case 5	-24.9044	8.6293	-4.5772	5.3061	-54.3907	18.3287	-5.1689	0.0772	-3.17E-06	3.13E-06

MV	Varying in EI Difference [%]		Varying in ρ Difference [%]		Varying in K_r Difference [%]		Varying in K_t Difference [%]		Varying in M_f Difference [%]	
	min	max	min	max	min	max	min	max	min	max
Case 1	-24.6756	19.6923	-4.7959	5.6022	-	-	-	-	-	-
Case 2	-13.2092	7.1639	-4.7959	5.6022	-47.0100	15.9709	-	-	-	-
Case 3	-12.9352	6.9539	-4.7959	5.6022	-46.5686	15.5526	-17.1766	0.5747	-	-
Case 4	-12.9330	6.9519	-4.7954	5.6016	-46.5659	15.5478	-18.0577	0.5787	-1.16E-04	1.16E-04
Case 5	-13.1154	7.2764	-4.7958	5.6021	-46.9366	15.9003	-3.6500	0.0977	-2.00E-05	2.00E-05

NO	Varying in EI Difference [%]		Varying in ρ Difference [%]		Varying in K_r Difference [%]		Varying in K_t Difference [%]		Varying in M_f Difference [%]	
	min	max	min	max	min	max	min	max	min	max
Case 1	-39.6284	27.8877	-4.8659	5.6980	-	-	-	-	-	-
Case 2	-33.4539	17.8311	-4.8659	5.6980	-35.3978	7.0022	-	-	-	-
Case 3	-33.2356	17.5478	-4.8659	5.6980	-35.1957	6.9296	-6.8178	0.2753	-	-
Case 4	-33.2351	17.5467	-4.8658	5.6979	-35.1952	6.9293	-6.9495	0.2760	-2.07E-05	2.07E-05
Case 5	-33.3738	17.9762	-4.8658	5.6980	-35.3287	6.9772	-2.4658	0.0948	-7.16E-06	7.16E-06

JuBi	Varying in EI Difference [%]		Varying in ρ Difference [%]		Varying in K_r Difference [%]		Varying in K_t Difference [%]		Varying in M_f Difference [%]	
	min	max	min	max	min	max	min	max	min	max
Case 1	-42.6155	29.2556	-4.1117	7.4031	-	-	-	-	-	-
Case 2	-34.2111	16.0428	-4.1117	7.4031	-45.0549	9.4766	-	-	-	-
Case 3	-33.7185	15.4829	-4.1117	7.4031	-44.5837	9.2447	-5.1897	0.5705	-	-
Case 4	-33.7156	15.4776	-4.1113	7.4022	-44.5810	9.2424	-5.3091	0.5743	-1.88E-04	1.88E-04
Case 5	-34.1707	16.0305	-4.1117	7.4031	-45.0191	9.4577	-0.4506	0.0469	-1.58E-05	1.58E-05

Oval	Varying in EI Difference [%]		Varying in ρ Difference [%]		Varying in K_r Difference [%]		Varying in K_t Difference [%]		Varying in M_f Difference [%]	
	min	max	min	max	min	max	min	max	min	max
Case 1	-42.5233	29.2147	-5.5802	6.7031	-	-	-	-	-	-
Case 2	-40.9162	25.8723	-5.5802	6.7031	-8.4513	1.7010	-	-	-	-
Case 3	-40.7435	25.5350	-5.5802	6.7031	-8.3972	1.6890	-1.7974	0.1985	-	-
Case 4	-40.7427	25.5323	-5.5801	6.7029	-8.3969	1.6889	-1.8295	0.1995	-4.75E-05	4.75E-05
Case 5	-40.6502	26.4483	-5.5800	6.7027	-8.3678	1.6824	-2.7887	0.3056	-7.24E-05	7.24E-05

For case 3, the translational spring is added to the base of the beam. This case behaves in the same way as the previous case. Once again, the smaller the non-dimensional translational stiffness, the larger the influence on the frequency. One notable difference is that for all 5 buildings, the average frequency (red line) nearly equates to the upper bound frequency of the translational spring stiffness. This can also be seen in table 3.32, the upper η_t values are significantly higher than the lower values. This means that a further increase in the translational spring stiffness, which would represent stiffer soil, will not have a large effect on the frequency. Another notable difference is that the influence of the varying bending stiffness and rotational stiffness is nearly unchanged with added degree of freedom. This would suggest that the translational spring is not as influential when it comes to determining the frequency. Again, as there is no mass added to this system, the influence of the varying density equates to that of the case 1 and 2.

For case 4, the foundation mass is added to the base of the beam. Figure 3.36 and table 3.33 show that this addition has a negligible effect on the frequency. As stated in the previous section, this is due to the position of the lumped mass being at the bottom of the beam and not taking part in the vibration.

When comparing the influence of the varying density for case 3 and 4, it can be seen that there is now a small difference between the two cases, but also a negligible amount.

For case 5, the rotational and translational springs and the foundation mass is added to the base of a Timoshenko beam. When comparing the averaged frequencies of case 4 and 5, for the respective buildings, it can be seen that there is no significant difference between the two cases. Figure 3.36 also shows that the difference between the influence of the varying bending stiffness, building density, rotational stiffness and foundation mass of the two cases is negligible. The only noticeable difference is the influence of the varying translational stiffness. For the NEMC, Montevideo, New Orleans and JuBi tower the influence of the lower bound of the translational spring stiffness is significantly less for the Timoshenko beam than for the Euler-Bernoulli beam, and that in the case of the JuBi tower, the varying translational stiffness has nearly no effect of the frequency. It is interesting to note that for the Oval tower, the influence of the lower bound of the translational stiffness has increased for the Timoshenko beam. Figure 3.37 shows the change in frequency for varying non-dimensional translational spring stiffness for the Euler-Bernoulli (red) and Timoshenko (blue) beam, for each building. In this figure, the frequency is normalized to that of a fixed base beam (case 1). In the figure, it can be seen that the for both the Euler-Bernoulli and Timoshenko beam, the curves flat out rather quickly. This again shows that further increases in the translational spring stiffnesses will have little effect on the frequencies. The positioning of each curve with respect to the y-axis can be related to the upper bound of the non-dimensional rotational stiffness, as this value increases, the normalized frequencies will increase. As the normalized frequency approaches 1, then the spring stiffnesses are so stiff that they represent a fixed base case.
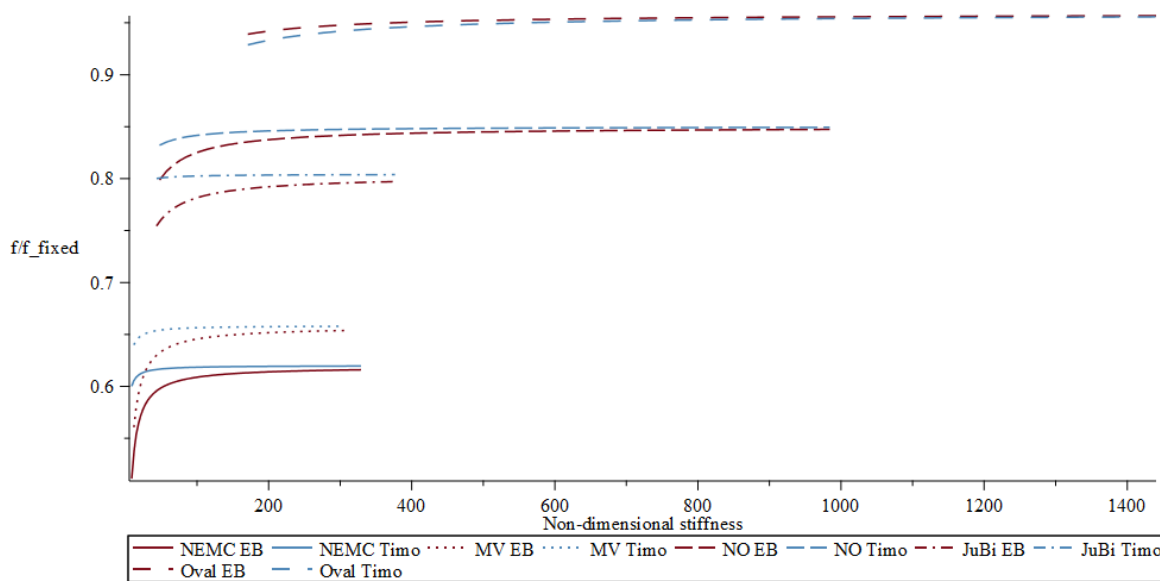
Figure 3.37: Normalized change in frequency for varying non-dimensional translational spring stiffness

To be able to determine why the behaviour of the Oval tower differs to that of the other 4 towers, a closer look is taken at how the frequency is determined using the method explained in appendix B.3. Equation 3.12 shows the boundary conditions of the Timoshenko beam. The boundary conditions are used to determine the coefficient matrix, from the coefficient matrix the determinant is calculated and equated to zero. The only unknown in this equation is the angular frequency, which can then be obtained. From case 4, it was seen that the addition of the foundation mass had nearly no effect on the frequency, so these terms can be ignored. For all 5 buildings, the magnitude of K_t and K_r fall in the same range, thus it is not likely that these are the variables which influence the behaviour of the Timoshenko beam. Variable a and the first term of b are both of a magnitude of 10^{-8} and is assumed not to be of great influence. This leaves variable c, which is the ratio between the shear and bending part of the beam.

At base (x = 0):

$$EI(\Phi''(0) + a\Phi(0)) - K_r\Phi'(0) + J\omega^2\Phi'(0) = 0$$

$$GkA((a + b + c)\Phi'(0) - \Phi'''(0)) - K_t\Phi(0) + M_f\omega^2\Phi(0) = 0$$

At free end (x = L):

$$\Phi''(L) + a\Phi'(0) = 0$$

$$d\Phi'(L) + \Phi'''(L) = 0$$

with   (3.12)

$$a = \frac{\omega^2\rho}{Gk}$$

$$b = \frac{\omega^2\rho}{E} - c$$

$$c = \frac{GkA}{EI}$$

$$\Phi = C1\cosh(\lambda_1 x) + C2\sinh(\lambda_1 x) + C3\cos(\lambda_2 x) + C4\sin(\lambda_2 x)$$

λ_1, λ_2 and d consist of a, b and c
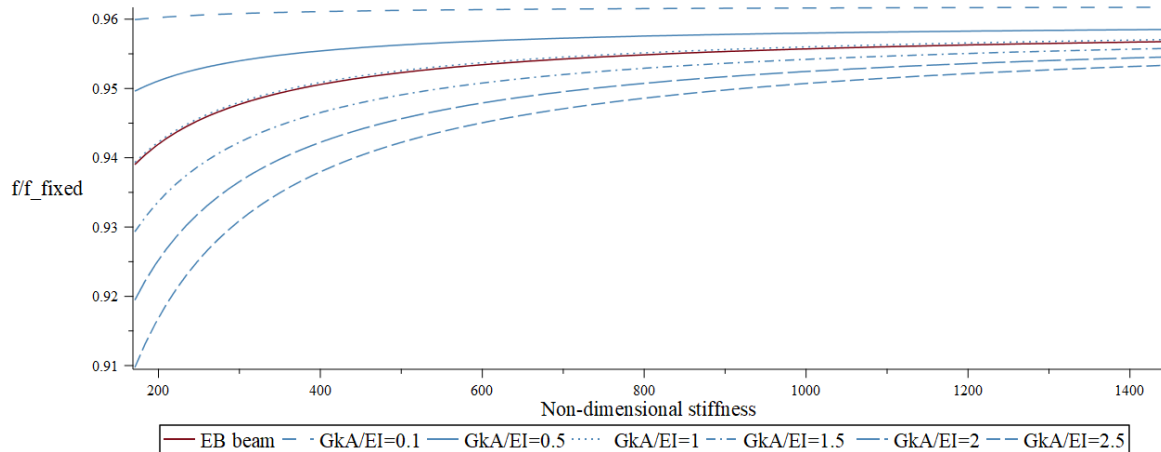
Figure 3.38: Normalized change in frequency vs varying non-dimensional translational spring stiffness for different $\frac{GkA}{EI}$ ratios for the Oval tower

In figure 3.38 the varying dimensionless translational spring stiffness vs the normalized frequency is plotted for different rations of $\frac{GkA}{EI}$. The figure shows that the larger the value of c, the more susceptible the frequency of the Timoshenko beam is to small values of η_t. For a c value of 1, the Timoshenko beam acts as an Euler-Bernoulli beam. As the c value approaches 0, the influence the translational spring has on the frequency also approaches 0. Taking another look at figure 3.37, the figure would suggest that the c values for the NEMC, Montevideo, New Orleans and JuBi tower are all smaller than 1, with that of the JuBi tower approaching 0, and that of the Oval tower being greater than 1. When comparing this with table 3.34,which shows the c values of the respective buildings, this indeed seems to be the case.

Table 3.34: c values

Building	$\frac{GkA}{EI}$
NEMC	0.16
MV	0.17
NO	0.34
JuBi	0.08
Oval	1.53

3.6.1.3 Frequency of Extreme Parameter Combinations

From figure 3.34 it was seen that when using the design parameters, the calculated frequency was well below the measured frequencies. In figure 3.36 is can be seen that if the upper bound of the bending and rotational spring stiffnesses, and the lower bound of the building density is reached, the frequency can be increased significantly. Figure 3.39 shows the frequency range of the first and second translational frequencies. In the calculation of the lower bound of the frequency range, the lower bound of the stiffness parameters and the upper bound of the mass parameters are used, and vice versa for the upper bound of the frequency range. In the figure it can be seen that for the first translational frequency, even when using the upper bound parameter combination, the frequencies still do not reach the measured frequencies. For the second translational frequency, the measured frequencies are only reached for the NEMC and the JuBi tower, and even then it is only reached by the upper bound of the frequency range.
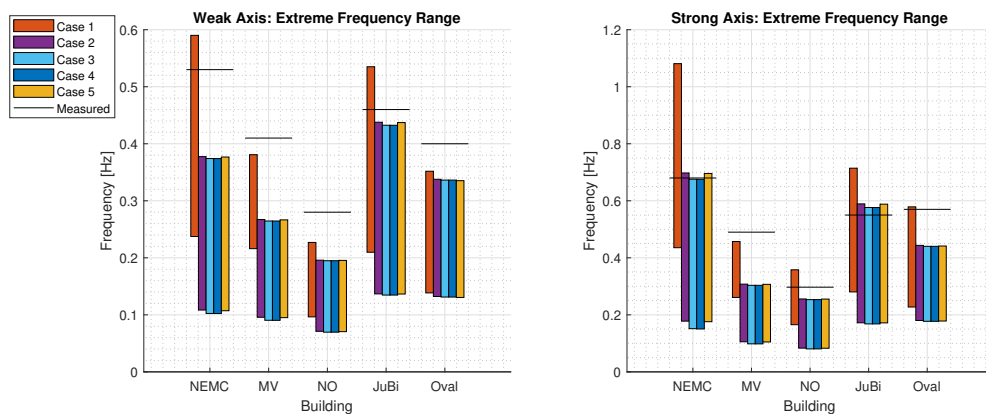
Figure 3.39: Frequency of extreme parameter combinations

The upper and lower bounds of the frequency ranges, shown in figure 3.39, do however give a false impression of the facts, as in reality the probability that the extreme parameter combinations occur is assumed to be rather small. For this reason, it would be more useful during the design phase to determine the frequency range for the 90% probability interval, rather than the extreme frequency range. There is little available literature shedding light on possible probability distributions of the structural parameters used in the beam models. For this reason, a Gaussian distribution will be used for each parameter. The mean of the Gaussian distribution will be the design value, and the standard deviation will be $\frac{0.5 mean}{1.64}$. The probability distribution will be restrained to the bound defined for the lower and upper bound of each parameter. The probability distribution will then be manipulated in such a way that the cumulative distribution between the bounds equates to 1. Figure 3.40 shows these steps for the E modulus of the Oval tower as an example. In the top plot of the figure, the original and manipulated probability distribution is seen. The middle plot shows the cumulative density, where it can be seen that the cumulative probability of the original probability density does not reach 1 when the upper limit is reached. After the original probability distribution is manipulated, the cumulative probability equates to 1 at the upper limit. The bottom plot of the figure shows 10000 random samples taken between the limits of the manipulated probability distribution.
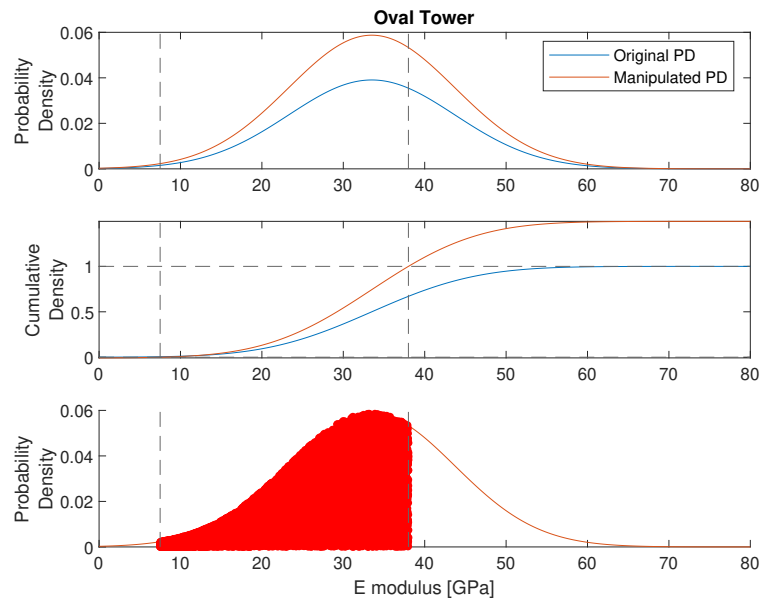
Figure 3.40: Probability density and cumulative density for the E modulus of the Oval tower.

As shown in the previous section, the translational stiffness, foundation mass and the use of the Timoshenko beam, only has a minimal effect on the frequency, thus the 90% probability interval will be calculated for case 2. For each parameter (EI, ρ and K_r), of each respective building, a new probability distribution is determined. The individual parameter probability and cumulative densities can be found in Appendix D.3. Random parameters combinations are then chosen according to each building's respective parameter probability distributions, these parameter combinations are then used to determine a frequency range. The 90% probability interval can then be determined from this frequency range and is show in table 3.36 for the respective buildings.

A recent article in Cement magazine [11] shows the dates the measured frequencies were determined and the dates the buildings were finished. This can be seen in table 3.35. In the table can be seen that for the NEMC, the measurements were done 2 years before construction was finished. Due to still being in the construction phase, it is assumed that only the structural loads are present. For this reason, the mean for the building density for the NEMC is taken as the lower bound.

Table 3.35: Date of the end of construction period and when measurements took place [11]

Building	End of Construction	Measurement
New Erasmus MC	2013	2011
Montevideo	2005	2009
New Orleans	2010	2011 - now
JuBi	2012	2016
Oval	2001	2002

Table 3.36: 90% probability interval for the first translational frequency

	90% Probability Interval
	f [Hz]
NEMC	0.149 - 0.334
Montevideo	0.123 - 0.248
New Orleans	0.095 - 0.174
JuBi	0.195 - 0.382
Oval	0.156 - 0.302

3.6.2. Multiple Beam Model

The general trend of high-rise structures is that as the height of the structure progresses, the stiffness and the density of the structure decreases. Table 3.37 shows the averaged uniform and sectional building stiffnesses and densities for the different buildings in the weak direction. In the table can be seen that for the Montevideo, New Orleans, Jubi and Oval towers, the stiffness of the top section is the smallest stiffness. For these 3 buildings, it can also be seen that the most of the mass sits in the lower half of the structure, only for the Oval tower, this does not apply. The NEMC is assumed to be constant in mass and stiffness over the height of the structure. Due to the use of a Timoshenko beam not having a significant influence on the frequency and large computational time needed for the calculations, the Timoshenko beam is left out of the multibeam calculations.

Table 3.37: Single- and multibeam bending stiffness and density comparison in the weak direction

	Level	Single-beam $EI[Nm^2]$	Multi-beam $EI[Nm^2]$	Single-beam $\rho[\frac{kg}{m^3}]$	Multi-beam $\rho[\frac{kg}{m^3}]$
NEMC	0-32	4.50E+13	4.50E+13	397	397
MV	0-1	3.53E+13	3.55E+13	426	263
	2-27	-	6.34E+13	-	454
	28-42	-	2.93E+12	-	405
NO	0-2	1.85E+13	2.05E+13	457	576
	3-10	-	2.12E+13	-	454
	11-46	-	1.98E+13	-	449
JuBi	0-9	1.24E+14	1.49E+14	448	493
	10-22	-	9.82E+13	-	482
	23-38	-	7.09E+13	-	366
Oval	0-14	5.60E+12	5.60E+12	284	281
	15-24	-	5.05E+12	-	287

As previously stated, a change in stiffness in the lower sections and a change in density in the upper sections of a structure will have the greatest effect on the frequency. Figure 3.41 shows the comparison of the first and second natural frequencies between the single- and multibeam models. As expected, there is a noticeable increase in frequency for the Montevideo, New Orleans and Jubi towers, with an increase in frequency for the JuBi tower as high as 15.2% for case 1, and ±12.5% for cases 2, 3 and 4. This is due to the reduction in density in the upper part of the beam models, and an increase in stiffness in the lower part of the beam models. Due to the density increase of the upper part of the beam for the Oval tower, and the uniform stiffness being equal or greater than the sectional stiffnesses of the multibeam model, there is a slight decrease in frequency. As there is no change in properties for the NEMC, the frequency also stays constant for the different beam models. The frequencies and percentile differences in frequency for the first and second translational frequencies can be found in tables 3.38 and 3.39.
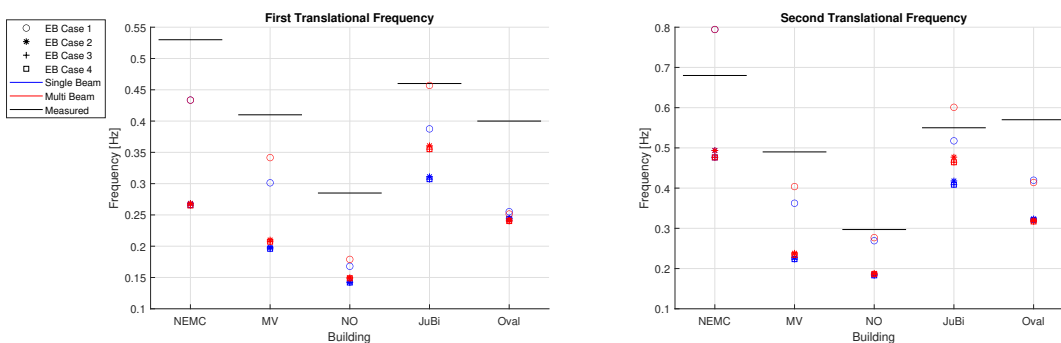
Figure 3.41: Single- and multibeam frequency comparison using the averaged parameters

Table 3.38: Comparison of the first translational frequencies for the single- and multibeam models

	NEMC			Montevideo			New Orleans			JuBi			Oval		
	Single Beam	Multi-beam	%	Single Beam	Multi-beam	%	Single Beam	Multi-beam	%	Single Beam	Multi-beam	%	Single Beam	Multi-beam	%
Case 1	0.434	0.434	0	0.301	0.342	11.792	0.168	0.179	6.166	0.387	0.457	15.208	0.255	0.251	-1.488
Case 2	0.268	0.268	0	0.198	0.210	5.612	0.143	0.150	4.647	0.311	0.361	13.722	0.245	0.241	-1.454
Case 3	0.266	0.266	0	0.196	0.207	5.466	0.142	0.149	4.573	0.307	0.355	13.521	0.244	0.240	-1.444
Case 4	0.265	0.265	0	0.196	0.207	5.465	0.142	0.149	4.596	0.307	0.355	13.518	0.244	0.240	-1.444

Table 3.39: Comparison of the second translational frequencies for the single- and multibeam models

	NEMC			Montevideo			New Orleans			JuBi			Oval		
	Single Beam	Multi-beam	%	Single Beam	Multi-beam	%	Single Beam	Multi-beam	%	Single Beam	Multi-beam	%	Single Beam	Multi-beam	%
Case 1	0.794	0.794	0	0.362	0.404	10.250	0.269	0.277	2.755	0.517	0.601	13.888	0.420	0.414	-1.378
Case 2	0.493	0.493	0	0.227	0.238	4.680	0.185	0.188	1.693	0.418	0.477	12.401	0.324	0.320	-1.250
Case 3	0.477	0.477	0	0.223	0.234	4.518	0.183	0.186	1.663	0.409	0.464	12.030	0.321	0.317	-1.236
Case 4	0.476	0.476	0	0.223	0.234	4.516	0.183	0.186	1.663	0.408	0.464	12.022	0.321	0.317	-1.236

The influence of the different structural parameters on the frequency and the extreme parameter combinations were also calculated for the multibeam models. The results of the multibeam models mimic that of the single beam models, with the only difference being slightly higher frequencies due to reason previously discussed. The results of the multibeam models can be found in Appendix D

3.7. Calibration of multibeam model

In figure 3.41 it was seen that, even though the multibeam model produces higher frequencies than the uniform beam model, the frequencies are still underestimated. It has been shown that the underestimation in frequency is most likely the cause of an underestimated superstructure stiffness. This begs the question if the stiffness can be calibrated realistically to fit the measured natural frequencies. Figure 3.42a) shows the change in frequencies as the E-modulus of concrete increases. In the analysis, the sectional densities are taken as the average between the lower and upper bounds, and the upper bounds for the foundation springs are used. The E-modulus for steel is still 210 GPa.

According to Gutierrez [24], the E-modulus of high strength concrete is between 40 GPa and 50 GPa. The black x in the graphs show the value of the E-modulus calibrated to fit the measured natural frequency, this can also be seen numerically in table 3.40. It can be seen that in most cases, the calibrated E-moduli are unrealistically high. The dash in the table means that the stiffness of the beam could not be calibrated to fit the measured data. It can be seen that for most cases, the extra stiffness needed in the two directions, differ quite significantly. This leads to the belief that the needed stiffness if most probably not provided by an inaccurate approximation of a material property, but rather originates from a source not yet taken into account.

Table 3.40: Calibrated E-modulus

	Direction		
	Weak	Strong	Weak (DynaPile)
	E-modulus [GPa]		
NEMC	-	53.5	58
Montevideo	-	-	195
New Orleans	155	135	83
JuBI	49	34.5	-
Oval	66.5	245	69.5

In an article by Bronkhorst [9], the foundations of the 5 structures we modelled in the Dynapile software, which makes use of the pile plan of the structure and the soil properties. Table 3.41 shows the single spring stiffnesses determined by Dynapile and the upper bounds determined in this thesis. Figure 3.42b) shows the change in frequency, for the weak axis, for the upper bound stiffnesses and the dynapile computed stiffnesses. For the NEMC, Montevideo and New Orleans tower, the dynapile

stiffnesses are higher than that of the upper bound, and in the case of the JuBi and Oval tower they are lower. These changes in stiffness significantly impact the frequencies. Literature and software provide many different methods of calculating the spring stiffnesses of foundations. The fact that the frequencies determined using different methods of calculating the spring stiffnesses, shows that approximating the foundation stiffness accurately is as important as accurately approximating the superstructure stiffness.

Table 3.41: Upper bound and Dynapile foundation spring stiffnesses

Spring stiffnesses			
Upper Bound		DynaPile	
Kr	Kt	Kr	Kt
1.75E+12	8.35E+09	5.94E+12	4.50E+09
1.42E+12	3.93E+09	4.45E+12	3.50E+09
2.29E+12	4.88E+09	5.33E+12	3.65E+09
1.16E+13	1.50E+10	3.80E+12	7.20E+09
4.49E+12	8.57E+09	3.46E+12	3.46E+09
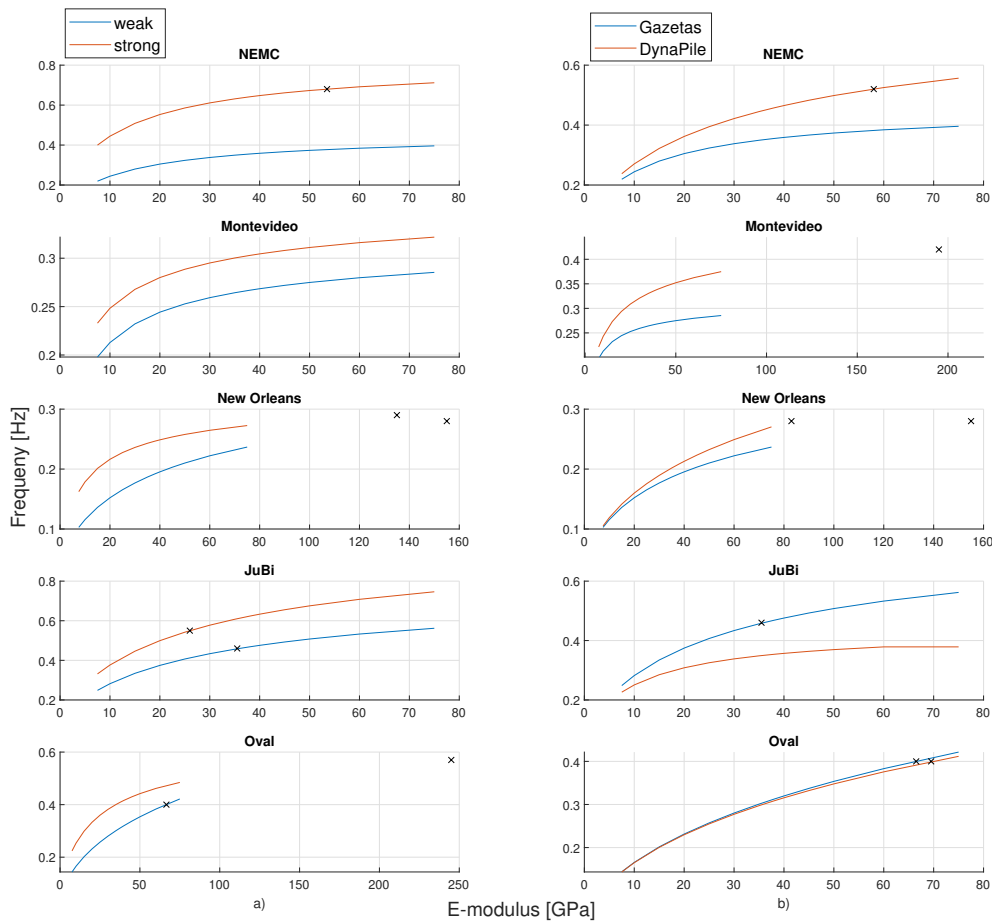
Figure 3.42: a) Weak and strong axis frequencies for increasing E-modulus. b) Frequencies for increasing E-modulus using different foundation spring stiffnesses.

3.8. Conclusions

The purpose of this chapter was to investigate factors influencing the natural frequencies of five existing structures in the Netherlands, by means of a sensitivity study. The frequencies were determined for 5 different beam models, each model providing insight to the influence a certain structural parameter has on the natural frequency. By making a conservative and extreme assumptions when calculating the different structural parameters, a lower and upper bound for each parameter was determined. This showed that there is a significant amount of uncertainty when it comes to determining structural parameters, which in the past were mostly taken as deterministic. These bounds were then used to quantify the influence each parameter has on the frequency.

First, the natural frequencies were determined for each beam model using the structural parameters given in the design documentation for each individual structure. From this calculation, it was immediately evident that the frequencies were underestimated when using the beam models. Even for case 1, representing a structure with a fixed base, the frequencies are underestimated. This lets one believe that the either stiffness of the structure is underestimated, or that the density of the structure is overestimated.

When comparing the results of the 5 different cases, it is evident that the density and the bending stiffness of the superstructure, and rotational stiffness of the substructure are the parameters which influence the natural frequency the most. As there was only a small decrease in frequency for case 3 and 4, when compared to case 2, it can be assumed that the translational stiffness and foundation mass don't play a significant role when determining the natural frequency of a structure.

After comparing the results of case 4 and 5, it was shown that the Timoshenko beam only differs slightly from the Euler-Bernoulli beam. Interestingly, the behaviour of the frequency of the Timoshenko beam is not the same for the different structures. For the NEMC, Montevideo, New Orleans and JuBi towers there is a slight increase in frequency, and for the Oval tower there is a slight decrease. The fact that the behaviour of the Timoshenko beam, and the fact that the magnitude of the change in frequency for the different cases, is not the same for each structure, shows that different parameter combinations lead to the frequency behaving differently for each structure.

To be able to quantify the influence each parameter has on the frequency, each individual parameter was varied from it's lower bound to it's upper bound while the other parameters in the system were kept constant. In this way, it could be seen how much the varying parameter influences the frequency.

The results obtained when respectively varying the bending stiffness and density of the superstructure are as expected. As the stiffness is increased, the frequency increases, and as the density increases, the frequency decreases. However, when comparing the influence the varying stiffness of case 1 and case 2 has on the frequency, a difference can be seen. This shows that the addition of the rotational spring, affects the influence of the bending stiffness has on the frequency.

After varying the rotational spring stiffness, it was seen that the influence the rotational spring stiffness has on the frequency largely relies on the ratio between the rotational spring stiffness and the building stiffness. This ratio can be express in a dimensionless stiffness. The smaller this non-dimensional rotation stiffness is, the larger the influence of the rotational spring and the smaller the influence of the bending stiffness, has on the frequency.

For the translational stiffness, there is no significant difference between the upper bound and the averaged frequencies. Only when the translational spring stiffness is very small, does this parameter have a noticeable influence on the frequency.

For the Timoshenko beam, the influence of the bending stiffness, density and rotational spring stiffness is similar to that of the Euler-Bernoulli beam. However, for the translational spring stiffness, it can be seen that the Timoshenko beam is a lot less susceptible to the translational spring stiffnesses when compared to that of the Euler-Bernoulli beam. For the structures where the Timoshenko beam provided increased frequencies, the influence of lower bound of the translational spring stiffness is less significant than in the cases of the Oval tower, where a decreased frequency was determined. It was found that the ratio between $\frac{G\kappa A}{EI}$ is what determines if the Timoshenko beam frequency increases or decreases in regard to the frequencies of the Euler-Bernoulli beam. If the ratio is greater than 1 the frequency decreases. if the frequency is smaller than 1 the frequency increases and When the ratio equates to 1, the Timoshenko beam and Euler-Bernoulli beam provide the same frequency.

For the multibeam models, new sectional parameters were determined. The section boundaries were

chosen at points over the height of the structures, where significant changes in stiffness occurred. When comparing the results of the single beam model with the multibeam model, it can be seen that, in most cases, the multibeam model provides and increased frequencies which is closer to the measured frequencies. This is due to the lower sections of the multibeam models having an increased stiffness, compared to the uniform stiffness of the single beam model. A second contributing factor to the increased frequencies is that a larger part of the mass of the structure is situated in the lower sections of the model, this results in less mass taking part in the vibration, which leads to higher frequencies. Even though the there is an increase in frequency, the frequencies are still significantly underestimated for most cases, when comparing them with the measured frequencies.
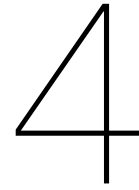
Sensitivity Study II: Finite Element Model of the new Erasmus Medical Centre

4.1. Introduction

The results given in chapter 3 show that the uncertainty of certain structural parameters can have a large effect on the natural frequency of the structure. Even after using the parameter combination which lead to the highest possible natural frequency, in most cases there is still an underestimation of the frequency compared to the measured data. As discussed in the literature of section 2.2.4, there are several structural and non-structural elements which provide extra stiffness to the structure, which are not taken into account in the stiffness calculation of the beams models. By adding the extra stiffness to the system, the natural frequency of the structure should increase. The following chapter provides insight into the influence different structural elements have on the natural frequency. This is done by creating a complete model of the new Erasmus Medical Centre and performing a modal analysis on the 3D model to determine the natural frequency. The FEM software used for the modal analysis is SCIA Engineer.

The chapter is structured in the following way. Section 4.2 described the original FEM Model modelled during the design phase of the structure and the alterations made to the original model. Section 4.3 gives the results of the different modal analyses done, quantifying the influence different structural systems have on the natural frequency of the structure. Lastly, section 4.4 discusses and provides concluding remarks on the results found in section 4.3.

4.2. The FEM Model

4.2.1. Original Model

During the design of the NEMC a model of the building was made in SCIA Engineer. Figure 4.2 shows the original model, where 4.1a shows the complete model, 4.1b shows an open view of the model and 4.1c shows the foundation plate and pile layout. The outer tube of the model exists of 640 2D wall elements. From the ground floor to level 4 the wall element are rigidly connected both horizontally and vertically to each other, due to these walls being cast in-situ in reality. Above level 4, stacked prefab concrete elements are used. The stacked elements are connected with DEMU fixing anchors and a connected horizontal joint. At the sides of the prefab elements, no joints are present. In the model, the 2D wall elements are rigidly connected to the wall elements above and below. To represent the absence of the joints between the horizontally placed wall elements, a gap of 20mm is modelled. The thickness of the wall elements range from 500mm to 320mm as specified in the design. The floors are modelled with 220mm thick 2D plate elements and are rigidly connected to the walls. The foundation slab is also modelled with a 2D plate elements and has a thickness of 2m. Connected to the foundation plate are 352 spring supports representing the piles under the foundation slab. In the design calculation, the 3 cores only comprised of 7% of the total moment of inertia of the structure, it was assumed to have little effect on the stiffness and was thus left out of the initial model.

(a) Complete original model   (b) Open original model   (c) Foundation with pile layout
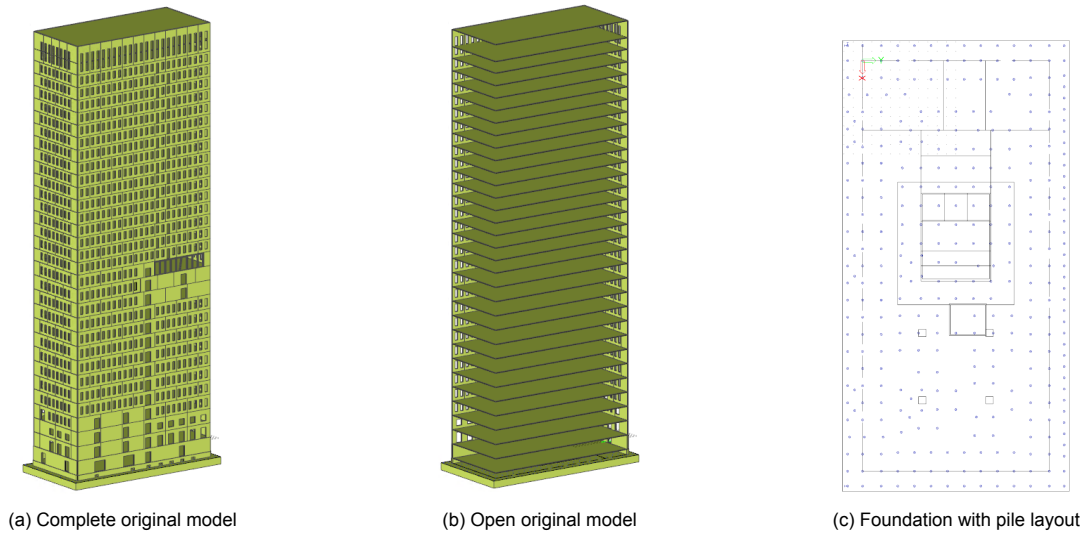
Figure 4.1: Original SCIA model showing outside view, inside view and pile layout

4.2.2. Complete Model

In the previous chapter, it was shown that there is an underestimation of the natural frequency when using the beam model. It is thought that this is due to an underestimation in the stiffness of the structure. For the complete model, the stability systems ignored in the initial model are added. These are the three main concrete cores and columns which stretch from the foundation to the roof, and the beams as shown in figures 4.2a, 4.2b and 4.2c. Figure 4.2d shows a connected view of the modelled systems.

The cores are each modelled with 2D wall elements with dimensions corresponding to the design specifications. Each wall element is connected with the adjacent element with a spring. The spring stiffness can be changed as to represent different interface conditions between the elements. The columns are modelled with 1D bar elements with properties corresponding to the design. Each bar element is connected rigidly at the top and bottom to the floors above and below. The beams are also modelled with 1D bar elements and are rigidly connected to the floors.

(a) Three concrete cores   (b) Columns   (c) Beams   (d) Connected cores, columns and beams
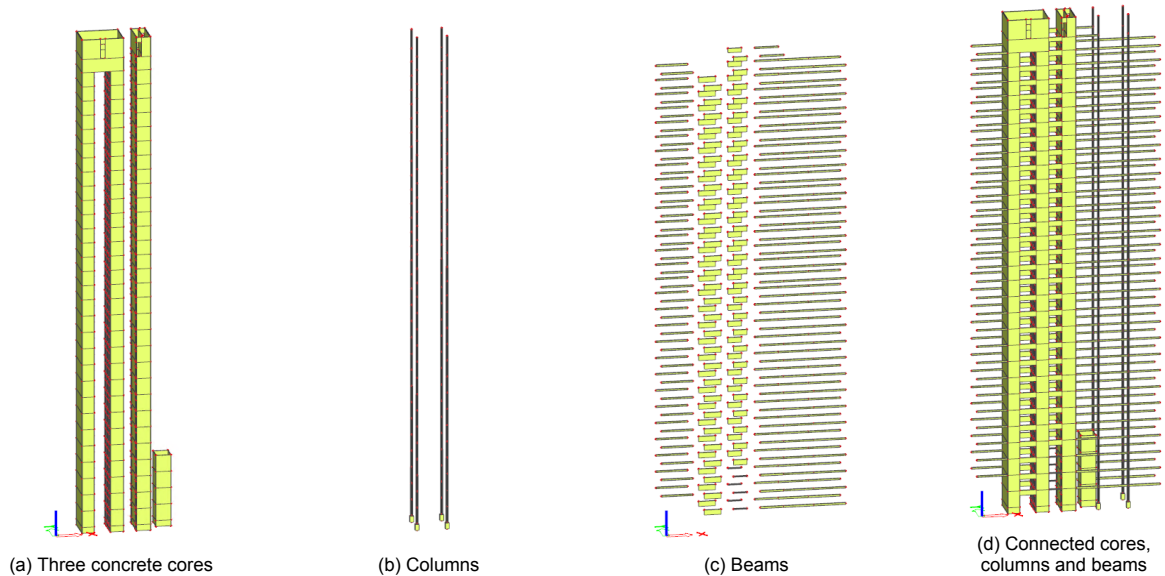
Figure 4.2: Added Stiffness systems

Table 4.1: SCIA Engineer model load summary

Load	Description	kN
Self weight	All modelled elements	358145
	Extra outer tube	69399
	Stairs and lifts	11228
Permanent	Floors, stairs and lifts	22141
Variable	Floors, stairs and lifts	64937
	Foundation	506

		$\frac{kg}{m^3}$
Density	Superstructure + foundation	493.76
	Superstructure	436.74

The loads added to the model were determined in the same way as the upper bound of the density in the previous chapter. A summary of the loads is given in table 4.1. As the prefab walls are modelled with 2D elements of a constant thickness, the total weight of the wall elements is less than in reality. The extra weight, as determined from the design specifications of the prefab elements, is added to the wall element with line loads. This can be seen in figure 4.4a. As the stairs and lift are not included in the model, these are also added as line loads on the respective floors where they are found, as shown in figure 4.4b. The permanent and variable loads of the stairs and lifts are added in the same way, whereas the permanent and variable loads for the floors are added as surface loads over the floors, as is the variable load of the foundation.

(a) Outer tube loads

(b) Loads due to stairs and lifts
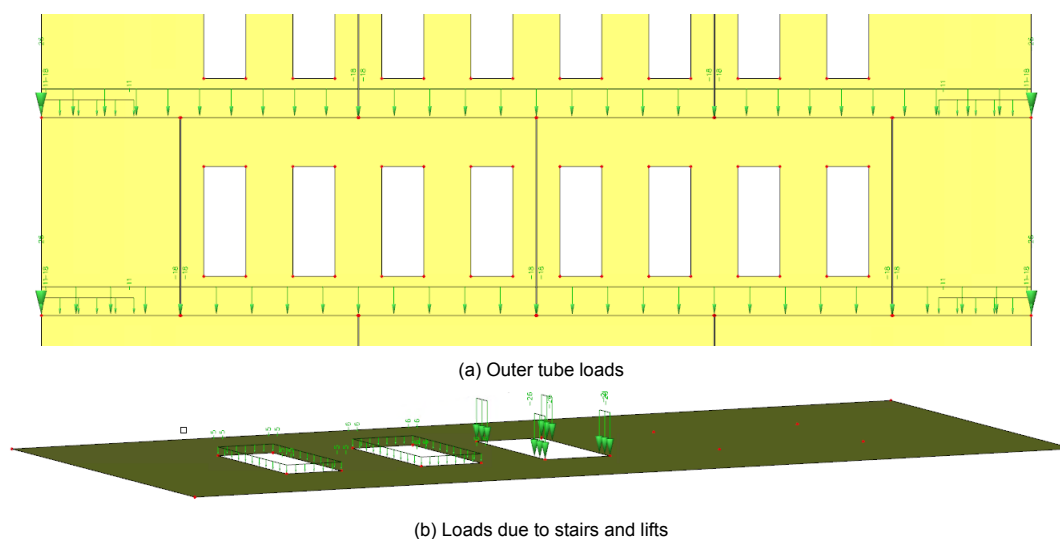
Figure 4.3: Loads added to SCIA model

4.3. Modal Analyses

To be able to quantify the influence of the different structural systems, each system contributing to the stiffness is created in its own layer, which can be turned on and off for each analysis. When a system is excluded from an analysis, the weight of the system is added to the structure in the form of an added mass. In this way, the total mass of the structure stays constant and the influence of the stiffness system can be determined. The different stiffness systems are the outer tube, floors, cores, foundation, beams and columns. Each pile of the foundation is modelled as a spring support. By changing the stiffness of the springs, the influence of soil-structure interaction can be seen, where infinitely stiff springs represent a fixed base of the superstructure, and specified spring stiffnesses represent the stiffness provided by the piles and soil. Each intersection between the walls, floors and cores are also modelled by springs to represent the type of connection between these elements, where

an infinitely stiff spring represents a rigid connection and a spring stiffness of zero represents hinged connections. By changing the stiffness of these spring connections in the FEM model, the influence of the connections can be quantified. Lastly, the Young's modulus of the different structural systems can also be changed to see what effect this has on the natural frequency. In all the analyses done, the outer tube, foundation and floors are present, whereas the cores, beams and columns are excluded in certain analyses.

Reference Case

The first modal analysis is performed for the model with a fixed base. This is achieved by prohibiting the springs in the foundation to translate or rotate in any direction. For the first case, all additional systems in the providing stiffness (cores, columns and beams) are present. The elasticity moduli for all concrete elements are $20GPa$ and the spring stiffness of the hinges are set to 10^{17} (maximum in SCIA Engineer) to represent a fixed connection. A summary of the properties and systems included in the model is shown in table 4.2. For the first analysis, the standard SCIA mesh size was taken, which is on average 1m for 2D elements and 1 intermediate point on 1D elements.

Table 4.2: Properties and systems included in first modal analysis

E [Gpa]				Included			Foundation						Hinges
Tube	Floors	Core	Foundation	Cores	Columns	Beams	Kx	Ky	Kz	Rx	Ry	Rz	ϕ_x
20	20	20	20	yes	yes	yes	clamped	clamped	clamped	clamped	clamped	clamped	1.00E+17

After performing the modal analysis, the eigen frequencies were obtained. The frequency calculated by SCIA was 0.322 Hz and 0.532 Hz for the first and second translational frequencies. When comparing this to the measured frequencies of 0.53 and 0.68 for the first and second translational frequencies, it can be seen that even for the fixed base case, there is still an underestimation of the frequencies. Just as for the beam models, the difference between the first translational frequency and the measured frequency is greater than that of the second translational frequency. SCIA Engineer does not have the feature to check the mode shapes of the different frequencies, however SCIA does provide the global deformation when the structure is excited at a chosen frequency. The deformation of the structure at 0.322 Hz and 0.532 Hz are shown in figure 4.4. Is can be seen that the global deformations for the two frequencies mimic the well-known first mode shape in each direction.

(a) Excited at 0.322 Hz

(b) Excited at 0.532 Hz
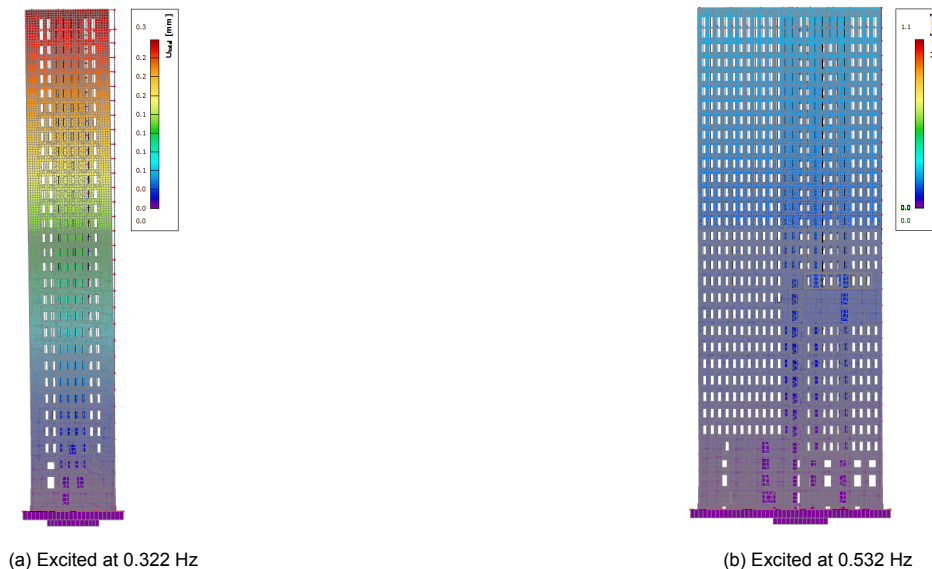
Figure 4.4: Mode shape represented by global displacement excited at chosen frequency

Mesh size and run time

Before changing the parameters of the model of excluding stiffness systems from the model, the in-

fluence the mesh size has on the frequency calculation is checked. Two more modal analyses are performed with the same model as mentioned above, the only difference is the mesh size. Table 4.3 shows the influence the change in mesh size has on the frequency and run time. The difference in calculated frequencies for run 2 and 3 are both related to run 1. It can be seen that there is a slight change in frequency when comparing runs 1 and 2, and that there is a negligible difference between runs 2 and 3. However, when looking at the run times of the respective analyses, it can be seen that the time increases exponentially as the mesh size decreases. As the difference in frequency is minimal for a smaller mesh size, but the run time increases significantly, the mesh size of run 1 was chosen for all future runs.

Table 4.3: Influence of mesh size on frequency and run time

	Mesh Size		Frequency		Difference		Run Time
	1D Elements	2D Elements	First	Second	%	%	
Run	Intermediate points	m	First	Second	%	%	Minutes
1	1	1	0.32210	0.53191	-	-	94
2	5	0.5	0.32476	0.53089	0.82614	-0.1933	172
3	10	0.25	0.32479	0.53085	0.83454	-0.2008	512

Elasticity modulus

For run 4 and 5, all structural systems are still included in the analysis. All spring supports of the foundation are still clamped, as to represent a fixed base. For run 4 and 5 the elasticity modulus for all concrete elements are changes to $38GPa$ and $7.5GPa$, respectively. This can be compared to the beam model for case 1 where the bending stiffness varies. To be able to compare the SCIA results with the beam model, the frequencies for the beam model were recalculated using an E-modulus of $20GPa$ and a density of $436\frac{kg}{m^3}$ as to match the parameters used in the SCIA model. The upper and lower bounds of the bending stiffness are the same as given in chapter 3. The frequencies for run 4 and 5, and the recalculated beam model frequencies, are shown in table 4.4. In the table can be seen that for run 4, the first translational frequency is still underestimated compared to the measured frequency of 0.53 Hz. However, the second translational frequency does surpass the measured frequency of 0.68 Hz.

When comparing the results of the SCIA model and the beam model, it can be seen that the beam model gives significantly higher frequencies. However, both models behave similarly when the E-moduli are changed. Comparing run 4 to run 1 for both models, there is an increase in frequency of 37,4% and 36.9% for the first and second frequency, for the SCIA model, and an increase of 37.8% in both directions for the beam model. When run 5 is compared to run 1, there is a reduction of ±38% for both models, in both direction.

Table 4.4: Parameter change and frequencies for runs 4 and 5 (left). Recalculated beam model frequencies for case 1 using matched parameters and varying stiffness (right).

	E [GPa]				Frequency [Hz]		Beam model Frequency [Hz]	
Runs	Tube	Floors	Core	Foundation	First	Second	First	Second
1	20	20	20	20	0.322	0.532	0.388	0.710
4	38	38	38	38	0.443	0.728	0.534	0.979
5	7.5	7.5	7.5	7.5	0.198	0.329	0.237	0.435

Foundation

In runs 6 to 16, the spring properties of the foundation is changed. Table 4.5 shows which parameters of the springs are change, their influence on the frequency and comparisons made between runs. In the table, K_x, K_y and K_z represent the translational restraints and R_x, R_y and R_z represent the rotational restraints of the springs. The stiffness of K_x and K_y is the translational stiffness of a single pile as determined in section 3.5.3. The stiffness of K_z is the stiffness determined by Deltares, as used in the

design documentation. Ar the rotational restraints are set to free, the rotational resistance is determined using the translational spring stiffnesses.

The table shows that the as K_x and K_y are relaxed, there is a decrease in the frequency in the corresponding directions. It can also be seen that the decrease in the second translational frequency is greater than that of the first, this is due to the fact that the difference between the stiffness of the substructure and superstructure is larger. This is the same behaviour as seen in the beam models. When considering run 9, it can be seen that when the vertical spring stiffness is relaxed, there is a noticeable decrease in frequency in both translational frequencies. Even though the springs are still restrained from rotating, the vertical displacement and deformation of the foundations results in a small amount of rotation. Just as in the beam models, it can be seen that the rotation of the foundation has a larger influence on the frequencies than the translation. It must be notes that the subscript of the rotational stiffnesses denotes the axis around which the rotation takes place, this is why the contradicting direction is influenced. When comparing the influence the rotation of the foundation has on the frequency, it is seen that the influence on the first translational frequency is greater. This is due to the fact that the foundation behaves stiffer when rotation around the strong axis. This is the result of the lever arm to the outer spring being much larger than in the weak direction. This results in a larger rotational resistance. The total decrease in frequency from run 1 and run 14 is 20% and 18% is the first and second natural frequencies. This is less than the 25.1% and 25.8% decrease in frequency for case 4 of the beam model, still the beam model gives significantly higher frequencies with 0.29 Hz and 0.53 Hz [1] for the first two natural frequencies.

Table 4.5: Change in foundation properties with corresponding frequencies

Runs	Foundation						Frequency [Hz]		difference %		
	K_x	K_y	K_z	R_x	R_y	R_z	First	Second	First	Second	between runs
1	clamped	clamped	clamped	clamped	clamped	clamped	0.322	0.532	-	-	-
6	1.56E+07	clamped	clamped	clamped	clamped	clamped	0.322	0.516	0.00	-3.06	6/1
7	clamped	1.56E+07	clamped	clamped	clamped	clamped	0.318	0.532	-1.16	0.00	7/1
8	1.56E+07	1.56E+07	clamped	clamped	clamped	clamped	0.318	0.516	-1.18	-3.06	8/1
9	clamped	clamped	8.70E+07	clamped	clamped	clamped	0.305	0.489	-5.43	-8.04	9/1
10	1.56E+07	1.56E+07	8.70E+07	clamped	clamped	clamped	0.301	0.476	-6.47	-10.58	10/1
11	1.56E+07	1.56E+07	8.70E+07	free	clamped	clamped	0.258	0.475	-14.21	-0.08	11/10
12	1.56E+07	1.56E+07	8.70E+07	clamped	free	clamped	0.301	0.436	-0.21	-8.32	12/10
13	1.56E+07	1.56E+07	8.70E+07	clamped	clamped	free	0.301	0.476	0.00	0.00	13/10
14	1.56E+07	1.56E+07	8.70E+07	free	free	free	0.258	0.436	-19.97	-18.09	14/1
15	1.56E+07	1.56E+07	group effect	free	free	free	0.264	0.443	2.25	1.64	15/14
16	group effect	group effect	group effect	free	free	free	0.264	0.443	-18.13	-16.63	16/1

It is difficult to simulate the group effect which takes place between the piles for such a large pile group, as there is little available literature found on this topic. It is well known that when a structure is excited by wind load, the outer piles of the foundation experience more of the force than the inner piles. A Geotechnical expert at Fugro has found that the axial forces in the piles can roughly be divided into three groups, this can be seen in figure 4.5. If the axial force in the middle pile group is F_z, then the outer pile group experiences $1.2F_z$ and the inner pile group $0.8F_z$. Applying the same factors to the spring stiffnesses of the SCIA model, the stiffnesses changes to those shown in table 4.6. The change in stiffness leads to a slightly higher frequency in both directions. This is due to the larger stiffness in the outer pile zone, leading to a larger rotational resistance.

Table 4.6: Change in vertical (left) and horizontal (right) spring stiffness due to group effect

Group effect	K_z $[\frac{kN}{m}]$	K_z $[\frac{kN}{m}]$	Group effect	$K_{x\&y}$ $[\frac{kN}{m}]$	$K_{x\&y}$ $[\frac{kN}{m}]$
Outer piles	8.7E+4×1.2	1.04E+05	Outer piles	1.56E+4×1.2	1.87E+04
Middle piles	8.7E+4	8.70E+04	Middle piles	1.56E+4	1.56E+04
Centre piles	8.7E+4×0.8	6.96E+04	Centre piles	1.56E+4×0.8	1.25E+04

---

[1]These frequencies were calculated using the upper bounds of the translational and rotational foundation stiffnesses, as these stiffnesses resemble the stiffnesses used in the SCIA model.
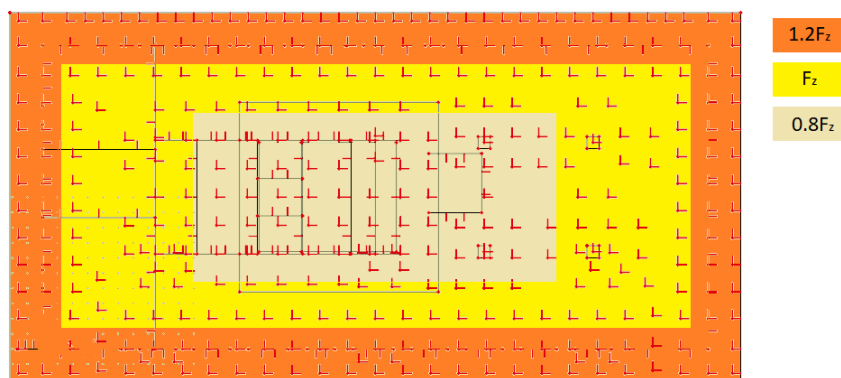
Figure 4.5: Three axial force zones in foundation piles

Change in E-modulus with flexible foundation

In the previous chapter, it was seen that when the flexible base (case 4) was introduced to the beam model, the change in frequency due to a change in the superstructure stiffness was significantly reduces when comparing it to the fixed base model. For the beam model, the reduction in frequency when using an E-modulus of $7.5GPa$ for concrete is ±28%, in both directions. When using an E-modulus of $38GPa$, the increase in frequency was ±16%. Both cases are compared to the frequencies calculated using an E-modulus of $20GPa$. Table 4.7 shows the change in frequency due to a change in E-modulus for the SCIA model with flexible foundation. It can be seen that the change in frequency is higher for the SCIA model compared to the beam model.

It was seen that when comparing the influence of the varying superstructure stiffness for the fixed base model, that the SCIA model and beam model behaved the same. This suggests that the difference in results lays in the foundation. In section 3.6.1.2 it was shown that the smaller the ratio between the substructure and superstructure stiffness ($\frac{K_r L}{EI}$), the greater a change in superstructure stiffness influences the frequency. As the SCIA model shows greater differences in frequency, it would suggest that the substructure stiffness is smaller than that of the beam model, even after the group effect is applied. This is probably due to the deformation of the foundation slab, which is not taken into account when determining the single spring stiffness of the beam model.

Table 4.7: Change in frequency due to a change in E-modulus for SCIA model with flexible foundation.

	E [GPa]				Frequency [Hz]		difference %	
Runs	Tube	Floors	Core	Foundation	First	Second	First	Second
16	20	20	20	20	0.264	0.443	-	-
17	38	38	38	38	0.320	0.540	21.42	21.73
18	7.5	7.5	7.5	7.5	0.181	0.305	-31.25	-31.19

Change in connection spring stiffness

In all the previous analyses, the spring connections between the 2D elements were models as rigid connections. In reality, this is an overestimation of the stiffness of the connection, as there is most likely some deformation in the connected area. To see if the connections between the 2D elements affect the frequency of the structure, the axial rotational stiffness in the springs are set to zero. This represents a hinged connection between the 2D elements. After the modal analysis was performed, a negligible reduction of 1% and 0.8% was seen in the first and second translational frequencies. However, the eigen frequencies of the individual 2D elements were affected significantly more by the change in the spring stiffness. Due to the relaxation of the boundary conditions of the individual 2D elements, they are more prone to vibration modes associated with plates.

Influence of stiffness systems

In the calculation for the bending stiffness of the superstructure done in the previous chapter, only the

outer tube and the three cores were taken into account. The stiffness of the floors and the addition of the columns and beams were assumed were not included in the calculation. To be able to quantify the influence each of the stiffness systems have on the frequency, each system was created in a separate layer in SCIA. These layers can be turned on or off during, as to be included or excluded during an analysis. The change in frequency can then be linked to the excluded stiffness system. Fo run 20 the beams were excluded from the model and a reduction of 0.23% and 1.66% was seen in the first and second frequency. It was expected that the beams would have a larger influence on the second translation frequency, as all beams are placed in the longitudinal direction of the structure. Table 4.8 shows which systems are excluded and the change in frequency.

If the columns were included in the bending moment calculations in the previous chapter, at most, the columns would only be 0.003% op the total bending stiffness. This validates the assumption that the columns can be ignored ion the bending stiffness calculation. For run 21, the columns were excluded from the analysis. Surprisingly, the reduction in frequency is 0.41% and 0.94% for the first and second frequency. Even though this is still a negligible decrease in frequency, it is significantly more than the contribution to the bending stiffness of the superstructure.

Apart from the tube, the cores contribute the most to the bending stiffness of the superstructure. In the calculation of the bending stiffness of the beam models, it was assumed that the cores work as separate stiffness systems, and that the floor does not transfer loads between cores and from the cores to the outer tube. With this assumption, the cores comprised of 6% of the total inertia in the weak direction, and 0.3% in the strong direction. After excluding the cores from the analysis, the first translational frequency was reduced by 4.5%. The second translational frequency was reduced with 4.25%. This would mean that the afore mentioned assumption is wrong, as the reduction in frequency is much larger than the assumed reduction in stiffness due to the exclusion of the cores. This would suggest that the floors do transfer load between systems. Interestingly, when comparing the reduction of the frequency caused by the columns and by the cores, the columns have a fairly large influence as the inertia of the columns is very small compared to that of the cores.

The floors can not be excluded from the model, as the walls will start to behave as 4 connected plates and not as a beam. To see how the floors affect the frequency, the E-modulus of the floors are changed. Even though the floors provide the structure with the integrity to behave as a beam, the change in stiffness does not greatly affect the frequency. In the table below, the change in frequency can be seen due to the change in floor stiffness. When comparing the reduction in frequency due to the exclusion of the beams and the change in frequency due to the change in floor stiffness, it can be seen that the beams have quite a large influence compared to the floor stiffness. One would not expect this, as the change in stiffness is thought to be significantly larger when the stiffness of the floors is reduced compared to when the beams are excluded.

Table 4.8: Change in frequency due to the exclusion of stiffness systems

Runs	E [GPa]				Included						Frequency [Hz]		difference %		between runs
	Tube	Floors	Core	Foundation	Tube	Foundation	Floors	Cores	Columns	Beams	First	Second	First	Second	
16	20	20	20	20	yes	yes	yes	yes	yes	yes	0.2637	0.4435	-	-	-
20	20	20	20	20	yes	yes	yes	yes	yes	no	0.2631	0.4361	-0.23	-1.66	20/16
21	20	20	20	20	yes	yes	yes	yes	no	yes	0.2626	0.4393	-0.41	-0.94	21//16
22	20	20	20	20	yes	yes	yes	no	yes	yes	0.2519	0.4246	-4.47	-4.25	22/16
23	20	20	20	20	yes	yes	yes	no	no	no	0.2510	0.4222	-4.82	-4.79	23/16
24	20	7.5	20	20	yes	yes	yes	no	no	no	0.2480	0.4174	-1.18	-1.15	24/23
25	20	38	20	20	yes	yes	yes	no	no	no	0.2527	0.4248	0.69	0.62	25/23

Reduced building density and the inclusion of non-structural walls and movement joints

Even after the addition of all the stiffness systems to the SCIA model, the frequencies are still under-estimated. Two possible partial reasons for this is that the stiffness is still underestimated and that the density of the structure is overestimated. As mentioned before, a recent article in Cement Magazine [11] stated that, for the NEMC, the frequency of the structure was done 2 years before the construction of the structure was finished. Assuming that the construction of all the stability systems were complete at the time the measurements were done, and that none of the finishing aspects were done, then the mass can be reduced significantly. Excluding all added mass representing the finishing and variable loads, the density of the superstructure decreases from $436.7 \frac{kg}{m^3}$ to $354 \frac{kg}{m^3}$. Due to this 19% decrease

of mass, the frequency increases by 10.7% in both direction in comparison to run 16. The first and second translational frequencies are 0.292 Hz and 0.491 Hz. Even after such a reduction in mass, the calculated frequencies are still underestimated. This leads to the belief that extra stiffness is provided to the structure, which is not taken into account in the current model.

On the west side of the NEMC, a low-rise building is connected to the NEMC. The low-rise structure is connected to the high-rise structure with movement joints. These movement joint make it possible for both structure to move independently of each other, and it was assumed that these joints provide no added stiffness to the high-rise structure. For the next analysis, it is assumed that the movement joints do not work and that the low-rise structure adds stiffness to the high-rise structure. At all locations where movement joints are found, a support is modelled. The support is free to rotate, but is restrained from translating horizontally. This is an overestimation of the possible stiffness movements joints could add to the system, as deformations will always be present in the connections or low-rise structure. after adding the supports, SCIA calculated a first and second translational frequency of 0.638 Hz and 0.981 Hz, respectively.

Another system which was assumed to provide no stiffness to the structure, are the partition walls. These are plasterboard walls which are installed after the floors are set. These walls are assumed to carry none of the load and are made of a panel with a relatively low stiffness. In literature mentioned in section 2, it was shown that these non-structural element can, in some cases, increase the structure's natural frequencies significantly. Using an architectural drawing, the basic layout of the NEMC was found. This was used to create the wall system, as shown in figure 4.6. In one study [53] it was found that the E-modulus of such plasterboard walls range between $2.1GPa$ and $4.1GPa$, an E-modulus of $2.5GPa$ was thus chosen for the modelled partitioning walls. The partitioning walls are connected to the floors and outer tube with hinged connection. To be able to quantify the amount of stiffness the walls add, the walls are massless, as the added mass will decrease the determined frequencies. After the walls were added, there was an increase of 8.5% and 6.9% in the first and second translational frequencies, the calculated frequencies are 0.317Hz and 0.525Hz.

(a) Floor layout of NEMC   (b) Modelled partitioning walls in SCIA
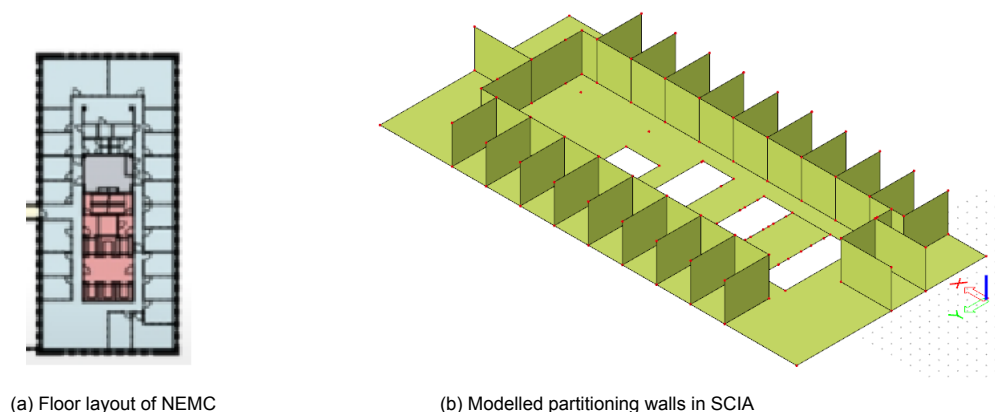
Figure 4.6: Floor plan and added partitioning walls to the SCIA model

4.4. Conclusion

The purpose of this chapter was to investigate the influence different structural systems have on the natural frequency using the finite element software SCIA Engineer. This was done by creating a model of the new Erasmus Medical Centre, consisting of all the structural systems specified in the design. The individual stiffness systems were all created in their own layer. These layers could be turned on or off for each analysis. In this way, it is possible to quantify the influence the turned off layer has on the frequency, by comparing the change in frequency between two analyses.

The first modal analysis was done for the model with a fixed base and includes all stiffness systems. This can be compared with case 1 of the beam models. The first two eigen frequencies calculated by SCIA Engineer were 0.32 Hz and 0.53 Hz. From this result, it can already be seen that the lacking frequency needed to reach the measured frequencies do not come from the stiffness systems which

were ignored in the beam models. This leads to the conclusion that the structure gains stiffness from a source which is still not taken into account.

For the model where a flexible foundation is assumed and where group effect is taken into account, the determined frequencies were 0.26 Hz and 0.44 Hz for the first and second frequencies. When comparing the results of the fixed base and flexible base SCIA models to the beams model results, the beam model provides higher frequencies, even though the columns, beams and floors are not taken into account when determining the bending stiffness.

In further analyses it was shown that the cores, contribute to ±4.5% of the frequency, whereas the contribution of the columns and beams are negligible for the NEMC model.

The results of the complete NEMC model, which includes all the stiffness systems, still underestimated the frequencies. This shows that either the stiffness is underestimated, the density is overestimated, or both. It was later found that the measurements done on the NEMC took place 2 years before the completion of the structure. After the assumption was made that all structural systems were in place at the time of the measurements and that the mass of the finishings and variable loads could be ignored, the frequency was calculated to be 0.29 Hz and 0.49 Hz for the first and second eigen frequency.

Next systems were added to the model which were initially assumed not to provide the structure with stiffness. One of these systems is the partitioning walls. After the walls were added, the frequency was increased with 8.5% and 6.9% is the first and second frequency, respectively. It must be noted that due to the fact that the layout for the partitioning walls are the same for all levels, the load in the partition walls transfers straight to the partition walls below and that no loads are transferred through the floors. In reality, the layout of the partition walls is most likely not constant for each level, this would result in a lesser increase in frequency.

Lastly, the assumption was made that the movement joints between the high-rise and low-rise structure are defective. At the location of each movement joint, a hinge support was placed to restrict the structure from translating horizontally. This essentially shortens the height of the structure, which increases the overall stiffness. This resulted in frequencies of 0.64 Hz and 0.98 Hz. It must however be noted that the assumption of defective movement joints being represented by hinged supports, is an unrealistic overestimation of the stiffness the low-rise structure could add to the high-rise structure.

5

Conclusion

The aim of this research was to determine the reason for the underestimation of the natural frequency for high-rise structures during the design phase. Commonly used methods to determine the natural frequency are by using empirical formulae based on measured data, calculating the frequencies using beam theory and creating elaborate models and using FEM software to determine the natural frequency. Each method having their own advantages and disadvantages. Often, over simplified assumptions have to be made when using these methods, with the result that there is often an error in the determination of the frequencies. According to an article on Gebiedsontwikkeling, by the year 2040, the predicted number of high-rise structures above 70 meters in the Netherlands will grow from the current 220 buildings to 450 buildings [36]. This shows the increasing need to be able to accurately predict the natural frequency during the design of these structures. Figure 5.1 shows that the underestimation of the natural frequency of 50%, which is not uncommon, can lead to an overestimation of the design base moment and base shear of between 20% to 30%. This could lead to the over designing of structures, which is uneconomical. The natural frequency is also often used in the determination of the damping and comfort of high-rise structures, which can have further influence on the design.

(a) Base Moment vs Frequency   (b) Base Shear vs Frequency
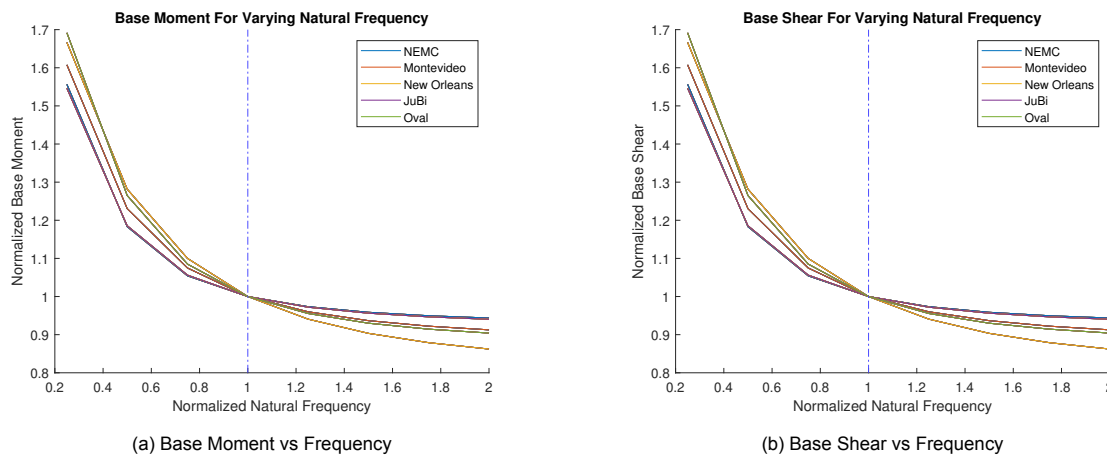
Figure 5.1: Normalized base moment and base shear for varying frequencies

To gain more understanding in factors influencing the natural frequency, five high-rise structures in the Netherlands were used as case studies. For all these structures, TNO have measured the natural frequencies. In Chapter 3, five different beam models were looked at, each model having the purpose of quantifying the influence of a certain parameter on the frequency of the model. From the parameters included in the five models, there were three parameters which had a significant influence on the frequency. These were the superstructure bending stiffness and density, and the rotational spring

stiffness of the foundation. For the models where the rotational spring was present, it was found that the influence the bending stiffness and the rotational stiffness had on the frequency, depended on the ratio between these two stiffnesses. The translational spring and foundation mass were found to have a negligible effect on the frequency. The influence different beam theories have on the natural frequencies of the five cases was also studies. The overall conclusion is that there is little difference in the results between the two beam theories. In four of the five cases, the Timoshenko beam provided slightly higher frequencies when compared to the Euler-Bernoulli beam. Only in the case of the Oval tower were lower frequencies computed. It was found that the ratio between $\frac{G\kappa A}{EI}$ was the factor which influences if the Timoshenko beam frequency increases or decreases from that of the Euler-Bernoulli beam. Even though the Timoshenko beam incorporates an extra parameter into the frequency calculation, when weighing the effort and computational time needed for the Timoshenko beam model, with the relative ease of the Euler beam, the slight difference in results is not worth it.

Often during the design phase of a high-rise structure, the parameters of the beam model are simplified to be uniform over the height of the beam. This is often an over simplification, as the stiffness and density of structures often decrease over their height. The analyses done in Chapter 3 were done for the simplified uniform beam and for a multibeam model. This proved to have a significant influence on the frequency, increasing the frequency as much as 15% in the case of the JuBi tower.

When comparing the results of the different beam models to the measured frequencies for the respected buildings, it was seen that for nearly all cases, the frequencies determined by the beam models were severely underestimated. Even in the case of a fixed base, the frequencies were underestimated. This leads to the conclusion that either the bending stiffness is underestimated or the density is overestimated. However, after the frequencies determined using the lower bound of the densities were still underestimated, it can be concluded the underestimation of the frequencies is due to the underestimation of the bending stiffness of the structures. This leads to the assumption that there are stiffness systems which are not yet taken into account in the bending stiffness calculations.

To be able to take into account all the stiffness systems in the structure, a complete model was created of the new Erasmus medical centre in SCIA Engineer as done in Chapter 4. Stiffness systems such as the columns, floors and beams, which were assumed negligible in Chapter 3, were added to the SCIA model. Each system was created in its own layer, these layers could be turned on or off in the modal analyses. In this way, the influence the specific systems have on the natural frequency could be quantified.

From the analyses done, it was concluded that the assumption that the beams and columns could be neglected in the stiffness calculation, was accurate. The influence these systems had on the first eigen frequency was less than 0.5%. It must be noted that the beams and columns should not be neglected for each case. Literature shows that when dealing with a frame like structure, that the beams and columns significantly influence the frequency of those structures.

To determine how the floors influence the frequencies, the E-modulus of the floors were changed from $20GPa$ to $7.5GPa$ and $38GPa$, respectively. It was found that these changes in E-modulus did not have a great effect on the frequencies, thus proving the floors can also be ignored in the stiffness calculations. The floors are however very important in the frequency calculation of the SCIA model. The floors effect the global behaviour of the structure. If the floors are omitted from the analyses, the global behaviour of the walls will be plate like, instead of the cantilever behaviour which is reached when the floors are present.

The addition of the cores and flexible foundation has the expected results. As the cores only comprise of 6% of the total bending stiffness, the influence on the frequency is just 4.5%. The addition of the flexible foundation results in a decrease in the frequency of around 20%, this is in the same range as that for the beam model.

Even with all the stiffness systems which were neglected in Chapter 3 added to the model, the frequency was still underestimated. This led to the belief that there might be sources of stiffness which provide the structure with extra stiffness. One such system could be the partition walls found in the building. A floor layout was assumed and the partition walls were added to the model. These were modelled as massless as to see how they affect the stiffness of the structure. The partition walls were modelled with plate element with an E-modulus of $2.5GPA$ as to represent gypsum walls. These plate elements were fixed to the walls and floors with hinged connections. The addition of these partition walls resulted in an increase in frequency of 8.5%. Even with the further increase, the measured frequencies were still

not reached.

Lastly, the assumption that the low-rise structure does not affect the high-rise structure was relaxed. Between the two structure, movement joints are placed. These joints were assumed not word work, thus making it possible for the high-rise structure to transfer loads to the low-rise structure. This was done by modelling supports at the locations of each movement joint. This finally led to frequencies which surpass the measured frequencies. It must however be noted that the assumption of defective movement joints being represented by hinged supports, is an unrealistic overestimation of the stiffness the low-rise structure could add to the high-rise structure. The effect defective movement joints might have on the high-rise building will have to be researched in more detail.

This thesis shed light on factors effecting the natural frequency of high-rise structures. by varying the magnitudes of various structural parameters, the influence these parameters have on the natural frequency were quantified. It was found that the three parameters which have the greatest effect on the natural frequency are the bending stiffness, density and rotational spring stiffness. Due to the underestimation of the computed natural frequencies, it was concluded that the in the calculations, the stiffness of the superstructure is underestimated and that there might be internal and external systems providing the structure with extra stiffness. Further research will have to be done to exactly pinpoint where this extra stiffness comes from. When comparing the different methods of determining the natural frequencies, in most cases, the empirical formula adopted by the NEN-EN 1991-1-4 provides frequencies the closest to the measured frequencies. The following chapter will provide recommendation for future research to further our understanding on the topics discussed in the thesis.

6

Recommendations

6.1. Measurements of dynamic properties

As the amount of high-rise structures is planned to be doubled in the next 20 years [36], it creates a good opportunity to use these structures to gain a better understanding of the dynamic properties of high-rise structures. By measuring the dynamic properties of these structures, the true behaviour of these structures can be seen. These measurements can be used to categorize different structural systems, determine empirical formulae specific to the Netherlands and determine the effectiveness of approximating a structure with different beams, just to name a few uses.

Empirical formula

The current method of determining the natural frequency adopted by the NEN-EN1991-4-1, is an empirical formula based on data of high-rise structures built in America and Japan. These are often structures built on foundations close to bedrock, resulting in the boundary conditions of the foundation being relatively stiff. This is often not the case in the Netherlands. With the existing high-rise structures, and all the planned high-rise structures, in the Netherlands, there are enough structures to form a sufficient data pool to create an empirical formula for the natural frequencies specific to structures in the Netherlands. The acceleration measurements are only needed at one height in the structure, as this is enough to determine the natural frequencies. As more measurements are made and added to the data pool used to determine the empirical formula, the more accurate the frequency approximation will be. If enough data is available, structures can be categorized according to their structural systems, and frequency equations can be made for the different structural systems.

Cataloguing different structural types

Due to the different types of complex high-rise structure designs, high-rise structures can not merely be classified as rigid frames or tubes, as once was possible. Kijewski-Correa has have catalogued more than 30 variations of structural systems used today. This shows that it is not possible to analyse high-rise structures with the assumption that they are going to behave the same. To gain a better understanding of the dynamic behaviour of these different types of high-rise structures, more measurements must be done. To be able to categorize these structures, special attention must be placed on the mode shapes. This means that measurements must be done on several heights in the structure, to be able to accurately capture the true mode shapes. The more discontinuous the structure is, the more measurements must be taken, as the different structural sections will behave differently. The accurate measurements of mode shapes can also provide insight about the influence of connecting structures. A method which can be used to catalogue the different structures, is by using the Differential Degree of Cantilever Action (dDCA) proposed by Bartolini [5], which compares the measured mode shapes with an ideal cantilever beam. If a correlation between the natural frequencies of structures with the same dDCA score is found, then these structures can be categorized together. If enough data is available for different categories, empirical formulae for the frequencies can also be determined for each category. By determining the dDCA score of different structural designs, it will also become more clear if a

73

bending beam is an accurate representation of these structures in the design phase. Further research can also be done on how to integrate the dDCA score of a structure with beam theory.
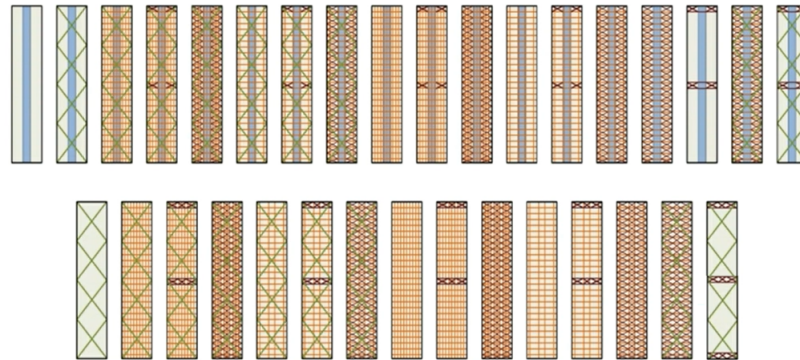
Figure 6.1: Different types of structural systems used in high-rise structures. *(Kijewski-Correa, T. (2020.* 'Predicting the energy dissipative potential of tall buildings: Insights from sustained full-scale monitoring'[conference presentation]. EURODYN 2020.

6.2. Influence of the low-rise structure

Structural pounding is a term often used in seismic engineering. Pounding occurs when two or more adjacent structures, which are in proximity, exert forces on each other due to collision caused by lateral loading. Many studies have been done studying pounding due to earthquakes [3, 34, 35, 40, 41, 47], but Abdullah et al. [1] stated that structural pounding can also occur due to the out-of-phase vibrations caused by wind excitation. As the oscillations caused by wind are less violent and in a more constant direction when compared to seismic excitations, the pounding could less noticeable. The contact between two adjacent structures is often due to the structures having different heights and stiffnesses. This leads the structures to vibrate out of phase, which can cause the structures to collide.
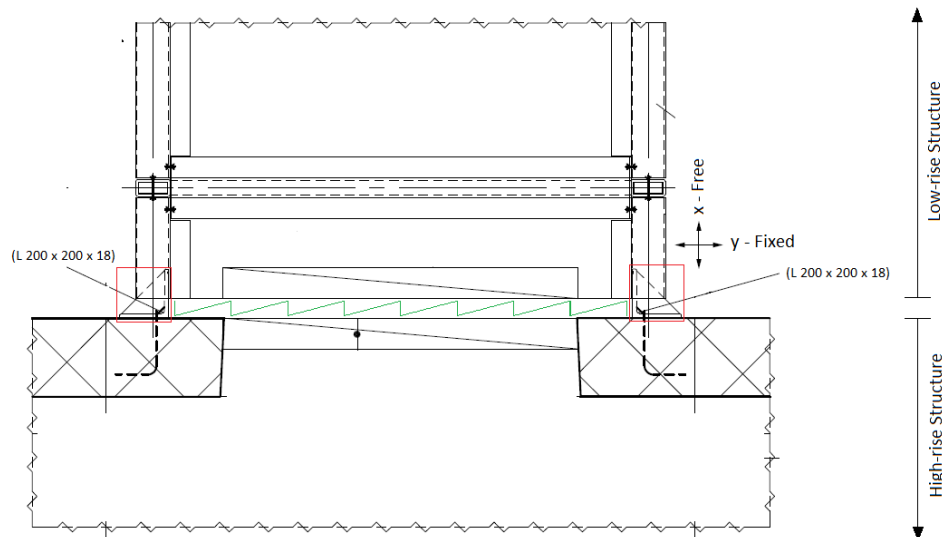
Figure 6.2: Top view of the movement joint between the low- and high-rise structures of the NEMC.

Between the high-rise and low-rise structures of the new Erasmus Medical Centre, movement joints are present at locations where the structures connect to each other. Figure 6.2 shows one of these movement joints. In the figure it can be seen that between the low- and high-rise building a gap, shown by the green lines, is present. It can also be seen that the floor of the low-rise building is connected to the high-rise building by two L-angles, shown in red. The figure shows that the angle is fixed to both

structures in the y-direction (strong), but free to move in the x-direction. His is due to the presence of an oil film between the angle and the floor of the low-rise structure. This would mean that the movement joints would provide negligible stiffness to the high-rise structure, but what is this is not the case?

FE Model
A modal analysis is not the only dynamic analysis which can be done in SCIA Engineer. The model can also be loaded with different types of dynamic loads, as to see how the model behaviours under certain conditions. The model can thus be excited by a dynamic wind load, and the motion of the structure can be determined. If the current FE model described in this thesis is excited by a dynamic load, the model will be able to deflect without any influence of the low-rise structure. The deflections of the nodes at the locations where the low-rise structure would be modelled must be considered. If these nodes deflect more than the distance between the two structures, then there is a possibility that the structures could touch. This would allow the high-rise structure to transfer load to the low-rise structure, resulting in the low-rise structure providing the high-rise structure with extra stiffness. If the deflections of the high-rise structure is small, this does not necessary mean that the structures do not touch. Due to the fact that the two structures have different heights and stiffnesses, the probability of the structures vibrating out of phase is quite high. Once the structures move out of phase, both structures must be considered in the dynamic analysis. The low-rise structure, as shown in figure 6.3, must be modelled next to the high-rise structure. The same dynamic load can now be applied to both structures, and the deflection of the structures can be determined. The nodes located in the circles, shown in figure 6.3, are most likely to collide if deflections are large enough. According to a study done by Jankowski [35], it is often the rotation of structures which lead to the contact between adjacent buildings. If the dynamic analysis proves that there is contact between the two structures when excited by a dynamic wind load, then it can be concluded that the possibility is present that the low-rise structure provided the high-rise structure with extra stiffness.
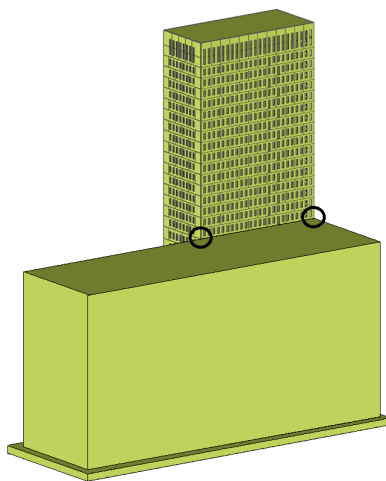
Figure 6.3: NEMC tower with proposed low-rise model.

If the low-rise structure is modelled, then the movement joints can also be added to the model. These can be modelled with springs at the specified locations of these joints given in the design documentation. The spring stiffnesses can be changed as to represent different assumptions made for the effectiveness of these joints. Modal analyses can be done using the two structure model. These results can then be compared to the single structure model to see how the low-rise building influences the frequency for different movement joint assumptions.

Measurements
To really understand if any forces are transferred from the high-rise structure to the low-rise structure, measurements at the movement joints can be taken. According to the design specifications of the movement joints, between the L-angles and the floor of the low-rise building, an oil film is present. The

purpose of the film is to let the two structure move freely in the x-direction, without load transfer. If the oil film is not effective, load will be transferred from one structure to the other through the L-angles. This load transfer will cause strains to form in the L-angles. These strains can be measured by placing strain gauges at certain sections of the angles. Section 1, marked in blue, in figure 6.4 is a section that could experience strains as loads are transferred between the two structures. The strains measured in these angles can be used to determine the influence of the ill effective movement joint. They can also provide insight to the magnitude of the spring stiffnesses, if these movement joints were modelled as springs in a FE model.
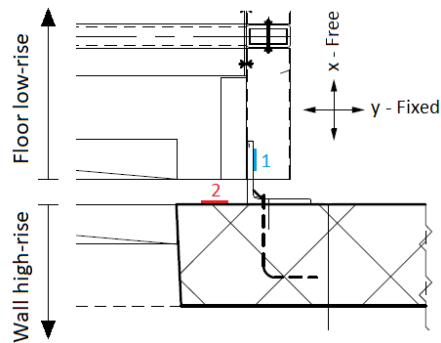
Figure 6.4: Proposed measurement apparatus setup.
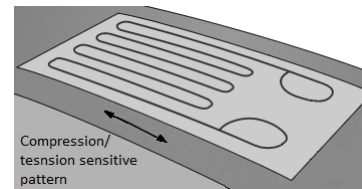
(a) Strain gauge
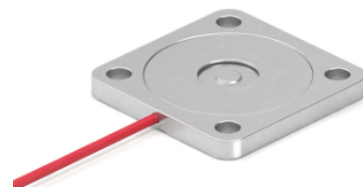
(b) Force gauge

Figure 6.5: Structural strain and force gauges

It could occur that the movement joints do work properly, but that load is still transferred. If the structures deflect out of phase, the motion in opposite directions could cause the structures to touch. This would mean that the floor of the low-rise structure slides past the movement joint until it reaches the wall of the high-rise structure. If contact takes place, force is transferred from one structure to the other. To see if this occurs, a force gauge can be placed between the floor of the low-rise structure and the wall of the high-rise structure, as shown in red in figure 6.4. Ideally, a thin button gauge as shown in figure 6.5b can be used, as these type of gauges will not significantly decrease the distance between the two structures.

6.3. Further recommendations

Update of beam models
In Chapter 3 only the translational and rotational springs are taken into account to represent the foundation. The beam models can be updated as to also take into account the coupling term between these translational and rotational spring. The beam models also ignore secondary effects, such as the axial loading in the structure. Further research can be done to quantify the influence of these effects.

E-modulus measurements
In Chapter 3 it can be seen that the E-modulus plays a large role in the stiffness of a structure. Various sources have reported that the E-modulus used in the design, and the E-modulus is reality, can differ [44, 42, 57]. By knowing the real value of the E-modulus, a better understanding of the stiffness of the structure will be obtained. Non-destructive methods, such as the Ultrasonic Pulse Method, can be used to determine the E-modulus of existing structures. The measured E-moduli can then be compared to the E-modulus given in the design documentation.

Partition walls
This thesis lightly touches on the effect non-structural elements, such as partition walls, have on the natural frequency of the NEMC. A floor layout was assumed and used for every floor. As the layout for each level was the same, the influence the partition walls have, might be overestimated. This is due to

the walls being able to transfer the load straight to the foundation. If different layouts for different levels are assumed, the influence these walls will have could be less. It is recommended to obtain the floor layout of the NEMC and model the partition walls accordingly. In the analyses done in Chapter 4, an E-modulus of the walls as assumed bases on values found in literature. Furthermore, the connections between the tube walls, floors and partition walls were modelled as hinges. Laboratory test could be done on the type of partition walls used in the NEMC, to find the true E-modulus and the stiffness of the connections. The connections can then be modelled by springs, to better represent the real connections.

Appendices

A
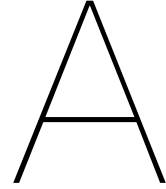
Beam Theory

In this appendix, the basic beam theories used throughout the report is given. The two theories discussed are the Euler-Bernoulli beam and the Timoshenko beam. The theories given here are based on [55].

A.1. Euler-Bernoulli Beam

The Euler-Bernoulli (EB) beam theory was first formulated in 1744 by Leonhard Euler and Daniel Bernoulli. The EB beam is one of the reference models for the analysis of slender homogeneous structures under bending loading [16]. For the EB beam, the following assumptions are made:

- Shear strains in all directions are zero.

- The displacements of the body are small.

- The longitudinal axis of the beam is straight and symmetric about the y-axis.

The last key assumption of this beam is that when the beam is subjected to loading, the plane cross-section remains plane and normal to the beam axis. This assumption is only valid due to the assumption that the shear and torsional deformations are small when comparing them to the deformations caused by normal stress and bending.

The sign convention shown in figure A.1 throughout this section.
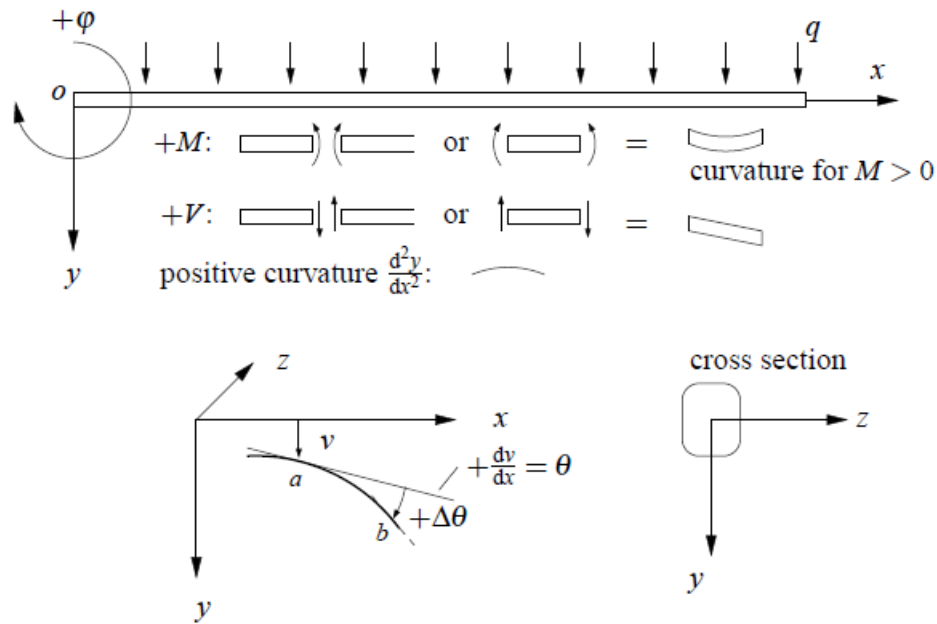
Figure A.1: Sign convention for Euler-Bernoulli beam

A.1.1. Relationship between deflection and curvature

In figure A.2a a curved 1D element can be seen. It is easy to see that the following equations hold for the curved element.

$$ds = \rho d\theta$$
$$\kappa = \frac{1}{\rho} = \frac{d\theta}{ds} \tag{A.1}$$

Where κ is the curvature of the element and ρ[1] is the radius of curvature. By differentiating the displacement of the element, the slope of the curve is found, which in turn can be related to the angle of rotation (θ) of the element, as shown in equation A.2 and can be seen in figure A.2b. As dx is infinitesimally small, ds can be approximated by a straight line, and as we only consider small rotations, the following can be approximated: $sin\theta \approx tan\theta \approx \theta$ and $cos\theta \approx 1$. Now taking the first derivative of θ, then equation A.3 holds. With v being the displacement in the y-direction.

$$\frac{dv}{ds} = tan\theta \tag{A.2}$$

$$\frac{d^2v}{dx^2} = \kappa = \frac{1}{\rho} \tag{A.3}$$

---

[1]Note that the ρ representing the radius of curvature in the Euler-Bernoulli beam theory has nothing to do with the ρ used throughout the rest of this report. In the main body of the report, ρ represents a density.

(a) Curved 1D element   (b) Curved element with small rotation approximation
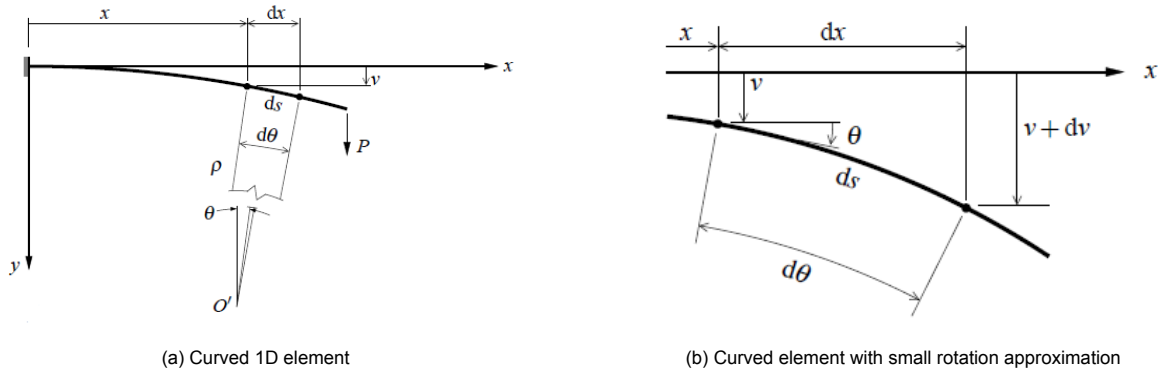
Figure A.2: Assumption of small rotations

A.1.2. Relationship between curvature and longitudinal strain

The relationship between the curvature of the beam and the longitudinal strain can be found by applying two coupled moments (M_0) on either side of a portion of the beam, as shown in figure A.3. The coupled moments produce a positive curvature and a negative bending moment in the beam element. As the beam element bends, the top fibres elongate, causing tension and the bottom fibres shorten, causing compression. On the neutral axis, there is no elongation or shortening of the fibres, this is shown by the dashed line in figure A.3. The point O' in the figure is where planes mn and pq of the deformed beam intersect. The angle between these two planes is given by $d\theta$ and the distance from O' to the neutral axis is ρ. As there is no change in length on the neutral axis, the distance between planes mn and pq (dx) can be related to the radius of curvature ass shown in equation A.4. Due to the shortening of the bottom fibre of the beam element, the length of segment ef is smaller than dx. At a distance y from the natural axis, segment ef has a length ds_{ef} as shown in equation A.4. The strain of segment ef can be found by dividing the difference in length of dx and ds_{ef} by the original length, as shown in equation A.5.

$$dx = \rho d\theta$$
$$ds_{ef} = (\rho - y)d\theta \tag{A.4}$$

$$\epsilon_{xx}^{ef} = \frac{ds_{ef} - dx}{dx} = -\kappa y \tag{A.5}$$
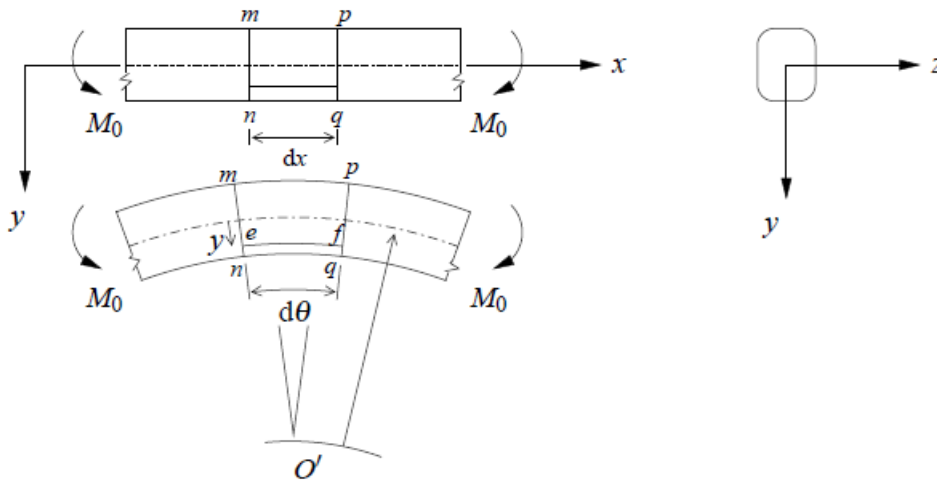
Figure A.3: Bending of a beam element

A.1.3. Relationship between external load, shear force and bending moment

Using an infinitesimal element dx as shown in figure A.4, equilibrium of the segment can be used to find the relationship between external load, shear force and bending moment. Using vertical force equilibrium, the relationship of the external force q and the shear force V can be expressed. This is shown in equation A.6. Similarly, using the moment equilibrium, the relationship between the bending moment and shear can be expressed and is given in equation A.7. It must be noted that the product of differentials $dxdV$ is taken to be zero, and that this equation only holds if the segment is loaded with a distributed load.

$$qdx + V + dV - V = 0$$
$$\frac{dV}{dx} = -q \tag{A.6}$$

$$-M - \frac{1}{2}dxV - \frac{1}{2}dxV - \frac{1}{2}dxdV + M + dM = 0$$
$$\frac{dM}{dx} = V \tag{A.7}$$
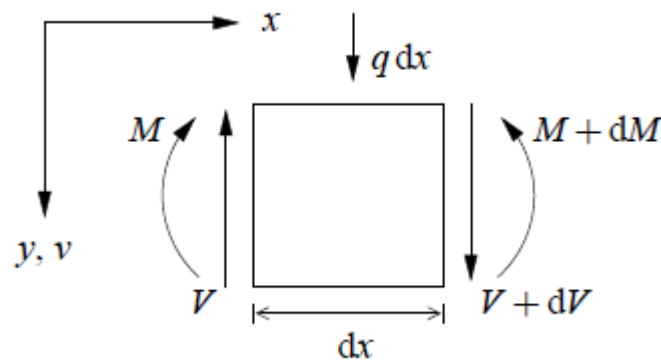
Figure A.4: Infinitesimal Euler-Bernoulli beam segment

A.1.4. Relationship between internal bending moment and curvature

Using Hooke's law, it is possible to relate strains and stresses by introducing the Young's modulus (E). Taking the stress in the x-direction as an example, the strain can be related to the stress as shown in equation A.8. Furthermore, using equation A.5, the stress can also be related to the curvature of the beam. Figure A.5 a beam element with an internal moment on one end and its corresponding stress distribution at the other end. Due to the beam element being in equilibrium, the internal moment can be equated to the internal coupling resulting from the stress distribution, as shown in equation A.9. By combining equations A.8 and A.9, the internal moment can be related to the curvature of the beam element, as done in equation A.10.

$$\sigma_x = E\epsilon_x = -\kappa y \tag{A.8}$$

$$M = \int dM = \int \sigma_x y dA \tag{A.9}$$

$$M = \int \sigma_x y dA = -\int E\kappa y^2 dA = -EI\kappa \tag{A.10}$$

where

$$I = \int y^2 \, dA \tag{A.11}$$

is the moment of inertia around the neutral axis. The product of the Youngs's modulus and moment of inertia (EI) is known as the bending stiffness of the beam element.
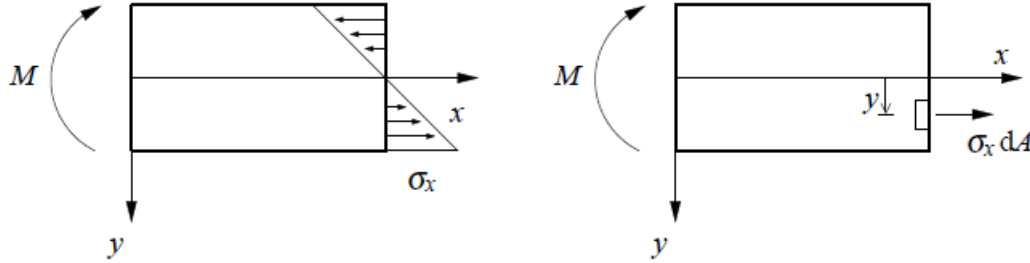
Figure A.5: Equilibrium due to internal moment and its corresponding stress distribution

A.1.5. Differential equation of the transverse deflection

Using equations A.3 and A.10 the differential equation of the deflection is obtained as given in equation A.12, where v is the deflection in the transverse direction. By manipulating equations A.6 and A.7 into equation A.12, the displacement can be related to the external force as shown in equation A.13, and when considering a beam which does not vary in EI, then the fourth order differential equation given in equation A.14 is obtained.

$$\frac{d^2 v}{dx^2} = -\frac{M}{EI} \tag{A.12}$$

$$\frac{d^2}{dx^2}\left(EI\frac{d^2 v}{dx^2}\right) = q \tag{A.13}$$

$$EI\frac{d^4 v}{dx^4} = q \tag{A.14}$$

A.2. Timoshenko Beam

The Timoshenko beam theory was proposed by Stepan Prokfyevich Timoshenko in 1922. The Timoshenko beam theory is an extension to the Euler-Bernoulli beam. The main difference is where Euler-Bernoulli assumed that plane sections remain plane and normal to the deformed centreline, Timoshenko relaxes this assumption and introduces a first-order transverse shear effect. This is done by introducing an additional degree of freedom describing the additional rotation of the bending slope.

A.2.1. Governing equations of a shear beam

Before being able to combine bending and shear, the governing equations of a beam in pure shear are needed. Shear distortion (γ) describes the shear deformation caused by a shear force, as shown in figure A.6. The shear distortion is related to a small displacement (dv) over the width of the infinitesimal segment, as shown in equation A.15. The constitutive equation of the shear element can again be formulated by using Hooke's law, using the shear stress (τ) and the shear distortion. The shear stress can also be related to the shear force (V) and the area the shear force is applied to (A_s). These two relations are shown in equation A.16.

$$\gamma \approx \frac{dv}{dx} \tag{A.15}$$

$$\tau = G\gamma$$
$$\tau = \frac{V}{A_s}$$

(A.16)

Using the above-mentioned equation, the shear deformation can be related to shear force and shear stiffness. This is shown in equation A.17, where GA_s is the shear stiffness of the beam. When considering moment equilibrium of the infinitesimal shear beam element, as done in the previous section, the same differential equation as given in A.6 is found. Combining equations A.17 and A.6 the second order differential equation A.18 is obtained.

$$\gamma = \frac{dv}{dx} = \frac{V}{GA_s}$$

(A.17)

$$-GA_s\frac{d^2v}{dx^2} = q$$

(A.18)
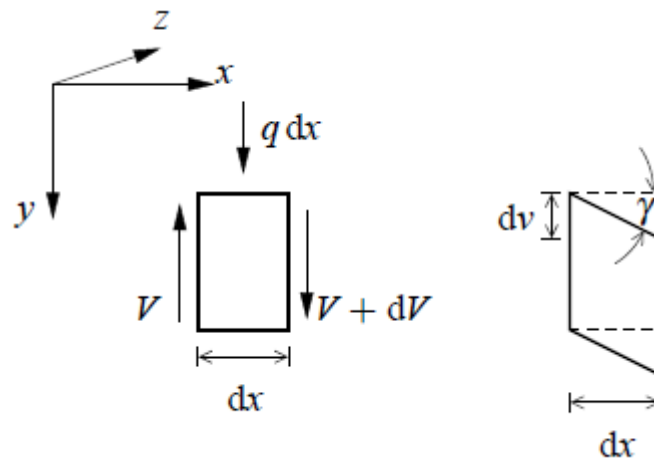
Figure A.6: Infinitesimal shear beam segment and deformed state

A.2.2. Kinematic assumptions for the Timoshenko beam

For the Timoshenko beam theory, there are two independent kinematic quantities. The first is the transverse deflection ($v(x)$) and the second is the cross-sectional rotation ($\phi(x)$), where ϕ is the rotation between the cross-section and the vertical-axis. Consider the point p, taken a distance y from the centre of the axis, as shown in figure A.7. The displacement field of the point can be described by equation A.19.

$$s_x(x, y) = -y\phi(x)$$
$$s_y(x, y) = v(x)$$

(A.19)
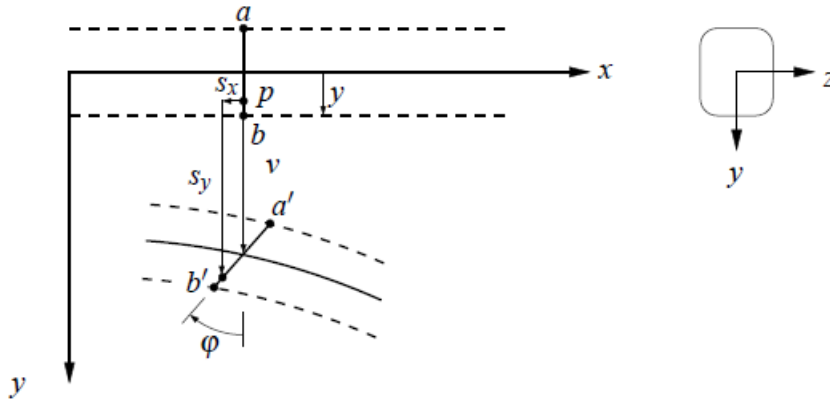
Figure A.7: Bending of a Timoshenko beam

By taking the derivatives of the non-zero components of the displacement field, the strain field shown below is obtained.

$$\epsilon_x = \frac{ds_x}{dx} = -y\frac{d\phi}{dx}$$
$$\gamma_{xy} = \frac{ds_x}{dy} + \frac{ds_y}{dx} = -\phi + \frac{dv}{dx}$$

(A.20)

A.2.3. Relationship between deformations and internal forces
By combining equation A.17 and the second equation of A.20 the shear force can be expressed as shown in A.21.

$$V = GA_s\gamma = GA_s(\frac{dv}{dx} - \phi)$$

(A.21)

Using Hooke's law and substituting in the first equation of A.20, the stress in the beam can be expressed as shown below.

$$\sigma_s = E\epsilon_x = -Ey\frac{d\phi}{dx}$$

(A.22)

Using the same method as shown in equations A.8, A.9 and A.10, and applying this to the Timoshenko beam, expression A.23 for the bending moment in the beam can be obtained.

$$M = -EI\frac{d\phi}{dx}$$

(A.23)

A.2.4. Differential equation for transverse deflection
When considering am infinitesimal beam segment of the Timoshenko beam, the equilibrium equations of the beam are unaffected by the shear deformation, and are thus the same as the equations A.6 and A.7. The differential equations are obtained by eliminating the shear force and bending moments in these equations.

Considering vertical equilibrium of the beam segment and substituting in equation A.21, the first differential equation shown below is found.

$$-q = \frac{dV}{dx} = \frac{d}{dx}(GA_s(\frac{dv}{dx} - \phi)) = GA_s(\frac{d^2v}{dx^2} - \frac{d\phi}{dx})$$

(A.24)

Doing the same for the moment equilibrium and substituting in equation A.23, the second differential equation is obtained.

$$0 = -\frac{dM}{dx} + V = -\frac{d}{dx}\left(-EI\frac{d\phi}{dx}\right) + GA_s\left(\frac{dv}{dx} - \phi\right) = -EI\frac{d^2\phi}{dx^2} + GA_s\left(\frac{dv}{dx} - \phi\right) \tag{A.25}$$

B

Dynamics

mention that all damping is left out due to not influencing the frequency

B.1. Single degree of freedom system

The most basic dynamic system which can be looked at is a lumped mass attached to a spring, as shown in figure B.1. This system is known as a single degree of freedom system, as the lumped mass can only move in the x-direction. Using Newton's second law, the equation of motion of the single degree of freedom system can be written down as shown in equation B.1.

$$m\ddot{x} + kx = F(t) \tag{B.1}$$

with:
$m =$ lumped mass
$k =$ spring stiffness
$x =$ displacement in x-direction
$\ddot{x} =$ acceleration in x-direction
$F(t) =$ external horizontal force
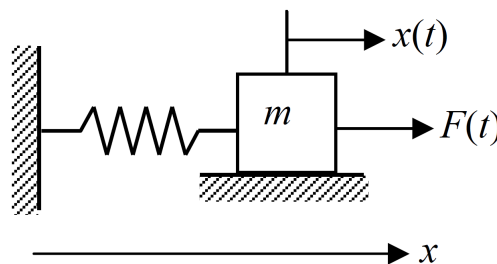
Figure B.1: Mass-spring system

As stated in section 2.2 of this report, the natural frequency is the frequency at which a system oscillates in the absence of an external force. The free vibration of a SDoF system can thus be represented by equation B.2, which is a well known second order ordinary linear differential equation.

$$m\ddot{x} + kx = 0 \tag{B.2}$$

Obtaining the general solution of the above-mentioned differential equation is rather simple and is shown in equation B.3

$$x(t) = A cos(\omega_n t) + B sin(\omega_n t) \tag{B.3}$$

where A and B are unknown constants which can be obtained using the initial conditions and where

$$\omega_n = \sqrt{\frac{k}{m}} \tag{B.4}$$

is the natural frequency of the system measured in $\frac{rad}{s}$. It can be seen in equation B.3 that for any given set of initial conditions, ω_n is the frequency the system will vibrate against. Often the angular frequency (ω) is converted to ordinary frequency measured in Hz. The conversion is done using the equation shown below.

$$f_n = \frac{\omega_n}{2\pi} \tag{B.5}$$

B.2. Continuous systems

In this section, the free vibration of the Euler-Bernoulli and Timoshenko beam will be discussed for several boundary conditions. The main focus of the proceeding sections will be on how the natural frequency of the beams are determined. For the determination of the equation of motion for the continuous beams in this section, the mass and stiffness is taken to be uniform throughout the height of the beam.

B.2.1. Euler-Bernoulli beam

As the external load applied to the beam is time dependent, the motion of the beam must also be time dependent. Consider the beam and infinitesimal beam segment shown in figure B.2. This is the same beam element as in Appendix A.1, with the exception that the external force is now time dependent. The method of obtaining the kinematic and constitutive relationships stays the same, but as the applied load changes with time, the kinematic and constitutive relationships are also time dependent and are given in equations B.6 and B.7.
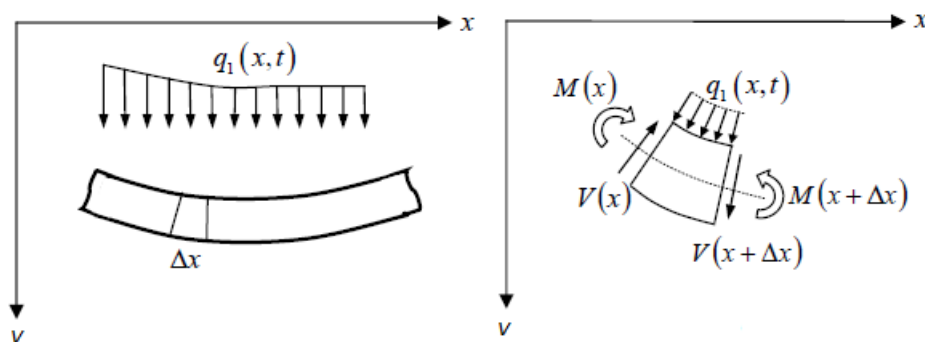
Figure B.2: Bending beam and infinitesimal beam segment with time dependent external load

$$\phi(x,t) = -\frac{dv(x,t)}{dx}$$
$$\kappa(x,t) = -\frac{d^2v(x,t)}{dx^2} \tag{B.6}$$
$$\epsilon(x,t) = -y\frac{d^2v(x,t)}{dx^2}$$

$$M = -EI\frac{d^2v(x,t)}{dx^2} \tag{B.7}$$

To obtain the equation of motion of the beam, the second law of Newton is used. Newton's second law states that force can be equated to the product of mass and acceleration, this is shown in equation B.8. Where m is the mass and a is the acceleration of the beam.

$$\Sigma F = ma \tag{B.8}$$

Considering vertical equilibrium of the infinitesimal beam segment in figure B.2 and combining this with Newton's second law, the first equation in B.9. After applying the Taylor expansion[1] and dividing by Δx, the second equation in B.9 is obtained.

$$\rho A \Delta x \frac{d^2v}{dt^2} = -V(x) + V(x + \Delta x) + q_1 \Delta x$$
$$\rho A \frac{d^2v}{dt^2} = \frac{dV}{dx} + q_1 \tag{B.9}$$

Using relationship A.7 and A.12, and combining them with equation B.2, the equation of motion of the beam is obtained.

$$\rho A \frac{d^2v}{dt^2} = \frac{dV}{dx} + q_1$$
$$\rho A \frac{d^2v}{dt^2} = \frac{d^2}{dx^2}M + q_1 \tag{B.10}$$
$$\rho A \frac{d^2v}{dt^2} + \frac{d^2}{dx^2}(EI\frac{d^2v}{dx^2}) = q_1$$

B.2.2. Free vibration of Euler-Bernoulli beam
As done for the single degree of freedom system, when calculating the natural frequencies of an Euler-Bernoulli beam, the external force must be set to zero. The equation of motion for the free vibration is then given by:

$$\rho A \frac{d^2v}{dt^2} + \frac{d^2}{dx^2}(EI\frac{d^2v}{dx^2}) = 0 \tag{B.11}$$

The separation of variables method is then used to split the equation of motion into a time dependent and a space dependent part. This is done by assuming that the displacement of the system can be described by the product of a time dependent term and a space dependent term, as shown in equation B.12. Here $W(x)$ and $\Psi(t)$ represent the spacial coordinate along the beam and time, respectively.

---

[1]The Taylor expansion used here is the approximation that $V(x + \Delta x) \approx V(x) + \frac{dV}{dx}\Delta x$

$$v(x,t) = W(x)\Psi(t) \tag{B.12}$$

Substituting this equation above in the equation of motion for free vibration and then dividing with $W(x)\Psi(t)\rho A$, the equation of motion can be written down in the following form:

$$\frac{1}{\Psi}\frac{d^2\Psi}{dt^2} + \frac{EI}{\rho A}\frac{1}{W}\frac{d^4W}{dx^4} = 0 \tag{B.13}$$

As can be seen in equation B.13, the first term is only dependent on time and the second term is only dependent on the spacial coordinate. The only way to satisfy the equation is if both terms are equal to a separation constant, as shown in equation B.14. The separation constant has to be introduced as shown below for the beam to be able to perform harmonic vibrations. In the equations ω represents the frequency of the vibration of the beam. For simplification of the second equation, a has been introduced as $a^2 = \frac{EI}{\rho A}$.

$$\frac{1}{\Psi}\frac{d^2\Psi}{dt^2} = -\omega^2$$
$$a^2\frac{1}{W}\frac{d^4W}{dx^4} = \omega^2 \tag{B.14}$$

The first equation of B.14 has a well known general solution which represents the harmonic motion and is given by

$$\Psi = A\sin(\omega t) + B\cos(\omega t) \tag{B.15}$$

Changing the form of the second equation in B.14 as shown below

$$\frac{d^4W}{dx^4} - \frac{\omega^2}{a^2}W = 0 \tag{B.16}$$

The general solution of this equation can be given in the form

$$W(x) = \Sigma_{n=1}^4 \tilde{C}_n exp(s_n x) \tag{B.17}$$

After differentiating equation B.17 four times and then substituting the general solution and the differentiated general solution in to equation B.16, the following characteristic equation is found

$$s_n^4 - \frac{\omega^2}{a^2} = 0 \tag{B.18}$$

Solving the characteristic equation, s_n can be expressed as follows

$$s_1 = \beta, \quad s_2 = -\beta, \quad s_3 = i\beta, \quad s_3 = -i\beta \tag{B.19}$$

with

$$\beta^4 = \frac{\omega^2}{a^2} \tag{B.20}$$

After substituting B.19 back in to the general solution and applying Euler's formula [2] and two complex trigonometric definitions [3] the general solution for the fourth order differential equation can be written as

$$W = C_1 \sin(\beta x) + C_2 \cos(\beta x) + C_3 \sinh(\beta x) + C_4 \cosh(\beta x) \tag{B.21}$$

The above-mentioned general solution has the following derivatives

$$
\begin{aligned}
\frac{dW}{dx} &= C_1 \beta \cos(\beta x) - C_2 \beta \sin(\beta x) + C_3 \beta \cosh(\beta x) + C_4 \beta \sinh(\beta x) \\
\frac{d^2 W}{dx^2} &= -C_1 \beta^2 \sin(\beta x) - C_2 \beta^2 \cos(\beta x) + C_3 \beta^2 \sinh(\beta x) + C_4 \beta^2 \cosh(\beta x) \\
\frac{d^3 W}{dx^3} &= -C_1 \beta^3 \cos(\beta x) + C_2 \beta^3 \sin(\beta x) + C_3 \beta^3 \cosh(\beta x) + C_4 \beta^3 \sinh(\beta x)
\end{aligned}
\tag{B.22}
$$

B.2.3. Boundary conditions

To be able to determine the coefficients in equation B.21 boundary conditions for the beam have to be defined. In this section, four different sets of boundary conditions are looked at. These are the boundary conditions considered in the body of this report, they are:

1. fixed support - free end

2. support with rotational spring - free end

3. support with rotational and translational spring - free end

4. support with rotational and translational spring and added foundation mass - free end

These boundary conditions are graphically shown in figure B.3.
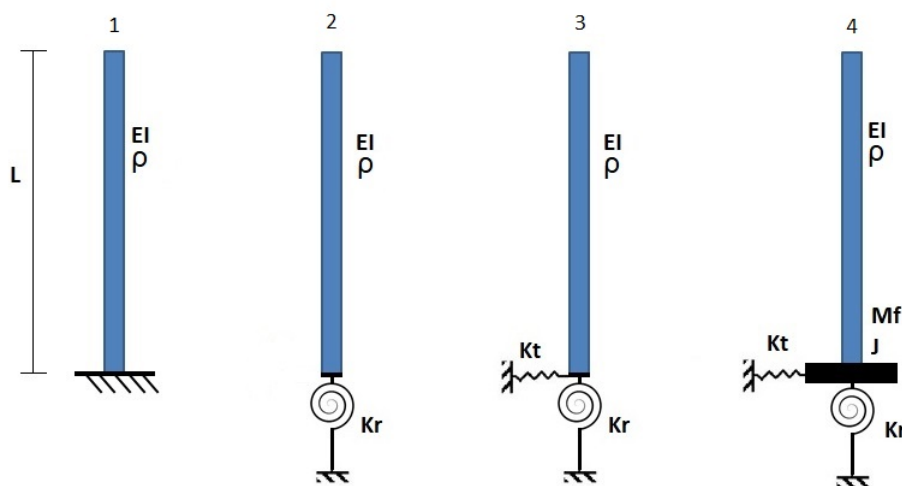
Figure B.3: Four boundary condition sets for Euler-Bernoulli beam

fixed support - free end

The boundary condition are the conditions found at the base and the free side of the beam. The boundary conditions for Case 1 case are shown below.

---

[2]Euler's formula: $e^{ix} = cos(x) + isin(x)$
[3]$\sinh x = -i \sin(ix)$ and $\cosh x = \cos(ix)$

At $x = 0$:

$W(x) = 0$

$\dfrac{dW(x)}{dx} = 0$

(B.23)

At $x = L$:

$\dfrac{d^2 W(x)}{dx^2} = 0$

$\dfrac{d^3 W(x)}{dx^3} = 0$

For the calculation of the natural frequencies of the beam, the coefficients $C1$ to $C4$ are not needed to be known. This leaves the following coefficient matrix determined using the boundary conditions.

$$M = \begin{bmatrix} 1 & 0 & 1 & 0 \\ 0 & \beta & 0 & \beta \\ -cos(\beta L) & -sin(\beta L) & cosh(\beta L) & sinh(\beta L) \\ sin(\beta L) & -cos(\beta L) & sinh(\beta L) & cosh(\beta L) \end{bmatrix}$$

(B.24)

The natural frequency can be determined by equating the determinant of the coefficient matrix to 0, ω is then the only unknown left in the equation. The equation will have several solutions, the smallest solution will result in the first natural frequency, the second smallest will be the second natural frequency, and so on. For a bending beam, the determinant of matrix M is rather straight forward and shown below. The

$$\beta(2cos(\beta L)cosh(\beta L) + 2) = 0$$

(B.25)

The equation can be simplified and ω can be isolated as shown below.

$$\omega_1 = \sqrt{\dfrac{EI}{\rho A}} \dfrac{(\beta_1 L)^2}{L^2} = \sqrt{\dfrac{EI}{\rho A}} \dfrac{(1.875104069)^2}{L^2}$$

(B.26)

Rotational spring support - free end
The boundary conditions for a cantilever beam with a rotational spring support is shown below.

At $x = 0$:

$W(x) = 0$

$EI\dfrac{dW^2(x)}{dx^2} - K_r \dfrac{dW(x)}{dx} = 0$

(B.27)

At $x = L$:

$\dfrac{d^2 W(x)}{dx^2} = 0$

$\dfrac{d^3 W(x)}{dx^3} = 0$

This set of boundary conditions lead to the following coefficient matrix.

$$M = \begin{bmatrix} -\beta^2 EI & -\beta K_r & \beta^2 EI & -\beta K_r \\ 1 & 0 & 1 & 0 \\ -cos(\beta L) & -sin(\beta L) & cosh(\beta L) & sinh(\beta L) \\ sin(\beta L) & -cos(\beta L) & sinh(\beta L) & cosh(\beta L) \end{bmatrix} \qquad (B.28)$$

Again, ω is the only unknown. By equating the determinant of matrix M to zero, the ω can be isolated, and the natural frequencies can be determined.

Rotational and translational spring support - free end
The boundary conditions for a cantilever beam with a rotational and translational spring support is shown below.

At $x = 0$:

$$EI\frac{dW^3(x)}{dx^3} + K_t W(x) = 0$$

$$EI\frac{dW^2(x)}{dx^2} - K_r\frac{dW(x)}{dx} = 0$$

$\qquad (B.29)$

At $x = L$:

$$\frac{d^2 W(x)}{dx^2} = 0$$

$$\frac{d^3 W(x)}{dx^3} = 0$$

This set of boundary conditions lead to the following coefficient matrix.

$$M = \begin{bmatrix} -\beta^2 EI & -\beta K_r & \beta^2 EI & -\beta K_r \\ K_t & -\beta^3 EI & K_t & \beta^3 EI \\ -cos(\beta L) & -sin(\beta L) & cosh(\beta L) & sinh(\beta L) \\ sin(\beta L) & -cos(\beta L) & sinh(\beta L) & cosh(\beta L) \end{bmatrix} \qquad (B.30)$$

Again, ω is the only unknown. By equating the determinant of matrix M to zero, the ω can be isolated, and the natural frequencies can be determined.

Rotational and translational spring support, with lumped foundation mass - free end
The boundary conditions for a cantilever beam with a rotational and translational spring support, with a lumped foundation mass is shown below.

At $x = 0$:

$$EI\frac{d^2 W(x)}{dx^2} - K_r\frac{dW(x)}{dx} + J\frac{\beta^4 EI}{\rho A}\frac{dW(x)}{dx} = 0$$

$$EI\frac{d^3 W(x)}{dx^3} + K_t W(x) - M_f\frac{\beta^4 EI}{\rho A}W(x) = 0$$

$\qquad (B.31)$

At $x = L$:

$$\frac{d^2 W(x)}{dx^2} = 0$$

$$\frac{d^3 W(x)}{dx^3} = 0$$

This set of boundary conditions lead to the following coefficient matrix.

$$
M = \begin{bmatrix}
-\beta^2 EI & \dfrac{EIJ\beta^5 - AK_r\rho\beta}{A\rho} & \beta^2 EI & \dfrac{EIJ\beta^5 - AK_r\rho\beta}{A\rho} \\
\dfrac{-EIM_f\beta^4 + AK_t\rho}{A\rho} & -\beta^3 EI & \dfrac{-EIM_f\beta^4 + AK_t\rho}{A\rho} & \beta^3 EI \\
-cos(\beta L) & -sin(\beta L) & cosh(\beta L) & sinh(\beta L) \\
sin(\beta L) & -cos(\beta L) & sinh(\beta L) & cosh(\beta L)
\end{bmatrix}
\tag{B.32}
$$

Again, ω is the only unknown. By equating the determinant of matrix M to zero, the ω can be isolated, and the natural frequencies can be determined.

B.2.4. Multibeam model
The theory behind the multibeam model is the same as the single beam model. The only difference is that there are three spatial equations W_n. Each W_n represents a different section of the beam. For a three beam model, the three spatial equations are:

for x from 0 to h_1
$$W_1 = A_1 \sin(\beta_1 x) + A_2 \cos(\beta_1 x) + A_3 \sinh(\beta_1 x) + A_4 \cosh(\beta_1 x)$$

for x from h_1 to h_2
$$W_2 = B_1 \sin(\beta_2 x) + B_2 \cos(\beta_2 x) + B_3 \sinh(\beta_2 x) + B_4 \cosh(\beta_2 x) \tag{B.33}$$

for x from h_2 to L
$$W_3 = C_1 \sin(\beta_3 x) + C_2 \cos(\beta_3 x) + C_3 \sinh(\beta_3 x) + C_4 \cosh(\beta_3 x)$$

Where $h1$, h_2 and L represent the sectional boundaries of the beam.

To be able to determine the coefficient matrix, a set of interface conditions are needed at the locations where two sections connect. The interface conditions for the three beam model is shown below.

at x = h_1

$$W_1(x) = W_2(x)$$
$$\frac{dW_1(x)}{dx} = \frac{dW_2(x)}{dx}$$
$$EI_1 \frac{d^2 W_1(x)}{dx^2} = \frac{d^2 W_2(x)}{dx^2}$$
$$EI_1 \frac{d^3 W_1(x)}{dx^3} = EI_2 \frac{d^3 W_2(x)}{dx^3}$$

$$\tag{B.34}$$

at x = h_2

$$W_2(x) = W_3(x)$$
$$\frac{dW_2(x)}{dx} = \frac{dW_3(x)}{dx}$$
$$EI_2 \frac{d^2 W_2(x)}{dx^2} = EI3 \frac{d^2 W_3(x)}{dx^2}$$
$$EI_2 \frac{d^3 W_2(x)}{dx^3} = EI3 \frac{d^3 W_3(x)}{dx^3}$$

In these equations the different $beta_n$ values are based on the sectional properties, but all have the

same ω, as shown below. This results in ω being the only unknown, and by equation the determinant of the coefficient matrix to 0, ω can be calculated.

$$\beta_n = \sqrt{\omega}\left(\frac{\rho_n A_n}{EI_n}\right)^{\frac{1}{4}}$$
(B.35)

B.3. Timoshenko Beam

The method used to determine the natural frequency of a Timoshenko beam is by means of a single difference equation. This method was proposed by Majkut [48] and is explained in detail in [48]. This section will only give the equations needed for the determination of the natural frequency.

The solution of the Timoshenko beam is in a similar form as that of the Euler-Bernoulli beam, and is shown in equation B.36. In this equation, $X(x)$ represents the vibration amplitude function of the beam.

$$X(x) = P_1 \sin(\lambda_1 x) + C_2 \cos(\lambda_1 x) + C_3 \sinh(\lambda x) + C_4 \cosh(\lambda x)$$
(B.36)

The above-mentioned general solution has the following derivatives

$$\frac{dX(x)}{dx} = P_1\lambda_1 \cos(\lambda_1 x) - P_2\lambda_1 \sin(\lambda_1 x) + P_3\lambda_2 \cosh(\lambda_2 x) + P_4\lambda_2 \sinh(\lambda_2 x)$$

$$\frac{d^2X(x)}{dx^2} = -P_1\lambda_1{}^2 \sin(\lambda_1 x) - P_2\lambda_1{}^2 \cos(\lambda_1 x) + P_3\lambda_2{}^2 \sinh(\lambda_2 x) + P_4\lambda_2{}^2 \cosh(\lambda_2 x)$$
(B.37)

$$\frac{d^3X(x)}{dx^3} = -P_1\lambda_1{}^3 \cos(\lambda_1 x) + P_2\lambda_1{}^3 \sin(\lambda_1 x) + P_3\lambda_2{}^3 \cosh(\lambda_2 x) + P_4\lambda_2{}^3 \sinh(\lambda_2 x)$$

For the sake of reading ease, the following simplifications have been made in the equation:

$$\lambda_1 = \frac{-d + \sqrt{(\Delta)}}{2}$$

$$\lambda_2 = \frac{d + \sqrt{(\Delta)}}{2}$$

$$d = a + b + c$$

$$\Delta = d^2 - 4e$$
(B.38)

$$a = \frac{\omega^2 \rho}{\kappa G}$$

$$b = \frac{\rho \omega^2}{E} - c$$

$$c = \frac{G\kappa A}{EI}$$

Rotational and translational spring support, with lumped foundation mass - free end
For the Timoshenko beam, only be cantilever beam with a rotational and translational spring support, with a lumped foundation mass, is considered. Thje boundary conditions for this case are:

at x = 0:

$$EI \left(\frac{d^2 X(x)}{dx^2} + aX(x) \right) - K_r \frac{dX(x)}{dx} + J\omega^2 \frac{dX(x)}{dx} = 0$$

$$GkA \left((a + b + c) \frac{dX(x)}{dx} - \frac{d^3 X(x)}{dx^3} \right) + K_t X(x) + M_f \omega^2 X(x) = 0$$

(B.39)

at x = L:

$$\frac{d^2 X(x)}{dx^2} + aX(x) = 0$$

$$d \frac{dX(x)}{dx} + \frac{d^3 X(x)}{dx^3} = 0$$

This set of boundary conditions lead to the following coefficient matrix. Just as in the case of the Euler-Bernoulli beam, the ω is the only unknown. By equating the determinant of matrix M to zero, the ω can be isolated, and the natural frequencies can be determined.

$$M = \begin{bmatrix} EI(\lambda_1^2 + a) & -\lambda_1(-J\omega^2 + K_r) & EI(-\lambda_2^2 + a) & -\lambda_2(-J\omega^2 + K_r) \\ M_f \omega^2 - K_t & AG\kappa\lambda_1(-\lambda_1^2 + a + b + c) & M_f \omega^2 - K_t & AG\kappa\lambda_2(\lambda_2^2 + a + b + c) \\ cosh(L\lambda_1)(\lambda_1^2 + a) & sinh(L\lambda_1)(\lambda_1^2 + a) & cos(L\lambda_2)(-\lambda_2^2 + a) & sin(L\lambda_2)(-\lambda_2^2 + a) \\ \lambda_1 sinh(L\lambda_1)(\lambda_1^2 + d) & \lambda_1 cosh(L\lambda_1)(\lambda_1^2 + d) & -\lambda_2 sin(L\lambda_2)(-\lambda_2^2 + d) & \lambda_2 cos(L\lambda_2)(-\lambda_2^2 + d) \end{bmatrix}$$ (B.40)

C
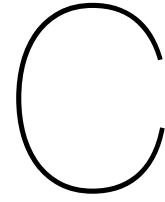
Structural Parameters

C.1. Building bending stiffness

In this appendix, the upper and lower bound for the bending stiffnesses for the five buildings discussed in section 3.2 will be calculated. This is done by calculating the moment of inertia of the stability system of the buildings and then multiplying the moment of inertia with the Young's modulus. For concrete elements, a Young's modulus of 7.5 GPa and 38 GPa is used for the lower and upper bound, respectively. The Young's modulus for steel sections is 210 GPa for both the lower and upper bound. The axes were chosen in such a way that the bending stiffness in the x-direction (bending around the y-axis) is the weak direction and that the bending stiffness in the y-direction (bending around the x-axis) is the strong direction. All distances are measured in meters and angles in degrees.

Determining the moment of inertia is done on the basis of the parallel axis theorem of a rectangle at an angle. Each concrete element contributing to the stiffness of the building gets 2 sets of x- and y-coordinates. The coordinates of the element are then used to calculate the length and the orientation of the element. The length, thickness and orientation are then used to determine the centroid and moment of inertia of each individual element. Hereafter, the centroid of the connected stability elements is determined. Finally, the parallel axis theorem is used to determine the moment of inertia of the connected stability systems. It must be noted that stability systems are only connected through walls and outriggers. Systems connected only by the floor are assumed to work independently. The equations used to determine the different properties are shown below. Each element of the different stability systems are given a number, the numbered elements are then tabulated with their respective parameters. It must be noted that for commonly used steel section the moment of inertia of the sections are not calculated as they are readily available.

$$\begin{aligned}
\text{Element length: } \; & b = \sqrt{(x_2 - x_1)^2 + (y_2 - y_1)^2} \\
\text{Centroid x: } \; & c_x = \frac{b\cos(\phi) + t\sin(\phi)}{2} \\
\text{Centriod y: } \; & c_y = \frac{t\cos(\phi) + b\sin(\phi)}{2} \\
\text{moment of inertia around y: } \; & I_{oy} = \frac{bt}{12}(b^2\cos^2\phi + t^2\sin^2\phi) \\
\text{moment of inertia around x: } \; & I_{ox} = \frac{bt}{12}(t^2\cos^2\phi + b^2\sin^2\phi) \\
\text{Parallel axis thetem y: } \; & I_x = I_{ox} + Ad_y^2 \\
\text{Parallel axis thetem x: } \; & I_y = I_{oy} + Ad_x^2
\end{aligned} \tag{C.1}$$

Where A, d_y and d_x are the area of the element and the distance from the element's own centroid to the global centroid in the y and x direction, respectively.

99
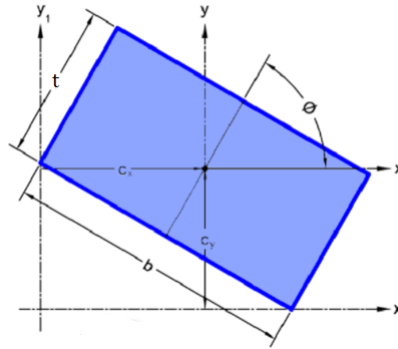
Figure C.1: Orientation of rotated rectangles used to determine moment of inertia

To illustrate the method, an example is shown below. In the example, the moment of inertia for a horizontally and vertically orientated wall connected at their ends, as shown in the figure, is calculated.

Table C.1: Moment of inertia example calculation

	Element	1	2	
	y1	0.00	44.02	
	x1	0.00	0.00	
	y2	44.02	44.02	
	x2	0.00	20.02	
	y2-y1	$44.02 - 0 = 44.02$	$0.00 - 0.00 = 0.00$	
	x2-x1	$0.00 - 0.00 = 0.00$	$20.02 - 0.00 = 20.02$	
$\sqrt{(y2-y1)^2 + (x2-x1)^2}$	b	$\sqrt{44.02^2 + 0^2} = 44.02$	$\sqrt{20.02^2 + 0^2} = 20.02$	
	t	0.32	0.32	
$b \times t$	A	$44.02 * 0.32 = 14.09$	$20.02 * 0.32 = 6.41$	$14.09 + 6.41 = 20.49$
	θ	0.00	90.00	
$abs(\theta - 90)$	ϕ	$abs(0.00 - 90.00) = 90.00$	$abs(90.00 - 90.00) = 0.00$	
$\frac{b\cos(\phi)+t\sin(\phi)}{2}$	cx	$\frac{44.02\cos(90)+0.32\sin(90)}{2} = 0.16$	$\frac{20.02\cos(0)+0.32\sin(0)}{2} = 10.01$	
	Acx	$14.09 * 0.16 = 2.25$	$6.41 * 10.01 = 64.13$	$2.25 + 64.13 = 66.38$
$\frac{\Sigma Acx}{\Sigma A}$	Cx	$\frac{66.38}{20.49} = 3.24$		
$\frac{bt}{12}(b^2 \cos^2 \phi + t^2 \sin^2 \phi)$	Iy0	$(\frac{44.02*0.32}{12})(44.02^2 \cos^2 90 + 0.32^2 \sin^2 90) = 0.12$	$(\frac{20.02*0.32}{12})(20.02^2 \cos^2 0 + 0.32^2 \sin^2 0) = 213.97$	
$A(Cx - cx)^2$	Ad^2	$14.09(3.24 - 0.16)^2 = 133.57$	$6.41(3.24 - 10.01)^2 = 293.69$	
$Iy0 + Ad^2$	Iyy	$0.12 + 133.57 = 133.69$	$213.97 + 293.69 = 507.66$	$133.69 + 507.66 = 641.35$

Figure C.2: Moment of inertia calculation example figure

C.1.1. New Erasmus Medical Center

The stability system of the NEMC exist of four parts. The outer tube given in red, and the three internal concrete cores given in blue, green and orange. The stability system of the NEMC is taken as constant throughout the height of the building. There is a small divergence of the moment of inertia from the ground floor to the fourth floor, but the effect it has on the bending stiffness is taken as negligible. In figure C.3 the four stability systems and their numbering can be seen. The tables C.4 to C.6 show the calculation of the moment of inertia of the different stability systems. Table C.2 is a summary of the results of the moment of inertia.

Table C.2: Moment of inertia of the stability systems of the NEMC

	Outer Tube	Left Core	Middle Core	Right Core	Total
I_{yy}	1863.67	37.59	34.37	41.67	1977.30
I_{xx}	6614.82	5.64	5.73	9.52	6635.70

The lower and upper bound bending stiffnesses can now be determined by multiplying the total moment of inertia with the respective Young's moduli.

Table C.3: Lower and upper bound of bending stiffness

	Lower Bound	Upper Bound
EI_x	1.48×10^{13}	7.51×10^{13}
EI_y	4.98×10^{13}	2.52×10^{14}
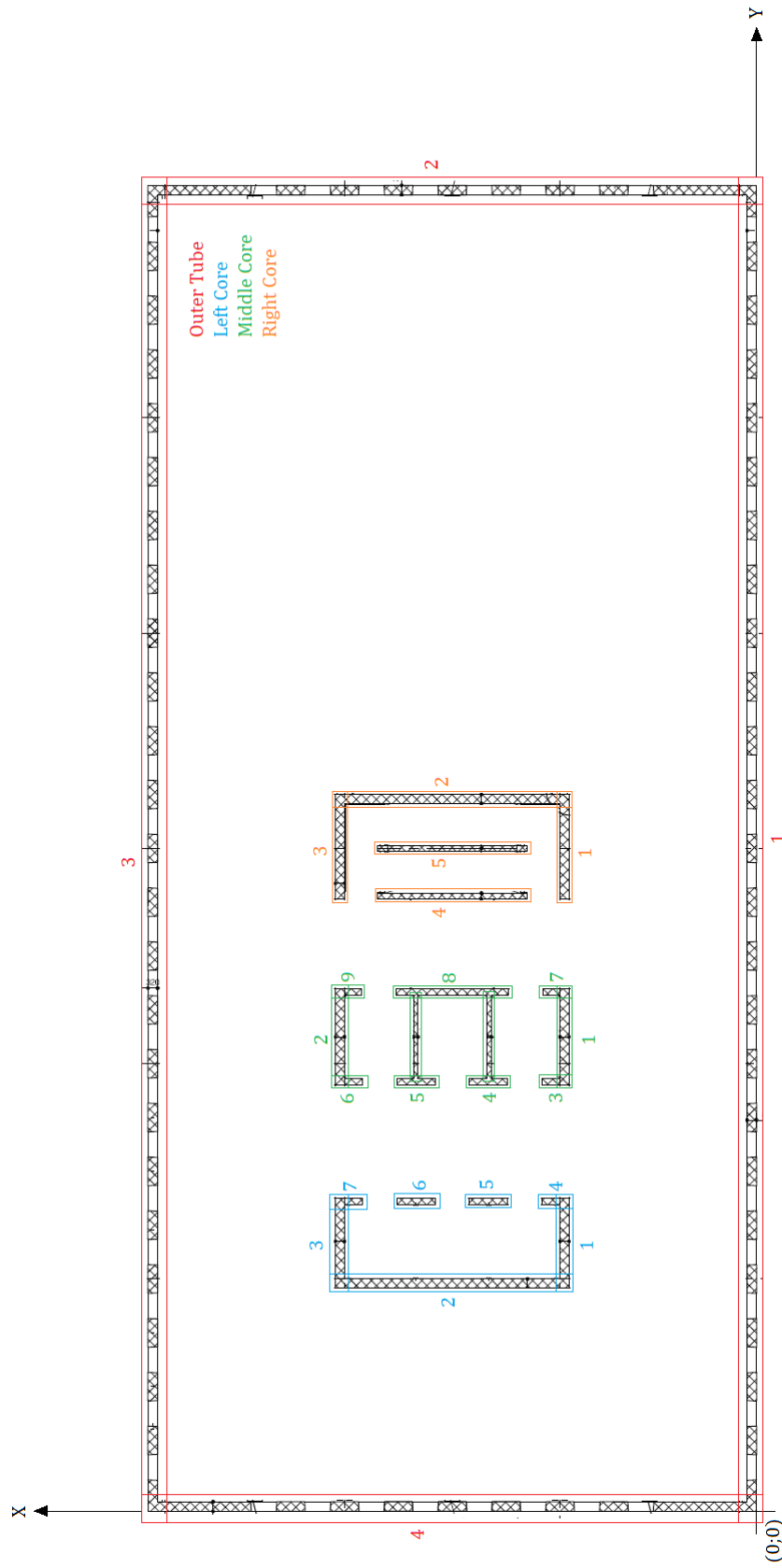
Figure C.3: NEMC stability system and element numbering

Table C.4: Moment of inertia calculation for the outer tube of the new Erasmus Medical Centre

Outer Tube

Element	y1	x1	y2	x2	y2-y1	x2-x1	b	t	A	θ	ϕ	cy	cy	Acy	Acx	Cy	Cx	Iy0	Adx^2	ORF	Iyy	Ix0	Ady^2	ORF	Ixx
1	0.00	0.00	44.02	0.00	44.02	0.00	44.02	0.32	14.09	0.00	90.00	22.01	0.16	310.04	2.25	22.01	10.01	0.12	1366.70	0.58	792.75	2274.67	0.00	0.58	1319.31
2	44.02	0.00	44.02	20.02	0.00	20.02	20.02	0.32	6.41	90.00	0.00	43.86	10.01	280.98	64.13			213.97	0.00	0.65	139.08	0.05	3058.56	0.65	1988.10
3	0.00	20.02	44.02	20.02	44.02	0.00	44.02	0.32	14.09	0.00	90.00	22.01	19.86	310.04	279.76			0.12	1366.70	0.58	792.75	2274.67	0.00	0.58	1319.31
4	0.00	0.00	0.00	20.02	0.00	20.02	20.02	0.32	6.41	90.00	0.00	0.16	10.01	1.03	64.13			213.97	0.00	0.65	139.08	0.05	3058.56	0.65	1988.10
									40.99					902.09	410.27						1863.67				6614.82

Table C.5: Moment of inertia calculation for the left core of the new Erasmus Medical Centre

Left Core

Element	y1	x1	y2	x2	y2-y1	x2-x1	b	t	A	θ	ϕ	cy	cy	Acy	Acx	Cy	Cx	Iy0	Adx^2	ORF	Iyy	Ix0	Ady^2	ORF	Ixx
1	7.46	6.26	10.21	6.26	2.75	0.00	2.75	0.30	0.83	0.00	90.00	8.84	6.26	7.29	5.16	8.37	10.01	0.01	11.60	1.00	11.61	0.52	0.18	1.00	0.70
2	7.46	6.26	7.46	13.76	0.00	7.50	7.50	0.30	2.25	90.00	0.00	7.46	10.01	16.79	22.52			10.55	0.00	1.00	10.55	0.02	1.86	1.00	1.88
3	7.46	13.76	10.21	13.76	2.75	0.00	2.75	0.30	0.83	0.00	90.00	8.84	13.76	7.29	11.35			0.01	11.60	1.00	11.61	0.52	0.18	1.00	0.70
4	10.21	6.26	14.21	6.94	0.00	0.68	0.68	0.20	0.14	90.00	0.00	10.21	6.60	1.39	0.90			0.01	1.58	1.00	1.59	0.00	0.46	1.00	0.46
5	10.21	8.28	14.21	9.34	0.00	1.06	1.06	0.20	0.21	90.00	0.00	10.21	8.81	2.16	1.87			0.01	0.31	1.00	0.33	0.00	0.72	1.00	0.72
6	10.21	10.68	14.21	11.74	0.00	1.06	1.06	0.20	0.21	90.00	0.00	10.21	11.21	2.16	2.38			0.02	0.31	1.00	0.33	0.00	0.72	1.00	0.72
7	10.21	13.08	10.21	13.76	0.00	0.68	0.68	0.20	0.14	90.00	0.00	10.21	13.42	1.39	1.83			0.01	1.58	1.00	1.59	0.00	0.46	1.00	0.46
									4.60					38.47	46.01						37.59				5.64

Table C.6: Moment of inertia calculation for the middle core of the new Erasmus Medical Centre

Middle Core

Element	y1	x1	y2	x2	y2-y1	x2-x1	b	t	A	θ	ϕ	cy	cy	Acy	Acx	Cy	Cx	Iy0	Adx^2	ORF	Iyy	Ix0	Ady^2	ORF	Ixx
1	14.21	6.26	17.21	6.26	3.00	0.00	3.00	0.30	0.90	0.00	90.00	15.71	6.26	14.14	5.63	15.80	10.01	0.01	12.66	1.00	12.66	0.68	0.01	1.00	0.68
2	14.21	13.76	17.21	13.76	3.00	0.00	3.00	0.30	0.90	0.00	90.00	15.71	13.76	14.14	12.38			0.01	12.66	1.00	12.66	0.68	0.01	1.00	0.68
3	14.21	6.26	14.21	6.94	0.00	0.68	0.68	0.20	0.14	90.00	0.00	14.21	6.60	1.93	0.90			0.01	1.58	1.00	1.59	0.00	0.34	1.00	0.35
4	14.21	8.28	14.21	9.34	0.00	1.06	1.06	0.20	0.21	90.00	0.00	14.21	8.81	3.01	1.87			0.02	0.31	1.00	0.33	0.00	0.54	1.00	0.54
5	14.21	10.68	14.21	11.74	0.00	1.06	1.06	0.20	0.21	90.00	0.00	14.21	11.21	3.01	2.38			0.02	0.31	1.00	0.33	0.00	0.54	1.00	0.54
6	14.21	13.08	14.21	13.76	0.00	0.68	0.68	0.20	0.14	90.00	0.00	14.21	13.42	1.93	1.83			0.01	1.58	1.00	1.59	0.00	0.34	1.00	0.35
7	17.21	6.26	17.21	6.94	0.00	0.68	0.68	0.20	0.14	90.00	0.00	17.21	6.60	2.34	0.90			0.01	1.58	1.00	1.59	0.00	0.27	1.00	0.27
8	17.21	8.28	17.21	11.74	0.00	3.46	3.46	0.20	0.69	90.00	0.00	17.21	10.01	11.91	6.93			0.69	0.00	1.00	0.69	0.00	1.37	1.00	1.37
9	17.21	13.08	17.21	13.76	0.00	0.68	0.68	0.20	0.14	90.00	0.00	17.21	13.42	2.34	1.83			0.01	1.58	1.00	1.59	0.00	0.27	1.00	0.27
10	14.21	8.79	17.21	8.79	3.00	0.00	3.00	0.15	0.45	0.00	90.00	15.71	8.79	7.07	3.95			0.00	0.68	1.00	0.68	0.34	0.00	1.00	0.34
11	14.21	11.24	17.21	11.24	3.00	0.00	3.00	0.15	0.45	0.00	90.00	15.71	11.24	7.07	5.06			0.00	0.68	1.00	0.68	0.34	0.00	1.00	0.34
									4.36					68.90	43.64						34.37				5.73

Table C.7: Moment of inertia calculation for the right core of the new Erasmus Medical Centre

Right Core

Element	y1	x1	y2	x2	y2-y1	x2-x1	b	t	A	θ	ϕ	cy	cy	Acy	Acx	Cy	Cx	Iy0	Adx^2	ORF	Iyy	Ix0	Ady^2	ORF	Ixx
1	20.41	6.26	23.66	6.26	3.25	0.00	3.25	0.30	0.98	0.00	90.00	22.04	6.26	21.48	6.10	22.37	10.01	0.01	13.71	1.00	13.72	0.86	0.11	1.00	0.97
2	23.66	6.26	23.66	13.76	0.00	7.50	7.50	0.30	2.25	90.00	0.00	23.66	10.01	53.24	22.52			10.55	0.00	1.00	10.55	0.02	3.72	1.00	3.74
3	20.41	13.76	23.66	13.76	3.25	0.00	3.25	0.30	0.98	0.00	90.00	22.04	13.76	21.48	13.42			0.01	13.71	1.00	13.72	0.86	0.11	1.00	0.97
4	20.41	7.61	20.41	12.41	0.00	4.80	4.80	0.20	0.96	90.00	0.00	20.41	10.01	19.59	9.61			1.84	0.00	1.00	1.84	0.00	3.70	1.00	3.70
5	22.01	7.61	22.01	12.41	0.00	4.80	4.80	0.20	0.96	90.00	0.00	22.01	10.01	21.13	9.61			1.84	0.00	1.00	1.84	0.00	0.13	1.00	0.13
									6.12					136.93	61.26						41.67				9.52

C.1.2. Montevideo

The stability system of the Montevideo tower is split into three sections over the height of the structure. For this reason, an upper and lower bound will be determined for each section. The first stability system stretches over the ground and first floor and consists of a concrete core and 14 steel columns. The second stability system ranges from the 2nd floor to the 27th floor and consists of a concrete core with connected concrete walls. The third section ranges from the 28th floor to the 42nd floor and consists of 14 steel columns. The three different stability systems and their element numbering can be seen in figures C.4 to C.6. The calculation of the moment of inertia of the different stability systems can be found in tables C.10 to C.13. In table C.8 the moment of inertia for the different sections can be found.

Table C.8: Moment of inertia of the stability systems of the Montevideo tower

		Concrete section	Steel section
Level 0 - 1	I_{yy}	315.00	134.82
	I_{xx}	549.70	153.64
Level 2 - 27	I_{yy}	2786.86	-
	I_{xx}	4421.06	-
Level 28 - 42	I_{yy}	-	13.95
	I_{xx}	-	16.67

The lower and upper bounds for the different sections can be determined by multiplying the concrete and steel parts with their respective Young's moduli. For the bending stiffness of levels 0 - 1 is taken as the product of the bending stiffness of the concrete and steel part. The results of the lower and upper bounds are shown below.

Table C.9: Lower and upper bound of bending stiffness

		Lower Bound	Upper Bound
Level 0 - 1	EI_x	3.07×10^{13}	4.03×10^{13}
	EI_y	3.64×10^{13}	5.32×10^{13}
Level 2 - 27	EI_x	2.09×10^{13}	1.06×10^{14}
	EI_y	3.32×10^{13}	1.68×10^{14}
Level 28 - 42	EI_x	2.93×10^{12}	2.93×10^{12}
	EI_y	3.50×10^{12}	3.50×10^{12}
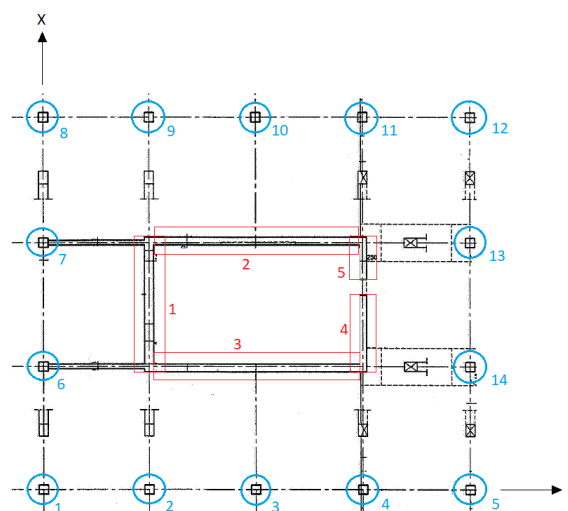
Figure C.4: Montevideo tower stability system and element numbering level 0-1
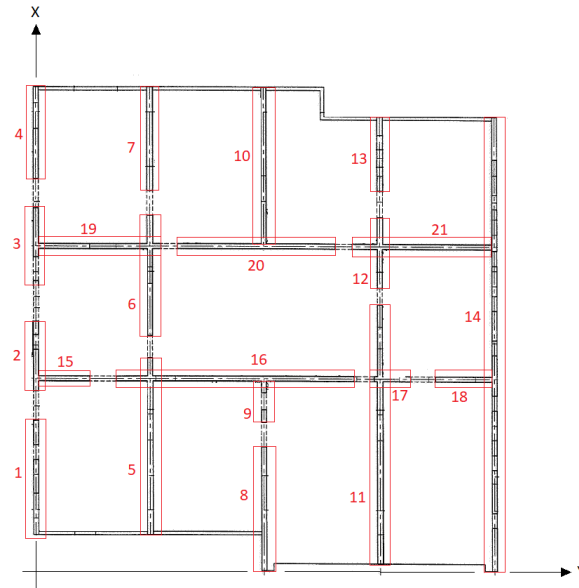
Figure C.5: Montevideo tower stability system and element numbering level 2-27
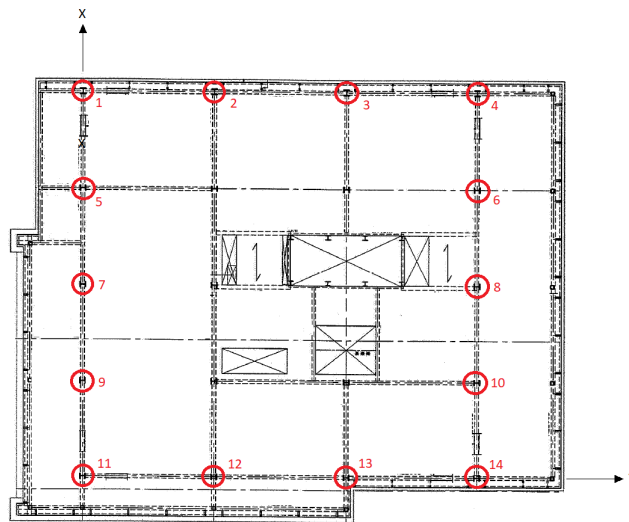
Figure C.6: Montevideo tower stability system and element numbering level 28-42

Table C.10: Moment of inertia calculation for the steel columns on levels 0-1 of the Montevideo tower

Level 0 - 1

Steel Columns	y	x	A (600x600x40)	Cy	Cx	Io	Ad^2	Iyy	Ad^2	Ixx
1	0.00	0.00	0.09	13.80	12.00	4.71E-03	12.90	12.91	17.06	17.07
2	6.90	0.00	0.09			4.71E-03	12.90	12.91	4.27	4.27
3	13.80	0.00	0.09			4.71E-03	12.90	12.91	0.00	0.005
4	20.70	0.00	0.09			4.71E-03	12.90	12.91	4.27	4.27
5	27.60	0.00	0.09			4.71E-03	12.90	12.91	17.06	17.07
6	0.00	8.00	0.09			4.71E-03	1.43	1.44	17.06	17.07
7	0.00	16.00	0.09			4.71E-03	1.43	1.44	17.06	17.07
8	0.00	24.00	0.09			4.71E-03	12.90	12.91	17.06	17.07
9	6.90	24.00	0.09			4.71E-03	12.90	12.91	4.27	4.27
10	13.80	24.00	0.09			4.71E-03	12.90	12.91	0.00	0.005
11	20.70	24.00	0.09			4.71E-03	12.90	12.91	4.27	4.27
12	27.60	24.00	0.09			4.71E-03	12.90	12.91	17.06	17.07
13	27.60	16.00	0.09			4.71E-03	1.43	1.44	17.06	17.07
14	27.60	8.00	0.09			4.71E-03	1.43	1.44	17.06	17.07
			1.25					134.82		153.64

Table C.11: Moment of inertia calculation for the concrete core on levels 0-1 of the Montevideo tower

Level 0 - 1

Concrete Core	y1	x1	y2	x2	y2-y1	x2-x1	b	t	A	θ	φ	cy	cy	Acy	Acx	Cy	Cx	Iy0	Adx^2	ORF	Iyy	Ix0	Ady^2	ORF	Ixx
1	6.90	8.00	6.90	16.00	0.00	8.00	8.00	0.60	4.80	90.00	0.00	6.90	12.00	33.12	57.60	13.23	11.45	25.60	1.45	1.00	27.05	0.14	192.05	1.00	192.19
2	6.90	16.00	20.70	16.00	13.80	0.00	13.80	0.50	6.90	0.00	90.00	13.80	16.00	95.22	110.40			0.14	142.86	1.00	143.00	109.50	2.28	1.00	111.78
3	6.90	8.00	12.50	8.00	13.80	0.00	13.80	0.50	6.90	0.00	90.00	13.80	8.00	95.22	55.20			0.14	82.12	1.00	82.26	109.50	2.28	1.00	111.78
4	20.70	8.00	12.50	8.00	-8.20	0.00	8.20	0.50	4.10	0.00	90.00	16.60	8.00	68.06	32.80			0.09	48.79	1.00	48.88	22.97	46.69	1.00	69.67
5	20.70	13.70	20.70	16.00	0.00	2.30	2.30	0.50	1.15	90.00	0.00	20.70	14.85	23.81	17.08			0.51	13.30	1.00	13.80	0.02	64.25	1.00	64.27
									23.85					315.43	273.08				273.08		315.00				549.70

Table C.12: Moment of inertia calculation for the concrete elements on levels 2-27 of the Montevideo tower

Level 2 - 27

Concrete Element	y1	x1	y2	x2	x2-x1	y2-y1	b	t	A	θ	φ	cy	cx	Acy	Acx	Cy	Cx	Iy0	Adx²	ORF	Iyy	Ix0	Ady²	ORF	Ixx
1	0.00	2.18	0.00	9.09	6.91	0.00	6.91	0.30	2.07	90.00	0.00	0.00	5.64	0.00	11.68	14.27	14.83	8.25	175.46	1.00	183.71	0.02	422.10	1.00	422.12
2	0.00	10.82	0.00	14.96	4.14	0.00	4.14	0.30	1.24	90.00	0.00	0.00	12.89	0.00	16.01			1.77	4.70	1.00	6.47	0.01	252.90	1.00	252.91
3	0.00	16.76	0.00	21.89	5.13	0.00	5.13	0.30	1.54	90.00	0.00	0.00	19.33	0.00	29.74			3.38	31.03	1.00	34.40	0.01	313.37	1.00	313.38
4	0.00	23.69	0.00	29.18	5.49	0.00	5.49	0.30	1.65	90.00	0.00	0.00	26.44	0.00	43.54			4.14	221.62	1.00	225.76	0.01	335.36	1.00	335.37
5	6.90	2.18	6.90	12.80	10.62	0.00	10.62	0.30	3.19	90.00	0.00	6.90	7.49	21.98	23.86			29.94	171.88	1.00	201.82	0.02	173.03	1.00	173.06
6	6.90	14.24	6.90	21.62	7.38	0.00	7.38	0.30	2.21	90.00	0.00	6.90	17.93	15.28	39.70			10.05	21.21	1.00	31.26	0.02	120.24	1.00	120.26
7	6.90	23.06	6.90	29.18	6.12	0.00	6.12	0.30	1.84	90.00	0.00	6.90	26.12	12.67	47.96			5.73	233.82	1.00	239.55	0.01	99.71	1.00	99.73
8	13.80	0.00	13.80	7.58	7.58	0.00	7.58	0.30	2.27	90.00	0.00	13.80	3.79	31.38	8.62			10.89	277.41	1.00	288.30	0.02	0.50	1.00	0.52
9	13.80	9.02	13.80	11.68	2.66	0.00	2.66	0.30	0.80	90.00	0.00	13.80	10.35	11.01	8.26			0.47	16.05	1.00	16.52	0.01	0.18	1.00	0.18
10	13.80	19.68	13.80	29.18	9.50	0.00	9.50	0.30	2.85	90.00	0.00	13.80	24.43	39.33	69.63			21.43	262.39	1.00	283.82	0.02	0.63	1.00	0.65
11	20.70	0.00	20.70	16.09	16.09	0.00	16.09	0.30	4.83	90.00	0.00	20.70	8.05	99.92	38.83			104.14	222.54	1.00	326.68	0.04	199.60	1.00	199.64
12	20.70	17.17	20.70	21.40	4.23	0.00	4.23	0.30	1.27	90.00	0.00	20.70	19.29	26.27	24.47			1.89	25.13	1.00	27.02	0.01	52.47	1.00	52.48
13	20.70	22.93	20.70	27.43	4.50	0.00	4.50	0.30	1.35	90.00	0.00	20.70	25.18	27.95	33.99			2.28	144.48	1.00	146.76	0.01	55.82	1.00	55.83
14	27.60	0.00	27.60	27.43	27.43	0.00	27.43	0.30	8.23	90.00	0.00	27.60	13.72	227.12	112.86			515.96	10.32	1.00	526.28	0.06	1462.30	1.00	1462.36
15	0.00	11.68	3.24	11.68	0.00	3.24	3.24	0.30	0.97	0.00	90.00	1.62	11.68	1.57	11.35			0.01	9.68	1.00	9.68	0.85	155.53	1.00	156.38
16	4.86	11.68	19.35	11.68	0.00	14.49	14.49	0.30	4.35	0.00	90.00	12.11	11.68	52.62	50.77			0.03	43.27	1.00	43.30	76.06	20.37	1.00	96.42
17	20.61	11.68	22.86	11.68	0.00	2.25	2.25	0.30	0.68	0.00	90.00	21.74	11.68	14.67	7.88			0.01	6.72	1.00	6.72	0.28	37.62	1.00	37.90
18	24.39	11.68	27.60	11.68	0.00	3.21	3.21	0.30	0.96	0.00	90.00	26.00	11.68	25.03	11.25			0.01	9.59	1.00	9.59	0.83	132.40	1.00	133.23
19	0.00	19.68	7.56	19.68	0.00	7.56	7.56	0.30	2.27	0.00	90.00	3.78	19.68	8.57	44.63			0.02	53.24	1.00	53.26	10.80	249.55	1.00	260.35
20	8.64	19.68	18.18	19.68	0.00	9.54	9.54	0.30	2.86	0.00	90.00	13.41	19.68	38.38	56.32			0.02	67.18	1.00	67.21	21.71	2.11	1.00	23.82
21	19.26	19.68	27.60	19.68	0.00	8.34	8.34	0.30	2.50	0.00	90.00	23.43	19.68	58.62	49.24			0.02	58.73	1.00	58.75	14.50	209.95	1.00	224.46
									49.92					712.38	740.61						2786.86				4421.06

Table C.13: Moment of inertia calculation for the steel columns on levels 28-42 of the Montevideo tower

Level 28 - 42   HE 300B

Steel section	y	x	Iyo	Ixo	A	Acy	Acx	Cy	Cx	Ad²	Iyy	Ad²	Ixx
1	0.00	20.40	2.52E-04	8.56E-05	0.01	0.00	0.30	10.35	10.20	1.55	1.55045	1.60	1.596
2	6.90	20.40	2.52E-04	8.56E-05	0.01	0.10	0.30			1.55	1.55045	0.18	0.177
3	13.80	20.40	2.52E-04	8.56E-05	0.01	0.21	0.30			1.55	1.55045	0.18	0.177
4	20.70	20.40	2.52E-04	8.56E-05	0.01	0.31	0.30			1.55	1.55045	1.60	1.596
5	0.00	15.30	8.56E-05	2.52E-04	0.01	0.00	0.23			0.39	0.38763	1.60	1.596
6	20.70	15.30	8.56E-05	2.52E-04	0.01	0.31	0.23			0.39	0.38763	1.60	1.596
7	0.00	10.20	8.56E-05	2.52E-04	0.01	0.00	0.15			0.00	0.00009	1.60	1.596
8	20.70	10.20	8.56E-05	2.52E-04	0.01	0.31	0.15			0.00	0.00009	1.60	1.596
9	0.00	5.10	8.56E-05	2.52E-04	0.01	0.00	0.08			0.39	0.38763	1.60	1.596
10	20.70	5.10	8.56E-05	2.52E-04	0.01	0.31	0.08			0.39	0.38763	1.60	1.596
11	0.00	0.00	8.56E-05	2.52E-04	0.01	0.00	0.00			1.55	1.55028	1.60	1.596
12	6.90	0.00	8.56E-05	2.52E-04	0.01	0.10	0.00			1.55	1.55028	0.18	0.178
13	13.80	0.00	8.56E-05	2.52E-04	0.01	0.21	0.00			1.55	1.55028	0.18	0.178
14	20.70	0.00	8.56E-05	2.52E-04	0.01	0.31	0.00			1.55	1.55028	1.60	1.596
					0.21	2.16	2.13			13.95	13.95	16.67	16.67

C.1.3. New Orleans

The stability system of the New Orleans tower is also split into three parts. The stiffness of levels 0 to 2 is provided by a concrete core and steel columns. The stability system of levels 3 to 10 is provided by a concrete core and walls, this can be seen in figure C.9. It must be noted that the walls are split into two groups, namely the connected and disconnected element, shown in red and blue respectively in figure C.9. When considering the connected walls, it is assumed that the system provides stiffness in both the x- and y-direction, this is due to all the walls being connected, and that load is transferred through the whole section when bending occurs. When considering the disconnected walls, it is assumed that the walls only provide significant stiffness in the y-direction. The reason for this is that the walls bend independently and that the moment of inertia around their respective y-axes (in the x-direction) is assumed to be negligible. The third stability section, ranging from levels 11 to 45, is largely the same as the previous system, the only difference is that wall 3 and 4 of the disconnected walls are not present and that wall 5 of the disconnected walls and 1 and 2 of the connected walls are shorter.c The stability system and element numbering can be seen in figure C.10. Throughout the whole height of the structure there is also a lift core providing stiffness in both directions. The moment of inertia calculation for all systems contributing to the stiffness are given in tables C.16 to C.23 with the results thereof given in table C.14.

Table C.14: Moment of inertia of the stability systems of the New Orleans tower

		Steel columns	Concrete core	Disconnected section	Connected section	Lift core
Level 0 - 2	I_{yy}	24.16	653.63	-	-	25.46
	I_{xx}	136.23	416.7	-	-	6.13
Level 3 - 10	I_{yy}	-	-	-	907.82	25.46
	I_{xx}	-	-	1149.32	1621.00	6.13
Level 11 - 45	I_{yy}	-	-	-	844.55	25.46
	I_{xx}	-	-	751.68	1299.87	6.13

The lower and upper bounds for the different sections can be determined by multiplying the concrete and steel parts with their respective Young's moduli. The total bending stiffness is taken as the product of the different bending stiffnesses of each section. The results of the lower and upper bounds are shown below.

Table C.15: Lower and upper bound of bending stiffness

		Lower Bound	Upper Bound
Level 0 - 2	EI_x	1.02×10^{13}	3.09×10^{13}
	EI_y	3.18×10^{13}	4.47×10^{13}
Level 3 - 10	EI_x	7.00×10^{12}	3.55×10^{13}
	EI_y	2.08×10^{13}	1.06×10^{14}
Level 11 - 45	EI_x	6.53×10^{12}	3.31×10^{13}
	EI_y	1.54×10^{12}	7.82×10^{13}
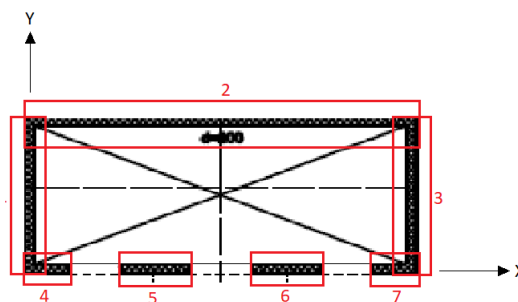
Figure C.7: New Orleans tower lift core element numbering level 0-45
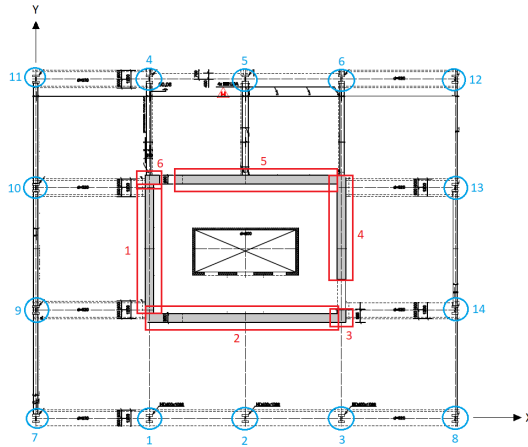
Figure C.8: New Orleans tower stability system and element numbering level 0-2
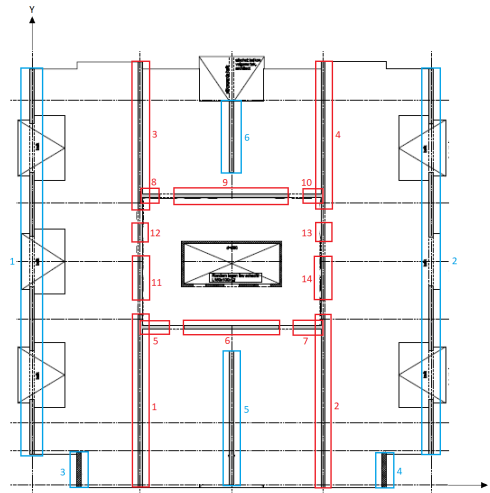
Figure C.9: New Orleans tower stability system and element numbering level 3-10
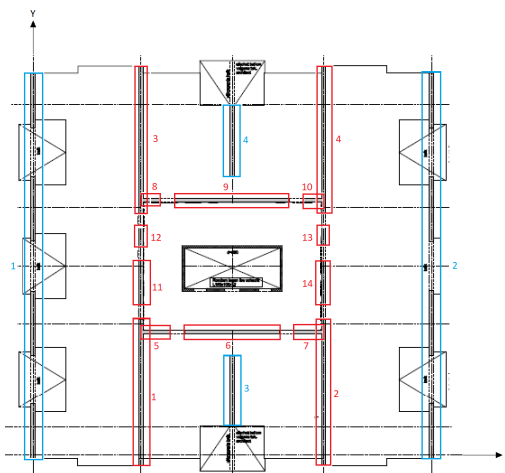
Figure C.10: New Orleans tower stability system and element numbering level 11-45

Table C.16: Moment of inertia calculation for the lift core on levels 0-2 of the New Orleans tower

Level 0 - 45

Life Core	x1	y1	x2	y2	(x2-x1)	(y2-y1)	b	t	A	θ	φ	cx	cy	Acx	Acy	Cx	Cy	Ixo	Ad²	ORF	Ixx	Iyo	Ad²	ORF	Iyy
1	10.850	14.635	10.850	17.735	0.000	3.100	3.100	0.200	0.620	90.000	0.000	10.850	16.185	6.727	10.035	14.400	16.452	0.497	0.044	1.000	0.541	0.002	7.814	1	7.816
2	10.850	17.735	17.950	17.735	7.100	0.000	7.100	0.200	1.420	0.000	90.000	14.400	17.735	20.448	25.184			0.005	2.337	1.000	2.341	5.965	0.000	1	5.965
3	17.950	14.635	17.950	17.735	0.000	3.100	3.100	0.200	0.620	90.000	0.000	17.950	16.185	11.129	10.035			0.497	0.044	1.000	0.541	0.002	7.814	1	7.816
4	10.850	14.635	11.600	14.635	0.750	0.000	0.750	0.200	0.150	0.000	90.000	11.225	14.635	1.684	2.195			0.001	0.495	1.000	0.496	0.007	1.512	1	1.519
5	12.550	14.635	13.850	14.635	1.300	0.000	1.300	0.200	0.260	0.000	90.000	13.200	14.635	3.432	3.805			0.001	0.859	1.000	0.859	0.037	0.374	1	0.411
6	14.950	14.635	16.250	14.635	1.300	0.000	1.300	0.200	0.260	0.000	90.000	15.600	14.635	4.056	3.805			0.001	0.859	1.000	0.859	0.037	0.374	1	0.411
7	17.200	14.635	17.950	14.635	0.750	0.000	0.750	0.200	0.150	0.000	90.000	17.575	14.635	2.636	2.195			0.001	0.495	1.000	0.496	0.007	1.512	1	1.519
									3.480					50.112	57.254						6.134				25.457

Table C.17: Moment of inertia calculation for the concrete core on levels 0-2 of the New Orleans tower

Level 0 - 2

Concrete Core	x1	y1	x2	y2	(x2-x1)	(y2-y1)	b	t	A	θ	φ	cx	cy	Acx	Acy	Cx	Cy	Ixo	Ad²	ORF	Ixx	Iyo	Ad²	ORF	Iyy
1	7.800	11.400	7.800	20.900	0.000	9.500	9.500	0.600	5.700	90.000	0.000	7.800	16.150	44.46	92.06	14.214	16.183	42.869	0.006	1.000	42.875	0.171	234.463	1.000	234.634
2	7.800	11.400	21.000	11.400	13.200	0.000	13.200	0.600	7.920	0.000	90.000	14.400	11.400	114.05	90.29			0.238	181.200	1.000	181.437	114.998	0.275	1.000	115.274
3	21.000	11.400	21.000	11.995	0.000	0.595	0.595	0.600	0.357	90.000	0.000	21.000	11.698	7.50	4.18			0.011	7.183	1.000	7.194	0.011	16.442	1.000	16.453
4	21.000	14.055	21.000	20.900	0.000	6.845	6.845	0.600	4.107	90.000	0.000	21.000	17.478	86.25	71.78			16.036	6.880	1.000	22.916	0.123	189.151	1.000	189.274
5	9.540	20.900	21.000	20.900	11.460	0.000	11.460	0.600	6.876	0.000	90.000	15.270	20.900	105.00	143.71			0.206	152.980	1.000	153.187	75.253	7.674	1.000	82.927
6	7.800	20.900	8.480	20.900	0.680	0.000	0.680	0.600	0.408	0.000	90.000	8.140	20.900	3.32	8.53			0.012	9.077	1.000	9.090	0.016	15.050	1.000	15.066
									25.368					360.57	410.53						416.699				653.627

Table C.18: Moment of inertia calculation for the steel columns on levels 0-2 of the New Orleans tower contributing in both directions

Level 0 - 2

Steel Columns	x	y	A	Acx	Acy	Ixx	Iyy	Cx	Cy	Ad²	Ixx	Ad²	Iyy
1	7.800	0.000	0.139	1.08	0.00	0.006	0.002	14.400	12.798	22.699	22.705	6.037	6.039
2	14.400	0.000	0.139	2.00	0.00	0.006	0.002			22.699	22.705	0.000	0.002
3	21.000	0.000	0.139	2.91	0.00	0.006	0.002			22.699	22.705	6.037	6.039
4	7.800	25.595	0.139	1.08	3.55	0.006	0.002			22.699	22.705	6.037	6.039
5	14.400	25.595	0.139	2.00	3.55	0.006	0.002			22.699	22.705	0.000	0.002
6	21.000	25.595	0.139	2.91	3.55	0.006	0.002			22.699	22.705	6.037	6.039
			0.832	11.98	10.64						136.232		24.161

Table C.19: Moment of inertia calculation for the steel columns on levels 0-2 of the New Orleans tower contributing in the xx-directions

Level 0 - 2 Steel Coulumns	x	y	A	Acy	Ixx	Ad²	Cy	Ixx
7	0.000	0.000	0.139	0.000	0.006	24.780	13.371	24.786
8	28.800	0.000	0.139	0.000	0.006	24.780		24.786
9	0.000	9.745	0.139	1.351	0.006	1.823		1.829
10	0.000	18.145	0.139	2.515	0.006	3.159		3.164
11	0.000	25.595	0.139	3.547	0.006	20.710		20.716
12	28.800	25.595	0.139	3.547	0.006	20.710		20.716
13	28.800	18.145	0.139	2.515	0.006	3.159		3.164
14	28.800	9.745	0.139	1.351	0.006	1.823		1.829
			1.109	14.826				100.990

Table C.20: Moment of inertia calculation for the disconnected concrete elements on levels 3-10 of the New Orleans tower

Level 3 - 10 Disconnected elements	x1	y1	x2	y2	x2-x1	y2-y1	b	t	A	θ	φ	cy	Acy	Cy	Ixo	ORF	Ixo	Ad²	Ixx
1	0	2.4	0	30.26	0	27.86	27.86	0.3	8.358	90	0	16.33	136.49	13.9	540.609	0.34		50.065	200.829
2	28.8	0	28.8	30.26	0	30.26	30.26	0.3	9.078	90	0	15.13	137.35		692.703	0.34		14.127	240.322
3	3.55	0	3.55	2.63	0	2.63	2.63	0.3	0.789	90	0	1.32	1.04		0.455	1		124.617	125.072
4	25.25	0	25.25	2.63	0	2.63	2.63	0.3	0.789	90	0	1.32	1.04		0.455	1		124.617	125.072
15	14.4	0	14.4	9.825	0	9.825	9.825	0.3	2.9475	90	0	4.91	14.48		23.710	1		342.493	366.203
16	14.4	20.675	14.4	25.83	0	5.155	5.155	0.3	1.5465	90	0	23.25	35.96		3.425	1		88.400	91.824
									23.508				326.35						1149.322

Table C.21: Moment of inertia calculation for the connected concrete elements on levels 3-10 of the New Orleans tower

Level 3 - 10 connected Core	x1	y1	x2	y2	x2-x1	y2-y1	b	t	A	θ	φ	cx	cy	Acx	Acy	Cy	Cx	Ixo	Ad²	ORF	Ixx	Iyo	Ad²	ORF	Iyy
1	7.8	0	7.8	20.135	0	20.135	20.135	0.3	6.0405	90	0	7.80	10.07	47.12	60.81	15.69	13.81	204.077	191.091	1	395.169	0.045	218.335	1	218.380
2	21	0	21	12.525	0	12.525	12.525	0.3	3.7575	90	0	21.00	6.26	78.91	23.53			49.122	334.100	1	383.222	0.028	194.136	1	194.164
3	7.8	20.135	7.8	30.76	0	10.625	10.625	0.3	3.1875	90	0	7.80	25.45	24.86	81.11			29.987	303.354	1	333.340	0.024	115.213	1	115.236
4	21	20.135	21	30.76	0	10.625	10.625	0.3	3.1875	90	0	21.00	25.45	66.94	81.11			29.987	303.354	1	333.340	0.024	164.686	1	164.710
5	7.8	11.525	9.945	11.525	2.145	0	2.145	0.3	0.6435	0	0	8.87	11.68	5.71	7.51			0.005	10.384	1	10.389	0.247	15.701	1	15.948
6	10.955	11.525	17.845	11.525	6.89	0	6.89	0.3	2.067	0	0	14.40	11.68	29.76	24.13			0.016	33.354	1	33.369	8.177	0.714	1	8.892
7	18.855	11.525	21	11.525	2.145	0	2.145	0.3	0.6435	0	0	19.93	11.68	12.82	7.51			0.005	10.384	1	10.389	0.247	24.066	1	24.313
8	7.8	21.35	9.245	21.35	1.445	0	1.445	0.3	0.4335	0	0	8.52	21.50	3.69	9.32			0.003	14.623	1	14.626	0.075	12.129	1	12.205
9	10.255	21.35	18.545	21.35	8.29	0	8.29	0.3	2.487	0	0	14.40	21.50	35.81	53.47			0.019	83.894	1	83.912	14.243	0.860	1	15.103
10	19.555	21.35	21	21.35	1.445	0	1.445	0.3	0.4335	0	0	20.28	21.50	8.79	9.32			0.003	14.623	1	14.626	0.075	18.121	1	18.196
11	7.8	13.535	7.8	16.725	0	3.19	3.19	0.3	0.957	90	0	7.80	15.13	7.46	14.48			0.812	0.302	1	1.114	0.007	34.591	1	34.598
12	7.8	17.735	7.8	19.125	0	1.39	1.39	0.3	0.417	90	0	7.80	18.43	3.25	7.69			0.067	3.126	1	3.193	0.003	15.073	1	15.076
13	21	13.535	21	16.725	0	3.19	3.19	0.3	0.957	90	0	21.00	15.13	20.10	14.48			0.812	0.302	1	1.114	0.007	49.445	1	49.452
14	21	17.735	21	19.125	0	1.39	1.39	0.3	0.417	90	0	21.00	18.43	8.76	7.69			0.067	3.126	1	3.193	0.003	21.545	1	21.548
									25.629					353.99	402.17						1620.996				907.819

Table C.22: Moment of inertia calculation for the disconnected concrete elements on levels 11–45 of the New Orleans tower

Level 11 - 45

Disconnected elements	x1	y1	x2	y2	x2-x1	y2-y1	b	t	A	θ	φ	cy	Acy	Cy	ORF	Ixo	Ad^2	Ixx
1	0	2.4	0	30.26	0	27.86	27.86	0.3	8.358	90	0	16.33	136.49	15.2	0.34	540.609	9.949	187.190
2	28.8	0	28.8	30.26	0	30.26	30.26	0.3	9.078	90	0	15.13	137.35		0.34	692.703	0.108	235.556
3	14.4	2.35	14.4	9.825	0	7.475	7.475	0.3	2.2425	90	0	6.09	13.65		1	10.442	245.695	256.136
4	14.4	20.675	14.4	25.83	0	5.155	5.155	0.3	1.5465	90	0	23.25	35.96		1	3.425	69.376	72.801
									21.225				323.45					751.683

Table C.23: Moment of inertia calculation for the connected concrete elements on levels 11–45 of the New Orleans tower

Level 11 - 45

Connected Core	x1	y1	x2	y2	x2-x1	y2-y1	b	t	A	θ	φ	cx	cy	Acx	Acy	Cx	Cy	Ixo	Ad^2	ORF	Ixx	Iyo	Ad^2	ORF	Iyy
1	7.8	2.4	7.8	20.135	0	17.735	17.735	0.3	5.3205	90	0	7.80	11.27	41.50	59.95	13.78	16.55	139.455	148.733	1	288.188	0.040	190.077	1	190.117
2	21	2.4	21	12.525	0	10.125	10.125	0.3	3.0375	90	0	21.00	7.46	63.79	22.67			25.949	251.106	1	277.055	0.023	158.468	1	158.491
3	7.8	20.135	7.8	30.76	0	10.625	10.625	0.3	3.1875	90	0	7.80	25.45	24.86	81.11			29.987	252.072	1	282.059	0.024	113.875	1	113.899
4	21	20.135	21	30.76	0	10.625	10.625	0.3	3.1875	90	0	21.00	25.45	66.94	81.11			29.987	252.072	1	282.059	0.024	166.294	1	166.318
5	7.8	11.525	9.945	11.525	2.145	0	2.145	0.3	0.6435	0	90	8.87	11.68	5.71	7.51			0.005	15.323	1	15.328	0.247	15.479	1	15.726
6	10.955	11.525	17.845	11.525	6.89	0	6.89	0.3	2.067	0	90	14.40	11.68	29.76	24.13			0.016	49.219	1	49.234	8.177	0.802	1	8.979
7	18.855	11.525	21	11.525	2.145	0	2.145	0.3	0.6435	0	90	19.93	11.68	12.82	7.51			0.005	15.323	1	15.328	0.247	24.342	1	24.589
8	7.8	21.35	9.245	21.35	1.445	0	1.445	0.3	0.4335	0	90	8.52	21.50	3.69	9.32			0.003	10.602	1	10.605	0.075	11.969	1	12.045
9	10.255	21.35	18.545	21.35	8.29	0	8.29	0.3	2.487	0	90	14.40	21.50	35.81	53.47			0.019	60.821	1	60.840	14.243	0.965	1	15.208
10	19.555	21.35	21	21.35	1.445	0	1.445	0.3	0.4335	0	90	20.28	21.50	8.79	9.32			0.003	10.602	1	10.605	0.075	18.318	1	18.393
11	7.8	13.535	7.8	16.725	0	3.19	3.19	0.3	0.957	90	0	7.80	15.13	7.46	14.48			0.812	1.943	1	2.754	0.007	34.189	1	34.196
12	7.8	17.735	7.8	19.125	0	1.39	1.39	0.3	0.417	90	0	7.80	18.43	3.25	7.69			0.067	1.466	1	1.534	0.003	14.898	1	14.901
13	21	13.535	21	16.725	0	3.19	3.19	0.3	0.957	90	0	21.00	15.13	20.10	14.48			0.812	1.943	1	2.754	0.007	49.927	1	49.934
14	21	17.735	21	19.125	0	1.39	1.39	0.3	0.417	90	0	21.00	18.43	8.76	7.69			0.067	1.466	1	1.534	0.003	21.755	1	21.758
									24.189					333.25	400.44						1299.875				844.554

C.1.4. JuBi Tower

The stability system of the JuBi tower can be split into three different sections. From the ground floor to the 9th floor, lateral stability is provided by thick concrete walls, a set of concrete columns and three concrete cores. This can be seen in figures C.11 and C.12. The second section ranges from the 10th floor to the 27th floor. This section consists of a concrete tube and three concrete cores. Only the left core of the second section differs from the cores of the first section. The concrete tube and cores can be seen in figures C.13 and C.14. The thirst section, which ranges from the 28th floor to the 38th floor, also exists of a concrete tube and three concrete cores, all differing from the previous section. The tube and cores are shown in figures C.15 and C.16. The moment of inertia calculation for all systems contributing to the stiffness of the structure are given in tables C.26 to C.36 and the results thereof are given in table C.24. The lower and upper bounds of the bending stiffnesses for each section are given in table C.25.

Table C.24: Moment of inertia of the stability systems of the JuBi tower

		Concrete columns	Concrete tube	Left core	Top core	Right core	Total
Level 0 - 9	I_{yy}	2015.06	4097.47	83.88	250.26	121.17	6567.84
	I_{xx}	1203.04	9276.85	496.88	68.28	596.81	11641.84
Level 10 - 27	I_{yy}	-	3917.20	29.14	250.26	121.17	4317.77
	I_{xx}	-	6767.62	321.51	68.28	596.81	7754.22
Level 28 - 38	I_{yy}	-	2907.33	11.67	149.05	49.12	3117.17
	I_{xx}	-	5658.1	109.00	39.01	150.48	5956.60

Table C.25: Lower and upper bound of bending stiffness

		Lower Bound	Upper Bound
Level 0 - 9	EI_x	4.93×10^{13}	2.50×10^{14}
	EI_y	8.73×10^{13}	4.42×10^{14}
Level 10 - 27	EI_x	3.24×10^{12}	1.64×10^{14}
	EI_y	5.82×10^{13}	2.95×10^{14}
Level 28 - 38	EI_x	2.34×10^{13}	1.18×10^{14}
	EI_y	4.47×10^{13}	2.26×10^{14}
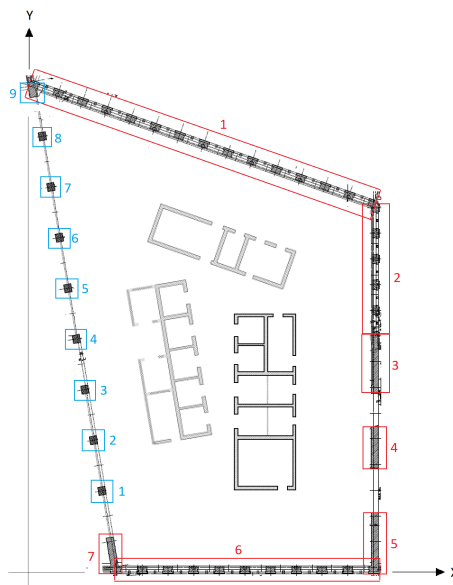
Figure C.11: JuBi tower outer tube element numbering level 0-9
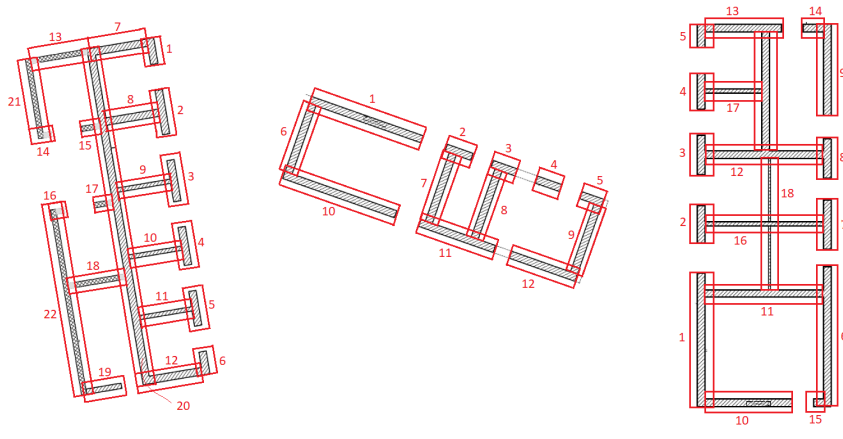
Figure C.12: JuBi tower core element numbering level 0-9
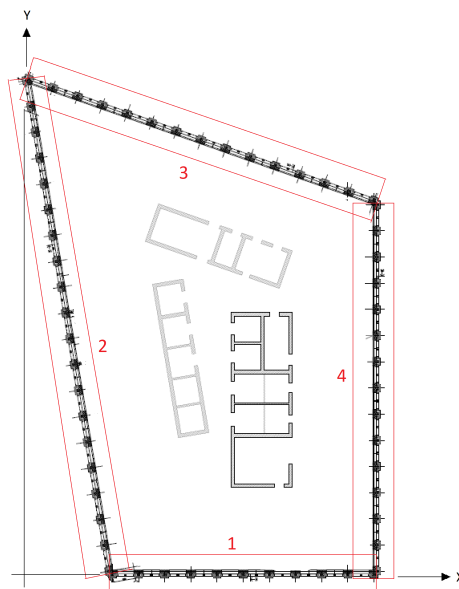
Figure C.13: JuBi tower outer tube element numbering level 10-27
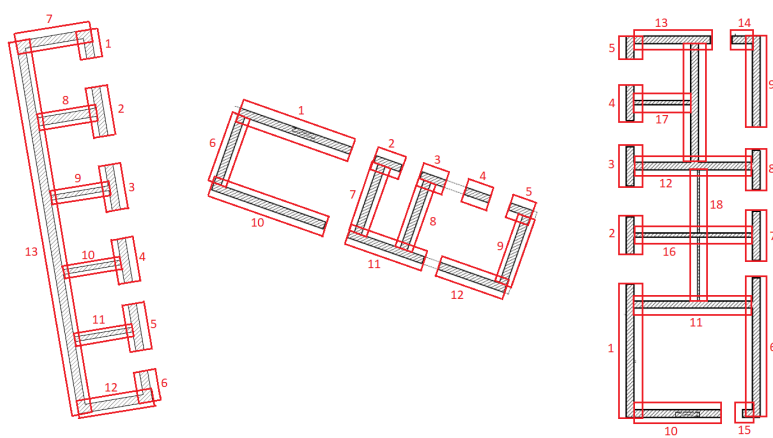
Figure C.14: JuBi tower core element numbering level 10-27
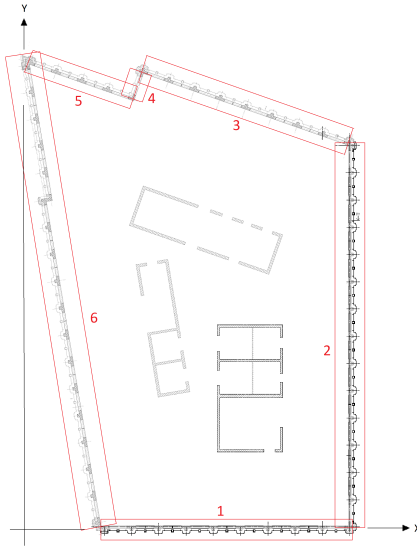
Figure C.15: JuBi tower outer tube element numbering level 28-38
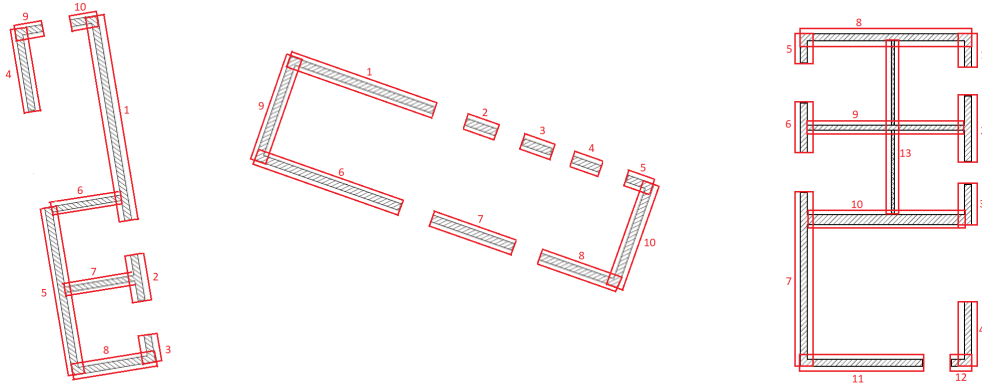
Figure C.16: JuBi tower core element numbering level 28-38

Table C.26: Moment of inertia calculation for the left core on levels 0-9 of the JuBi tower

left core	x1	y1	x2	y2	x2-x1	y2-y1	b	t	A	θ	ϕ	cx	cy	Acx	Acy	Cx	Cy	Ixo	Ad^2	ORF	Ixx	Iyo	Ad^2	ORF	Iyy
1	22.53	30.21	22.71	29.17	0.18	-1.04	1.230	0.35	0.43	79.96	10.04	22.62	29.69	9.74	12.78	21.22	21.93	0.053	25.936	1	25.989	0.006	0.843	1	0.849
2	22.93	27.95	23.30	25.87	0.37	-2.08	2.110	0.35	0.74	79.96	10.04	23.11	26.91	17.07	19.87			0.266	18.329	1	18.595	0.016	2.643	1	2.659
3	23.51	24.65	23.88	24.72	0.37	-1.93	1.960	0.35	0.69	79.96	10.04	23.70	23.69	16.26	16.25			0.213	2.118	1	2.331	0.013	4.205	1	4.218
4	24.10	21.50	24.41	19.72	0.32	-1.78	1.810	0.35	0.63	79.96	10.04	24.26	20.61	15.37	13.06			0.168	1.101	1	1.268	0.012	5.830	1	5.842
5	24.63	18.49	24.92	16.86	0.29	-1.63	1.660	0.35	0.58	79.96	10.04	24.77	17.68	14.39	10.27			0.130	10.510	1	10.639	0.010	7.332	1	7.341
6	25.14	15.64	25.29	14.75	0.16	-0.89	1.080	0.35	0.38	79.96	10.04	25.21	15.20	9.53	5.74			0.036	17.136	1	17.172	0.005	6.024	1	6.029
7	19.72	29.71	22.53	30.21	2.81	0.50	2.500	0.35	0.88	79.96	10.04	21.13	29.96	18.48	26.22			0.023	56.448	1	56.470	0.442	0.008	1	0.450
8	20.30	26.41	23.11	26.91	2.81	0.50	2.500	0.35	0.88	10.04	79.96	21.71	26.66	18.99	23.33			0.023	19.592	1	19.615	0.442	0.204	1	0.646
9	20.89	23.11	23.69	23.61	2.80	0.50	2.500	0.2	0.50	10.04	79.96	22.29	23.36	11.15	11.68			0.010	1.025	1	1.035	0.253	0.570	1	0.823
10	21.46	19.89	24.27	20.39	2.81	0.50	2.500	0.2	0.50	10.04	79.96	22.87	20.14	11.43	10.07			0.010	1.599	1	1.608	0.253	1.349	1	1.602
11	21.96	17.03	24.77	17.53	2.81	0.50	2.500	0.2	0.50	10.04	79.96	23.37	17.28	11.68	8.64			0.010	10.802	1	10.812	0.253	2.296	1	2.548
12	22.48	14.25	25.27	14.75	2.79	0.50	2.500	0.35	0.88	10.04	79.96	23.88	14.50	20.89	12.69			0.023	48.279	1	48.302	0.442	6.157	1	6.600
13	16.76	29.19	19.72	29.71	2.96	0.52	2.700	0.25	0.68	10.04	79.96	18.24	29.45	12.31	19.88			0.016	38.191	1	38.207	0.398	6.003	1	6.401
14	17.40	25.69	17.90	25.78	0.50	0.09	0.380	0.25	0.10	79.96	10.04	17.65	25.74	1.68	2.44			0.001	1.377	1	1.377	0.001	1.212	1	1.213
15	19.32	26.03	20.36	26.21	1.04	0.18	0.880	0.25	0.22	79.96	10.04	19.84	26.12	4.36	5.75			0.002	3.866	1	3.867	0.014	0.420	1	0.434
16	18.03	21.51	18.53	21.60	0.50	0.09	0.380	0.25	0.10	10.04	79.96	18.28	21.56	1.74	2.05			0.001	0.013	1	0.014	0.001	0.822	1	0.824
17	19.95	21.85	20.99	22.03	1.04	0.18	0.880	0.25	0.22	10.04	79.96	20.47	21.94	4.50	4.83			0.002	0.000	1	0.002	0.014	0.124	1	0.138
18	18.65	18.01	21.61	18.53	2.96	0.52	2.700	0.25	0.68	10.04	79.96	20.13	18.27	13.59	12.33			0.016	9.033	1	9.048	0.398	0.805	1	1.203
19	19.50	13.73	21.33	14.05	1.83	0.32	1.805	0.25	0.45	10.04	79.96	20.42	13.89	9.21	6.27			0.006	29.156	1	29.162	0.119	0.294	1	0.413
20	19.72	29.71	22.46	14.25	2.74	-15.46	15.700	0.35	5.50	79.96	10.04	21.09	21.98	115.89	120.78			109.443	0.015	1	109.458	3.485	0.096	1	3.581
21	16.76	29.19	17.38	25.69	0.62	-3.50	3.800	0.25	0.95	79.96	10.04	17.07	27.44	16.22	26.07			1.109	28.862	1	29.971	0.040	16.379	1	16.419
22	18.03	21.51	19.53	13.04	1.50	-8.47	8.850	0.25	2.21	79.96	10.04	18.78	17.28	41.55	38.22			14.002	47.903	1	61.905	0.450	13.197	1	13.647
									18.66					396.03	409.21						496.847				83.880

Table C.27: Moment of inertia calculation for the top core on levels 0-9 of the JuBi tower

Top core	x1	y1	x2	y2	x2-x1	y2-y1	b	t	A	θ	ϕ	cx	cy	Acx	Acy	Cx	Cy	Ixo	Ad^2	ORF	Ixx	Iyo	Ad^2	ORF	Iyy
1	20.39	38.02	25.47	36.15	5.08	-1.87	5.59	0.35	1.96	20.17	69.84	22.93	37.09	44.86	72.56	26.32	33.63	0.623	23.312	1	23.935	4.492	22.495	1	26.986
2	26.62	35.73	27.83	35.29	1.21	-0.44	1.285	0.35	0.45	20.17	69.84	27.23	35.51	12.24	15.97			0.011	1.584	1	1.596	0.055	0.368	1	0.423
3	28.78	34.94	29.91	34.52	1.13	-0.42	1.205	0.35	0.42	20.17	69.84	29.35	34.73	12.38	14.65			0.010	0.507	1	0.517	0.045	3.857	1	3.903
4	30.87	34.17	32.00	33.76	1.13	-0.41	1.205	0.35	0.42	20.17	69.84	31.44	33.97	13.26	14.32			0.010	0.046	1	0.056	0.045	11.031	1	11.076
5	32.96	33.40	33.80	33.09	0.84	-0.31	1.07	0.35	0.37	20.17	69.84	33.38	33.25	12.50	12.45			0.008	0.056	1	0.064	0.032	18.662	1	18.694
6	19.10	34.33	20.39	38.02	1.29	3.69	3.4	0.35	1.19	69.84	20.17	19.75	36.18	23.50	43.05			1.012	7.689	1	8.700	0.147	51.457	1	51.604
7	25.69	31.91	26.98	35.59	1.29	3.68	3.4	0.35	1.19	69.84	20.17	26.34	33.75	31.34	40.16			1.012	0.016	1	1.028	0.147	0.000	1	0.147
8	27.84	31.13	29.13	34.81	1.29	3.68	3.4	0.35	1.19	69.84	20.17	28.49	32.97	33.90	39.23			1.012	0.523	1	1.535	0.147	5.574	1	5.721
9	32.51	29.41	33.80	33.09	1.29	3.68	3.4	0.35	1.19	69.84	20.17	33.16	31.25	39.45	37.19			1.012	6.758	1	7.770	0.147	55.581	1	55.728
10	19.10	34.33	24.18	32.46	5.08	-1.87	5.59	0.35	1.96	20.17	69.84	21.64	33.40	42.34	65.34			0.623	0.111	1	0.734	4.492	42.866	1	47.358
11	25.33	32.05	28.82	30.77	3.49	-1.28	3.723	0.35	1.30	20.17	69.84	27.08	31.41	35.28	40.93			0.191	6.440	1	6.631	1.328	0.741	1	2.069
12	29.58	30.49	32.51	29.41	2.93	-1.08	3.282	0.35	1.15	20.17	69.84	31.05	29.95	35.66	34.40			0.133	15.583	1	15.716	0.910	25.637	1	26.547
									12.79					336.71	430.25						68.282				250.256

level 0 - 9

Right Core	x1	y1	x2	y2	x2-x1	y2-y1	b	t	A	θ	φ	cx	cy	Acx	Acy	Cx	Cy	Ixo	Ad²	ORF	Ixx	Iyo	Ad²	ORF	Iyy
1	27.70	9.01	27.70	15.18	0.00	6.18	6.28	0.35	2.20	90.00	0.00	27.70	12.09	60.88	26.58	30.89	17.56	7.224	65.660	1	72.883	0.022	22.308	1	22.330
2	27.70	16.62	27.70	18.31	0.00	1.69	1.76	0.35	0.62	90.00	0.00	27.70	17.47	17.06	10.76			0.159	0.005	1	0.164	0.006	6.252	1	6.258
3	27.70	19.75	27.70	21.61	0.00	1.86	1.86	0.35	0.65	90.00	0.00	27.70	20.68	18.03	13.46			0.188	6.345	1	6.533	0.007	6.607	1	6.614
4	27.70	22.85	27.70	24.51	0.00	1.66	1.66	0.35	0.58	90.00	0.00	27.70	23.68	16.09	13.76			0.133	21.775	1	21.908	0.006	5.897	1	5.903
5	27.70	25.75	27.70	26.65	0.00	0.90	1.08	0.35	0.38	90.00	0.00	27.70	26.20	10.47	9.90			0.037	28.230	1	28.267	0.004	3.836	1	3.840
6	34.00	9.01	34.00	15.42	0.00	6.42	6.59	0.35	2.31	90.00	0.00	34.00	12.21	78.42	28.17			8.347	65.909	1	74.256	0.024	22.370	1	22.393
7	34.00	16.24	34.00	18.57	0.00	2.33	2.33	0.35	0.82	90.00	0.00	34.00	17.41	27.73	14.19			0.369	0.019	1	0.388	0.008	7.909	1	7.917
8	34.00	19.59	34.00	21.27	0.00	1.68	1.85	0.35	0.65	90.00	0.00	34.00	20.43	22.02	13.23			0.185	5.331	1	5.516	0.007	6.280	1	6.286
9	34.00	22.37	34.00	26.65	0.00	4.29	4.29	0.35	1.50	90.00	0.00	34.00	24.51	51.05	36.80			2.303	72.514	1	74.817	0.015	14.562	1	14.578
10	27.70	9.01	32.16	9.01	4.46	0.00	4.105	0.35	1.44	0.00	90.00	29.93	9.01	43.00	12.94			0.015	105.105	1	105.120	2.018	1.319	1	3.337
11	27.70	14.23	34.00	14.23	6.30	0.00	5.6	0.35	1.96	0.00	90.00	30.85	14.23	60.47	27.88			0.020	21.774	1	21.794	5.122	0.003	1	5.125
12	27.70	20.61	34.00	20.61	6.30	0.00	5.6	0.35	1.96	0.00	90.00	30.85	20.61	60.47	40.39			0.020	18.196	1	18.216	5.122	0.003	1	5.125
13	27.70	26.65	31.32	26.65	3.62	0.00	3.62	0.35	1.27	0.00	90.00	29.51	26.65	37.39	33.77			0.013	104.734	1	104.747	1.384	2.398	1	3.782
14	32.34	26.65	34.00	26.65	1.66	0.00	0.96	0.35	0.34	0.00	90.00	33.17	26.65	11.15	8.95			0.003	27.775	1	27.778	0.026	1.753	1	1.779
15	33.18	9.01	34.00	9.01	0.83	0.00	0.475	0.35	0.17	0.00	90.00	33.59	9.01	5.58	1.50			0.002	12.162	1	12.164	0.003	1.214	1	1.217
16	27.70	17.43	34.00	17.43	6.30	0.00	5.6	0.2	1.12	0.00	90.00	30.85	17.43	34.55	19.52			0.004	0.018	1	0.022	2.927	0.001	1	2.928
17	27.70	23.68	31.32	23.68	3.62	0.00	2.7	0.2	0.54	0.00	90.00	29.51	23.68	15.94	12.79			0.002	20.238	1	20.240	0.328	1.022	1	1.350
18	31.70	14.23	31.70	20.61	0.00	6.38	6.2	0.1	0.62	90.00	0.00	31.70	17.42	19.65	10.80			1.986	0.013	1	1.999	0.001	0.411	1	0.412
									19.10					589.95	335.38						596.813				121.173

Table C.28: Moment of inertia calculation for the right core on levels 0-9 of the JuBi tower

level 0 - 9

Tube	x1	y1	x2	y2	x2-x1	y2-y1	b	t	A	θ	φ	cx	cy	Acx	Acy	Cx	Cy	Ixo	Ad²	ORF	Ixx	Iyo	Ad²	ORF	Iyy
4	42.00	37.80	5.98	51.03	-36.03	13.23	38.378	0.5	19.19	20.17	69.84	23.99	44.42	460.29	852.27	28.40	24.65	280.227	7499.812	0.393	3057.555	2075.326	374.280	0.393	962.695
5	42.00	23.67	42.00	37.80	0.00	14.13	14.127	0.35	4.94	90.00	0.00	42.00	30.74	207.67	151.98			82.231	183.457	0.393	104.416	0.050	913.992	0.393	359.219
6	42.00	17.16	42.00	23.67	0.00	6.52	6.515	0.61	3.97	90.00	0.00	42.00	20.42	166.91	81.13			14.057	71.100	1	85.157	0.123	734.630	1	734.753
7	42.00	10.16	42.00	14.45	0.00	4.29	4.288	0.75	3.22	90.00	0.00	42.00	12.30	135.07	39.57			4.928	489.815	1	494.743	0.151	594.485	1	594.635
8	42.00	0.00	42.00	5.64	0.00	5.64	5.64	0.75	4.23	90.00	0.00	42.00	2.82	177.66	11.93			11.213	2014.920	1	2026.133	0.198	781.925	1	782.123
9	15.00	0.00	42.00	0.00	27.00	0.00	27	0.35	9.45	0.00	90.00	28.50	0.00	269.33	0.00			0.096	5739.807	0.393	2255.782	574.088	0.087	0.393	225.651
	15.00	0.00	14.46	3.08	-0.54	3.08	3.125	0.75	2.34	79.96	10.04	14.73	1.54	34.52	3.61			1.853	1251.214	1	1253.067	0.164	438.228	1	438.393
									47.35					1451.45	1140.49						9276.853				4097.469

Table C.29: Moment of inertia calculation for the outer tube on levels 0-9 of the JuBi tower

Table C.30: Moment of inertia calculation for the concrete columns on levels 0-9 of the JuBi tower

level 0 - 9 Concrete Columns	x	y	A	Acx	cy	Cx	Cy	Ixo	Iyo	Ad^2	Ixx	Ad^2	Iyy
1	13.59	7.98	0.64	8.6636	5.0873	28.404	24.645	0.0302	0.0381	177.05	177.08	139.9	139.94
2	12.65	13.29	0.64	8.0644	8.4724			0.0302	0.0381	82.20	82.23	158.22	158.26
3	11.71	18.61	0.64	7.4651	11.864			0.0302	0.0381	23.22	23.25	177.66	177.70
4	10.76	23.93	0.64	6.8595	15.255			0.0302	0.0381	0.33	0.36	198.46	198.50
5	9.82	29.25	0.64	6.2603	18.647			0.0302	0.0381	13.52	13.55	220.17	220.21
6	8.88	34.56	0.64	5.661	22.032			0.0302	0.0381	62.67	62.70	243.01	243.04
7	7.94	39.88	0.64	5.0618	25.424			0.0302	0.0381	147.96	147.99	266.97	267.01
8	7.00	45.20	0.64	4.4625	28.815			0.0302	0.0381	269.34	269.37	292.06	292.10
9	6.06	50.51	0.64	3.8633	32.2			0.0302	0.0381	426.48	426.51	318.27	318.31
			5.74	56.361	167.8						1203.04		2015.06

Table C.31: Moment of inertia calculation for the left core on levels 10-27 of the JuBi tower

Level 10-27 Left core	x1	y1	x2	y2	x2-x1	y2-y1	b	t	A	θ	φ	cx	cy	Acx	Acy	Cx	Cy	Ixo	Iyo	Ad^2	ORF	Ixx	Iyo	Ad^2	ORF	Iyy
1	22.53	30.21	22.71	29.17	0.18	-1.04	1.230	0.35	0.43	79.96	10.04	22.62	29.69	9.74	12.78	22.26	22.30	0.053	0.006	23.527	1	23.580	0.006	0.057	1	0.063
2	22.93	27.95	23.30	25.87	0.37	-2.08	2.110	0.35	0.74	79.96	10.04	23.11	26.91	17.07	19.87			0.266	0.016	15.712	1	15.978	0.016	0.540	1	0.555
3	23.51	24.65	23.88	22.72	0.37	-1.93	1.960	0.35	0.69	79.96	10.04	23.70	23.69	16.26	16.25			0.213	0.013	1.321	1	1.534	0.013	1.420	1	1.434
4	24.10	21.50	24.41	19.72	0.32	-1.78	1.810	0.35	0.63	79.96	10.04	24.26	20.61	15.37	13.06			0.168	0.012	1.804	1	1.972	0.012	2.526	1	2.537
5	24.63	18.49	24.92	16.86	0.29	-1.63	1.660	0.35	0.58	79.96	10.04	24.77	17.68	14.39	10.27			0.130	0.010	12.414	1	12.544	0.010	3.676	1	3.686
6	25.14	15.64	25.29	14.75	0.16	-0.89	1.080	0.35	0.38	79.96	10.04	25.21	15.20	9.53	5.74			0.036	0.005	19.068	1	19.104	0.005	3.301	1	3.306
7	19.72	29.71	22.53	30.21	2.81	0.50	2.500	0.35	0.88	10.04	79.96	21.13	29.96	18.48	26.22			0.023	0.442	51.375	1	51.398	0.442	1.126	1	1.568
8	20.30	26.41	23.11	26.91	2.81	0.50	2.500	0.35	0.88	10.04	79.96	21.71	26.66	18.99	23.33			0.023	0.442	16.653	1	16.675	0.442	0.269	1	0.711
9	20.89	23.11	23.69	23.61	2.80	0.50	2.500	0.2	0.50	10.04	79.96	22.29	23.36	11.15	11.68			0.010	0.253	0.565	1	0.574	0.253	0.000	1	0.253
10	21.46	19.89	24.27	20.39	2.81	0.50	2.500	0.2	0.50	10.04	79.96	22.87	20.14	11.43	10.07			0.010	0.253	2.327	1	2.337	0.253	0.183	1	0.436
11	21.96	17.03	24.77	17.53	2.81	0.50	2.500	0.2	0.50	10.04	79.96	23.37	17.28	11.68	8.64			0.010	0.253	12.587	1	12.597	0.253	0.611	1	0.864
12	22.48	14.25	25.27	14.75	2.79	0.50	2.500	0.35	0.88	10.04	79.96	23.88	14.50	20.89	12.69			0.023	0.442	53.200	1	53.223	0.442	2.284	1	2.726
13	19.72	29.71	22.46	14.25	2.74	-15.46	15.7	0.35	5.50	79.96	10.04	21.09	21.98	115.89	120.78			109.443	3.485	0.554	1	109.997	3.485	7.513	1	10.998
									13.07					290.87	291.37							321.511				29.135

Table C.32: Moment of inertia calculation for the outer tube on levels 10-27 of the JuBi tower

Level 10-27 Tube	x1	y1	x2	y2	x2-x1	y2-y1	b	t	A	θ	φ	cx	cy	Acx	Acy	Cx	Cy	Ixo	Iyo	Ad^2	ORF	Ixx	Iyo	Ad^2	ORF	Iyy
1	15.00	0.00	42.00	0.00	27.00	0.00	27	0.35	9.45	0.00	90.00	28.50	0.00	269.33	0.00	24.65	24.14	0.096	574.088	5505.439	0.395	2174.686	574.088	139.872	0.395	282.014
2	15.00	0.00	5.98	51.03	-9.03	51.03	51.822	0.35	18.14	79.96	10.04	10.49	25.52	190.22	462.78			3935.716	123.547	34.450	0.395	1568.216	123.547	3639.404	0.395	1486.366
3	5.98	51.03	42.00	37.80	36.03	-13.23	38.378	0.35	13.43	20.17	69.84	23.99	44.42	322.20	596.59			196.033	1452.711	5523.353	0.395	2259.158	1452.711	5.945	0.395	576.169
4	42.00	0.00	42.00	37.80	0.00	37.80	37.8	0.35	13.23	90.00	0.00	42.00	18.90	555.66	250.05			1575.296	0.135	362.823	0.395	765.557	0.135	3981.263	0.395	1572.652
									54.25					1337.41	1309.42							6767.617				3917.201

Level 28 - 38

Right Core	x1	y1	x2	y2	x2-x1	y2-y1	b	t	A	θ	φ	cx	cy	Acx	Acy	Cx	Cy	Ixo	Ad^2	ORF	Ixx	Iyo	Ad^2	ORF	Iyy
1	33.78	19.59	33.78	20.65	0.00	1.06	1.19	0.25	0.30	90	0.00	33.78	20.12	10.05	5.99	30.69	15.15	0.035	7.360	1	7.395	0.002	2.832	1	2.834
2	33.78	16.24	33.78	18.57	0.00	2.33	2.33	0.25	0.58	90	0.00	33.78	17.41	19.67	10.14			0.264	2.972	1	3.236	0.003	5.546	1	5.549
3	33.78	14.16	33.78	15.42	0.00	1.27	1.44	0.25	0.36	90	0.00	33.78	14.79	12.16	5.32			0.062	0.046	1	0.109	0.002	3.427	1	3.429
4	33.78	9.06	33.78	11.22	0.00	2.17	2.29	0.25	0.57	90	0.00	33.78	10.14	19.34	5.80			0.250	14.362	1	14.613	0.003	5.450	1	5.453
5	27.93	18.75	27.93	20.66	0.00	1.91	1.03	0.25	0.26	90	0.00	27.93	19.70	7.19	5.07			0.023	5.346	1	5.368	0.001	1.968	1	1.969
6	27.93	16.55	27.93	18.31	0.00	1.76	1.76	0.25	0.44	90	0.00	27.93	17.43	12.29	7.67			0.114	2.295	1	2.408	0.002	3.363	1	3.365
7	27.93	9.06	27.93	15.11	0.00	6.06	6.18	0.25	1.55	90	0.00	27.93	12.08	43.14	18.67			4.917	14.502	1	19.419	0.008	11.807	1	11.816
8	27.93	20.66	33.78	20.66	5.85	0.00	5.6	0.25	1.40	0	90.00	30.85	20.66	43.19	28.92			0.007	42.485	1	42.493	3.659	0.036	1	3.695
9	27.93	17.43	33.78	17.43	5.85	0.00	5.6	0.2	1.12	0	90.00	30.85	17.43	34.55	19.52			0.004	5.842	1	5.845	2.927	0.029	1	2.956
10	27.93	14.16	33.78	14.16	5.85	0.00	5.6	0.35	1.96	0	90.00	30.85	14.16	60.47	27.74			0.020	1.926	1	1.946	5.122	0.050	1	5.173
11	27.93	9.06	32.16	9.06	4.23	0.00	4.105	0.25	1.03	0	90.00	30.04	9.06	30.83	9.29			0.005	38.077	1	38.082	1.441	0.433	1	1.874
12	33.18	9.06	33.78	9.06	0.60	0.00	0.475	0.25	0.12	0	90.00	33.48	9.06	3.98	1.08			0.001	4.406	1	4.407	0.002	0.921	1	0.924
13	31.05	14.16	31.05	20.67	0.00	6.51	6.2	0.1	0.62	90	0.00	31.05	17.41	19.25	10.79			1.986	3.177	1	5.163	0.001	0.081	1	0.081
									10.30					316.10	156.01						150.483				49.117

Table C.33: Moment of inertia calculation for the right core on levels 28-38 of the JuBi tower

Level 28 - 38

Left Core	x1	y1	x2	y2	x2-x1	y2-y1	b	t	A	θ	φ	cx	cy	Acx	Acy	Cx	Cy	Ixo	Ad^2	ORF	Ixx	Iyo	Ad^2	ORF	Iyy
1	24.36	19.59	23.1	26.73	-1.26	7.14	7.38	0.25	1.85	79.96	10.04	23.73	23.16	43.78	42.73	22.937	20.071	8.120	17.602	1	25.721	0.264	1.160	1	1.424
2	24.87	16.73	24.58	18.37	-0.29	1.64	1.66	0.25	0.42	79.96	10.04	24.73	17.55	10.26	7.28			0.092	2.638	1	2.731	0.005	1.327	1	1.332
3	25.24	14.69	25.09	15.51	-0.15	0.82	0.98	0.25	0.25	79.96	10.04	25.17	15.10	6.17	3.70			0.019	6.055	1	6.074	0.002	1.216	1	1.218
4	20.88	23.49	20.39	26.27	-0.49	2.78	2.95	0.25	0.74	79.96	10.04	20.64	24.88	15.22	18.35			0.519	17.054	1	17.573	0.020	3.909	1	3.929
5	22.53	14.21	21.51	19.95	-1.02	5.74	6.05	0.25	1.51	79.96	10.04	22.02	17.08	33.31	25.83			4.473	13.533	1	18.007	0.148	1.272	1	1.420
6	21.51	19.95	24.22	20.4	2.71	0.45	2.5	0.2	0.50	10.04	79.96	22.87	20.18	11.43	10.09			0.010	0.005	1	0.015	0.253	0.003	1	0.255
7	22.02	17.09	24.73	17.55	2.71	0.46	2.5	0.2	0.50	10.04	79.96	23.38	17.32	11.69	8.66			0.010	3.785	1	3.794	0.253	0.096	1	0.348
8	22.53	14.21	25.24	14.69	2.71	0.48	2.5	0.25	0.63	10.04	79.96	23.89	14.45	14.93	9.03			0.013	19.749	1	19.762	0.316	0.562	1	0.877
9	20.39	26.27	21.24	26.42	0.85	0.15	0.74	0.25	0.19	10.04	79.96	20.82	26.35	3.85	4.87			0.001	7.282	1	7.283	0.008	0.833	1	0.841
10	22.25	26.6	23.1	26.73	0.85	0.13	0.74	0.25	0.19	10.04	79.96	22.68	26.67	4.19	4.93			0.001	8.043	1	8.044	0.008	0.013	1	0.021
									6.75					154.83	135.48						109.004				11.665

Table C.34: Moment of inertia calculation for the left core on levels 28-38 of the JuBi tower

Table C.35: Moment of inertia calculation for the top core on levels 28-38 of the JuBi tower

Level 28 - 38

Top Core	x1	y1	x2	y2	x2-x1	y2-y1	b	t	A	θ	φ	cx	cy	Acx	Acy	Cx	Cy	Ixo	Ad²	ORF	Ixx	Iyo	Ad²	ORF	Iyy
1	26.05	31.86	21.04	33.70	-5.01	1.84	5.46	0.25	1.36	20.17	69.84	23.55	32.78	32.11	44.70	26.35	29.68	0.41	13.11	1.00	13.52	2.98	10.72	1.00	13.70
2	28.27	31.04	27.19	31.44	-1.08	0.40	1.15	0.25	0.29	20.17	69.84	27.73	31.24	7.97	8.98			0.01	0.70	1.00	0.71	0.03	0.55	1.00	0.58
3	30.22	30.33	29.23	30.69	-0.99	0.36	1.05	0.25	0.26	20.17	69.84	29.73	30.51	7.80	8.01			0.00	0.18	1.00	0.19	0.02	2.99	1.00	3.01
4	31.97	29.69	30.98	30.05	-0.99	0.36	1.05	0.25	0.26	20.17	69.84	31.48	29.87	8.26	7.84			0.00	0.01	1.00	0.01	0.02	6.90	1.00	6.92
5	33.72	29.04	32.93	29.34	-0.79	0.30	0.97	0.25	0.24	20.17	69.84	33.33	29.19	8.08	7.08			0.00	0.06	1.00	0.06	0.02	11.80	1.00	11.82
6	24.79	28.44	19.79	30.27	-5.00	1.83	5.46	0.25	1.36	20.17	69.84	22.29	29.36	30.40	40.03			0.41	0.14	1.00	0.55	2.98	22.47	1.00	25.45
7	28.82	26.96	25.94	28.02	-2.88	1.06	3.07	0.25	0.77	20.17	69.84	27.38	27.49	21.01	21.10			0.08	3.68	1.00	3.76	0.53	0.82	1.00	1.35
8	32.46	25.62	29.77	26.61	-2.69	0.99	2.99	0.25	0.75	20.17	69.84	31.12	26.12	23.26	19.52			0.07	9.50	1.00	9.57	0.49	16.98	1.00	17.47
9	19.79	30.27	21.04	33.70	1.25	3.43	3.40	0.25	0.85	69.84	20.17	20.42	31.99	17.35	27.19			0.72	4.52	1.00	5.24	0.10	29.93	1.00	30.03
10	32.46	25.62	33.72	29.04	1.26	3.42	3.40	0.25	0.85	69.84	20.17	33.09	27.33	28.13	23.23			0.72	4.69	1.00	5.41	0.10	38.62	1.00	38.72
									7.00					184.38	207.68						39.01				149.05

Table C.36: Moment of inertia calculation for the outer tube on levels 28-38 of the JuBi tower

Level 28 - 38

Tube	x1	y1	x2	y2	x2-x1	y2-y1	b	t	A	θ	φ	cx	cy	Acx	Acy	Cx	Cy	Ixo	Ad²	ORF	Ixx	Iyo	Ad²	ORF	Iyy
1	17.70	0.00	42.00	0.00	24.30	0.00	27.00	0.35	9.45	0.00	90.00	29.85	0.00	282.08	0.00	27.13	22.46	0.10	4768.43	0.395	1883.57	574.09	69.78	0.395	254.33
2	42.00	0.00	42.00	37.80	0.00	37.80	37.80	0.35	13.23	90.00	0.00	42.00	18.90	555.66	250.05			1575.30	167.97	0.395	688.59	0.14	2924.33	0.395	1155.16
3	42.00	37.80	21.72	45.25	-20.28	7.45	21.60	0.35	7.56	20.17	69.84	31.86	41.53	240.86	313.93			35.00	2746.94	0.395	1098.87	259.01	168.95	0.395	169.04
4	20.72	42.54	21.72	45.25	1.00	2.71	2.89	0.35	1.01	69.84	20.17	21.22	43.90	21.46	44.40			0.62	464.60	0.395	183.76	0.09	35.36	0.395	14.00
5	20.72	42.54	10.58	46.26	-10.14	3.72	10.80	0.35	3.78	20.17	69.84	15.65	44.40	59.16	167.83			4.40	1819.02	0.395	720.25	32.38	498.40	0.395	209.66
6	17.70	0.00	10.58	46.26	-7.12	46.26	45.90	0.35	16.07	79.96	10.04	14.14	23.13	227.16	371.58			2734.77	7.14	0.395	1083.06	85.88	2711.92	0.395	1105.13
									51.10					1386.38	1147.79						5658.10				2907.33

C.1.5. Oval

The stability system of the Oval tower is split into two sections. The first section stretching from the ground floor to the 13th floor, and the second section stretching from the 14th floor to the 28th floor. For both sections, the stiffness is provided by two cores and four columns attached to each core by an outrigger on the top floor. Between the two sections, there is only a small difference in the configuration of the cores. The cores and the attached columns can be found in figures C.17 to C.19. The calculations of the moment of inertia for the two sections are given in tables C.39 to C.42, where the results of these calculations are summarized in table C.37. The lower and upper bound of the bending stiffness for the two sections are shown in table C.38.

Table C.37: Moment of inertia of the stability systems of the New Orleans tower

		Concrete columns	Left core	Right core	Total
Level 0 - 13	I_{yy}	18.78	97.11	110.22	246.17
	I_{xx}	187.14	142.96	147.60	664.86
Level 14 - 28	I_{yy}	20.05	84.86	99.41	221.86
	I_{xx}	187.15	138.50	145.56	658.39

Table C.38: Lower and upper bound of bending stiffness

		Lower Bound	Upper Bound
Level 0 - 13	EI_x	1.85×10^{12}	9.35×10^{12}
	EI_y	4.99×10^{12}	2.53×10^{13}
Level 14 - 28	EI_x	1.66×10^{12}	8.43×10^{12}
	EI_y	4.94×10^{12}	2.50×10^{13}
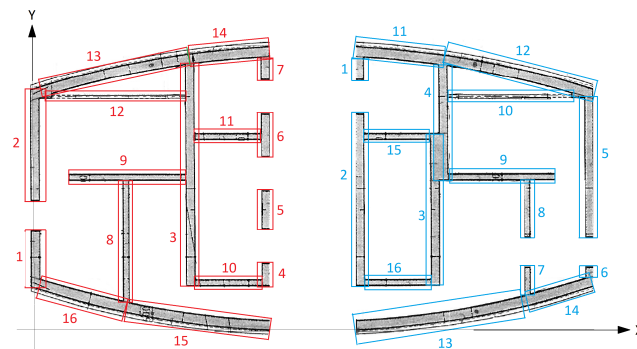
Figure C.17: Oval tower core element numbering level 0-13
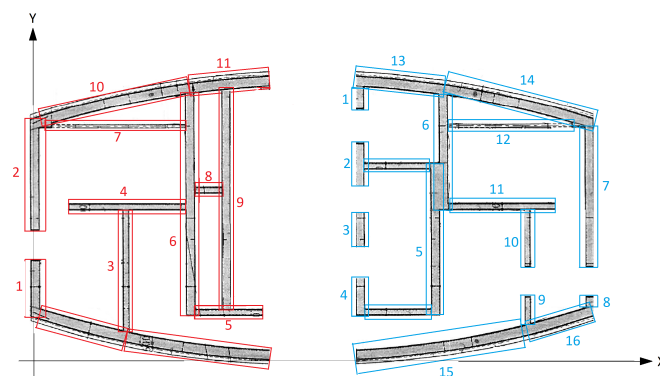
Figure C.18: Oval tower core element numbering level 14-28
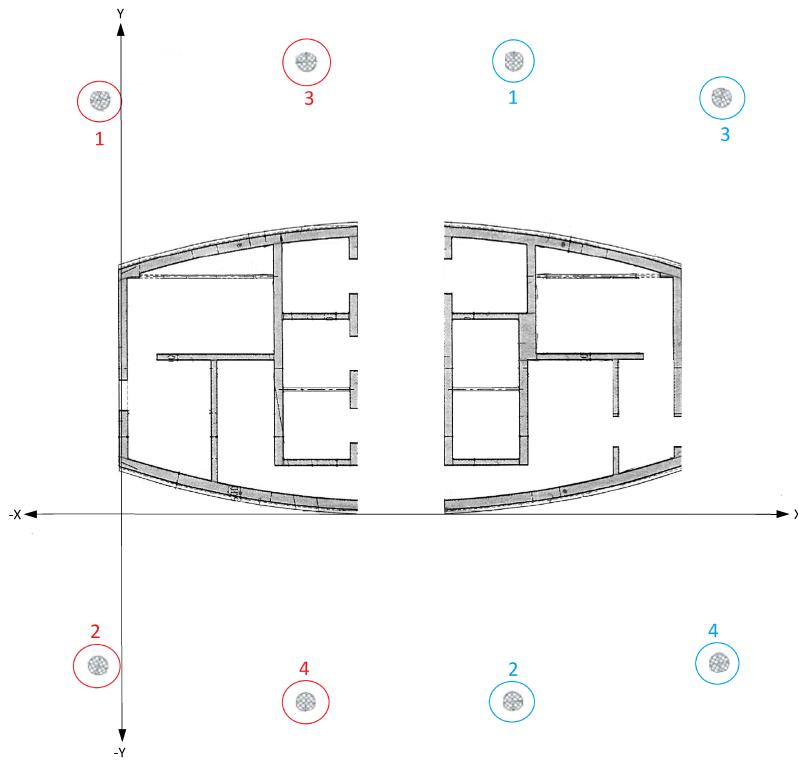
Figure C.19: Oval tower core column numbering level 0-28

Table C.39: Moment of inertia calculation for the left core on levels 0-13 of the Oval tower

level 0 - 13 left core	x1	y1	x2	y2	x2-x1	y2-y1	b	t	A	θ	φ	cx	cy	Acx	Acy	Cx	Cy	Ixo	Ad^2	ORF	Ixx	Iyo	Ad^2	ORF	Iyy
1	0.00	1.69	0.00	3.51	0.00	1.81	1.81	0.30	0.54	90.00	0.00	0.00	2.60	0.00	1.41	4.07	5.21	0.15	3.70	1	3.85	0.00	9.03	1	9.04
2	0.00	4.56	0.00	8.28	0.00	3.72	3.72	0.30	1.12	90.00	0.00	0.00	6.42	0.00	7.16			1.29	1.64	1	2.92	0.01	18.53	1	18.54
3	5.60	1.84	5.60	9.45	0.00	7.61	7.61	0.30	2.28	90.00	0.00	5.60	5.65	12.78	12.89			11.02	0.44	1	11.46	0.02	5.31	1	5.33
4	8.10	1.84	8.10	2.45	0.00	0.61	0.61	0.30	0.18	90.00	0.00	8.10	2.15	1.48	0.39			0.01	1.71	1	1.72	0.00	2.97	1	2.97
5	8.10	3.83	8.10	4.95	0.00	1.12	1.12	0.30	0.34	90.00	0.00	8.10	4.39	2.72	1.48			0.04	0.22	1	0.26	0.00	5.45	1	5.45
6	8.10	6.23	8.10	7.45	0.00	1.22	1.22	0.30	0.37	90.00	0.00	8.10	6.84	2.96	2.50			0.05	0.98	1	1.02	0.00	5.93	1	5.93
7	8.10	8.83	8.10	9.81	0.00	0.98	0.98	0.30	0.29	90.00	0.00	8.10	9.32	2.37	2.73			0.02	4.94	1	4.97	0.00	4.74	1	4.74
8	3.20	1.01	3.20	5.38	0.00	4.37	4.37	0.20	0.87	90.00	0.00	3.20	3.19	2.80	2.79			1.39	3.54	1	4.93	0.00	0.67	1	0.67
9	1.20	5.38	5.60	5.38	4.40	0.00	4.40	0.20	0.88	0.00	90.00	3.40	5.48	2.99	4.82			0.00	0.07	1	0.07	1.42	0.40	1	1.82
10	5.60	1.84	8.10	1.84	2.50	0.00	2.50	0.20	0.50	0.00	90.00	6.85	1.94	3.43	0.97			0.00	5.33	1	5.34	0.26	3.85	1	4.11
11	5.60	6.91	8.10	6.91	2.50	0.00	2.50	0.20	0.50	0.00	90.00	6.85	7.01	3.43	3.51			0.00	1.63	1	1.63	0.26	3.85	1	4.11
12	0.00	8.19	5.60	8.19	5.60	0.00	5.60	0.12	0.67	0.00	90.00	2.80	8.25	1.88	5.54			0.00	6.23	1	6.23	1.76	1.09	1	2.85
13	5.60	8.28	5.60	9.45	5.60	1.17	5.72	0.35	2.00	11.83	78.17	2.80	8.86	5.61	17.75			0.25	26.79	1	27.03	5.23	3.25	1	8.49
14	5.60	9.45	8.10	9.81	2.50	0.36	2.53	0.35	0.88	8.08	81.92	6.85	9.63	6.05	8.51			0.02	17.28	1	17.29	0.46	6.81	1	7.27
15	3.20	1.01	8.10	0.18	4.90	-0.83	4.97	0.35	1.74	-9.66	80.34	5.65	0.59	9.83	1.03			0.12	37.04	1	37.16	3.48	4.32	1	7.80
16	0.00	1.69	3.20	1.01	3.20	-0.68	3.27	0.35	1.15	-12.05	77.95	1.60	1.35	1.83	1.55			0.06	17.03	1	17.08	0.98	7.01	1	7.99
									14.32					60.17	75.03						142.96				97.11

Table C.40: Moment of inertia calculation for the left core columns on levels 0-13 of the Oval tower

level 0 - 13 columns	x	y	A	Acx	cy	Cx	Cy	Ixo	Ad^2	Ixx	Iyo	Ad^2	Iyy
1	6.19	17.32	0.33	2.06	5.75	4.07	5.21	0.01	48.70	48.71	0.01	1.49	1.50
2	6.19	-7.64	0.33	2.06	-2.54			0.01	54.77	54.78	0.01	1.49	1.50
3	-0.80	16.06	0.33	-0.27	5.33			0.01	39.09	39.10	0.01	7.88	7.89
4	-0.80	-6.38	0.33	-0.27	-2.12			0.01	44.55	44.55	0.01	7.88	7.89
			1.33	3.58	6.42					187.14			18.78

Table C.41: Moment of inertia calculation for the right core on levels 0-13 of the Oval tower

Right Core	x1	y1	x2	y2	x2-x1	y2-y1	b	t	A	θ	φ	cx	cy	Acx	Acy	Cx	Cy	Ixo	Ad²	ORF	Ixx	Iyo	Ad²	ORF	Iyy
1	11.40	8.83	11.40	9.81	0.00	0.98	0.98	0.30	0.29	90.00	0.00	11.40	9.32	3.33	2.73	15.11	5.22	0.02	4.91	1	4.94	0.00	4.03	1	4.03
2	11.40	1.84	11.40	7.45	0.00	5.61	5.61	0.30	1.68	90.00	0.00	11.40	4.65	19.19	7.82			4.41	0.55	1	4.97	0.01	23.19	1	23.20
3	13.90	1.84	13.90	6.91	0.00	5.07	5.07	0.30	1.52	90.00	0.00	13.90	4.38	21.15	6.66			3.26	1.08	1	4.34	0.01	2.23	1	2.25
4	14.20	5.24	14.20	9.45	0.00	4.21	4.21	0.30	1.26	90.00	0.00	14.20	7.35	17.92	9.27			1.86	5.72	1	7.58	0.01	1.05	1	1.06
5	19.50	3.37	19.50	8.28	0.00	4.91	4.91	0.30	1.47	90.00	0.00	19.50	5.82	28.72	8.57			2.96	0.54	1	3.49	0.01	28.36	1	28.37
6	19.50	1.69	19.50	1.99	0.00	0.30	0.30	0.30	0.09	90.00	0.00	19.50	1.84	1.77	0.17			0.00	1.03	1	1.03	0.00	1.74	1	1.75
7	17.30	1.01	17.30	1.99	0.00	0.99	0.99	0.20	0.20	90.00	0.00	17.30	1.50	3.41	0.30			0.02	2.72	1	2.74	0.00	0.94	1	0.94
8	17.30	3.04	17.30	5.24	0.00	2.20	2.20	0.20	0.44	90.00	0.00	17.30	4.14	7.61	1.82			0.18	0.51	1	0.69	0.00	2.11	1	2.11
9	13.90	5.24	17.30	5.24	3.40	0.00	3.40	0.20	0.68	90.00	90.00	15.60	5.34	10.61	3.63			0.00	0.01	1	0.01	0.66	0.16	1	0.82
10	14.20	8.19	19.50	8.19	5.30	0.00	5.30	0.12	0.64	0.00	90.00	16.85	8.25	10.72	5.25			0.00	5.84	1	5.84	1.49	1.92	1	3.41
11	11.40	9.81	14.20	9.45	2.80	-0.36	2.82	0.35	0.99	-7.23	82.77	12.80	9.63	12.64	9.51			0.02	19.20	1	19.22	0.65	5.28	1	5.92
12	14.20	9.45	19.50	8.28	5.30	-1.17	5.43	0.35	1.90	-12.48	77.52	16.85	8.86	32.01	16.84			0.24	25.24	1	25.48	4.45	5.74	1	10.19
13	11.40	0.18	17.30	1.01	5.90	0.83	5.96	0.35	2.09	8.05	81.95	14.35	0.59	29.93	1.23			0.14	44.64	1	44.78	6.05	1.21	1	7.26
14	17.30	1.01	19.50	1.69	2.20	0.68	2.30	0.35	0.81	17.25	72.75	18.40	1.35	14.84	1.09			0.04	12.06	1	12.10	0.33	8.72	1	9.04
15	11.40	6.91	13.90	6.91	2.50	0.00	2.50	0.30	0.75	0.00	90.00	12.65	7.06	9.49	5.30			0.01	2.55	1	2.56	0.39	4.55	1	4.94
16	11.40	1.84	13.90	1.84	2.50	0.00	2.50	0.30	0.75	0.00	90.00	12.65	1.99	9.49	1.49			0.01	7.82	1	7.82	0.39	4.55	1	4.94
									15.56					232.82	81.68						147.60				110.22

Table C.42: Moment of inertia calculation for the right core columns on levels 0-13 of the Oval tower

columns	x	y	A	Acx	cy	Cx	Cy	Ixo	Ad²	Ixx	Iyo	Ad²	Iyy
1	13.31	17.32	0.33	4.42	5.75	15.11	5.22	0.01	48.60	48.61	0.01	1.08	1.09
2	13.31	-7.64	0.33	4.42	-2.54			0.01	54.88	54.88	0.01	1.08	1.09
3	20.30	16.06	0.33	6.74	5.33			0.01	39.00	39.01	0.01	8.93	8.94
4	20.30	-6.38	0.33	6.74	-2.12			0.01	44.64	44.65	0.01	8.93	8.94
			1.33	22.31	6.42					187.15			20.05

level 0 - 13

Level 14 - 28

left core	x1	y1	x2	y2	x2-x1	y2-y1	b	t	A	θ	φ	cx	cy	Acx	Acy	Cx	Cy	Ixo	Ad²	ORF	Ixx	Iyo	Ad²	ORF	Iyy
1	0	1.692	0	3.506	0	1.814	1.81	0.30	0.54	90.00	0.00	0.00	2.60	0.00	1.41	3.94	5.19	0.15	3.65	1	3.80	0.0041	8.46	1	8.47
2	0	4.556	0	8.277	0	3.721	3.72	0.30	1.12	90.00	0.00	0.00	6.42	0.00	7.16			1.29	1.68	1	2.97	0.0084	17.36	1	17.37
3	3.2	1.009	3.2	5.38	0	4.371	4.37	0.20	0.87	90.00	0.00	3.20	3.19	2.80	2.79			1.39	3.48	1	4.87	0.0029	0.48	1	0.49
4	1.2	5.38	5.6	5.38	4.4		4.40	0.20	0.88	0.00	90.00	3.40	5.48	2.99	4.82			0.00	0.07	1	0.08	1.4197	0.26	1	1.68
5	5.6	1.84	6.9	1.84	1.3	0	1.30	0.20	0.26	0.00	90.00	6.25	1.94	1.63	0.50			0.00	2.75	1	2.75	0.0366	1.38	1	1.42
6	5.6	1.84	5.6	9.45	0	7.61	7.61	0.30	2.28	90.00	0.00	5.60	5.65	12.78	12.89			11.02	0.47	1	11.49	0.0171	6.26	1	6.28
7	0	8.19	5.6	8.19	5.6	0	5.60	0.12	0.67	0.00	90.00	2.80	8.25	1.88	5.54			0.00	6.29	1	6.29	1.7562	0.88	1	2.64
8	5.6	5.6	6.9	5.6	1.3	0	1.30	0.20	0.26	0.00	90.00	6.25	5.70	1.63	1.48			0.00	0.07	1	0.07	0.0366	1.38	1	1.42
9	6.9	1.84	6.9	9.54	0	7.7	7.70	0.20	1.54	90.00	0.00	6.90	5.69	10.63	8.76			7.61	0.38	1	7.99	0.0051	13.46	1	13.46
10	0	8.277	3.2	8.971	3.2	0.694	3.27	0.35	1.15	12.24	77.76	1.60	8.62	1.83	9.88			0.06	13.51	1	13.57	0.9785	6.29	1	7.27
11	3.2	8.971	8.1	9.805	4.9	0.834	4.97	0.35	1.74	9.66	80.34	5.65	9.39	9.83	16.33			0.12	30.66	1	30.78	3.4813	5.07	1	8.55
12	0	1.692	3.2	1.009	3.2	-0.683	3.27	0.35	1.15	-12.05	77.95	1.60	1.35	1.83	1.55			0.06	16.88	1	16.94	0.9778	6.29	1	7.27
13	3.2	1.009	8.1	0.175	4.9	-0.834	4.97	0.35	1.74	-9.66	80.34	5.65	0.59	9.83	1.03			0.12	36.78	1	36.90	3.4813	5.07	1	8.55
									14.20					57.66	74.16						138.50				84.86

Table C.43: Moment of inertia calculation for the left core on levels 14-28 of the Oval tower

Level 14 - 28

columns	x	y	A	Acx	cy	Cx	Cy	Ixo	Ad²	Ixx	Iyo	Ad²	Iyy
1	6.19	17.32	0.33	2.06	5.75	5.74	5.20	0.01	48.71	48.72	0.01	0.07	0.08
2	6.19	-7.64	0.33	2.06	-2.54			0.01	54.76	54.76	0.01	0.07	0.08
3	-0.80	16.06	0.33	-0.27	5.33			0.01	39.10	39.11	0.01	14.21	14.22
4	-0.80	-6.38	0.33	-0.27	-2.12			0.01	44.53	44.54	0.01	14.21	14.22
			1.33	3.58	6.42					187.14			28.59

Table C.44: Moment of inertia calculation for the left core columns on levels 14-28 of the Oval tower

Table C.45: Moment of inertia calculation for the right core on levels 14-28 of the Oval tower

Right Core	x1	y1	x2	y2	x2-x1	y2-y1	b	t	A	θ	φ	cx	cy	Acx	Acy	Cx	Cy	Ixo	Ad^2	ORF	Ixx	Iyo	Ad^2	ORF	Iyy
1	11.4	8.83	11.4	9.805	0	0.975	0.98	0.30	0.29	90.00	0.00	11.40	9.32	3.33	2.73	15.30	5.26	0.02	4.81	1	4.83	0.00	4.44	1	4.44
2	11.44	6.23	11.4	7.45	-0.04	1.22	1.22	0.30	0.37	-88.12	1.88	11.42	6.84	4.18	2.50			0.05	0.91	1	0.96	0.00	5.50	1	5.51
3	11.4	3.83	11.4	4.95	0	1.12	1.12	0.30	0.34	90.00	0.00	11.40	4.39	3.83	1.48			0.04	0.26	1	0.29	0.00	5.10	1	5.10
4	11.4	1.84	11.4	2.45	0	0.61	0.61	0.30	0.18	90.00	0.00	11.40	2.15	2.09	0.39			0.01	1.78	1	1.79	0.00	2.78	1	2.78
5	13.9	1.84	13.9	6.913	0	5.073	5.07	0.30	1.52	90.00	0.00	13.90	4.38	21.15	6.66			3.26	1.20	1	4.46	0.01	2.97	1	2.98
6	14.2	5.244	14.2	9.45	0	4.206	4.21	0.30	1.26	90.00	0.00	14.20	7.35	17.92	9.27			1.86	5.48	1	7.34	0.01	1.52	1	1.53
7	19.5	3.368	19.5	8.277	0	4.909	4.91	0.30	1.47	90.00	0.00	19.50	5.82	28.72	8.57			2.96	0.46	1	3.42	0.01	26.02	1	26.03
8	19.5	1.692	19.5	1.994	0	0.302	0.30	0.30	0.09	90.00	0.00	19.50	1.84	1.77	0.17			0.00	1.06	1	1.06	0.00	1.60	1	1.60
9	17.3	1.009	17.3	1.994	0	0.985	0.99	0.20	0.20	90.00	0.00	17.30	1.50	3.41	0.30			0.02	2.79	1	2.80	0.00	0.79	1	0.79
10	17.3	3.044	17.3	5.244	0	2.2	2.20	0.20	0.44	90.00	0.00	17.30	4.14	7.61	1.82			0.18	0.55	1	0.73	0.00	1.77	1	1.77
11	13.9	5.244	17.3	5.244	3.4	0	3.40	0.20	0.68	0.00	0.00	15.60	5.34	10.61	3.63			0.00	0.00	1	0.01	0.66	0.06	1	0.72
12	14.2	8.19	19.5	8.19	5.3	0	5.30	0.12	0.64	0.00	0.00	16.85	8.25	10.72	5.25			0.00	5.67	1	5.67	1.49	1.54	1	3.02
13	11.4	9.805	14.2	9.45	2.8	-0.355	2.82	0.35	0.99	-7.23	82.77	12.80	9.63	12.64	9.51			0.02	18.81	1	18.83	0.65	6.16	1	6.80
14	14.2	9.45	19.5	8.277	5.3	-1.173	5.43	0.35	1.90	-12.48	77.52	16.85	8.86	32.01	16.84			0.24	24.62	1	24.86	4.45	4.59	1	9.03
15	11.4	0.175	17.3	1.009	5.9	0.834	5.96	0.35	2.09	8.05	81.95	14.35	0.59	29.93	1.23			0.14	45.51	1	45.65	6.05	1.87	1	7.92
16	17.3	1.009	19.5	1.692	2.2	0.683	2.30	0.35	0.81	17.25	72.75	18.40	1.35	14.84	1.09			0.04	12.34	1	12.38	0.33	7.77	1	8.09
17	11.4	6.913	13.9	6.913	2.5	0	2.50	0.30	0.75	0.00	90.00	12.65	7.06	9.49	5.30			0.01	2.43	1	2.43	0.39	5.25	1	5.64
18	11.4	1.84	13.9	1.84	2.5	0	2.50	0.30	0.75	0.00	90.00	12.65	1.99	9.49	1.49			0.01	8.04	1	8.04	0.39	5.25	1	5.64
									14.76					223.73	78.23						145.56				99.41

Table C.46: Moment of inertia calculation for the right core columns on levels 14-28 of the Oval tower

columns	x	y	A	Acx	cy	Cx	Cy	Ixo	Ad^2	Ixx	Iyo	Ad^2	Iyy
1	13.31	17.32	0.33	4.42	5.75	15.30	5.26	0.01	48.24	48.25	0.01	1.31	1.32
2	13.31	-7.64	0.33	4.42	-2.54			0.01	55.26	55.27	0.01	1.31	1.32
3	20.30	16.06	0.33	6.74	5.33			0.01	38.68	38.69	0.01	8.31	8.32
4	20.30	-6.38	0.33	6.74	-2.12			0.01	44.99	44.99	0.01	8.31	8.32
			1.33	22.31	6.42					187.20			19.27

C.2. Building Density

To determine the lower and upper bounds for the building density of the 5 structure, the loads contributing to the mass of the structure is divided into three parts, the structural load, the permanent load and the variable load. The structural loads consist of all the dead loads originating from all the systems contributing to the structural integrity of the structure. These are the dead loads of the load bearing walls, cores, floors etc. The permanent loads are all dead loads which do not contribute to the structural integrity of the structure. These are the loads of the floor finishings, piping, ceilings etc. Lastly, the variable loads are all the live loads which originate due to the functionality of the building. The lower bound of the building density is determined by the summation of all the structural loads. The upper bound of the building density is the sum of all the structural loads, permanent loads and variable loads. The equations for the lower and upper bounds are given in equation C.2. It must be noted that the variable load is multiplied by a combination factor as used in the European Standards. This is due to the assumption that not all variable loads are present at the same time.

$$
\rho_{lower} = \frac{\Sigma G_{structural}}{gAL}
$$
$$
\rho_{upper} = \frac{\Sigma(G_{structural} + G_{permanent} + \Psi Q_{variable})}{gAL} \tag{C.2}
$$

For the multibeam models, the building density is again split into different sections. These sections coincide with the sections made for the bending stiffnesses. For the single beam model, the density is determined by dividing the total mass with the volume of the structure. The density in the x- and y-direction is taken as constant. To determine the loads for the bounds, a combination of the design documentation and technical drawings of each building was used.

(a) Sectional building densities

Building	Section	Density [$\frac{kg}{m^3}$]	
		Lower	Upper
NEMC	Level 0-32	358	436
Montevideo	Level 0-1	257	269
	Level 2-27	406	503
	Level 28-42	362	448
New Orleans	Level 0-2	495	656
	Level 3-10	405	502
	Level 11-45	405	493
JuBi	Level 0-9	444	542
	Level 10-27	433	532
	Level 28-38	314	418
Oval	Level 0-13	248	314
	Level 14-28	250	324

(b) Uniform building densities

Building	Density [$\frac{kg}{m^3}$]		
	Lower	Design	Upper
NEMC	358	400	436
Montevideo	382	460	470
New Orleans	410	500	504
JuBi	393	530	504
Oval	249	340	318

The following sections provide tables with the density calculations for the respective structures. Due to confidentiality reasons, the technical drawings and design documentation regarding the load calculations are not added.

C.2.1. New Erasmus Medical Centre

Table C.48: NEMC load calculation

Description	A [m^2]	$w_{structural}$ [$\frac{kN}{m^2}$]	$G_{structural}$ [kN]	$w_{permanent}$ [$\frac{kN}{m^2}$]	$G_{permanent}$ [kN]	$q_{variable}$ [$\frac{kN}{m^2}$]	$Q_{variable}$ [kN]	Ψ	$\Psi Q_{variable}$
Roof									
Core	99	24.00	2369						
roof	861	5.28	4546			1	861	0	0
Beams and Columns			364						
Façade	839	10.30	8637						
Façade Massive	128	15.40	1964						
Floor 30									
Core	57.568	24.00	1381.63						
Floor Technical Space	732.190	7.20	5271.77	0.70	512.53	7.5	5491.43	0.7	3844.00
Standard Floor	12.000	5.28	63.36	0.70	8.40	4	48.00	0.5	24.00
Saved Space	-17.160	7.20	-123.55	0.70	-12.01				
Floor Lift Shaft	43.125	5.28	227.70	2.10	90.56	4	172.50	0.5	86.25
Stair Platform	24.375	7.56	184.28	1.40	34.13	4	97.50	0.5	48.75
Beams and Columns			315.60						
Façade	403	10.30	4152.96						
Façade Massive	40	15.40	608.30						
Floor 29									
Core	58	24.00	1381.63						
Standard Floor	793	5.28	4189.10	0.70	555.37	4	3174	0.5	1587
Saved Space		5.28	0.00	0.70	0.00				
Floor Lift Shaft	43.125	5.28	227.70	2.10	90.56	4	173	0.5	86
Stair Platform	24.375	7.65	186.47	1.40	34.13	4	98	0.5	49
Beams and Columns			315.60						
Façade	403	10.30	4152.96						
Façade Massive	40	15.40	608.30						
Floor 28									
same as 29			11061.76		680.06		3444		1722
Floor 27									
same as 29			11061.76		680.06		3444		1722
Floor 26									
same as 29			11061.76		680.06		3444		1722
Floor 25									
same as 29			11061.76		680.06		3444		1722
Floor 24									
same as 29			11061.76		680.06		3444		1722
Floor 23									
same as 29			11061.76		680.06		3444		1722
Floor 22									
same as 29			11061.76		680.06		3444		1722
Floor 21									
Core	58	24.00	1382						
Floor 0.3m	0	7.20	0	3.00	0.00	4	0	0.5	0
Standard Floor	793	5.28	4189	0.70	555.38	4	3174	0.5	1587
Saved Space	0	7.20	0	3.00	0.00				
Floor Lift Shaft	43.125	5.28	228	2.10	90.56	4	173	0.5	86
Stair Platform	24.375	7.65	186	1.40	34.13	4	98	0.5	49
Beams and Columns			316						
Façade	403	10.30	4153						
Façade Massive	40	15.40	608						

Description	$A\ [m^2]$	$w_{structural}$ $[\frac{kN}{m^2}]$	$G_{structural}$ $[kN]$	$w_{permanent}$ $[\frac{kN}{m^2}]$	$G_{permanent}$ $[kN]$	$q_{variable}$ $[\frac{kN}{m^2}]$	$Q_{variable}$ $[kN]$	Ψ	$\Psi Q_{variable}$
Floor 20									
Core	58	24.00	1382						
Floor 0.3m	0	7.20	0	0.70	0	7.5	0	0.7	0
Standard Floor	793	5.28	4187	0.70	555	4	3172	0.5	1586
Saved Space	0	7.20	0	0.70	0				
Floor Lift Shaft	43.125	5.28	228	2.10	91	4	173	0.5	86
Stair Platform	24.375	7.65	186	1.40	34	4	98	0.5	49
Beams and Columns			316						
Façade	403	10.30	4153						
Façade Massive	40	15.40	608						
Floor 19									
same as 29			11062		680		3444		1722
Floor 19									
same as 29			11062		680		3444		1722
Floor 19									
same as 29			11062		680		3444		1722
Floor 19									
same as 29			11062		680		3444		1722
Floor 19									
same as 29			11062		680		3444		1722
Floor 14									
Core	66	24.00	1579						
Floor 0.3m	0	7.20	0	3.00	0	4	0	0.5	0
Standard Floor	793	5.28	4187	0.70	555	4	3172	0.5	1586
Saved Space	0	7.20	0	3.00	0				
Floor Lift Shaft	43.125	5.28	228	2.10	91	4	173	0.5	86
Stair Platform	24.375	7.65	186	1.40	34	4	98	0.5	49
Beams and Columns			354						
Façade	461	10.30	4746						
Façade Massive	45	15.40	695						
Floor 13									
Core	66	24.00	1579						
Floor Technical Space	0	7.20	0	0.70	0	7.5	0	0.7	0
Standard Floor	793	5.28	4187	0.70	555	4	3172	0.5	1586
Saved Space	0	7.20	0	0.70	0				
Floor Lift Shaft	43.125	5.28	228	2.10	91	4	173	0.5	86
Stair Platform	24.375	7.60	185	1.40	34	4	98	0.5	49
Beams and Columns			354						
Façade	461	10.50	4838						
Façade Massive	45	15.40	695						
Floor 12									
Core	66	24.00	1579						
Standard Floor	793	5.28	4187	0.70	555	4	3172	0.5	1586
Saved Space	0	5.28	0	0.70	0				
Floor Lift Shaft	43.125	5.28	228	2.10	91	4	173	0.5	86
Stair Platform	24.375	7.60	185	1.40	34	4	98	0.5	49
Beams and Columns			354						
Façade	461	10.50	4838						
Façade Massive	45	15.40	695						
Floor 11									
Core	66	24.00	1579						
Standard Floor	793	5.28	4187	0.70	555	4	3172	0.5	1586
Saved Space	0	5.28	0	0.70	0				
Floor Lift Shaft	43.125	5.28	228	2.10	91	4	173	0.5	86
Stair Platform	24.375	7.60	185	1.40	34	4	98	0.5	49
Beams and Columns			354						
Façade	461	10.50	4838						
Façade Massive	45	15.40	695						

Description	A [m^2]	$w_{structural}$ [$\frac{kN}{m^2}$]	$G_{structural}$ [kN]	$w_{permanent}$ [$\frac{kN}{m^2}$]	$G_{permanent}$ [kN]	$q_{variable}$ [$\frac{kN}{m^2}$]	$Q_{variable}$ [kN]	Ψ	$\Psi Q_{variable}$
Floor 10									
Core	66	24.00	1579						
Standard Floor	793	5.28	4187	0.70	555	4	3172	0.5	1586
Saved Space	0	5.28	0	0.70	0				
Floor Lift Shaft	43.125	5.28	228	2.10	91	4	173	0.5	86
Stair Platform	24.375	7.60	185	1.40	34	4	98	0.5	49
Beams and Columns			354						
Façade	461	10.50	4838						
Façade Massive	45	15.40	695						
Floor 9									
same as 10			12066		680		3442		1721
Floor 8									
Core	66	24.00	1579						
Floor 0.3m	0	7.20	0	3.00	0	4	0	0.5	0
Standard Floor	793	5.28	4187	0.70	555	4	3172	0.5	1586
Saved Space	0	7.20	0	3.00	0				
Floor Lift Shaft	43.125	5.28	228	2.10	91	4	173	0.5	86
Stair Platform	24.375	7.60	185	1.40	34	4	98	0.5	49
Beams and Columns	354		354						
Façade	461	10.50	4838						
Façade Massive	45	15.40	695						
Floor 7									
Core	66	24.00	1579						
Floor 0.3m	793	7.20	5710	0.70	555	7.5	5948	0.7	4163
Standard Floor	17	5.28	90	0.70	12	4	68	0.5	34
Saved Space	-17	7.20	-124	3.00	-51				
Floor Lift Shaft	43.125	5.28	228	2.10	91	4	173	0.5	86
Stair Platform	24.375	7.60	185	1.40	34	4	98	0.5	49
Beams and Columns	354		354						
Façade	461	10.50	4838						
Façade Massive	45	15.40	695						
Floor 6									
same as 10			12066		680		3442		1721
Floor 5									
same as 10			12066		680		3442		1721
floor 4									
Core	66	24.00	1579						
Standard Floor	793	5.28	4187	0.70	555	4	3172	0.5	1586
Saved Space	0	5.28	0	0.70	0				
Floor Lift Shaft	43.125	5.28	228	2.10	91	4	173	0.5	86
Stair Platform	24.375	7.60	185	1.40	34	4	98	0.5	49
Beams and Columns			354						
Façade	461	10.50	4838						
Façade Massive	45	15.40	695						
Floor 3									
Core	66	24.00	1579						
Standard Floor	779	5.28	4115	0.70	546	4	3117	0.5	1559
Saved Space	0	5.28	0	0.70	0				
Floor Lift Shaft	56.780	5.28	300	2.10	119	4	227	0.5	114
Stair Platform	24.375	7.60	185	1.40	34	4	98	0.5	49
Beams and Columns			354						
Façade	461	10.50	4838						
Façade Massive	45	15.40	695						
Floor 2									
Core	66	24.00	1579						
Standard Floor	779	5.28	4115	0.70	546	4	3117	0.5	1559
Saved Space	0	5.28	0	0.70	0		0		
Floor Lift Shaft	56.780	5.28	300	2.10	119	4	227	0.5	114
Stair Platform	24.375	7.60	185	1.40	34	4	98	0.5	49
Beams and Columns			354						
Façade	461	9.90	4564						
Façade Massive	45	15.40	693						

Description	$A\,[m^2]$	$w_{structural}$ $[\frac{kN}{m^2}]$	$G_{structural}$ $[kN]$	$w_{permanent}$ $[\frac{kN}{m^2}]$	$G_{permanent}$ $[kN]$	$q_{variable}$ $[\frac{kN}{m^2}]$	$Q_{variable}$ $[kN]$	Ψ	$\Psi Q_{variable}$
Floor 1									
Core	66	24.00	1579						
Standard Floor	779	5.28	4115	0.70	546	4	3117	0.5	1559
Saved Space	0	5.28	0	0.70	0				
Floor Lift Shaft	56.780	5.28	300	2.10	119	4	227	0.5	114
Stair Platform	24.375	7.60	185	1.40	34	4	98	0.5	49
Beams and Columns			354						
Concrete walls	512	8.10	4150						
			0						
Gound Floor			0						
Core	20	24.00	478						
Floor 0.25m	779	6.00	4676	1.20	935	10	7794	0.5	3897
Standard Floor	0	5.28	0	0.70	0	4	0	0.5	0
Floor Lift Shaft	56.780	5.28	300	2.10	119	4	227	0.5	114
Stair Platform	24.375	7.60	185	1.40	34	4	98	0.5	49
Stubs	14	24.00	335						
Concrete Walls	146	24.00	3505						
Total			374019		21458		117472		60593

Table C.49: NEMC density lower and upper bound calculation

Density			Lower		Upper	
floor	$L\,[m]$	$A\,[m2]$	$mass\,[kg]$	$\rho\,[\frac{kg}{m^3}]$	$mass\,[kg]$	$\rho\,[\frac{kg}{m^3}]$
All	121	881	38126301.42	357.65	46490309.27	436.12

C.2.2. Montevideo Tower

Table C.50: Montevideo load calculation

Floor	Description	$A\,[m^2]$	n Floors	$w_{structural}$ $[\frac{kN}{m^2}]$	$G_{structural}$ $[kN]$	$w_{permanent}$ $[\frac{kN}{m^2}]$	$G_{permanent}$ $[kN]$	$q_{variable}$ $[\frac{kN}{m^2}]$	$Q_{variable}$ $[kN]$	Ψ	$\Psi Q_{variable}$
43	Roof	290.70	1.00	5.28	1534.90	0.20	58.14	1.00	290.70	0.00	0.00
43	Roof Installation Space	16.64	1.00	5.28	87.86	0.35	5.82	7.00	116.48	1.00	116.48
42 to 29	Living Space	624.80	14.00	5.28	46185.09	2.10	18369.07	1.75	15307.56	0.40	6123.02
28	Living Space	751.68	1.00	5.28	3968.87	2.10	1578.53	1.75	1315.44	0.40	526.18
28	Balconies	71.76	1.00	5.28	378.89	2.10	150.70	2.50	179.40	0.50	89.70
27A	Installation Space	751.68	1.00	7.20	5412.09	0.00	0.00	7.00	5261.76	1.00	5261.76
43 - 27A	masonry walls				21767.26						
43 - 27A	structural steel				57913.08						
27 to 24	Living Space	691.45	4.00	5.28	14603.40	2.10	5808.17	1.75	4840.14	0.40	1936.06
	Balconies	28.91	4.00	5.28	610.47	2.10	242.80	2.50	289.05	0.50	144.53
23 to 5	Living Space	756.23	19.00	5.28	75865.39	2.10	30173.74	1.75	25144.78	0.40	10057.91
	Balconies	28.91	19.00	5.28	2899.75	2.10	1153.31	2.50	1372.99	0.50	686.49
4 & 3	Living Space	771.53	2.00	5.28	8147.40	2.10	3240.44	1.75	2700.37	0.40	1080.15
4 & 3 Balconies	Balconies	28.91	2.00	5.28	305.24	2.10	121.40	2.50	144.53	0.50	72.26
2	Commercial Space	745.20	1.00	7.20	5365.44	1.60	1192.32	5.00	3726.00	0.40	1490.40
27-2	concrete core				116332.99						
27-2	masonry walls				14849.28						
1 & 0	Core Floor	110.40	2.00	5.28	1165.82	2.10	463.68	1.75	386.40	0.40	154.56
1-0	concrete core				5146.92						
1-0	structural steel				7226.46						
Total					389766.61		62558.12				27739.50

Table C.51: Montevideo density lower and upper bound calculation

Density			Lower		Upper	
floor	$L\,[m]$	$A\,[m2]$	$mass\,[kg]$	$\rho\,[\frac{kg}{m^3}]$	$mass\,[kg]$	$\rho\,[\frac{kg}{m^3}]$
0-1	8.1	662.4	1380142.5	257.2	1443163.9	269.0
2-27	80.6	745	24360791.9	405.7	30211962.3	503.1
28-42	51.4	751	13990626.0	362.4	17281084.0	447.7
Uniform	140.1	743	39731560.4	381.6	48936210.3	470.0

C.2.3. New Orleans Tower

Table C.52: New Orleans load calculation

Floor	Description	A [m^2]	n Floors	$w_{structural}$ [$\frac{kN}{m^2}$]	$G_{structural}$ [kN]	$w_{permanent}$ [$\frac{kN}{m^2}$]	$G_{permanent}$ [kN]	$q_{variable}$ [$\frac{kN}{m^2}$]	$Q_{variable}$ [kN]	Ψ	$\Psi Q_{variable}$
0	entrance	700.7	1	9.81	6873.89	1	700.70	10	7007.02	0.25	1751.75
		129.6	1	7.85	1017.10	1	129.6	10	1296	0.25	324
		97.68	1		0	3.6	351.64				0
		99.93	1	4.91	490.19	1.2	119.92	3	299.81	0.25	74.95
1	shops and bike storage	827.42	1	3.8	3144.20	1.2	992.90	5	4137.11	0.25	1034.27
		827.42	1		0	0.5	413.71				0
		827.42	1		0	1.75	1447.98				0
		99.93	1	4.91	490.19	1.2	119.92	3	299.81	0.25	74.95
2	installation space	697.82	1	7.36	5134.22	1.2	837.38	5	3489.11	1	3489.11
		99.93	1	4.91	490.19	1.2	119.95	3	299.81	0.25	74.95
3	storage	697.82	1	7.36	5134.22	1.2	837.38	5	3489.11	1	3489.11
		697.82	1		0	0.5	348.91				0
		99.93	1	4.91	490.19	1.2	119.92	3	299.81	0.25	74.95
4-5	living space	710.62	2	7.36	10456.75	1.2	1705.48	1.75	2487.16	0.25	621.79
		710.62	2		0	1.2	1705.48				0
		99.93	2	4.91	980.38	1.2	239.85	3	599.62	0.25	149.90
		53.76	2	6.87	738.40	1.3	139.78	2.5	268.82	0.5	134.41
6-10	living space	679.6	5	7.36	25000.72	1.2	4077.59	1.75	5946.48	0.25	1486.62
		679.6	5		0	1.2	4077.59				0
		99.93	5	4.91	2450.96	1.2	599.62	3	1499.06	0.25	374.76
		102.7	5	6.87	3526.03	1.3	667.51	2.5	1283.68	0.5	641.84
11	living space	635.01	1	7.36	4672.07	1.2	762.01	1.75	1111.26	0.25	277.81
		635.01	1		0	1.2	762.01				0
		99.93	1	4.91	490.19	1.2	119.92	3	299.81	0.25	74.95
		87.42	1	6.87	600.31	1.3	113.64	2.5	218.55	0.5	109.27
12-39	living space	699.55	28	7.36	144114.39	1.2	23504.89	1.75	34277.97	0.25	8569.49
		699.55	28		0	1.2	23504.89				0
		99.93	28	4.91	13725.41	1.2	3357.9	3	8394.75	0.25	2098.68
		91.65	28	6.87	17622.09	1.3	3336.06	2.5	6415.5	0.5	3207.75
40-41	living space	686.3	2	7.36	10098.94	1.2	1647.12	1.75	2402.05	0.25	600.51
		686.3	2		0	1.2	1647.12				0
		99.93	2	4.91	980.38	1.2	239.85	3	599.62	0.25	149.90
Floor	Description	A [m^2]	n Floors	$w_{structural}$ [$\frac{kN}{m^2}$]	$G_{structural}$ [kN]	$w_{permanent}$ [$\frac{kN}{m^2}$]	$G_{permanent}$ [kN]	$q_{variable}$ [$\frac{kN}{m^2}$]	$Q_{variable}$ [kN]	Ψ	$\Psi Q_{variable}$
0	entrance	700.7	1	9.81	6873.891525	1	700.7025	10		686.3	2
	0	1.2	1647.126				0				
		99.93	2	4.91	980.38	1.2	239.85	3	599.62	0.25	149.90
43	living space	568.22	1	7.36	4180.69	1.2	681.86	1.75	994.385	0.25	248.59
		568.22	1		0	1.2	681.867				0
		99.98	1	4.91	490.19	1.2	119.95	3	299.81	0.25	74.95
44	living space	473.36	1	7.36	3482.76	1.2	568.03	1.75	828.38	0.25	207.09
		473.36	1		0	1.2	568.03				0
		99.93	1	4.91	490.19	1.2	119.92	3	299.81	0.25	74.95
45-46	living space	155.06	2	7.36	2281.74	1.2	372.15	1.75	542.71	0.25	135.67
		155.06	2		0	1.2	372.15				0
		99.93	2	4.91	980.38	1.2	239.85	3	599.62	0.25	149.90
all	lift	21.503	47	5.28	5336.06		0	6	6063.70	0.25	1515.92
all	beams				0						
all	columns				0						
all	Concrete core and outriggers				0						
all	masonry and cladding				0						
Total					275963.56		82472.12		96050.44		31292.92

Table C.53: New Orleans density lower and upper bound calculation

Density			Lower		Upper	
floor	L [m]	A [$m2$]	mass [kg]	ρ [$\frac{kg}{m^3}$]	mass [kg]	ρ [$\frac{kg}{m^3}$]
0-2	11.47	671	3812195.69	495.32	5051185.251	656.30749
3-10	26.64	856	9240444.76	405.21	11457630.51	502.44303
11-46	116.735	789	37263429.5	404.58	45404099.07	492.96601
Uniform	154.845	793	50316070	409.83	61912914.84	504.29051

C.2.4. JuBi Tower

Table C.54: JuBi load calculation

Floor	Description	$A\ [m^2]$	n Floors	$w_{structural}$ $[\frac{kN}{m^2}]$	$G_{structural}$ $[kN]$	$w_{permanent}$ $[\frac{kN}{m^2}]$	$G_{permanent}$ $[kN]$	$q_{variable}$ $[\frac{kN}{m^2}]$	$Q_{variable}$ $[kN]$	Ψ	$\Psi Q_{variable}$
0-9	concrete floor 390	1168.4	10	8.2	95808.8	1.6	18694.4	4	46736	0.5	23368
0-9	core floor 200	69.2	10	5	3460	1.6	1107.2	3	2076	0.5	1038
0-9	Staircase	39.9	10	5	1995	1.6	638.4	3	1197	0.25	299.25
0-9	lift	77.5	10	5.28	4092	0		6	4650	0.25	1162.5
0-9	prefab façade				0						
0-9	concrete columns				0						
0-9	concrete core				0						
0-9	connecting floors				0		0				0
10-22	concrete floor 350	1190.6	13	7.2	111440.16	1.6	24764.48	4	61911.2	0.5	30955.6
10-22	core floor 200	69.2	13	5	4498	1.6	1439.36	3	2698.8	0.5	1349.4
10-22	Staircase	26.6	13	5	1729	1.6	553.28	3	1037.4	0.25	259.35
10-22	lift	68.6	13	5.28	4708.704			6	5350.8	0.25	1337.7
10-22	façade				0						
10-22	concrete columns				0						
10-22	concrete core				0						
23-27	concrete floor 350	979.6	5	7.2	35265.6	1.6	7836.8	4	19592	0.5	9796
23-27	core floor 200	69.2	5	5	1730	1.6	553.6	3	1038	0.5	519
23-27	Staircase	26.6	5	5	665	1.6	212.8	3	399	0.25	99.75
23-27	lift	68.6	5	5.28	1811.04			6	2058	0.25	514.5
28-38	concrete floor 350	980.2	11	7.2	77631.84	1.6	17251.52	4	43128.8	0.5	21564.4
28-38	core floor 200	63.3	11	5	3481.5	1.6	1114.08	3	2088.9	0.5	1044.45
28-38	Staircase	26.6	11	5	1463	1.6	468.16	3	877.8	0.25	219.45
28-38	lift	31.5	11	5.28	1829.52			6	2079	0.25	519.75
23-38	façade				0						
23-38	concrete columns				0						
23-38	concrete core				0						
					351609.164		74634.08				94047.1

Table C.55: JuBi density lower and upper bound calculation

Density			Lower		Upper	
floor	$L\ [m]$	$A\ [m2]$	$mass\ [kg]$	$\rho\ [\frac{kg}{m^3}]$	$mass\ [kg]$	$\rho\ [\frac{kg}{m^3}]$
0-9	41	1355	23872047.17	429.70	29322006.40	527.80
10-22	46.02	1355	25914756.74	415.59	32098158.37	514.75
23-38	59.26	1144	20957390.13	309.14	27248344.26	401.93
Uniform	146.28	1268	70744194.05	381.27	88668509.03	477.88

C.2.5. Oval Tower

Table C.56: Oval load calculation

Force moved to column	Floor	Description	$A\ [m^2]$	n Floors	$w_{structural}$ $[\frac{kN}{m^2}]$	$G_{structural}$ $[kN]$	$w_{permanent}$ $[\frac{kN}{m^2}]$	$G_{permanent}$ $[kN]$	$q_{variable}$ $[\frac{kN}{m^2}]$	$Q_{variable}$ $[kN]$	Ψ	$\Psi Q_{variable}$
column V	roof	roof floor	23.19	1	2.35	54.50	3.70	85.80				
		Wood midsection	6.40	1	2.00	12.80	0.00	0.00	0.55	12.80	0.00	0.00
	1 to 24	floor	727.69	1	2.43	1768.28	1.94	1411.72	117.19	750.00	0.50	375.00
	1 to 24	floor	44.49	1	2.43	108.10	1.94	86.30	0.05	35.00	0.50	17.50
	0	floor	17.60	1	6.70	117.91	2.50	43.99	0.79	35.20	0.50	17.60
	all	prefab façade		1		1481.00		0.00				0.00
	0	edge beam		1		229.10		0.00		76.80	0.50	38.40
	1 to 24	bottom part façade		1		400.80		0.00				
	all	column		1		820.90		0.00				
	all	stub		1		82.90		0.00				
column Z	roof	roof floor	23.00	1	2.35	54.05	3.70	85.10				
		midsection	6.40	1	2.00	12.80	0.00	0.00	0.56	12.80	0.00	0.00
	1 to 24	floor	727.69	1	2.43	1768.28	1.94	1411.72	117.19	750.00	0.50	375.00
		concrete strip	44.49	1	2.43	108.10	1.94	86.30	0.05	35.00	0.50	17.50
	0	floor	17.60	1	6.70	117.91	2.50	43.99	0.79	35.20	0.50	17.60
	all	prefab façade		1		1481.00		0.00				
	0	edge beam		1		229.10		0.00		76.80	0.50	38.40
	all	column		1		820.90		0.00				
	all	stub		1		82.90		0.00				
		sprinkler basin		1		77.70		0.00		440.00	0.70	308.00

Force moved to column	Floor	Description	A [m²]	n Floors	$w_{structural}$ [$\frac{kN}{m^2}$]	$G_{structural}$ [kN]	$w_{permanent}$ [$\frac{kN}{m^2}$]	$G_{permanent}$ [kN]	$q_{variable}$ [$\frac{kN}{m^2}$]	$Q_{variable}$ [kN]	Ψ	$\Psi Q_{variable}$
column A & H	roof	floor	12.50	2	2.35	58.73	3.70	92.47			0.00	0.00
	1 to 24	floor	248.79	2	2.43	1209.11	1.94	965.29	31.61	395.00	0.50	395.00
	0	floor	22.80	2	6.70	305.58	2.50	114.02	0.18	45.60	0.50	45.60
	all	prefab façade		2		3147.00		0.00				
	0	edge beam		2		486.80		0.00		81.60	0.50	81.60
	all	walls		2		647.80		0.00				
	all	columns		2		1641.80		0.00				
	all	stubs		2		202.20		0.00				
column J	roof	floor	12.50	1	2.35	29.37	3.70	46.23			0.00	0.00
	1 to 24	floor	248.79	1	2.43	604.55	1.94	482.65	31.61	395.00	0.50	197.50
	0	floor	22.80	1	6.70	152.79	2.50	57.01	0.18	45.60	0.50	22.80
	all	prefab façade		1		1573.50						
	0	edge beam		1		243.40				81.60	0.50	40.80
	all	walls		1		323.90						
	all	columns		1		820.90						
	all	stubs		1		101.10						
		installation strip	10.25	1	2.00	20.50				20.50		
column R	roof	floor	12.50	1	2.35	29.37	3.70	46.23	0.00		0.00	0.00
	1 to 24	floor	248.79	1	2.43	604.55	1.94	482.65	31.61	395.00	0.50	197.50
	0	floor	22.80	1	6.70	152.79	2.50	57.01	0.18	45.60	0.50	22.80
	all	prefab façade		1		1573.50						
	0	edge beam		1		243.40				81.60	0.50	40.80
	all	walls		1		323.90						
	all	columns		1		820.90						
	all	stubs		1		101.10						
		installation strip	10.25	1	2.00	20.50				20.50	0.50	10.25
		strinkler basin		1		32.60			55.61	570.00	0.70	399.00
column B	roof	roof floor	11.70	1	2.35	27.50	3.70	43.30			0.00	0.00
	roof	roof floor	21.40	1	8.10	173.30	0.00	0.00			0.00	0.00
	roof	Technical space	3.01	1	2.35	7.07	2.50	7.53	0.28	6.00	0.50	3.00
	roof	25th field	26.63	1	7.15	190.39	1.45	38.61	49.76	149.80	1.00	149.80
	roof	extra concrete		1		204.90		0.00				
	1 to 24	floor	221.33	1	2.43	537.83	1.94	429.37		395.00	0.50	197.50
		floor	301.12	1	2.43	731.72	1.94	584.18	2.56	566.70	0.50	283.35
	0	floor	28.16	1	6.70	188.69	2.50	70.41	0.15	46.30	0.50	23.15
	all	prefab façade		1		1666.10						
	0	edge beam		1		257.80				86.40	0.50	43.20
	all	walls		1		342.90						
	all	columns		1		820.90						
	all	stubs		1		82.90						
column G	roof	roof floor	11.70	1	2.35	27.50	3.70	43.30			0.00	0.00
		roof floor	21.40	1	8.10	173.30					0.00	0.00
		Technical space	3.01	1	2.35	7.07	2.50	7.53	0.28	6.00	0.50	3.00
		25th field	26.63	1	7.15	190.39	1.45	38.61	49.76	149.80	1.00	149.80
		extra concrete		1		204.90						
	1 to 24	floor	221.33	1	2.43	537.83	1.94	429.37		395.00	0.50	197.50
		floor	301.12	1	2.43	731.72	1.94	584.18	2.56	566.70	0.50	283.35
	0	floor	28.16	1	6.70	188.69	2.50	70.41	0.15	46.30	0.50	23.15
	all	prefab façade		1		1666.10						
	0	edge beam		1		257.80				86.40	0.50	43.20
	all	walls		1		342.90						
	all	columns		1		820.90						
	all	stubs		1		82.90						
		floor stairs	18.38	1	6.00	110.30				36.80	0.50	18.40
Column K	roof	roof floor	11.70	1	2.35	27.50	3.70	43.30			0.00	0.00
		Concrete wall		1		173.30						
		25th field	26.63	1	7.15	190.39	1.45	38.61		149.80	1.00	149.80
	1 to 24	floor	221.33	1	2.43	537.83	1.94	429.37	14.83	395.00	0.50	197.50
		floor	301.12	1	2.43	731.72	1.94	584.18	2.56	566.70	0.50	283.35
	0	floor	28.16	1	6.70	188.69	2.50	70.41	0.15	46.30	0.50	23.15
	all	prefab façade		1		1666.10						
	0	edge beam		1		257.80				86.40	0.50	43.20
	all	walls		1		342.90						
	all	columns		1		820.90						
	all	stubs		1		82.90						
		intermidiate strip technical space	10.85	1	2.00	21.70				21.70	0.50	10.85
		concrete walls installation space		1		113.90						
Column Q	roof	roof floor	11.70	1	2.35	27.50	3.70	43.30				
		Concrete walls		1		173.30						
		25th field	26.63	1	7.15	190.39	1.45	38.61		149.80	1.00	149.80
	1 to 24	floor	221.33	1	2.43	537.83	1.94	429.37	14.83	395.00	0.50	197.50
		floor	301.12	1	2.43	731.72	1.94	584.18	2.56	566.70	0.50	283.35
	0	floor	28.16	1	6.70	188.69	2.50	70.41	0.15	46.30	0.50	23.15
	all	prefab façade		1		1666.10						
	0	edge beam		1		257.80				86.40	0.50	43.20
	all	walls		1		342.90						
	all	columns		1		820.90						
	all	stubs		1		82.90						
		intermidiate strip technical space	10.85	1	2.00	21.70				21.70	0.50	10.85
		concrete walls installation space		1		113.90						
		Extra wall filling		1		99.20						
		water		1		0.00				625.00	1.00	625.00
column 2W	roof	roof floor	75.95	1	2.35	178.48	3.70	281.02				
		intermediate floor	10.85	1	2.00	21.70			0.29	21.70	0.50	10.85
		25th field	44.79	1	7.15	320.25	1.45	64.95	23.23	252.00	1.00	252.00
		prefab façade		1		227.70						0.00
	1 to 24	floor	3368.79	1	2.43	8186.15	1.94	6535.45		4598.80	0.50	2299.40
	0	floor	65.39	1	6.70	438.12	2.50	163.48	0.04	135.60	0.50	67.80
	all	columns		1		1108.50						
	all	stubs		1		186.60						

Force moved to column	Floor	Description	A [m^2]	n Floors	$w_{structural}$ [$\frac{kN}{m^2}$]	$G_{structural}$ [kN]	$w_{permanent}$ [$\frac{kN}{m^2}$]	$G_{permanent}$ [kN]	$q_{variable}$ [$\frac{kN}{m^2}$]	$Q_{variable}$ [kN]	Ψ	$\Psi Q_{variable}$
column 2Y	roof	roof floor	75.95	1	2.35	178.48	3.70	281.02			0.00	0.00
		intermediate floor	10.85	1	2.00	21.70			0.29	21.70	0.50	10.85
		25th field	44.79	1	7.15	320.25	1.45	64.95	23.23	252.00	1.00	252.00
		prefab façade		1		227.70						
	1 to 24	floor	3368.79	1	2.43	8186.15	1.94	6535.45		4598.80	0.50	2299.40
	0	floor	65.39	1	6.70	438.12	2.50	163.48	0.04	135.60	0.50	67.80
	all	columns		1		1108.50						
	all	stubs		1		186.60						
		walls sprinkler system		1		217.80				888.00	1.00	888.00
Column C	roof	roof floor	30.00	1	8.10	243.00					0.00	0.00
		intermediate floor	27.51	1	2.35	64.64	2.50	68.76	1.83	55.00	0.50	27.50
		25th field	34.07	1	7.15	243.60	1.45	49.40	6.62	182.00	1.00	182.00
		extra concrete		1		91.10						
		steel outrigger		1		41.00						
	1 to 24	floor	328.33	1	2.43	797.84	1.94	636.96		623.30	0.50	311.65
		floor	288.33	1	2.43	700.64	1.94	559.36	1.65	542.50	0.50	271.25
	0	floor	12.96	1	6.00	77.79	2.50	32.41	0.09	25.90	0.50	12.95
	all	prefab façade		1		1666.10						
	0	edge beam		1		257.80				86.40	0.50	43.20
	all	walls		1		342.90						
	all	columns		1		782.70						
	all	stubs		1		82.90						
column F	roof	roof floor	30.00	1	8.10	243.00					0.00	0.00
		intermediate floor	27.51	1	2.35	64.64	2.50	68.76	1.83	55.00	0.50	27.50
		25th field	34.07	1	7.15	243.60	1.45	49.40	6.62	182.00	1.00	182.00
		extra concrete		1		91.10						
		steel outrigger		1		41.00						
	1 to 24	floor	328.33	1	2.43	797.84	1.94	636.96		623.30	0.50	311.65
		floor	288.33	1	2.43	700.64	1.94	559.36	1.65	542.50	0.50	271.25
	0	floor	12.96	1	6.00	77.79	2.50	32.41	0.09	25.90	0.50	12.95
	all	prefab façade		1		1666.10						
	0	edge beam		1		257.80				86.40	0.50	43.20
	all	walls		1		342.90						
	all	columns		1		782.70						
	all	stubs		1		82.90						
		stairs	12.97	1	6.00	77.80				25.90	0.50	12.95
column L	roof	roof floor	15.93	1	8.10	129.00					0.00	0.00
		gridfloor	1.75	1	8.00	14.00					0.00	0.00
		25th field	33.91	1	7.15	242.43	1.45	49.17	101.71	178.00	1.00	178.00
		outrigger		1		41.00						
	3 to 24	floor	264.30	1	2.43	642.25	1.94	512.75		499.10	0.50	249.55
	1 to 24	floor	328.33	1	2.43	797.84	1.94	636.96	2.36	623.30	0.50	311.65
	0	floor	11.98	1	6.70	80.25	2.50	29.95	0.08	25.90	0.50	12.95
	all	prefab façade		1		1634.00						
	0	edge beam		1		128.90				43.20	0.50	21.60
	all	walls		1		342.90						
	all	columns		1		782.70						
	all	stubs		1		82.90						
	2	awning		1		432.00				28.70	0.50	14.35
		inner walls		1		58.30						
	0	dividers		1		75.60						
column P	roof	roof floor	15.93	1	8.10	129.00					0.00	0.00
		gridfloor	1.75	1	8.00	14.00					0.00	0.00
		25th field	33.91	1	7.15	242.43	1.45	49.17	101.71	178.00	1.00	178.00
		outrigger		1		41.00						
	1 to 24	floor	616.66	1	2.43	1498.48	1.94	1196.32		1165.80	0.50	582.90
	0	floor	12.96	1	6.00	77.79	2.50	32.41	0.04	25.90	0.50	12.95
	all	prefab façade		1		1661.10						
	0	edge beam		1		257.80				86.40	0.50	43.20
	all	walls		1		342.90						
	all	columns		1		782.70						
	all	stubs		1		82.90						
	2	awning		1		751.70						
columns D & E	roof	roof floor	29.00	2	8.10	469.80					0.00	0.00
		gridfloor	29.01	2	2.35	136.35	2.50	145.05	2.00	58.00	0.00	0.00
		25th field	32.83	2	7.15	469.41	1.45	95.19	5.00	145.00	1.00	290.00
		extra concrete		2		182.20						
		outrigger		2		82.00						
	1 to 24	floor	576.66	2	2.43	2802.56	1.94	2237.44		1085.00	0.50	1085.00
	0	floor	11.98	2	6.70	160.51	2.50	59.89	0.04	25.90	0.50	25.90
	all	prefab façade		2		3332.20						
	0	edge beam		2		515.60				86.40	0.50	86.40
	all	walls		2		685.80						
	all	columns		2		1565.40						
	all	stubs		2		165.80						
column M	roof	gridfloor	3.63	1	8.00	29.00					0.00	0.00
		25th field	29.34	1	7.15	209.76	1.45	42.54	56.00	203.00	1.00	203.00
		outrigger		1		41.00						
	2 to 24	floor	552.63	1	2.43	1342.89	1.94	1072.11		1041.60	0.50	520.80
	0	floor	18.00	1	6.00	108.00	2.50	45.00	0.07	36.00	0.50	18.00
	all	prefab façade		1		1602.00						
	0	edge beam		1		128.90				43.20	0.50	21.60
	all	walls		1		342.90						
	all	columns		1		782.70						
	all	stubs		1		82.90						
	2	awning		1		759.00						

Force moved to column	Floor	Description	A [m²]	n Floors	$w_{structural}$ [$\frac{kN}{m^2}$]	$G_{structural}$ [kN]	$w_{permanent}$ [$\frac{kN}{m^2}$]	$G_{permanent}$ [kN]	$q_{variable}$ [$\frac{kN}{m^2}$]	$Q_{variable}$ [kN]	Ψ	$\Psi Q_{variable}$
column N	roof	roof floor	3.63	1	8.00	29.00	0.00				0.00	0.00
		25th field	29.34	1	7.15	209.76	1.45	42.54	56.00	203.00	1.00	203.00
		outrigger		1		41.00						
	2 to 24	floor	552.63	1	2.43	1342.89	1.94	1072.11		1041.60	0.50	520.80
	1	floor	3.59	1	2.43	8.73	1.94	6.97	0.01	7.20	0.50	3.60
	0	floor	12.96	1	6.00	77.79	2.50	32.41	7.21	25.90	0.50	12.95
	all	prefab façade		1		1610.00						
	0	edge beam		1		257.80				86.40	0.50	43.20
	all	walls		1		342.90						
	all	columns		1		782.70						
	all	stubs		1		82.90						
	2	awning		1		759.00						
						0.00						
Right side core (inner loads)	25 and roof	concrete core		1		1678.30						
	15 to 24	concrete core		1		11975.00						
	0 to 14	concrete core		1		18882.70						
	all	stairs	292.03	1	6.00	1752.16	1.50	438.04		337.00	0.50	168.50
	all	stairs and lift shafs		1		2297.00						
	roof	roof and technical space		1		1312.70				166.20	1.00	166.20
	0 to 25	floors	512.21	1	6.00	3073.28	1.50	768.32		1058.40	0.50	529.20
	all	mid section	442.00	1	6.00	2652.00	1.50	663.00	1.78	910.00	0.50	455.00
	all	beams		1		765.50						
right side core (outer loads)	all	floors and outriggers		1		24681.00				9708.50	0.50	4854.25
left side core (inner loads)	25 and roof	concrete core		1		1776.90						
	15 to 24	concrete core		1		11923.20						
	0 to 14	concrete core		1		17755.20						
	all	stairs	292.03	1	6.00	1752.16	1.50	438.04		337.00	0.50	168.50
	roof	roof and technical space		1		1301.00				164.70	1.00	164.70
	all	stairs and lift shafs		1		1638.70						
	0 to 25	floors	436.43	1	6.00	2618.56	1.50	654.64		901.80	0.50	450.90
	all	mid section	442.00	1	6.00	2652.00	1.50	663.00	2.09	910.00	0.50	455.00
	all	beams		1		765.50						
left side core (outer loads)	all	floors and outriggers		1		24704.40				9665.00	0.50	4832.50
Total						247564.37		38043.58		55192.60		30860.05

Table C.57: Oval density lower and upper bound calculation

Density			Lower		Upper	
floor	L [m]	A [m2]	mass [kg]	ρ [$\frac{kg}{m^3}$]	mass [kg]	ρ [$\frac{kg}{m^3}$]
0-14	57.4	1030	14663037.87	248.01	18583946.25	314.33
15-24	41	1030	10572881.57	250.36	13675788.71	323.84
Uniform	98.4	1030	25235919.45	248.99	32259734.96	318.29

C.3. Foundation Mass

For the foundation mass, the same principle was used as for the building density. The only difference being that the total mass is determined, and not the density, as shown in equation C.3. For the foundation mass, all sub-zero levels are taken into account. As the foundation mass is added to the single beam and multibeam models, by adding a lumped mass to the bottom of the beam, the determined added mass is the same for both models.

$$M_{flower} = \frac{\Sigma G_{structural}}{g}$$
$$M_{fupper} = \frac{\Sigma(G_{structural} + G_{permanent} + \Psi Q_{variable})}{g} \tag{C.3}$$

Table C.58 shows the lower and upper bound for the foundation mass for each building.

Table C.58: Lower and upper bound of the foundation mass

Foundation Mass [kg]	
Lower Bound	Upper Bound
5.97E+06	6.03E+06
6.06E+06	6.32E+06
4.98E+06	5.21E+06
8.90E+06	9.54E+06
5.95E+06	6.38E+06

Below, the tables with the foundation mass calculations are given.

Table C.59: Foundation mass calculation of the NEMC

Foundation	A $[m^2]$	$w_{structural}$ $[\frac{kN}{m^2}]$	$G_{structural}$ $[kN]$	$q_{variable}$ $[\frac{kN}{m^2}]$	$Q_{variable}$ $[kN]$	Ψ	$variable$ $[kN]$	M_f	$[kg]$
Concrete Plate	2342.52	24.00	56220.48					Lower Bound	5969018.72
Deep Plate	205.77	24.00	4938.60					Upper Bound	6028102.39
Saved Space	-105.45	24.00	-2530.77						
Saved Space	-3.01	24.00	-72.23	4.00	-12.04	0.50	-6.02		
Crawl Space	1171.26			1.00	1171.26	0.50	585.63		
Total			58556.07		1159.22		579.61		

Table C.60: Foundation mass calculation of the Montevideo tower

Description	Floor	A $[m^2]$	Description	$w_{structural}$ $[\frac{kN}{m^2}]$	$G_{structural}$ $[kN]$	$q_{variable}$ $[\frac{kN}{m^2}]$	Q	Φ	$variable$ $[kN]$	M_f	$[kg]$
Parking A $[m^2]$	-1	630.66	Concrete floor 210	5.04	3178.53	2.00	1261.32	0.70	882.92	Lower	6062900.89
Parking A $[m^2]$	-1	264.96	Concrete Floor 500	12.00	3179.52	2.00	529.92	0.70	370.94	Upper	6318531.47
Foundation Slab	-2	895.62	Concrete slab	48.00	42989.76	2.00	1791.24	0.70	1253.87		
Concrete core & columns	-1 & -2		Concrete		9712.07				0.00		
Structural Steel	-1 & -3		Steel		417.18				0.00		
Total					59477.06				2507.74		

Table C.61: Foundation mass calculation of the New Orleans tower

Description	Floor	A $[m^2]$	Description	$w_{structural}$ $[\frac{kN}{m^2}]$	$G_{structural}$ $[kN]$	$q_{variable}$ $[\frac{kN}{m^2}]$	$Q_{variable}$ $[kN]$	Ψ	$variable$ $[kN]$	M_f	$[kg]$
Parking	-1	797.76	concrete floor 260mm	6.38	5086.92	2.00	1595.52	0.70	1116.86	Lower	4995035.32
			beams		1065.60				0.00	Upper	5222734.41
Parking + slab	-2	797.76	foundation slab 2m	48.00	38292.48	2.00	1595.52	0.70	1116.86		
	-1&-2		core		4009.95				0.00		
	-1&-2		lift core		546.35				0.00		
Total					49001.30				2233.73		

Table C.62: Foundation mass calculation of the JuBi tower

Description	Floor	A $[m^2]$	Description	$w_{structural}$ $[\frac{kN}{m^2}]$	$G_{structural}$ $[kN]$	$w_{permanent}$ $[\frac{kN}{m^2}]$	$G_{permanent}$ $[kN]$	$q_{variable}$ $[\frac{kN}{m^2}]$	$Q_{variable}$ $[kN]$	Ψ	$variable$ $[kN]$	M_f	$[kg]$
parking	-1	1355	concrete floor	4.40	5962.00	1.80	2439.00	2.00	2710.00	0.70	1897.00	Lower	8903802.93
Parking + slab	-2	1355	concrete floor	48.00	65040.00	0.00	0.00	2.00	2710.00	0.70	1897.00	Upper	9539175.00
core walls	-2 & -1				13902.56		0.00				0.00		
columns	-2 & -1				2441.75		0.00				0.00		
Total					87346.31		2439.00		5420.00		3794.00		

Table C.63: Foundation mass calculation of the Oval tower

Description	Floor	A $[m^2]$	$w_{structural}$ $[\frac{kN}{m^2}]$	$G_{structural}$ $[kN]$	$w_{permanent}$ $[\frac{kN}{m^2}]$	$G_{permanent}$ $[kN]$	$q_{variable}$ $[\frac{kN}{m^2}]$	$Q_{variable}$ $[kN]$	Ψ	$variable$ $[kN]$	M_f	$[kg]$
Concrete Plate	-1	1030.00	37.50	38625.00		0.00					Lower Bound	5952476.48
floor	-1	488.02	9.60	4684.99	1.00	488.02	5.00	2440.10	1.00	2440.10	Upperbound	6375270.13
foundation	-1	1008.00	7.50	7560.00				1050.00	1.00	1050.00		
mid section foundation	-1	22.00	13.75	302.40				157.60	1.00	157.60		
columns	-1			782.70		0.00						
concrete core	-1			4441.90								
walls	-1			1996.80								
Total				58393.79		488.02		3647.70		3647.70		

C.4. Foundation Spring Stiffnesses

C.4.1. Rotational Stiffness

Lower Bound

In a study done by Furgo, the rotational spring stiffnesses of the structures were determined using the D-Pile Group software. During the D-Pile Group analysis, the pile group is modelled with an infinitely stiff foundation slab. Due to the size of the pile group, the software calculates the rotational stiffness using the Poulus model. This is a static model which considers two layers of fully elastic soil. The top layer is along the entire height of the piles, the second layer is located below the tip of the pile. The stiffness of these soil layers is specified by the user. In the analysis done by Furgo, large shear strains in the soil were assumed. This leads to a relatively small E-modulus of the soil, which is approximated by $E = 2G(1+\nu)$, with G being the shear modulus and ν the Poisson's ratio. The large strain assumption made for the D-Pile Group analysis is seen as conservative, and thus this analysis is used as the lower bound. After the pile group and foundation slab is modelled, and the soil stiffness is specified, a moment is applied to the foundation. D-Pile Group then determined the rotation of the pile heads. Using the determined rotation and the applied force, the rotational spring stiffness can then be determined. Table C.64 shows the input parameters and the results of the D-Pile Group analysis.

Table C.64: Input parameters and the results of the D-Pile Group analysis for the rotational spring stiffness

Building	E surface	E below pile	Applied Moment	Rotation pile head		Kr	
	$\frac{kN}{m^2}$	$\frac{kN}{m^2}$	kNm	x direction [rad]	y direction [rad]	x direction [$\frac{kNm}{rad}$]	y direction [$\frac{kNm}{rad}$]
NEMC	3000	60000	1.00E+06	7.57E-03	2.96E-03	1.23E+08	3.38E+08
Montevideo	6000	70000	1.00E+06	6.98E-03	5.98E-03	1.42E+08	1.67E+08
New Orleans	5000	70000	1.00E+06	4.78E-03	5.65E-03	2.10E+08	1.77E+08
JuBi	35000	100000	1.00E+06	1.19E-03	8.12E-04	8.40E+08	1.23E+09
Oval	25000	70000	1.00E+06	1.29E-03	2.88E-03	7.75E+08	3.47E+08

Upper Bound

Accompanying the explanation of the upper bound of the rotational spring stiffness is an Excel file named "***Kr Upper Bound Calculation***". The calculations of the upper bound of the rotational spring stiffness can be found there, as the calculations consist of tables too long to add to the appendix.

For the upper bound of the rotational spring stiffness, each pile under the foundation slab is represented by a vertical spring. For each building, the vertical spring stiffness was determined in the design phase by geotechnical institutions. These spring stiffnesses are shown in table C.65.

Table C.65: Vertical spring stiffness of an individual pile

	NEMC	Montevideo	New Orleans	JuBi	Oval
K_z [$\frac{kN}{m}$]	87000	90000	85000	210000	190000

The assumption is then made that the foundation slab is infinitely stiff and that it does not deform when the slab rotates. The slab is then rotated around the pile group's centre of gravity, as shown in figure C.20. Due to the shortening and elongation of the springs, a force is exerted on to the foundation slab. By combining the well-known equations in C.4, the single rotational spring stiffness of equation C.5 can be obtained.

$$F_i = k_z \delta_i$$

$$M_i = F_i a_i$$

$$\delta_i = \theta a_i$$

$$k_{r,i} = \frac{M_i}{\theta}$$

where,

F_i is the force of an individual pile,   (C.4)

k_z is the vertical spring stiffness,

δ, i is the shortening/elongation of the springs,

M, i is the moment due to the spring forces,

a, i is the lever arm of the different springs,

θ is the angle of rotation of the foundation slab, and

$k_{r,i}$ is the rotational stiffness of each spring.

$$K_r = \Sigma k_{z,i} a_i^2$$ (C.5)
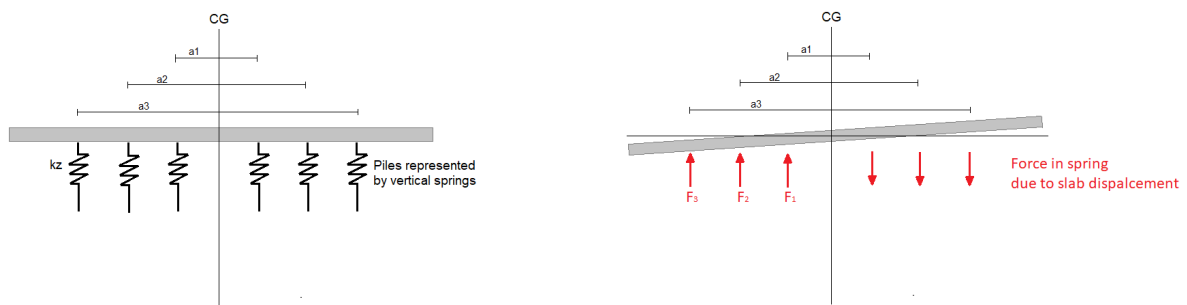
Figure C.20: Foundation with piles represented by vertical springs (left). Rotated foundation slap with vertical force equilibrium (right)

Following this method, the rotational stiffnesses of the foundations can be determined for each structure in each direction. The rotational stiffnesses in both direction are shown in the table below for each structure.

Table C.66: Rotational Spring stiffnesses for each structure in both directions

	Rotational Spring Stiffness [kNm/rad]	
Building	K_{rx}	K_{ry}
NEMC	1.75E+9	6.05E+9
Montevideo	1.42E+9	1.75E+9
New Orleans	2.29E+9	2.04E+9
JuBi	1.16E+10	2.16E+10
Oval	4.48E+9	1.49E+9

C.4.2. Translational Stiffness

Lower Bound

In the same study done by Fugro, as mentioned for the lower bound of the rotational stiffness, the translational spring stiffness was determined. Again the D-Pile Group software, with the same input parameters, was used. This time, instead of applying a moment to the pile heads, a horizontal force was applied. The software then calculated the displacements of the pile heads. The displacement and the applied force is then used to determine the translational spring stiffness. Table C.67 shows the input parameters and the results of the D-Pile Group analysis.

Table C.67: Input parameters and the results of the D-Pile Group analysis for the rotational spring stiffness

Building	E surface $\frac{kN}{m^2}$	E below pile $\frac{kN}{m^2}$	Applied Force kN	Translation pile head x direction [rad]	y direction [rad]	K_t x direction [$\frac{kN}{m}$]	y direction [$\frac{kN}{m}$]
NEMC	3000	60000	1000	7.39E-03	8.13E-03	1.35E+05	1.23E+05
Montevideo	6000	70000	1000	9.00E-03	9.28E-03	1.11E+05	1.08E+05
New Orleans	5000	70000	1000	5.33E-03	5.42E-03	1.89E+05	1.85E+05
JuBi	35000	100000	1000	6.27E-04	5.97E-04	1.59E+06	1.68E+06
Oval	25000	70000	1000	1.06E-03	1.16E-03	9.40E+05	8.62E+05

Upper Bound

Accompanying the explanation of the upper bound of the translational spring stiffness are 3 Excel files named "***Kx Upper bound - Shallow foundation - weak***", "***Kx Upper bound - Shallow foundation - strong***" and "***Kx Upper bound - Piles***". The calculations of the upper bound of the translational spring stiffness can be found there, as the calculations consist of tables too long to add to the appendix.

The upper bound of the translational stiffness is a combination of two methods proposed by Gazetas [21]. The first part is calculating the translational stiffness provided by a surface foundation on deep inhomogeneous soil. This represents the resistance of the foundation slab. The translational stiffness is determined with equation 3.9. Where G_0 is the shear stiffness of the soil at the surface, and α and n are variables determined by finding the best fit line to the shear stiffness of the soil profile. The method is described in detail in Foundation Engineering Handbook [21]. The translational stiffness is determined for a foundation strip of 1m and then multiplied by the total width of the foundation.

$$K_t = \frac{2}{2 - \nu} G_0 (1 + \frac{2}{3}\alpha)^n \tag{C.6}$$

Example: Surface foundation stiffness of NEMC

In figure C.21, the shear stiffness of the soil is shown by the blue line. This is the shear stiffness of measurements done in the design phase of the NEMC. The best fit line, shown in orange, is plotted using equation C.7. Using the well known least square method, α and n can be iterated until the best fit is determined.

For the NEMC $\alpha = 0.006$ and $n = 148.5$. From the figure of the shear stiffness, it can be seen that $G_0 = 31.22 GPa$. The foundation has a width $(2B)$ of 24m. A Poisson ratio of 0.3 is used. All unknowns are now known, and equation C.6 can be used to determine the translational stiffness for a strip of 1m. Multiplying this strip with the length of the foundation $(48m)$, the total translational stiffness can be determined. This is shown in equation C.8.

$$G(z) = G_0 \left(1 + \alpha\frac{2}{3}\right)^n \tag{C.7}$$
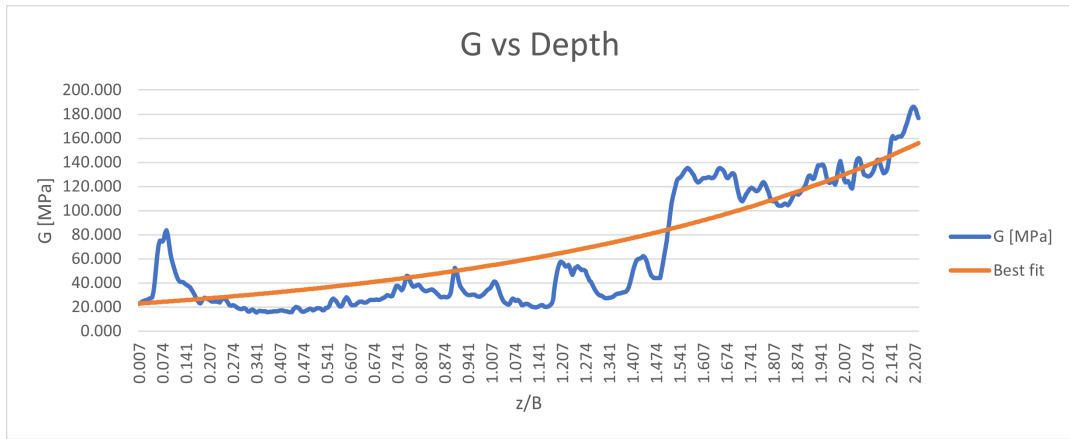
Figure C.21: Shear stiffness vs depth for the NEMC

$$K_t = \frac{2}{2-v} G_0 \left(1 + \frac{2}{3}\alpha\right)^n = \left(\frac{2}{2-0.3}\right)(31.22 \times 10^6)\left(1 + \frac{2 \times 0.006}{3}\right)^{148.5} \times 48 = 3.12 \times 10^9 \frac{N}{m} \quad (C.8)$$

This calculation is done is both directions, to determine the translational stiffness in the strong and weak direction.

The second part of the calculation is determining the translational stiffness of a single pile. The translational stiffness of a pile can be determined with the first part of equation C.9. where d is the diameter of the pile, $\tilde{E}_s$ is a reference E-modulus of the soil determined using the best fit line of the E-modulus profile of the soil, and E_p is the E-modulus of the pile. After the translational stiffness is determined for a single pile, the stiffness is multiplied by the number of piles in the foundation.

$$K_t = 0.6d\tilde{E}_s \left(\frac{E_p}{\tilde{E}_s}\right)^{0.35} \times n_{piles} \quad (C.9)$$

Example: Pile stiffness of NEMC

In figure C.22, the elasticity modulus of the soil is shown by the blue line. This is the elasticity modulus of measurements done in the design phase of the NEMC. The best fit line, shown in orange, is plotted using equation C.10, where z id the depth and d is the pile diameter. Using the well known least square method, $\tilde{E}_s$ can be iterated until the best fit is determined.

For the NEMC $\tilde{E}_s = 2.07 MPa$. The piles have a diameter (d) of 0.508m and elasticity modulus (E_P) =f $20 GPa$. All unknowns are now known, and equation C.9 can be used to determine the translational stiffness for 1 pile. Multiplying the stiffness for 1 pile with the total number of piles, the total translational stiffness of the pile group can be determined. This is shown in equation C.11.

$$E_s = \tilde{E}_s \left(\frac{z}{d}\right) \quad (C.10)$$
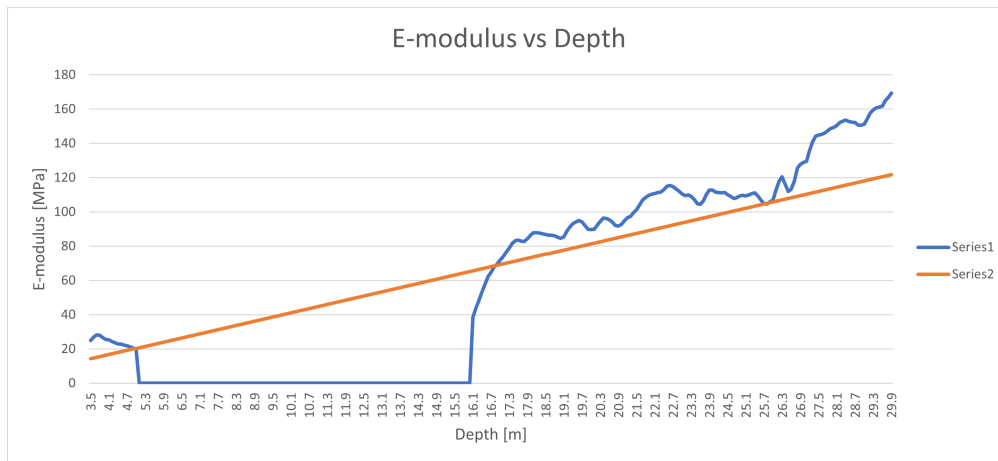
Figure C.22: Elasticity modulus vs depth for the NEMC

$$K_t = 0.6d\tilde{E}_s\left(\frac{E_p}{\tilde{E}_s}\right)^{0.35} \times n_{piles}$$

$$= 0.6(0.508)(2.06 \times 10^6)\left(\frac{20 \times 10^9}{(2.06 \times 10^6)}\right)^{0.35} \times 334 = 5.23 \times 10^9 \quad \text{(C.11)}$$

The translational stiffness of a single pile is assumed to be the same in both directions.

The total translational spring stiffness is then calculated by the product of equations C.6 and C.9. The spring stiffness for each structure is given in table C.68 and C.69. The full calculations can be found in the added Excel files.

Table C.68: Translational spring stiffness weak direction

	K_{tx} [$\frac{kN}{m}$]		
	Shallow Foundation	n piles	Total
NEMC	3.12E+06	5.23E+06	8.35E+06
MV	1.53E+06	2.40E+06	3.93E+06
NO	1.60E+06	3.28E+06	4.88E+06
JuBi	5.00E+06	9.99E+06	1.50E+07
Oval	4.63E+06	3.94E+06	8.57E+06

Table C.69: Translational spring stiffness strong direction

	K_{ty} [$\frac{kN}{m}$]		
	Shallow Foundation	n piles	Total
NEMC	2.76E+06	5.23E+06	7.98E+06
MV	1.44E+06	2.40E+06	3.84E+06
NO	1.54E+06	3.28E+06	4.82E+06
JuBi	5.20E+06	9.99E+06	1.52E+07
Oval	4.85E+06	3.94E+06	8.79E+06

D
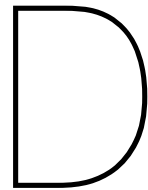
Sensitivity Study Results

This chapter provides the results of the sensitivity study, which were not added to the body of the thesis.

D.1. Varying Parameters

This section shows the results of the single and multibeam for the analyses done where different parameters are varied. In each case, one parameter varies from its lower bound to its upper bound, while all other parameters are kept constant.

D.1.1. Single Beam Model
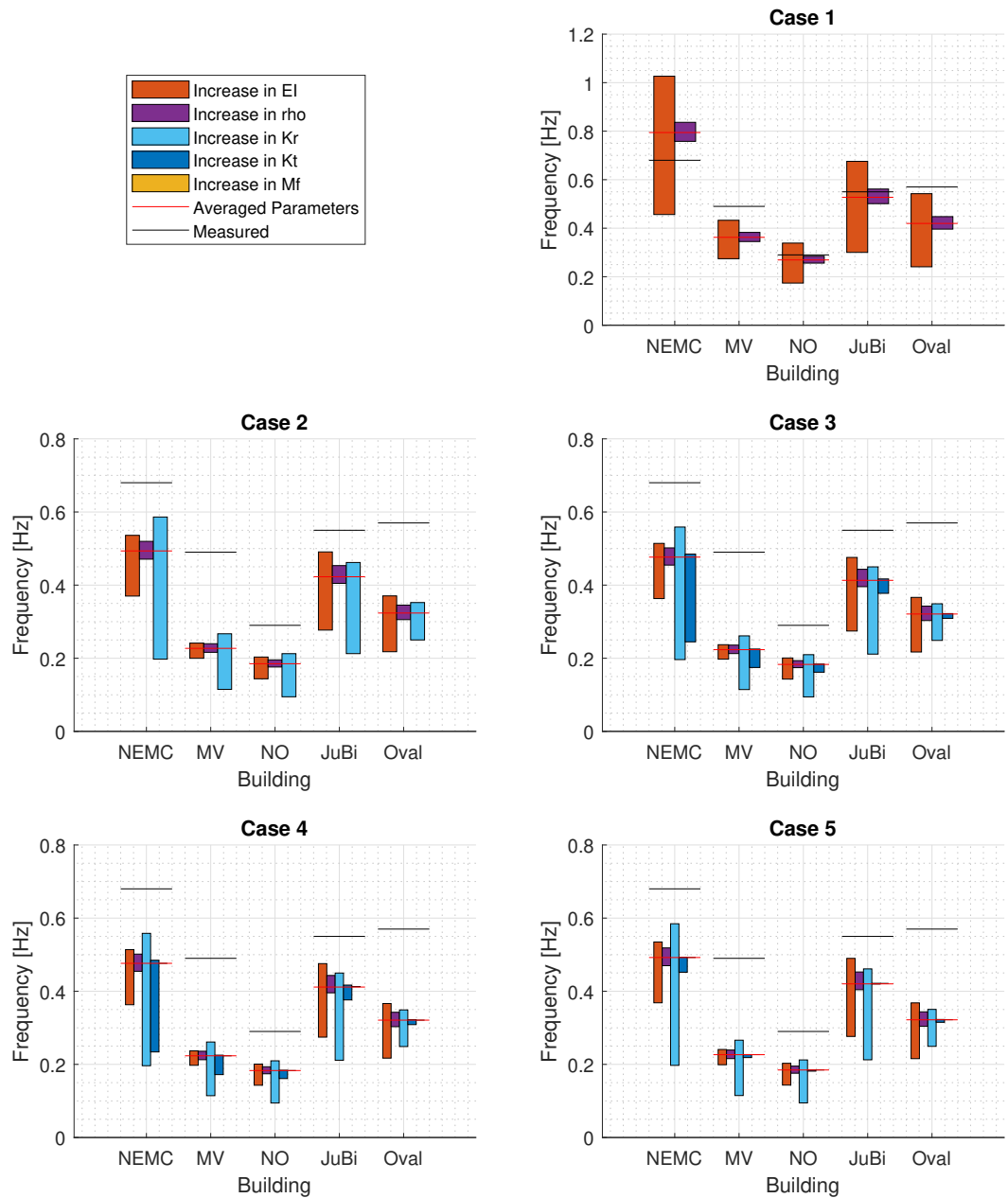
Figure D.1: Influence of varying parameters on the second translational frequency

D.1.2. Multibeam Beam Model
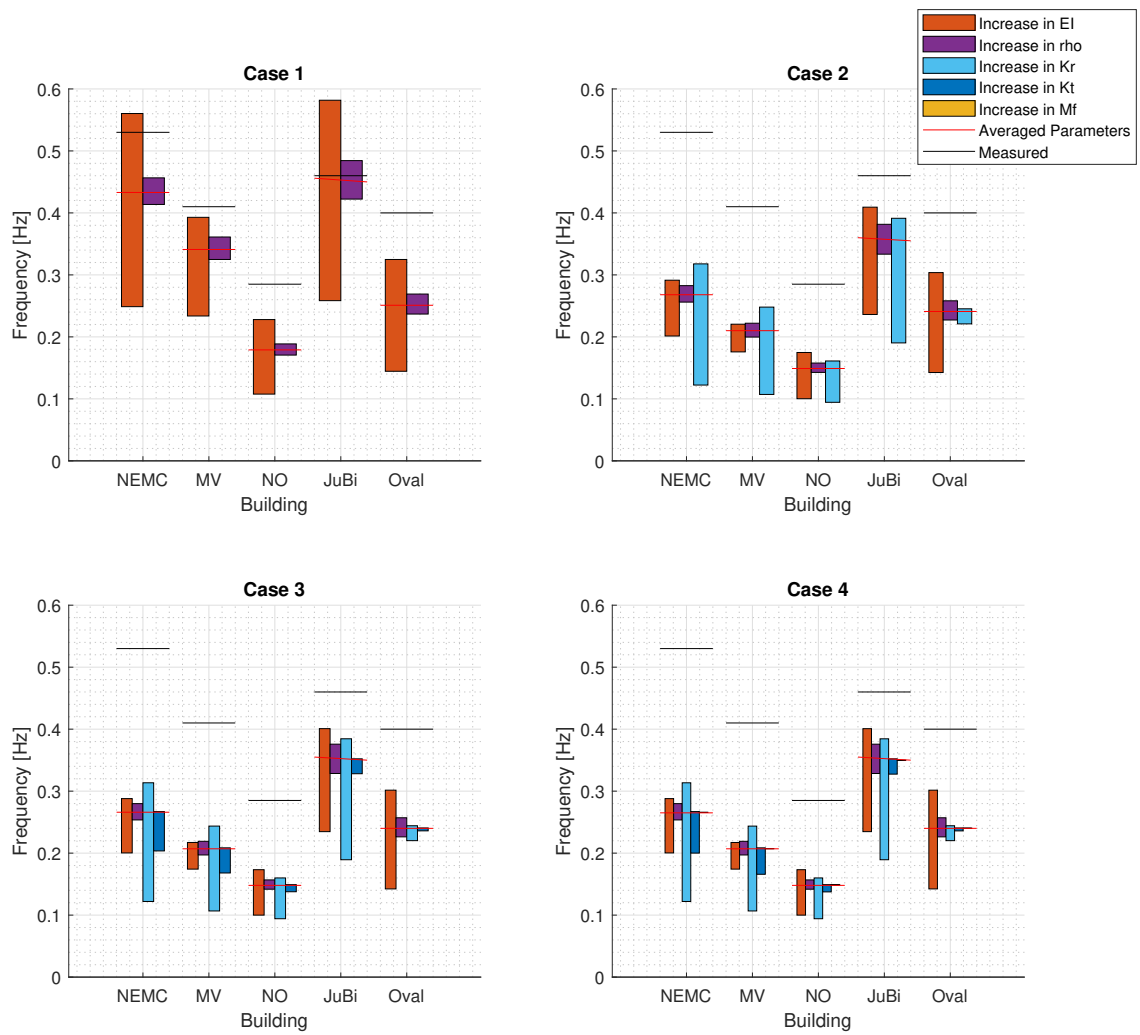
Figure D.2: Influence of varying parameters on the first translational frequency
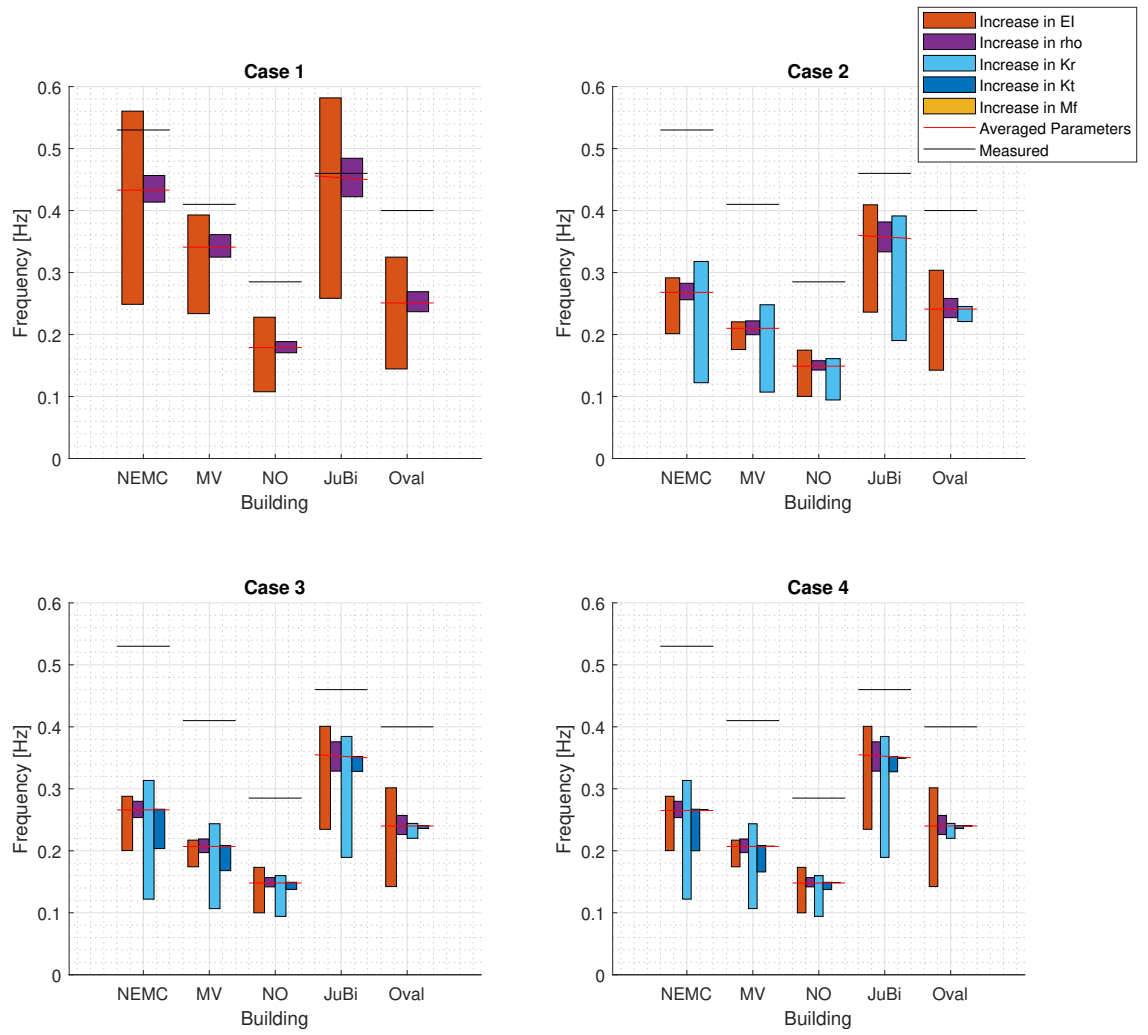
Figure D.3: Influence of varying parameters on the second translational frequency

D.2. Extreme Parameter Combinations
D.2.1. Multibeam Beam Model
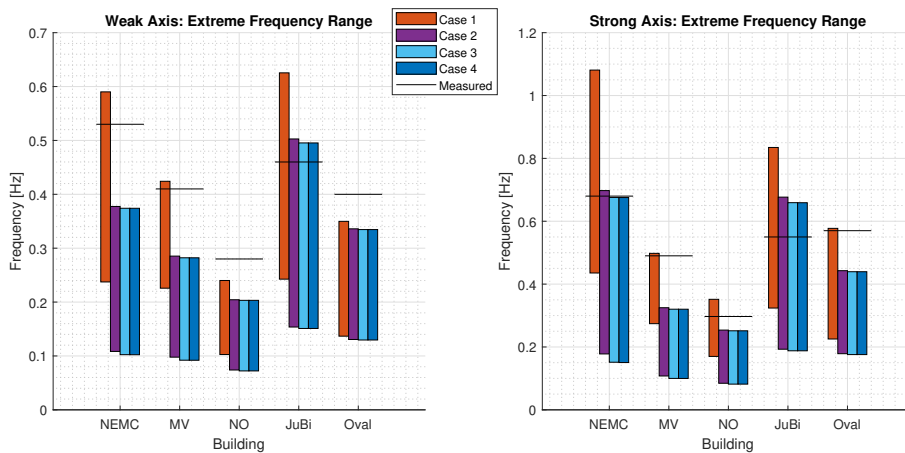
Figure D.4: Frequency of extreme parameter combinations

D.3. 90% Probability Interval
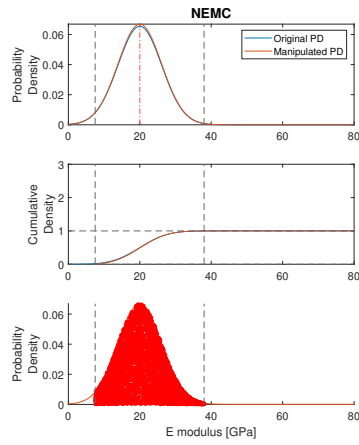
(a) Probability density and cumulative density for the E modulus of the NEMC tower.
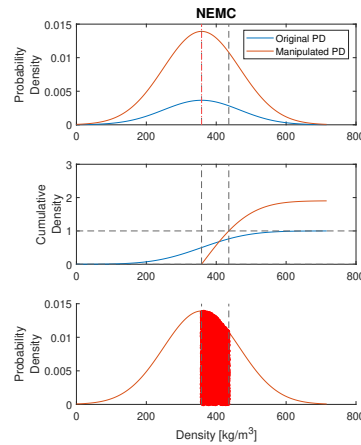
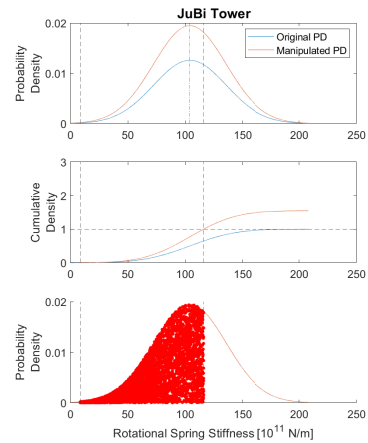(b) Probability density and cumulative density for the density of the NEMC tower.
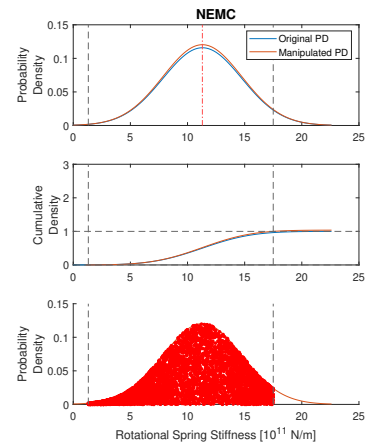
(c) Probability density and cumulative density for the rotational stiffness of the NEMC tower.
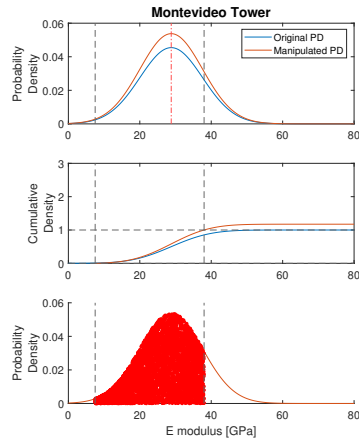
(a) Probability density and cumulative density for the E modulus of the Montevideo tower.
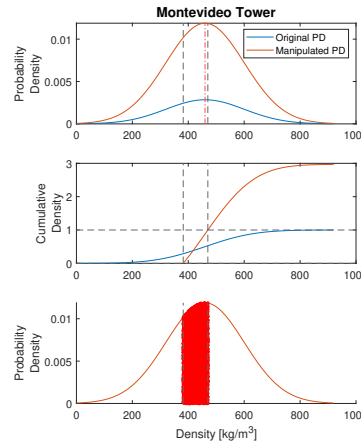
(b) Probability density and cumulative density for the density of the Montevideo tower.
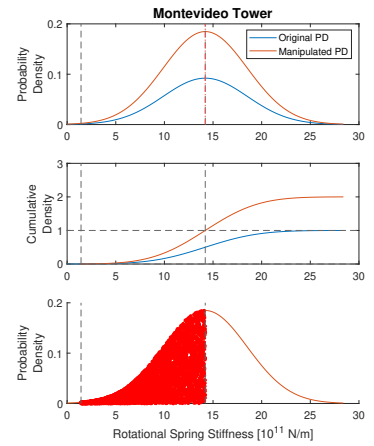
(c) Probability density and cumulative density for the rotational stiffness of the Montevideo tower.
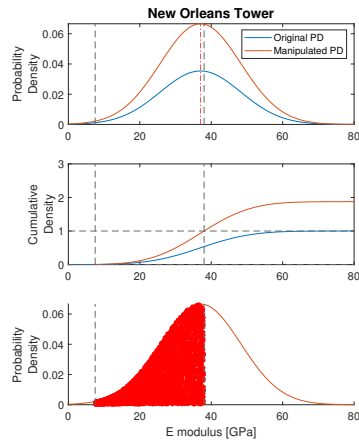
(a) Probability density and cumulative density for the E modulus of the New Orleans tower.
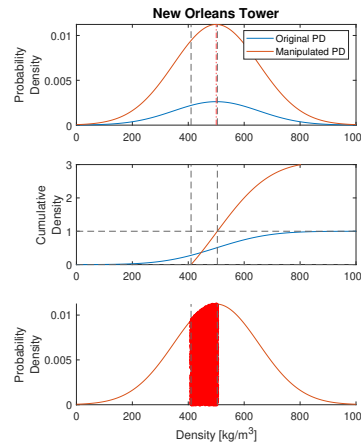
(b) Probability density and cumulative density for the density of the New Orleans tower.
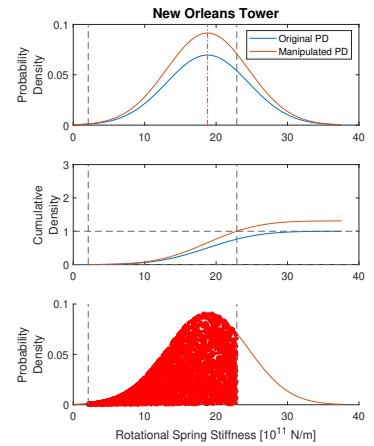
(c) Probability density and cumulative density for the rotational stiffness of the New Orleans tower.
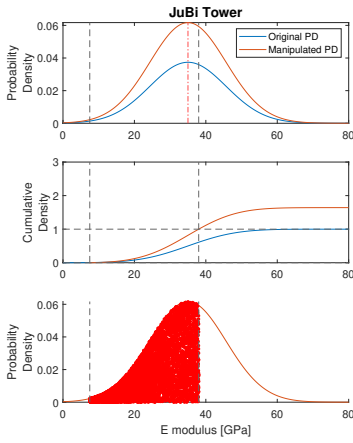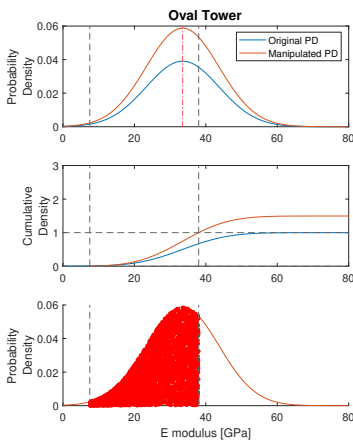
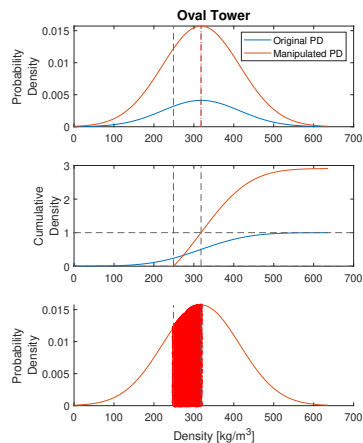(a) Probability density and cumulative density for the density of the JuBi tower.
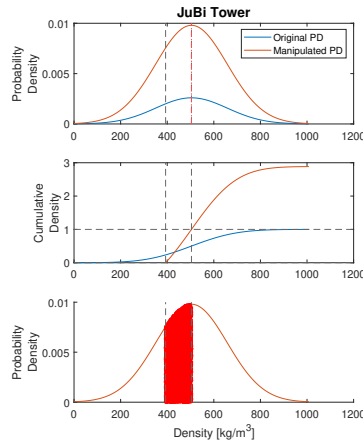
(b) Probability density and cumulative density for the rotational stiffness of the JuBi tower.
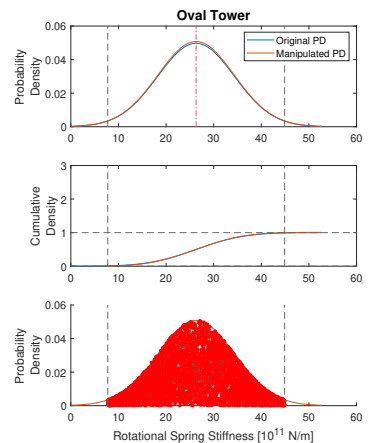
(c) Probability density and cumulative density for the rotational stiffness the JuBi tower.

(a) Probability density and cumulative density for the E modulus of the Oval tower.

(b) Probability density and cumulative density for the density of the Oval tower.

(c) Probability density and cumulative density for the rotational stiffness of the Oval tower.

Bibliography

[1] Makola M. Abdullah et al. "Use of a shared tuned mass damper (STMD) to reduce vibration and pounding in adjacent structures". In: *Earthquake Engineering and Structural Dynamics* 30.8 (2001), pp. 1185–1201. ISSN: 00988847. DOI: `10.1002/eqe.58`.

[2] American Society of Civil Engineers. *ASCE 7: Minimum Design Loads for Buildings and Other Structures*. Tech. rep. 2012.

[3] Stavros A. Anagnostopoulos. "Pounding of buildings in series during earthquakes". In: *Earthquake Engineering & Structural Dynamics* 16.3 (1988), pp. 443–456. ISSN: 10969845. DOI: `10.1002/eqe.4290160311`.

[4] L. Arany et al. "An analytical model to predict the natural frequency of offshore wind turbines on three-spring flexible foundations using two different beam models". In: *Soil Dynamics and Earthquake Engineering* 74 (2015), pp. 40–45. ISSN: 02677261. DOI: `10.1016/j.soildyn.2015.03.007`. URL: `http://dx.doi.org/10.1016/j.soildyn.2015.03.007`.

[5] Andrew Bartolini. "Advancements in Full☐Scale Monitoring Hardware for Improved Modeling of Tall Buildings: A System Behavior Perspective". PhD thesis. University of Notre Dame, 2019.

[6] R.L.J. van den Berg and Steenbergen R.D.J.M. "Identifying the Damping Contribution of Building components based on measured top vibration". In: *4th ECCOMAS Thematic Conference on Computational Methods in Structural Dynamics and Earthquake Engineering*. 2013.

[7] R. E.D. Bishop, S. M. Cannon, and S. Miao. *On coupled bending and torsional vibration of uniform beams*. 1989. DOI: `10.1016/0022-460X(89)91005-5`.

[8] Rune Brincker, Lingmi Zhang, and Palle Andersen. "Modal identification from ambient responses using frequency domain decomposition". In: *Proceedings of the IMAC 18, International Modal Analysis COnference*. 2000.

[9] A J Bronkhorst, C A Van Bentum, and S S Gomez. *Wind-induced vibrations and damping in high-rise buildings*. Tech. rep. 2018.

[10] A J Bronkhorst and D Moretti. *Application of the Frequency Domain Decomposition method on the residential tower New Orleans*. Tech. rep. 2021, p. 17.

[11] Okke Bronkhorst and Chris Geurts. "HIVIBE - Monitoring van trillinggen in hoogbouw: Naar een Nationaal Programma Hoogbouwmonitoring". In: *Cement* (2021).

[12] J. M.W. Brownjohn, T. C. Pan, and X. Y. Deng. "Correlating dynamic characteristics from field measurements and numerical analysis of a high-rise building". In: *Earthquake Engineering and Structural Dynamics* 29.4 (2000), pp. 523–543. ISSN: 00988847. DOI: `10.1002/(SICI)1096-9845(200004)29:4<523::AID-EQE920>3.0.CO;2-L`.

[13] Bureau of Indian Standards. "Criteria for earthquake resistant design of structures". In: *Earthquake Resistant Design of Structures* (2002).

[14] S. Campbell, K. C.S. Kwok, and P. A. Hitchcock. "Dynamic characteristics and wind-induced response of two high-rise residential buildings during typhoons". In: *Journal of Wind Engineering and Industrial Aerodynamics* 93.6 (2005), pp. 461–482. ISSN: 01676105. DOI: `10.1016/j.jweia.2005.03.005`.

[15] Canadian Commission on Building and Fire Codes and National Research Council of Canada. *National Building Code of Canada 2005*. Tech. rep. 2005, pp. 182–183.

[16] E Carrera, G Giunta, and M Petrolo. *Beam Structures Beam Structures*. 2001. ISBN: 9780470972007.

[17] Helen Crowley and Rui Pinho. "Revisiting Eurocode 8 formulae for periods of vibration and their employment in linear seismic analysis". In: *Earthquake Engineering and Structural Dynamics* 39.2 (2010), pp. 223–235. ISSN: 10969845. DOI: `10.1002/eqe.949`.

[18] Clive L. Dym and Harry E. Williams. *Analytical estimates of structural behavior*. CRC Press, Feb. 2012, pp. 1–214. ISBN: 9781439870914. DOI: `10.1201/b11638`.

[19] B. R. Ellis. "An assessment of the accuracy of prediction the fundamental frequencies of buildings". In: *Institution of Civil engineers* 69 (1980), pp. 763–776.

[20] EUROPEAN COMMITTEE FOR STANDARDIZATION. *Eurocode 8: Design of structures for earthquake resistance - Part 1 : General rules, seismic actions and rules for buildings*. Tech. rep. 2005. 2011.

[21] G Gazetas. "Foundation Engineering Handbook". In: *Foundation Engineering Handbook*. Ed. by H Fang. 1991. Chap. Foundation, pp. 553–593. DOI: `10.1007/978-1-4757-5271-7`.

[22] Damien Gilles. "IN SITU DYNAMIC CHARACTERISTICS OF REINFORCED By requirements of the degree of Doctor of Philosophy". In: February (2011).

[23] Rakesh K. Goel and Anil K. Chopra. "Period Formulas for Moment-Resisting Frame Buildings". In: *Journal of Structural Engineering* 123.11 (Nov. 1997), pp. 1454–1461. ISSN: 0733-9445. DOI: `10.1061/(ASCE)0733-9445(1997)123:11(1454)`.

[24] Pilar Alaejos Gutierrez and Manuel Fernandez Canovas. "The modulus of elasticity of high performance concrete". In: *Materials and Structures* 28.10 (1995), pp. 559–568. ISSN: 00255432. DOI: `10.1007/BF02473187`.

[25] George D. Hatzigeorgiou and George Kanapitsas. "Evaluation of fundamental period of low-rise and mid-rise reinforced concrete buildings". In: *Earthquake Engineering and Structural Dynamics* 42.11 (2013), pp. 1599–1616. ISSN: 10969845. DOI: `10.1002/eqe.2289`.

[26] Ward Heylen, Stefan Lammens, and Paul Sas. "Modal Analysis Theory and Testing". In: (1997), p. 340. URL: `https://asset-pdf.scinapse.io/prod/156689764/156689764.pdf%0Ahttps://pdfs.semanticscholar.org/bad9/0f4967dc926830c47226f2157ce4727a3983.pdf`.

[27] E Ho and L Kong. "Full scale and wind tunnel comparison of wind-induced responses of tall buildings". In: *Proceedings of 12th international conference on wind engineering*. 2007, pp. 1231–8.

[28] Li-Ling Hong and Woei-Luen Hwang. "Empirical formula for fundamental vibration periods of reinforced concrete buildings in Taiwan". In: *Earthquake Engineering & Structural Dynamics* 29.3 (Mar. 2000), pp. 327–337. ISSN: 0098-8847. DOI: `10.1002/(SICI)1096-9845(200003)29:3<327::AID-EQE907>3.0.CO;2-0`.

[29] Jorrit van Ingen. "Stabiliteitskern met tweede-orde-effecten". In: *Cement* (2021), pp. 54–61.

[30] International Conference of Building Officials. *Uniform building code - 1970*. Tech. rep. 1970.

[31] International Conference of Building Officials. *Uniform building code - 1997*. Tech. rep. 1997.

[32] S. K. Jang and C. W. Bert. "Free vibration of stepped beams: Exact and numerical solutions". In: *Journal of Sound and Vibration* 130.2 (1989), pp. 342–346. ISSN: 10958568. DOI: `10.1016/0022-460X(89)90561-0`.

[33] S. K. Jang and C. W. Bert. "Free vibration of stepped beams: Exact and numerical solutions". In: *Journal of Sound and Vibration* 132.2 (1989), pp. 164–168.

[34] Robert Jankowski. "Non-linear FEM analysis of earthquake-induced pounding between the main building and the stairway tower of the Olive View Hospital". In: *Engineering Structures* 31.8 (2009), pp. 1851–1864. ISSN: 01410296. DOI: `10.1016/j.engstruct.2009.03.024`. URL: `http://dx.doi.org/10.1016/j.engstruct.2009.03.024`.

[35] Robert Jankowski. "Non-linear FEM analysis of pounding-involved response of buildings under non-uniform earthquake excitation". In: *Engineering Structures* 37 (2012), pp. 99–105. ISSN: 01410296. DOI: `10.1016/j.engstruct.2011.12.035`. URL: `http://dx.doi.org/10.1016/j.engstruct.2011.12.035`.

[36] Jasper Monster. *Hoogbouw is de ideale oplossing in de strijd tegen woningnood. Of toch niet? – Gebiedsontwikkeling.nu*. 2021. URL: `https://www.gebiedsontwikkeling.nu/artikelen/hoogbouw-is-de-ideale-oplossing-in-de-strijd-tegen-woningnood-of-toch-niet/`.

[37] R. Jategaonkar and D.S. Chehil. "Natural frequencies of a beam with varying section properties". In: 133 (1989), pp. 303–322.

[38] F. Ju, H. P. Lee, and K. H. Lee. "On the free vibration of stepped beams". In: *International Journal of Solids and Structures* 31.22 (1994), pp. 3125–3137. ISSN: 00207683. DOI: `10.1016/0020-7683(94)90045-0`.

[39] Ahsan Kareem. "Effects of Parametric Uncertainty on Wind Excited Structural Response." In: *Journal of Wind Engineering and Industrial Aerodynamics* 30 (1988), pp. 233–241. ISSN: 01676105. DOI: `10.1016/j.jweia.2013.08.007`.

[40] Kazuhiko Kasai and Bruce F. Maison. "Building pounding damage during the 1989 Loma Prieta earthquake". In: *Engineering Structures* 19.3 (1997), pp. 195–207. ISSN: 01410296. DOI: `10.1016/S0141-0296(96)00082-X`.

[41] Hemant B. Kaushik et al. "Performance of structures during the Sikkim earthquake of 14 February 2006". In: *Current Science* 91.4 (2006), pp. 449–455. ISSN: 00113891.

[42] Do Hyun Kim and Ji Young Kim. "Assessment on Natural Frequencies of Structures using Field Measurement and FE Analysis". In: *International Journal of High-Rise Buildings* 3.4 (2014), pp. 305–310. ISSN: 2234-7224. DOI: `10.21022/IJHRB.2014.3.4.305`.

[43] J.Y. Kim et al. "Evaluations of dynamic structural properties using wind-induced responses". In: *Proceedings of annual conference of KSSC*. 2007.

[44] Ji Young Kim et al. "Calibration of analytical models to assess wind-induced acceleration responses of tall buildings in serviceability level". In: *Engineering Structures* 31.9 (2009), pp. 2086–2096. ISSN: 01410296. DOI: `10.1016/j.engstruct.2009.03.010`.

[45] Q. S. Li et al. "Full-scale measurements and numerical evaluation of wind-induced vibration of a 63-story reinforced concrete tall building". In: *Engineering Structures* 26.12 (2004), pp. 1779–1794. ISSN: 01410296. DOI: `10.1016/j.engstruct.2004.06.014`.

[46] Q. S. Li et al. "Full-scale measurements of wind effects on the Jin Mao building". In: *Journal of Wind Engineering and Industrial Aerodynamics* 95.6 (2007), pp. 445–466. ISSN: 01676105. DOI: `10.1016/j.jweia.2006.09.002`.

[47] Bruce F. Maison and Kazuhiko Kasai. "Dynamics of pounding when two buildings collide". In: *Earthquake Engineering & Structural Dynamics* 21.9 (1992), pp. 771–786. ISSN: 10969845. DOI: `10.1002/eqe.4290210903`.

[48] Leszek Majkut. "Free and forced vibrations of timoshenko beams described by single difference equation". In: *Journal of Theoretical and Applied Mechanics* 47.1 (2009), pp. 193–210. ISSN: 14292955.

[49] C. Michel et al. "Comparison between seismic vulnerability models and experimental dynamic properties of existing buildings in France". In: *Bulletin of Earthquake Engineering* 8.6 (Dec. 2010), pp. 1295–1307. ISSN: 1570-761X. DOI: `10.1007/s10518-010-9185-7`.

[50] M. Miwa et al. "Modal identification by FEM analysis of a building with CFT columns". In: *Proceedings of the 20th international modal analysis conference*. 2002, pp. 1618–22.

[51] NEN-EN. *NEN 6702: Technical principles for building structures - TGB 1990 - Loadings and deformations*. Tech. rep. 2007.

[52] Tso-Chien Pan, Key Seng Goh, and Kusnowidjaja Megawati. "Empirical relationships between natural vibration period and height of buildings in Singapore". In: *Earthquake Engineering & Structural Dynamics* 43.3 (Mar. 2014), pp. 449–465. ISSN: 00988847. DOI: `10.1002/eqe.2356`.

[53] C Petrone et al. "Stress-Strain Behavior of Plasterboards Subjected in Tension and Compression". In: (2017).

[54] S Sánchez Gómez. "Energy flux method for identification of damping in high-rise buildings subject to wind". PhD thesis. Technical University of Delft, 2019, p. 161. DOI: `10.4233/uuid:bc4fe937-2711-4ee0-95b7-baad7c5d234c`.

[55] Angelo Simone. *An Introduction to the Analysis of Slender Structures*. 2011.

[56] M Sonneveld. *Sensitivities and prerequisites of the application of the Energy Flux Analysis to high-rise structures excited by wind using in situ measurements*. Tech. rep. Technical University of Delft, 2020, p. 204.

[57] R. K.L. Su et al. "Influence of non-structural components on lateral stiffness of tall buildings". In: *Structural Design of Tall and Special Buildings* 14.2 (2005), pp. 143–164. ISSN: 15417794. DOI: `10.1002/tal.266`.

[58] Y. Tamura et al. "Measurement of wind-induced response of buildings using RTK-GPS". In: *Journal of Wind Engineering and Industrial Aerodynamics* 90.12-15 (2002), pp. 1783–1793. ISSN: 01676105. DOI: `10.1016/S0167-6105(02)00287-8`.

[59] Pulkit Dilip ; Velani and P K Ramancharla. "New Empirical Formula for Fundamental Period of Tall Buildings in India By Ambient Vibration Test". In: *16th World Conference on Earthquake Engineering* (2017).

[60] Peter D. Welch. "The Use of Fast Fourier Transform for the Estimation of Power Spectra: A Method Based on Time Averaging Over Short, Modified Periodograms". In: *IEEE Transactions*

on Audio and Electroacoustics 15.2 (1967), pp. 70–73. ISSN: 00189278. DOI: `10.1109/TAU.1967.1161901`.

[61]   Yun Zhou et al. "Operational Modal Analysis and Rational Finite-Element Model Selection for Ten High-Rise Buildings based on On-Site Ambient Vibration Measurements". In: *Journal of Performance of Constructed Facilities* 31.5 (Oct. 2017), p. 04017043. ISSN: 0887-3828. DOI: `10.1061/(ASCE)CF.1943-5509.0001019`.